

# **AIR FLOW MANAGEMENT INSIDE DATA CENTRES**

**Ali M A S Almoli**

Submitted in accordance with the requirements for the degree of  
Doctor of Philosophy

The University of Leeds  
School of Mechanical Engineering

February, 2013

The candidate confirms that the work submitted is his own, except where work has formed jointly-authored publication has been included. The contribution of the candidate and other authors to this work has been explicitly indicated overleaf. The candidate confirms that appropriate credit has been given within the thesis where reference has been made to the work of others.

This copy has been supplied on the understanding that it is copyrighted material and that no quotation from the thesis may be published without proper acknowledgement.

## **Work Formed from Jointly Authored Publication**

During the PhD. study the publication has been done with help of my supervisors and colleague. The candidate did the CFD modelling for the publication. Also the analysis of the result, meshing, and results presentation have been carried out by candidate.

The study in chapter 7, which is in section 7.3 has been published by candidate and others. In this study, the comparison between two types of back door coolers (active back door cooler and passive back door cooler) with respect to the cooling load inside the data centre has been done. This paper has been accepted in the Journal of Applied Energy in 3 February 2011 and presented online at 25 February 2011[Almoli et al., 2011]. The CFD analysis and results presentation have been done by candidate. Whereas, the paper has been written by Dr. Jonathan Summers and Prof. Harvey Thompson. The experimental part has been done by Adam Thompson, and Dr. Nikil Kapur. The experimental part has been done at Airedal International Air Conditioning Ltd. Leeds, United Kingdom under supervision of George Hannah.

## **Acknowledgements**

I would like to express my extreme gratefulness to my supervisors, Dr. Jonathan Summers, Prof. Harvey Thompson and Dr. Nikil Kapur. I cannot find any suitable words to express my deep respect and appreciation to you. You helped me a lot with my PhD, you left your doors open to me, you gave me your advice and put me on the right path. Most importantly, you supplied useful hints in my PhD research. I will always keep your advice and instructions in mind.

I cannot deny and forget the role of my colleague, Adam Thompson, and his help with the experimental work involved in this research. You are easy to work with and I hope that you achieve your goals in the future.

I would like to extend my great thanks and regards to Mr. George Hannah, at Airedale International Air Conditioning, Ltd., for his help and for letting me use the facilities of the company. You helped me a lot; thank you very much indeed.

Above all else, I thank my family, father ,mother and my wife so much for their support and prayers. You gave me a lot, but most especially, you gave me the strength to go on. Thank you very much.

## **Abstract**

A data centre can be defined as an infrastructure facility that houses file servers, processors and other computer equipment, along with a standby power supply. These servers are kept inside cabinets and those cabinets are called racks. These racks are located close to each other inside a data centre to form rows. These rows are located front to front and back to back to form the aisles. These aisles could be used to supply the chilled air and also to provide room for operational purposes.

Data centres are now widespread due to the high demand of infrastructure requirements, such as the network to operate Internet services. In this thesis, research is focused on the air cooling method, a popular method of cooling that is used to cool many data centres. The aim of this thesis is to understand the capabilities and limitations of Computational Fluid Dynamics (CFD) analysis of cooling air flow in data centres. The data centre components, which are the server blade and rack, have been simulated in order to study the environmental conditions (temperature, pressure and velocity fields) inside the data centre; as such, CFD analysis has been carried out at server, rack and room levels. The proposed method of a porous media model has been implemented to simulate servers and racks and has been tested and validated through corresponding experiments. It is shown from the results that the porous media model provides good agreement with experimental data of an actual case at the server level. The server racks have been simulated as a porous media with different permeability values in each direction ( $x$ ,  $y$ ,  $z$ ). In addition, a 3-dimensional CFD model has been used to explore the performance of three different room level cooling strategies based on the aisle containment (cold and hot aisle containments) and back door cooler. It is shown that using either cold

or hot aisle containment within a data centre provides significant improvement inside the data centre with respect to temperature distribution and the avoidance of hot spots.

Finally, the power input to the computer room air conditioning (CRAC) unit has been analysed for different cooling configurations when assuming the Coefficient of Performance (COP) of either direct expansion CRAC unit or a chiller system. Furthermore, the comparison between active and passive back door coolers has been done to evaluate the power consumption in the CRAC unit. It is shown that the supply temperature inside the data centre has a significant effect on the CRAC power input (compressor work) of the DX CRAC unit. With respect to comparison between the active and passive back door coolers, it has been found that the reduction of the CRAC unit load is higher when using the active back door cooler compared to the passive back door cooler, so the active back door cooler is better than passive back door cooler with respect to reduction of load on CRAC unit.

## Table of Contents

<b>CHAPTER 1: INTRODUCTION .....</b>	<b>1</b>
1.1 General overview .....	1
1.2 Thesis Plan .....	4
<b>CHAPTER 2: LITERATURE REVIEW.....</b>	<b>6</b>
2.1 Introduction .....	6
2.2 Data centre overview.....	6
2.3 Data centre power system layout .....	8
2.4 Environmental requirements .....	10
2.5 Data centre efficiency .....	11
2.6 Layout and cooling.....	13
2.6.1 Data centre layout .....	14
2.6.2 Data centre cooling .....	21
Overhead cooling method .....	35
Portable data centre with a cooling system .....	38
Back door cooling system .....	39
2.7 High Performance Computing (HPC) data centre .....	41
2.8 Thermodynamics of a data centre .....	44

2.8.1 CRAC unit types .....	45
2.8.2 Coefficient of Performance (COP) of the data centre.....	48
2.9 Conclusion .....	50
<b>CHAPTER 3: THE SCOPE OF THE CURRENT WORK .....</b>	<b>52</b>
3.1 Introduction.....	52
3.2 Objective and new knowledge .....	52
<b>CHAPTER 4 : MODELLING .....</b>	<b>55</b>
4.1 Introduction.....	55
4.2 Computational Fluid Dynamics (CFD) modelling.....	56
4.2.1 CFD modelling of data centre air flows.....	58
4.2.2 Non-dimensional analysis for the governing equations.....	60
4.3 Laminar flow.....	63
4.4 Turbulent flow.....	63
4.4.1 Reynolds Averaged Navier-Stokes model (RANS).....	64
4.4.2 Turbulence k- $\epsilon$ models.....	68
4.4.3 Standard k- $\epsilon$ model: .....	68
4.4.4 RNG k- $\epsilon$ model: .....	69
4.4.5 Realizable k- $\epsilon$ model:.....	70
4.4.6 Boundary conditions .....	73
4.5 Porous flow modelling.....	73
4.5.1 Darcy's law .....	74

4.5.2 Inertial losses in porous media.....	75
4.6 Fan modelling .....	76
4.6.1 Fan modelling for the traditional rack server.....	76
4.6.2 Fan modelling for active back cooler.....	80
4.7 CFD analysis of server blade .....	81
4.8 Traditional server (1U server).....	83
4.8.1 CPU analysis in the 1U traditional server.....	83
4.8.2 Server Modelling.....	91
4.8.3 Boundary Conditions .....	94
4.9 Blade server.....	105
4.9.1 HP server modelling.....	107
4.9.2 Boundary Conditions .....	107
4.9.3 Results and Discussion.....	109
4.10 Conclusion .....	112
<b>CHAPTER 5 : CFD ANALYSIS OF FLOW-THROUGH LEVEL RACKS .....</b>	<b>113</b>
5.1 Introduction .....	113
5.2 Rack Cooling Scenarios .....	115
5.2.1 Traditional cooling for the rack.....	115
5.2.2 CFD analysis for the rack.....	116
5.3 Results and Discussion.....	120
5.4 Conclusion .....	136



<b>CHAPTER 6: DATA CENTRE COOLING CONFIGURATIONS.....</b>	<b>137</b>
6.1 Introduction.....	137
6.2 3-D Analysis for cold-hot aisle arrangement. ....	137
6.3 An Assessment of the cold aisle containment technique .....	140
6.4 An Assessment of the hot aisle containment technique .....	141
6.5 An assessment of a back door cooler .....	142
6.5.1 Active back door cooler .....	143
6.5.2 Passive back door cooler.....	143
6.5.3 CFD analysis of the back door cooler .....	144
6.6 Result and Discussion .....	147
6.7 Conclusion .....	158
<b>CHAPTER 7 :CFD ANALYSIS OF DIFFERENT COOLING CONFIGURATIONS OF HPC DATA CENTRES.....</b>	<b>159</b>
7.1 Introduction.....	159
7.2 CRAC power input for different cooling configurations .....	159
7.2.1 CRAC power input for cold-hot aisle arrangement .....	160
7.2.2 CRAC power input of cold aisle and hot aisle containment configurations.....	162
7.2.3 CRAC power input for active and passive backdoor coolers .....	167
7.3 Back door cooler in HPC data centre.....	171
7.3.1 CFD analysis of back door cooler inside a HPC data centre .....	173
7.3.2 Results and discussion .....	174

7.4 Conclusion .....	179
<b>CHAPTER 8: CONCLUSIONS .....</b>	<b>180</b>
8.1 General discussion .....	180
8.2 Future Work .....	185
<b>BIBLIOGRAPHY .....</b>	<b>186</b>
<b>APPENDIX.....</b>	<b>197</b>

## List of Tables

Table 4.1 Electrical specification of studied fan [77].	77
Table 4.2 Mechanical specification of studied fan [77].	77
Table 4.3 Pressure distribution against the velocity for fan [77].	78
Table 4.4 Pressure distribution against the velocity at 15000 RPM for active back door cooler fan.	80
Table 4.5 Velocity for different k- $\epsilon$ models against the pressure drop.	97
Table 4.6 Turbulent intensity specification for both inlet and outlet.	98
Table 4.7 Number of cells vs. the velocity point for 1U server blade.	102
Table 4.8 Comparison between experimental and CFD (RNG k- $\epsilon$ model) with respect to the temperature difference across the server.	104
Table 4.9 Velocity profile for HP blade server with respect to the pressure drop across the server.	109
Table 4.10 Permeability values for CPU, 1U server, and HP server blade.	112
Table 5.1 Boundary conditions used in Fluent.	120
Table 5.2 Number of cells vs. the maximum temperature for the rack of 32 server blades.	122
Table 6.1 Number of cells vs. the maximum temperature for the traditional data centre.	139
Table 7.1 CRAC power input values for different supply temperatures in cold aisle containment technique at COP =3.5.	163

Table 7.2 CRAC power input values for different supply temperatures in hot aisle containment technique at COP=3.5. ....	163
Table 7.3 Power input values for different supply temperatures in passive back door cooler at COP =3.5. ....	168
Table 7.4 Power input values for different supply temperatures in active back door cooler at COP =3.5. ....	168
Table 7.5 CFD analysis for rack intake temperatures for both active and passive back door cooler for different rack heat consumption (kW). ....	176
Table 7.6 CFD analysis for rack exhaust temperatures for both active and passive back door cooler for different rack heat consumption (kW). ....	177
Table 7.7 Heat load calculations for the CRAC unit and a back door cooler for a data centre with four racks at 25 kW each. ....	178

## List of Figures

Figure 1.1 Schematic of the data centre energy system.....	3
Figure 1.2 Heat load trend in data centres [5].....	4
Figure 2.1 The cold-hot aisle arrangement [11].....	7
Figure 2.2 Typical raised-floor data centre configuration [15].....	8
Figure 2.3 The main components of a typical data centre [14].....	9
Figure 2.4 ASHRAE-recommended environmental conditions for data centres [17].....	10
Figure 2.5 Partitions' location that covers the cold aisles in the data centre [25].....	16
Figure 2.6 The cold aisle containment technique [31].....	18
Figure 2.7 In-row cooling with hot aisle containment technique [31].....	18
Figure 2.8 The ducted exhaust cabinet technique [32] . ....	20
Figure 2.9 Breakdown for the power inside a typical data centre [33].....	21
Figure 2.10 Comparison between a 1U rack and a blade rack [34].....	23
Figure 2.11 Six types of air distribution systems [11].....	25
Figure 2.12 Effect of installation of blanking panel on server air inlet temperature [35].....	27
Figure 2.13 Five alternative cooling systems for data centre [6].....	33
Figure 2.14 Air side economizer system [40]. ....	34
Figure 2.15 Data Cool system in cold-hot aisle arrangement [41]. ....	36

Figure 2.16 Overhead cooling system in a data centre [43].....	38
Figure 2.17 Ice cube cooling technique [44].....	39
Figure 2.18 Rack backdoor cooler. ....	40
Figure 2.19 Supercomputers countries share [52].....	42
Figure 2.20 Direct expansion CRAC unit type [56]. ....	46
Figure 2.21 Cooling loop for the data centre with chiller system[58] .....	46
Figure 2.22 COP vs. CRAC supply temperature from the HP experiment [51].....	50
Figure 3.1 Scope of the thesis work. ....	54
Figure 4.1 Flow analysis in server, rack and room of the data centre.....	56
Figure 4.2 The flow modes over the smooth airfoil [68].....	64
Figure 4.3 Pressure-based method to solve governing equations [69]. ....	67
Figure 4.4 Schematic of the fluid flow across the porous block [55]. ....	74
Figure 4.5 Location of the fan on the traditional server [32]. ....	76
Figure 4.6 Fan drawing [77].....	78
Figure 4.7 Polynomial fitting of fan curve.....	79
Figure 4.8 Fitting curve of the pressure difference with respect to the fan velocity at 15000RPM for active back door cooler fan. ....	80
Figure 4.9 Thunder K8S Pro S882 server mother board [78].....	82
Figure 4.10 Hp G7 server blade [79]. ....	83
Figure 4.11 Actual and approximated CPU geometries.....	85
Figure 4.12 Diagram for the flow-through channel .....	86

Figure 4.13 Comparison between the actual analysis and approximation analysis of the CPU.....	89
Figure 4.14 Temperature, pressure and velocity gradient for both actual and approximation CPUs in the longitudinal direction (Z) of the CPU. ....	90
Figure 4.15 The block diagram of the server’s internal parts. ....	92
Figure 4.16 Experimental set-up geometry for the 1U server.....	92
Figure 4.17 The boundary condition used in the CFD analysis of a 1U server rack.....	95
Figure 4.18 Velocity versus the pressure drop for different turbulence intensities. ....	99
Figure 4.19 The comparison between k-ε models and the experimental data for the server. ....	101
Figure 4.20 Mesh independence study for 1U server blade.....	103
Figure 4.21 Comparison between experimental measurements and CFD analysis with respect to the temperature difference across the server. ....	104
Figure 4.22 Power consumption for both blade and rack servers with two processors [88]. ....	106
Figure 4.23 HP blade server geometry with attached tunnel [77].....	107
Figure 4.24 Boundary condition used in the CFD analysis of an HP blade server.....	108
Figure 4.25 Velocity profile vs. pressure drop in a HP blade server. ....	110
Figure 5.1 IT rack inside the data centre [89]. ....	114
Figure 5.2 Plan view of air flow through racks in a data centre. ....	115

Figure 5.3 Rack configuration.....	117
Figure 5.4 Five porous blocks approximation. ....	118
Figure 5.5 Boundary conditions for tested rack inside a data centre. ....	119
Figure 5.6 Temperature distribution in a rack inside the data centre.....	121
Figure 5.7 Mesh independence study for the 32 server rack.....	122
Figure 5.8 Temperature distribution along both rack inlet and rack exhaust.....	123
Figure 5.9 Velocity field (m/s) for a 32-server rack inside a data centre.....	124
Figure 5.10 Comparison between inlet and outlet temperature distributions for the 32-server rack and 16 porous blocks.....	126
Figure 5.11 Comparison between inlet and outlet temperature distributions for the 32-server rack and 8 porous blocks.....	127
Figure 5.12 Comparison between inlet and outlet temperature distributions for the 32-server rack and 4 porous blocks.....	128
Figure 5.13 Comparison between inlet and outlet temperature distributions for the 32-server rack and 2 porous blocks.....	129
Figure 5.14 Comparison between inlet and outlet temperature distributions for the 32-server rack and 1 porous block. ....	130
Figure 5.15 Temperature fields for the 16 and 8 porous blocks configurations. ....	132
Figure 5.16 Temperature fields for the 4 and 2 porous blocks configurations. ....	133
Figure 5.17 Temperature fields for 1 porous block configuration.....	134
Figure 5.18 Velocity fields (m/s) through 16 and 8 porous blocks configurations. ....	135



Figure 6.1 Top view for the tested data centre with a cold-hot aisle arrangement.....	138
Figure 6.2 Mesh independence study for the traditional data centre. ....	140
Figure 6.3 Cold aisle containment in the data centre.....	141
Figure 6.4 Hot aisle containment in the data centre.....	142
Figure 6.5 Schematic of the active back door cooler.....	143
Figure 6.6 Schematic of passive back door cooler.....	144
Figure 6.7 The boundary conditions and governing equations that are used to solve back door coolers.....	145
Figure 6.8 The experimental data for air side convective heat transfer coefficient for different speed values.....	146
Figure 6.9 Temperature fields for the cold-hot aisle arrangement.....	148
Figure 6.10 Cold and Hot aisle containment techniques [29].....	149
Figure 6.11 CFD analysis for both hot and cold aisle containments with respect to temperature distribution.....	150
Figure 6.12 Comparison between the cold aisle containment technique, the hot aisle containment technique and the traditional data centre with respect to rack inlet temperature. ....	152
Figure 6.13 Comparison between the cold aisle containment technique, the hot aisle containment technique and the traditional data centre with respect to rack exhaust temperature. ....	153
Figure 6.14 Rack inlet and exhaust temperatures for both active and passive back door coolers. ....	155

Figure 6.15 Temperature field inside the data centre for the back door cooler technique. ....	156
Figure 6.16 Temperature profile for cold aisle containment, hot aisle containment, active back door cooler, and passive back door cooler. ....	157
Figure 7.1 Relationship between CRAC power input and supply temperature for both cold and hot aisle containments at COP=3.5. ....	164
Figure 7.2 CRAC power input vs. room temperature for both hot and cold aisle containments at COP=3.5. ....	166
Figure 7.3 Relationship between CRAC power input and supply temperature for both passive and active back door coolers at COP=3.5. ....	169
Figure 7.4 Total cooling power input of DX CRAC and chiller units vs. CRAC supply temperature four cooling configurations at COP=3.5. ....	170

## Nomenclature

A	Area ( $\text{m}^2$ )
$C_p$	Specific heat constant at constant pressure ( $\text{kJ/kg.K}$ )
$D_h$	Hydraulic diameter (m)
H	Head losses across the rack (m)
$\kappa$	Kinetic energy ( $\text{m}^2/\text{s}^2$ )
P	Power (kW)
PD	Power density ( $\text{kW/m}^2$ )
Pe	Peclet number
Pr	Prandtl number
R	Radius (m)
Re	Reynolds number
S	Source term for the momentum equation ( $\text{kPa/m}$ )
T	Temperature ( $^{\circ}\text{C}$ )
$\underline{U}$	Velocity vector
(u,v,w)	Velocities in x, y and z directions, respectively.
(x,y,z)	Cartesian Coordinates
$W_{in}$	Compressor work of DX CRAC unit (kW)

***Greek Symbols***

$\rho$	Density (kg/m <sup>3</sup> )
$\alpha$	Permeability (m <sup>2</sup> )
$\nu$	Kinematic viscosity (m <sup>2</sup> /s)
$\mu$	Dynamic viscosity (N.s/m <sup>2</sup> )
$\gamma$	Specific weight (N/m <sup>3</sup> )
$\mu_t$	Eddy viscosity (N.s/m <sup>2</sup> )
$\vartheta$	Velocity scale for the turbulent model (m/s)
$\ell$	Length scale for the turbulent model (m)
$\varepsilon$	Dissipation (m <sup>2</sup> /s <sup>3</sup> )

***Superscripts***

*	Non-Dimensional quantities
---	----------------------------

***Subscripts***

Equip	Equipment
H	Outside environment
HI	High range
i	Inlet
Lo	Low temperature range
o	Outlet
R,Carnot	Refrigeration Carnot cycle

Return	Return air to the cooling unit
s	Surface
Supply	Supply air to the data centre
tot	Total
(u,v,w)	The components of velocity in x, y, and z directions, respectively

***Acronyms***

ADS	Air Distribution Systems
ADU	Air Distribution Unit
CFD	Computational Fluid Dynamics
CI	Cooling Index
CLF	Cooling Load Factor
COP	Coefficient of Performance
CRAC	Computer Room Air Conditioning
DCE	Data Centre Efficiency
DCIE	Data Centre Infrastructure Efficiency
DCP	Data Centre Productivity
IT	Information Technology
O-CS/CR	Overhead distribution – CRAC flooded supply/CRAC flooded Return
O-CS/FR	Overhead distribution – CRAC flooded supply/Fully ducted Return
O-CS/LR	Overhead distribution – CRAC flooded supply/Locally ducted Return

O-LS/CR Return	Overhead distribution – Locally ducted Supply/CRAC flooded
O-LS/FR	Overhead distribution – Locally ducted Supply/Fully ducted Return
O-LS/LR Return	Overhead distribution – Locally ducted Supply/Locally ducted
PDUS	Power Distribution Unit Supply
PLF	Power Load Factor
PUE	Power Usage Effectiveness
RCI	Rack Cooling Index
RTI	Return Temperature Index
SHI	Supply Heat Index
U-FS/CR	Underfloor distribution – Fully ducted supply/ CRAC flooded Return
U-FS/FR	Underfloor distribution – Fully ducted supply/ Fully ducted Return
U-FS/LR	Underfloor distribution – Fully ducted supply/ Locally ducted Return
U-LS/CR Return	Underfloor distribution – Locally ducted supply/ CRAC flooded
U-LS/FR	Underfloor distribution – Locally ducted supply/ Fully ducted Return
U-LS/LR Return	Underfloor distribution – Locally ducted supply/Locally ducted
UPS	Uninterruptible Power Supply

## CHAPTER 1: INTRODUCTION

### 1.1 General overview

With the technological advancements in recent times and a mammoth leap in communication technology over the last couple of decades, our reliance on computing has increased sharply and will continue to do so for the foreseeable future. As we rely more and more on computing power for things as crucial as business continuity and operations, we need dedicated facilities to house these computer systems and associated components, such as telecommunication and storage systems; these dedicated facilities are called Data Centres [1],[2] and [3].

According to a report from the ‘Renewable Energy Policy Project on Energy Smart Data Centres’, Data Centres are:

*“... an essential component of the infrastructure supporting the Internet and the digital commerce and electronic communication sector. Continued growth of these sectors requires a reliable infrastructure because ... interruptions in digital services can have significant economic consequences.”[4].*

The main purpose of a data centre is running the applications that handle the core business and operational data of an organization. This can occupy one room of a building, one or more floors, or even an entire building.

A data centre may house several file servers, processors, and other computer equipment along with standby power supply. These servers are kept inside cabinets called racks. The racks are placed close to each other, front to front and back to back, in rows, forming corridors called aisles. These aisles not only provide the room for accessing the front and rear of each cabinet, but could be of immense use to supply the chilled air, which is the method currently used for cooling of the data centres.

Data centres are now widespread due to the high demand of infrastructure requirements such as networks to operate Internet services [1]. A wide range of telecommunication services such as web searching engines, bank systems and computer communications systems are operated by using data centres. The power used by the data centre operates the server racks that dissipate heat inside the data centre, as shown in Figure 1.1. Heat dissipation from servers increase inside the data centre so the cooling power is expected to rise significantly [5], as shown in Figure 1.2.

The heat dissipation of a modern data centre varies between 1 kW to 3 kW per rack and it is expected that the average heat dissipation per rack will increase up to 15 kW per rack [6]. Some High-performance Computing (HPC) data centres now even have racks with 30 kW or more per rack [6].

The high demand for using the infrastructure systems increases the density of the data centre beyond what was expected at the design stage whilst building the data centre, which means that the data centre cooling loads increases due to increased IT heat load. For this reason, the air management system inside the data centre is critical in order to cool the racks inside it. Moreover the integration of both mechanical and computer



sciences with electrical engineering is also very important to maintain the good condition of the server racks inside the data centre.

Mechanical engineering science considers the thermal flow aspects, such as the temperature and air flow, inside the data centre. Hence, the mechanical engineer focuses on how to meet the cooling target of the data centre by optimizing the design parameters of its geometry and operating conditions. In most cases the cooling of a data centre is over-specified because the servers are running below capacity and the air conditioning is keeping the data centre cooler than is required [5] . The main reason for hot spots inside the data centre is due to the air recirculation phenomena [6],[7] and[8]. Recirculation happens when the exhaust hot air from the racks mixes with the cold air stream at the rack inlet, which leads to the accumulation of hot air at the cold aisle affecting the reliability of the rack servers. Therefore, improving the cooling system either by changing air management systems or by changing the design of the data centre geometry is necessary. The aim of air management systems is to separate the exhaust hot air from the intake cold air to prevent air recirculation, which means that the hot air migrates from the hot aisle to mix with cold air in the cold aisle; this is the focus of this research. Whereas, the controlling of the data centre geometry is implemented to meet the same aim.

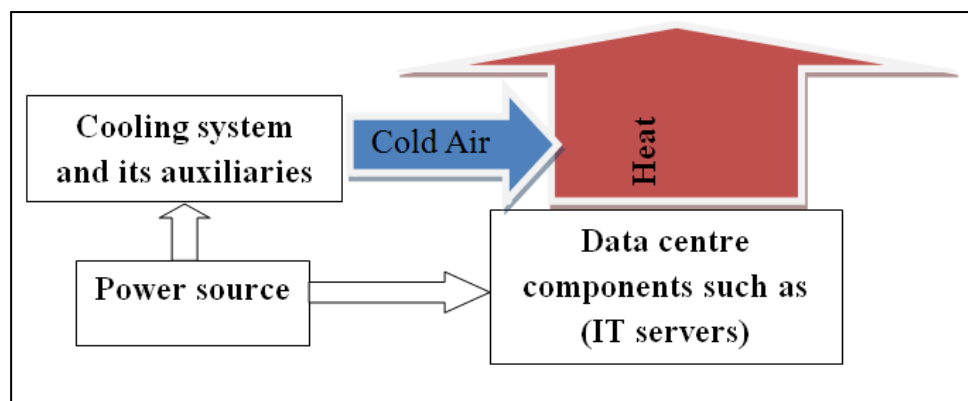


Figure 1.1 Schematic of the data centre energy system.

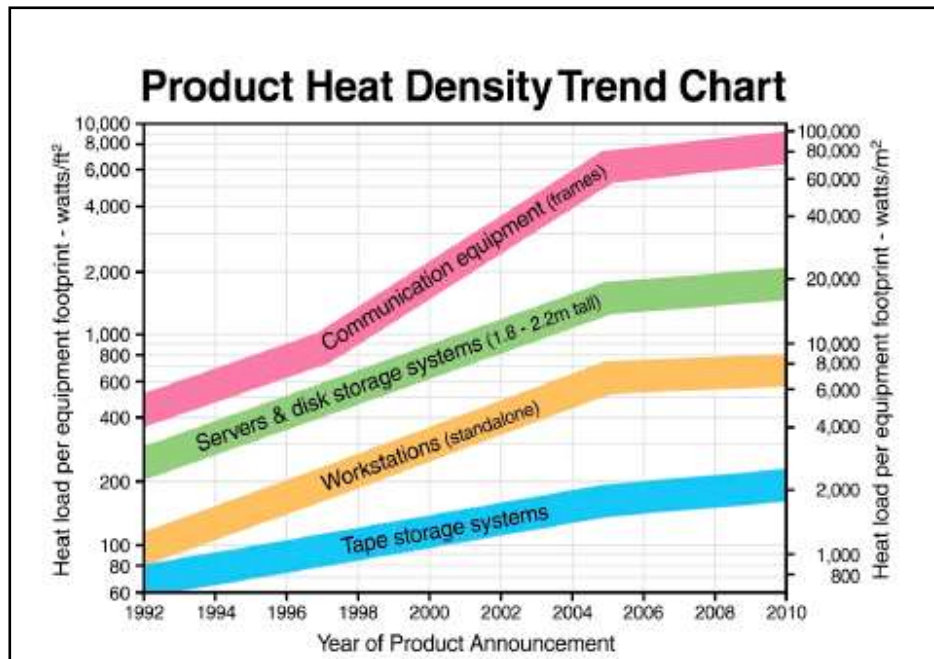


Figure 1.2 Heat load trend in data centres [5]

## 1.2 Thesis Plan

In this thesis the air management inside the data centre will be discussed in detail with respect to the design criteria and the energy load as will be shown in the following chapters. The thesis sequence will be described as the following:

1. Chapter 2 : which contain the literature review for the current work.
2. Chapter 3: which describes the scope of the current work.
3. Chapter 4: which describes the Computational Fluid Dynamics (CFD) modelling methodology for the server and its internal components.
4. Chapter 5: which describes the CFD modelling of the rack level.
5. Chapter 6: which describes the different cooling configurations inside the data centre.

6. Chapter 7 : which determines the energy loads calculations for Direct expansion CRAC unit for different cooling configurations.
7. Chapter 8: which shows both conclusions and future wok.

## **CHAPTER 2: LITERATURE REVIEW**

### **2.1 Introduction**

This chapter deals with literature review about the cooling of data centre. In this chapter several studies have been addressed to describe the data centre several areas such as the configuration of data centre layout, the power supplied to the data centre, the environmental condition inside the data centre, the cooling configuration that can be applied inside the data centre, and the thermal analysis inside the data centre.

The IT density within data centres increases extremely rapidly with time, thus the efficiency of the cooling process to keep the data centre in good condition is an important criteria [9]. The power required to operate the data centre is approximately 40 times more than that required in operating a standard office building [10] and [11]. The rate of heat load that is produced by the data centre increases as the server loads increase in density. Therefore, the energy required to maintain the data centre at the correct temperature and humidity increases along with increasing the heat load inside the data centre. The power that is used to operate the data centre IT equipment and electronics varies; on average, it is about 30% to 40% of the total power required to operate the data centre. The remainder of this power is used for the purpose of cooling [11],[12] and[13].

### **2.2 Data centre overview**

The cold-hot aisle arrangement is a popular arrangement that is used in most data centres to minimize the recirculation problem. The supply air and the exhaust air of the units are divided into zones. Figure 2.1 shows the arrangement of the rack

servers in the data centre. There are two aisles, which are cold aisles and hot aisles. The cold aisles contain the floor tiles or vents that supply the air at the front of each server rack. The cold aisles separate the rack rows at the front (intakes); whereas, the hot aisles separate the rack server rows at the back (outlet). So the rows of racks are positioned so that they are facing each other at the front in the cold aisle [11] and [14].

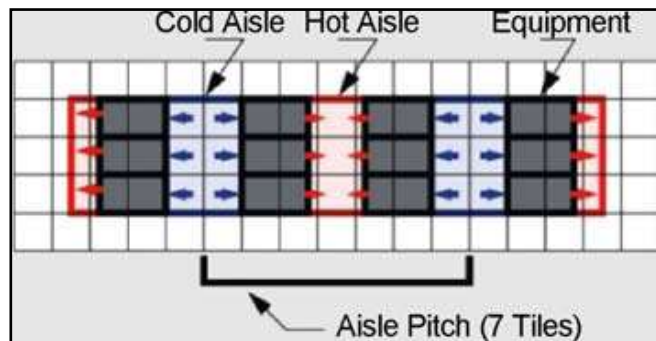


Figure 2.1 The cold-hot aisle arrangement [11].

In the raised floor data centre situation, the cool air is supplied by the computer room air conditioning (CRAC) units to the plenum, as shown in Figure 2.2. It then flows through the tiles that face the rack at the front, passing through the servers and exiting at a higher temperature through the rear of the rack. The hot air flows back to the CRAC units to cool them down and supply it again to the rack servers. The CRAC contains fans and cooling coils. The cooling process takes place in the cooling coil. It acts as a heat exchanger between the cooling agent in the cooling coil and the hot air pushed by the fans. The heated cooling agent is sent to the cooling tower to cool it down and then recirculated to the cooling coil in the CRAC units. The CRAC supplies the air at 16-20°C but it reaches the rack at 18-20°C due to the

recirculation action within the data centre and gaining heat on its way to the servers [14]. The air temperature exits the rear of the server racks around 27°C [11].

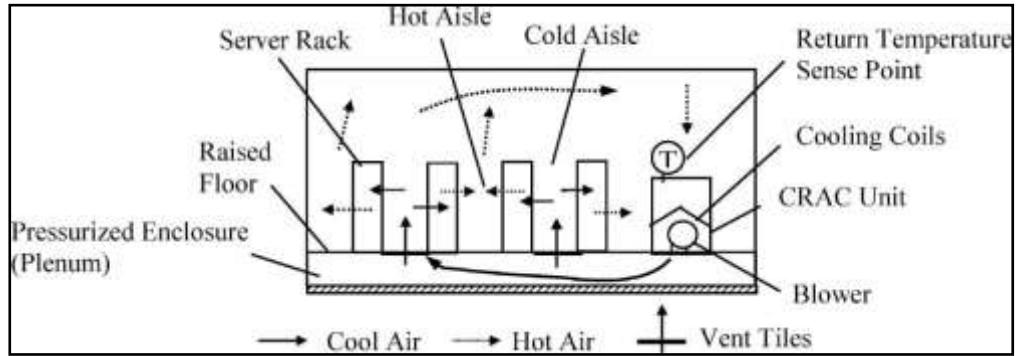


Figure 2.2 Typical raised-floor data centre configuration [15].

### 2.3 Data centre power system layout

Figure 2.3 shows the main components in most data centres. The power is supplied from outside the data centre by transformers located in the utility substation. The voltage is reduced by switchgear and the power then passes the UPS system. A second feed is usually supplied from diesel generators to the UPS system to act as a back-up when power fails [14].

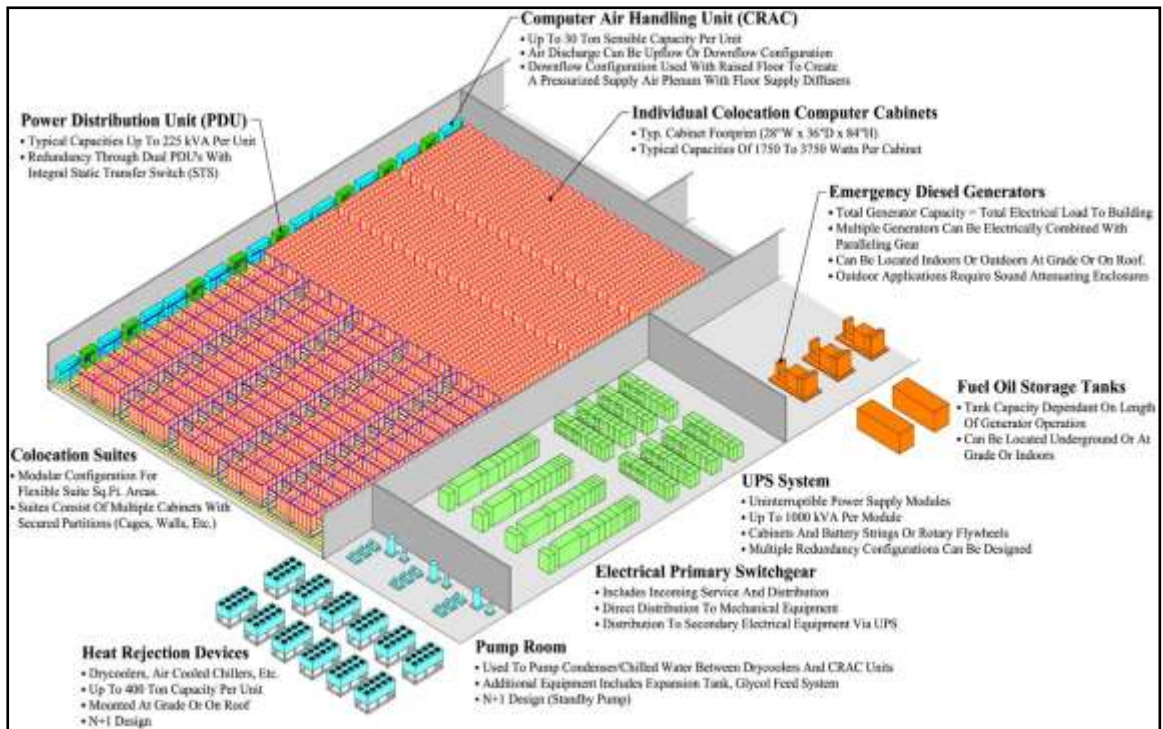


Figure 2.3 The main components of a typical data centre [14].

Electrical power is provided to the system and utilized in the computer equipment, CRAC units, the office, the uninterruptible power supply (UPS), and lighting, as well as the chiller system, e.g., the compressors. The power density (PD) of the data centre is expressed as power supply divided by area.

$$PD = \frac{P_{tot}}{A} \quad (2.1)$$

Total electricity supply ( $P_{tot}$ ) and its include the power rate of the equipment, the office, UPS, lighting, CRAC units and electricity demand in the chiller system, e.g., the compressors. Area (A) could be expressed as the area occupied by rack, the so-called “footprint”, the total area of the computer room or the total area of the whole data centre facility [4].

## 2.4 Environmental requirements

To achieve good operating conditions inside the data centre, suitable temperatures and humidity should be taken into account during the design stage. According to the ASHRAE TC 9.9 standards, the appropriate inlet temperature should be between 15°C and 25°C and the humidity should be between 40% and 60%. Data centre design that gives poor temperature or humidity control could damage the equipment in the data centre [11] and [16]. The recommended zone for operating the data centre is specified by using a Psychrometric chart, as shown in Figure 2.4. The recommended envelope, as shown in Figure 2.4, demonstrate the recommended temperatures and the humidity limits that can be applied in a data centre. However, A1 envelope, A2 envelope, A3 envelope and A4 envelope are the allowable envelopes for the specific range of the server blades with controlling of dew point temperature inside the data centre [17].

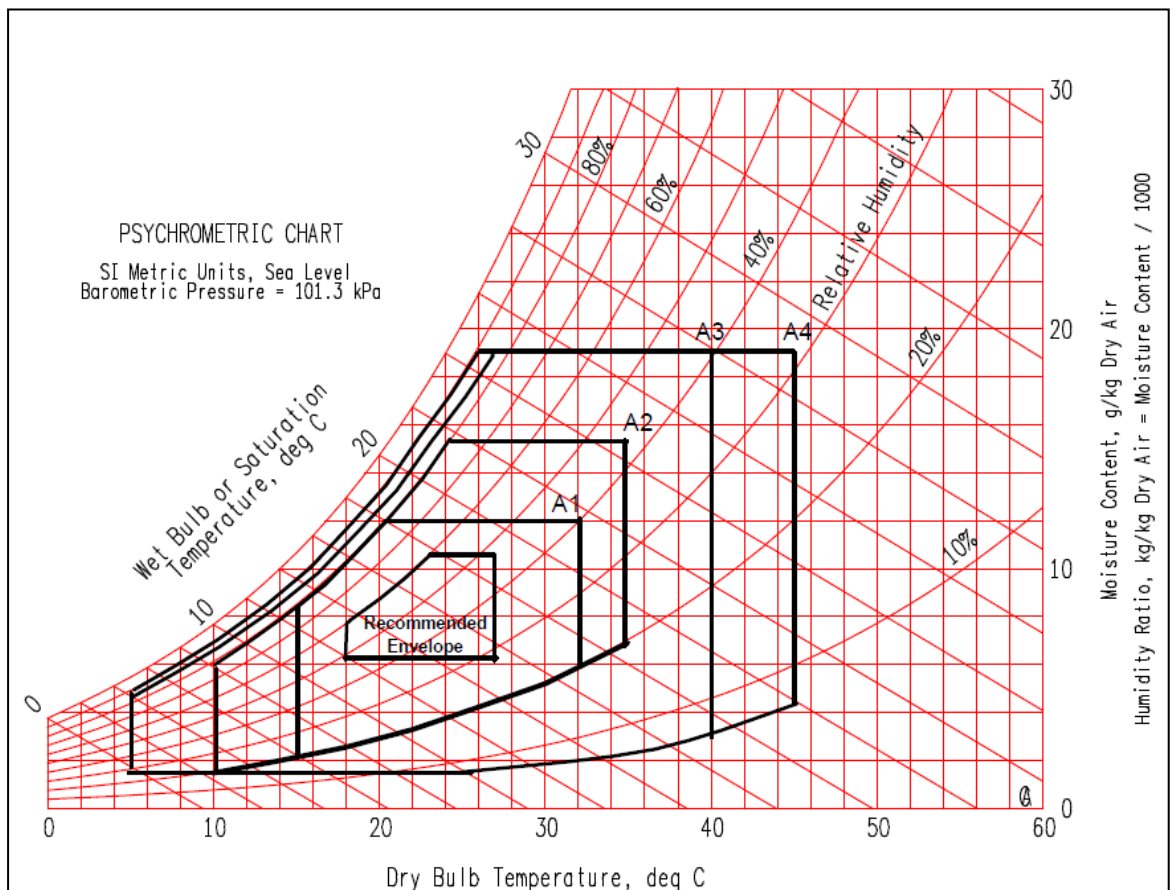


Figure 2.4 ASHRAE-recommended environmental conditions for data centres [17].



## 2.5 Data centre efficiency

With regards to the data centre efficiency, there is a term in common use called power usage effectiveness (PUE), which is the amount of total power divided by the amount of power used to power the computer infrastructure. The best efficiency of the data centre can be achieved as the PUE value reduces to reach 1 [18]. Most data centres have an operational PUE value between 1.2 and 3, where the PUE of 1.2 is a very efficient data centre. On the other hand, the data centre with 3 is considered to be a very inefficient data centre [19]. The data centre efficiency (DCE) is defined as the inverse of the PUE value multiplied by 100, and its value varies between 0 to 100%.

The PUE and DCE were proposed by Haywood et al.[19], and Green Grid [12] to estimate the energy efficiency of their data centres and compare it with others. The PUE varies between 1 to infinity [20], but for proper design, the PUE value of 1.2 can be achieved [20]. The data centre productivity (DCP) is a new factor and has been defined by Green Grid [20]. DCP is defined as the useful work divided by the total facility power. The Green Grid expressed the PUE, as follows

$$PUE = 1 + \text{Cooling Load Factor (CLF)} + \text{Power Load Factor (PLF)} \quad (2.2)$$

Where,

1 represents the normalization of the IT load.

$$CLF = \frac{\text{Total Power Consumed by the cooling system and its Auxiliaries}}{\text{IT load}} \quad (2.3)$$

$$PLF = \frac{\text{Total Power Consumed by switch gear, UPS and power distribution unit}}{\text{IT load}} \quad (2.4)$$

The calculation of the PUE is not straightforward because it is difficult to calculate the exact amount of both total power and IT equipment power. Furthermore, there is no exact point to measure either total power or IT power. This difficulty was solved by Avelar [21] by defining a standard method to calculate PUE. Four main reasons that make the calculation of PUE difficult are listed, as follows:

- a) The way to calculate the power used by devices in a data centre is not clear.
- b) Sometimes some systems used by data centres are outside the data centre.
- c) Some systems can be classified as both data centre and non data centre equipment.
- d) The difficulty in specifying the proper location to take the power measurements.

A three-part methodology has been developed by Avelar [21] to overcome most problems that face the calculation of PUE. This method states the following;

- The description of the types of subsystem used in data centre: whether it is IT load, infrastructure or not-included load.
- The approximate assumption can be used, either if subsystems are joined with other non-data centre loads or the measurement load of the subsystem is difficult due to technical problems.
- The estimation of power consumed by the subsystem, such as Power Distribution Unit (PDU), can be done when there is a difficulty

performing the measurement, such as the existence of obstruction barriers.

## **2.6 Layout and cooling**

Data centre energy efficiency can be enhanced in several ways, such as improving the cooling system, improving the rack layout, using the concept of a green data centre ( data centre in which the mechanical, lighting, electrical and computer systems are designed for maximum energy efficiency and minimum environmental impact) and improving the data centre power system by decreasing the power required to cool data centre by using some cooling techniques such as air side economizer.

Efficiency losses in the data centre are due to overloaded cooling system and its auxiliaries by using a lot of power to cool down the data centre with wrong rack layout, so careful design of the data centre and the best operation might help to improve the data centre efficiency [14].

The reduction of electricity consumption of data centres is a very important issue because as the power goes to high demand, then the cost increases and the environment will be impacted [22]. Energy saving procedures were discussed by the CERN open lab. Electricity is used to operate both IT equipment and the cooling systems of data centres, and CERN found that saving energy was better than improving the cooling efficiency with respect to the return on investment. To focus on the reduction of energy consumption by changing the type of the processor of servers to an updated one will reduce the energy consumption and increase the useful life of the data centre while reducing costs.

Rasmussen [23] discussed common mistakes that could occur during the design and operation of data centres. There are several issues that might reduce the cooling efficiency by 20% or more. The most important parameters that affect the cooling performance of data centres can be summarized, as follows:

- Rack air flow.
- Rack layout.
- Layout of delivered and returned air of data centre.
- Cooling setting
- Distribution of load.

The air flow problems appear either as mixing of hot and cold air before the CRAC intake or if air flow is blocked by obstructions. The blanking panel which is a panel that is use inside rake to fill the gaps between server blades and it could be used to improve the cooling performance in the rack by avoiding the mixing of hot and cold air streams. The cooling setting (such as changing the supply temperature and air flow rate) is another critical parameter that has a direct effect on the cooling performance of data centres. So, as the supply temperature of the CRAC unit increases within an acceptable range (20°C-25°C) as the cooling performance of the CRAC unit increases, and vice versa.

### **2.6.1 Data centre layout**

The servers with high demand should be distributed and deployed so as to eliminate recirculation and hot spot problems without adding new CRAC units or changing the inlet temperature. The layout of delivered and returned air is very important in terms of the cooling performance. The correct layout leads to minimised hot spots and to reduce recirculation, as well. Therefore, the cooling efficiency will be improved. Also the data centre layout can be improved by

changing the geometry inside the data centre, such as moving the vents closer to the intake of the racks in the cold aisle to provide the rack with sufficient cooling requirements.

The effect of the floor plan on the number of racks, IT power densities, power and cooling and electricity consumption was analyzed by Rasmussen and Torell [24], who also introduced a method for designing the floor layout of a data centre. The number of racks in a data centre can be estimated by dividing the room area by  $2.6 \text{ m}^2/\text{rack}$ . The basic principle layout involves many parameters that should be taken into account, such as controlling the air flow using hot-cold aisles, controlling the tiles' location, reducing the isolated IT devices and predesigning for the equipment layout. Additionally, the structure layout plays a significant role in power and cooling performance by locating the windows and walls in a data centre.

Radmehr et al. [25] said that using CFD to determine the temperature and air flow within the data centre is the best way to optimise the cooling system. Optimisation of the cooling system of the data centre can be achieved by changing the rack layout and cooling settings. In terms of rack layout, the cooling performance can be improved by using the partitions at the end of cold aisles to reduce the recirculation phenomena, as shown in Figure 2.5.

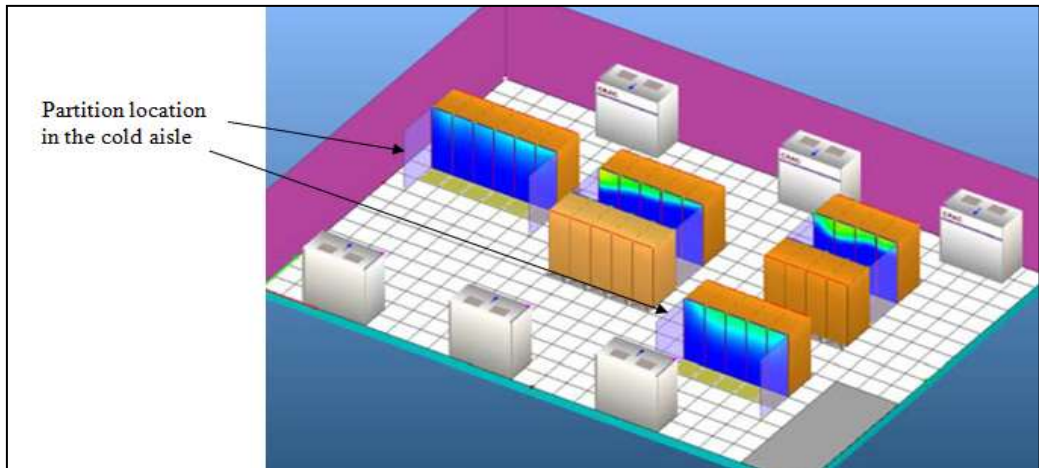


**Figure 2.5 Partitions' location that covers the cold aisles in the data centre [25].**

The cooling and design principles have been discussed by Intel information technology [26] in order to cool a high-performance data centre (HPC). The affecting factors on the cooling system have been tested by studying four data centre layouts. There are several factors that have a significant effect on the data centre, such as using a return ducted type, using barriers on the top and bottom of the racks, changing the location of the cables to under the floor in the hot aisles, and placing racks such that they are parallel to the air flow from the CRAC units. The results show that the combination of these factors leads to huge improvements in cooling efficiency by raising the supply temperature to 21°C instead of 15°C.

Changing the data centre layout corresponding with the capture index (CI) was discussed by Jensen [27]. The capture index (CI) is an index that is calculated via CFD analysis and it is based on the flow rate concept. CI is used to detect the air flow rate streams for both cold and hot aisles at each rack which is an important parameter to define the air flow path inside the data centre. Two CIs are extracted from the main capture index, which are for hot and cold aisles. If  $CI = 100\%$  then the paths of all air flow streams for both cold and hot aisles reach the correct points

(where all the cold air flow to the rack inlet section, and the all the exhaust hot air flow to the CRAC unit) and when  $CI= 0\%$ , the path of all air flow streams for both cold and hot aisles is not optimal.

The best rack layout leads to high values of CI, which means the air stream flow path is optimal to carry out the all heat dissipated from the racks. The results given from the real-time measurements show that a symmetrical layout of racks based on the best cold-hot aisles arrangement leads to the highest possible CI percentage (70%-90%).

Bhopte et al. [28] discussed the strategy to minimize the inlet air temperature to the rack by analysing the room layout, including the depth of plenum and the ceiling height. Also, optimization has been applied to obtain the best design with respect of the inlet air temperature of the racks. The results are as follows:

- Large plenum depth leads to more uniform distribution of cold air.
- Increasing ceiling height leads to an increase in the recirculation phenomenon, thus the inlet air temperature will be increased.

#### **Cold aisle containment and in-row cooling with hot aisle containment.**

The cold aisle and hot aisle containments were presented by Niemann [29]. These two methodologies have been applied in the data centre to manage the air flow inside in order to eliminate the hot/cold air mixing. Also the comparison between these two techniques has been discussed in this study. The concept of cold aisle technique is to apply the physical barriers on the cold aisle to prevent the mixing between the hot and cold streams, as shown in Figure 2.6. The concept of using hot and cold air containments is to obtain a high degree of separation between the hot and the cold air streams [30].

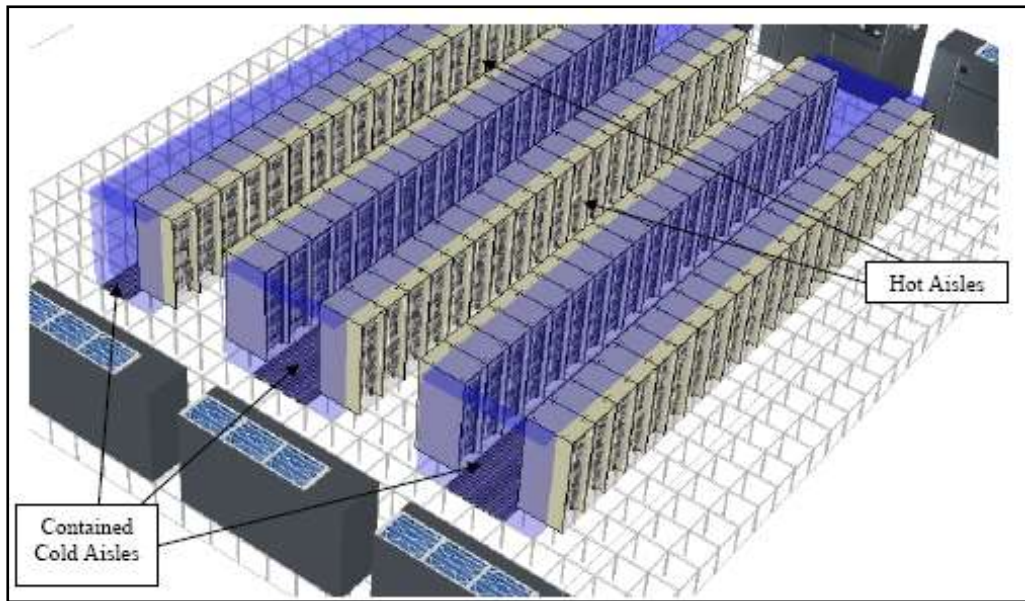


Figure 2.6 The cold aisle containment technique [31].

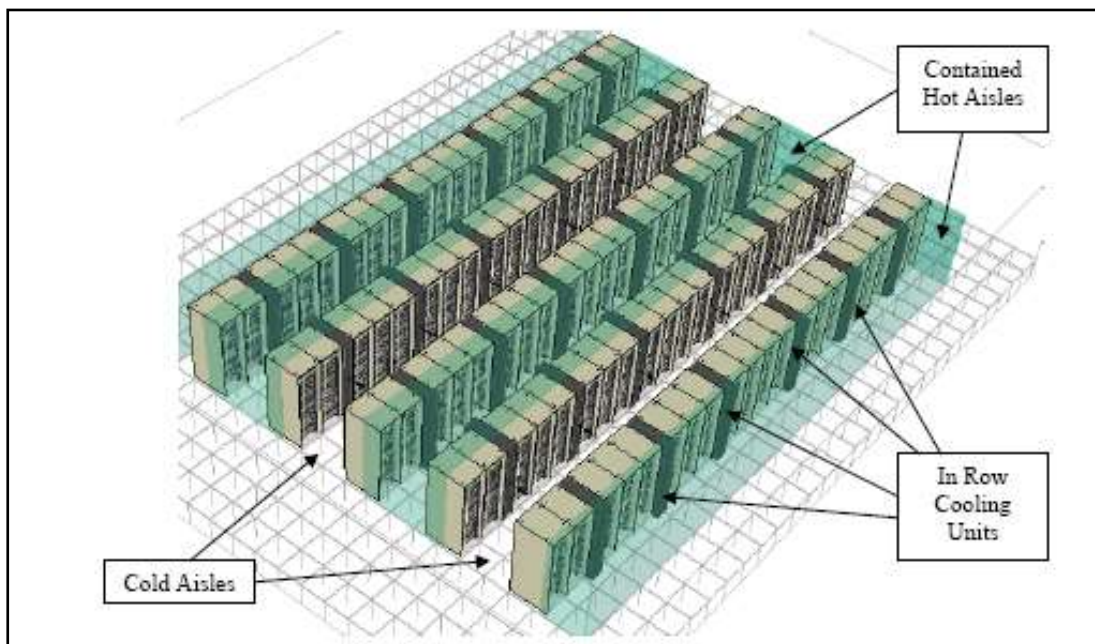


Figure 2.7 In-row cooling with hot aisle containment technique [31].



With respect to the hot aisle containment, the hot aisle is covered with barriers to block the exhausted hot air and send it to the in-row cooling units. The cooling units then cool the air and distribute it again to the cold aisle, as shown in Figure 2.7. Once these techniques are applied, a lot of benefits might be captured to improve the power performance and cooling efficiency; for example, the recirculation phenomena will be dismissed and the supply temperature can be increased within the acceptable operation temperature range (15°C-25°C) because the supply temperature will be equal to the rack inlet temperature (i.e., there is no increasing of temperature due to the hot stream migration) [30]. Thus, energy will be saved and the cooling efficiency will be improved; also, the humidification and dehumidification can be reduced because the hot and cold air streams are separated.

However, the cold aisle containment technique has some drawbacks, such as all cold aisles should be covered to improve the cooling efficiency. This means if there are any racks missing in the row, a blank panel should be filled to connect the row [30]. Another issue is that the room temperature will increase due to the separation of the cold and hot aisles. So, these drawbacks will affect the operating condition but this technique is still better than the traditional one. These drawbacks could be overcome by using in-row cooling with hot aisle containment.

### **Cabinet ducted to hot air plenum**

Chatsworth Products, Inc. [32] invented a new approach to manage the exhaust air flow within the cold-hot aisle data centre by taking it directly to the cooling source without any mixing with cold air streams. This method is called the ducted exhaust cabinet. The ducts are attached at the top rear of the rack cabinets to suck all hot air and send it through the top plenum to the cooling source (CRAC), as shown in Figure 2.8.

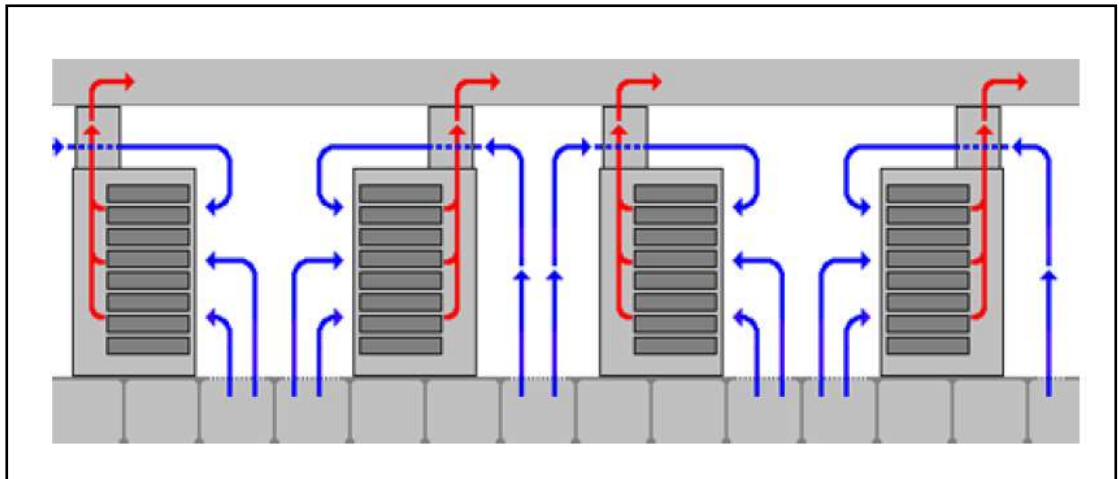


**Figure 2.8 The ducted exhaust cabinet technique [32] .**

There are several benefits that are claimed by Chatsworth Products in using this technique, such as controlling the rack orientation (i.e., no need for front-to-front and back-to-back arrangements) and also the ability to use all exposed floor as the supply for the cold air, which means that all servers will take enough flow rate to improve their cooling efficiency. Furthermore, the supply air from the raised floor is not the only technique to supply the air; other supply techniques can be implemented in a high density data centre. In addition, the above ducted system is adequate for up to 30 kW per rack. So, it offers a good solution for the high density data centre. Thus, this technique can be installed easily without any constraints and it offers a high degree of separation between cold and hot air streams. However, the pressure drop might increase so that additional fan power would be required to overcome this pressure drop [32].

## 2.6.2 Data centre cooling

### IT load in data centre

The power required for data centres has been increasing due to the introduction of high-performance computer facilities (HPC) [5]. Thus, the need to provide additional cooling will increase strongly. Furthermore, the traditional hot-cold aisle configuration is not sufficient to carry away dissipated heat in a high density data centre due to the increase in rack exhaust temperatures [30]. So, new cooling approaches have been invented to assist the traditional cooling system (hot-cold aisle cooling system).

Recently these methods have been deployed in some data centres to cope with the excessive heat dissipation from the racks. In such, the power consumption trend is increasing.

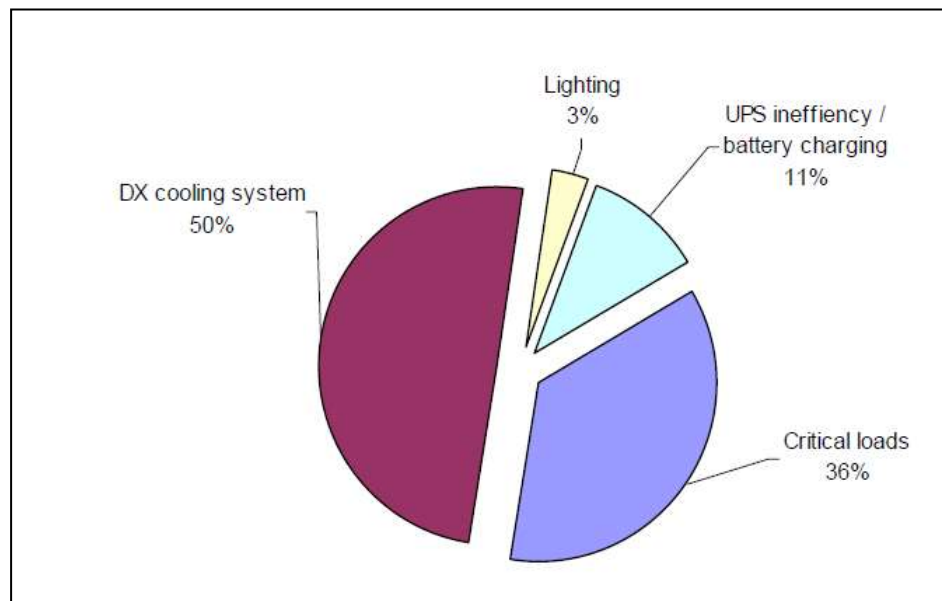


Figure 2.9 Breakdown for the power inside a typical data centre [33].

Some HPC data centres now have racks with 30 kW or more per rack (University of Leeds, as an example). It is shown in Figure 2.9 that the most power goes to the cooling system, whereas the IT load draws 36% of the total input power for the data centre with an area of 465 m<sup>2</sup>, and with rack units of 50 kW [33].

Malone et al. [34] came up with a new rack design that uses blade servers in order to reduce the power consumption associated with groups of fans that have the ability to carry higher back pressure to minimize the air flow bypass (the cold air goes to non desired place which is server exhaust). The concept behind Malone's approach is to reduce the back air flow of the servers, thus decreasing the power consumption of the rack fans. As a result of using blade servers, the air flow can be reduced by up to 25% of the air flow value of traditional 1U rack servers; also, the power consumption can be reduced by up to 48% when using blade servers rather than 1U rack servers, as shown in Figure 2.10. Also, in this analysis, the comparison of using blade and 1U rack servers has been discussed. In such, the recirculation problem can be eliminated by implementing blade servers in cold-hot aisle data centres. Thus, the CRAC air flow can be reduced, leading to a saving in the energy requirements of the CRAC unit. Furthermore, the inlet temperature of 1U servers is 8 K higher than the blades for the same CRAC temperature set-point, due to the recirculation problem. So, as the supply air temperature from the CRAC increases, the coefficient of performance (COP) of the CRAC increases, indicating that the data centre becomes more efficient and consumes less power. As a result of back flow air from the servers, migration of hot air to the cold aisle has less possibility of occurring, so the amount of air flow required in a blade rack data centre is less than

the air flow required in a data centre with 1U rack servers. Thus, the saving of fan power in the CRAC unit has been accomplished.

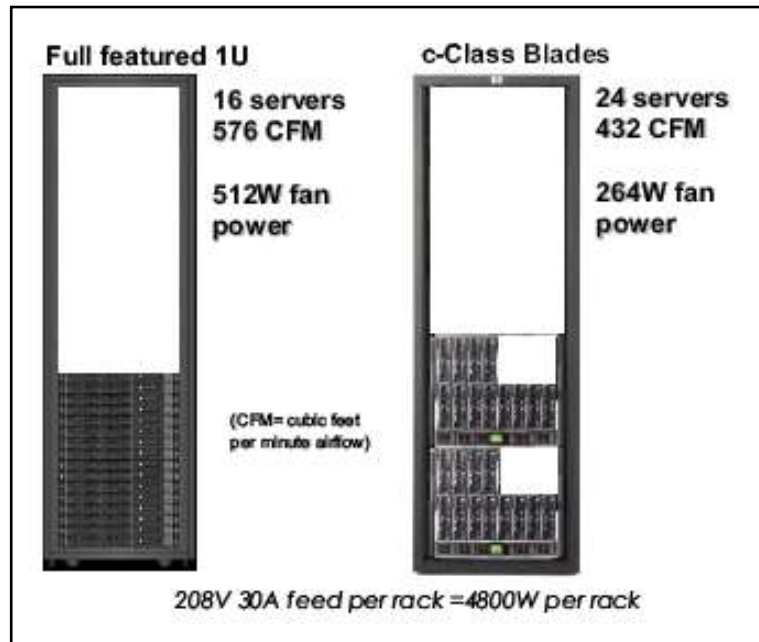


Figure 2.10 Comparison between a 1U rack and a blade rack [34].

### Air distribution systems for a data centre

Six air distribution systems were introduced by Cho et al. [11]. Each of these systems have different return and supply types. Here, six air distribution types have been implemented and evaluated with respect to the temperature and velocity fields. The six distribution systems are as follows:

- Overhead distribution-CRAC flooded supply/fully ducted return (O-CS/CR). In this configuration, the cold air is supplied by CRAC unit to the data centre. Whereas the hot air coming from the rack exhaust is ducted. In this case insufficient chilled air will be provided for the racks that are far away from the CRAC unit. Also, mixing between hot air and cold air will occur.

- Overhead distribution-CRAC flooded supply/locally ducted return (O-CS/LR). In this configuration, the cold air is supplied by CRAC by using over head duct at the rack inlet. Whereas, the hot exhaust air return directly to the CRAC unit.
- Overhead distribution-locally ducted supply/CRAC flooded return (O-LS/CR). It is good to provide the chilled air to the upper server's inside racks, but this does not provide enough chilled air to the bottom server. The recirculation of hot air may be reduced by using an overhead supply.
- Overhead distribution-locally ducted supply/locally ducted return (O-LS/LR). In this case, the supply air from the CRAC unit is introduced to the rack by using duct. Similarly, the hot exhaust air is sucked by the over head duct at the hot aisle. Then Case 4 is the best case among other cases due to its ducted return method to prevent the recirculation of hot air to the cold aisle.
- Underfloor distribution-locally ducted supply/CRAC flooded return ( U-LS/CR). This is the most common configuration that used in data centres. This configuration is beneficial in providing the chilled air to the lower servers' inside rack. However, the mixing between hot and cold air may occur.

- Underfloor distribution-locally ducted supply/locally ducted return (U-LS/LR), as shown in Figure 2.11. As in case 4, this case is used to avoid recirculation by using a return duct.

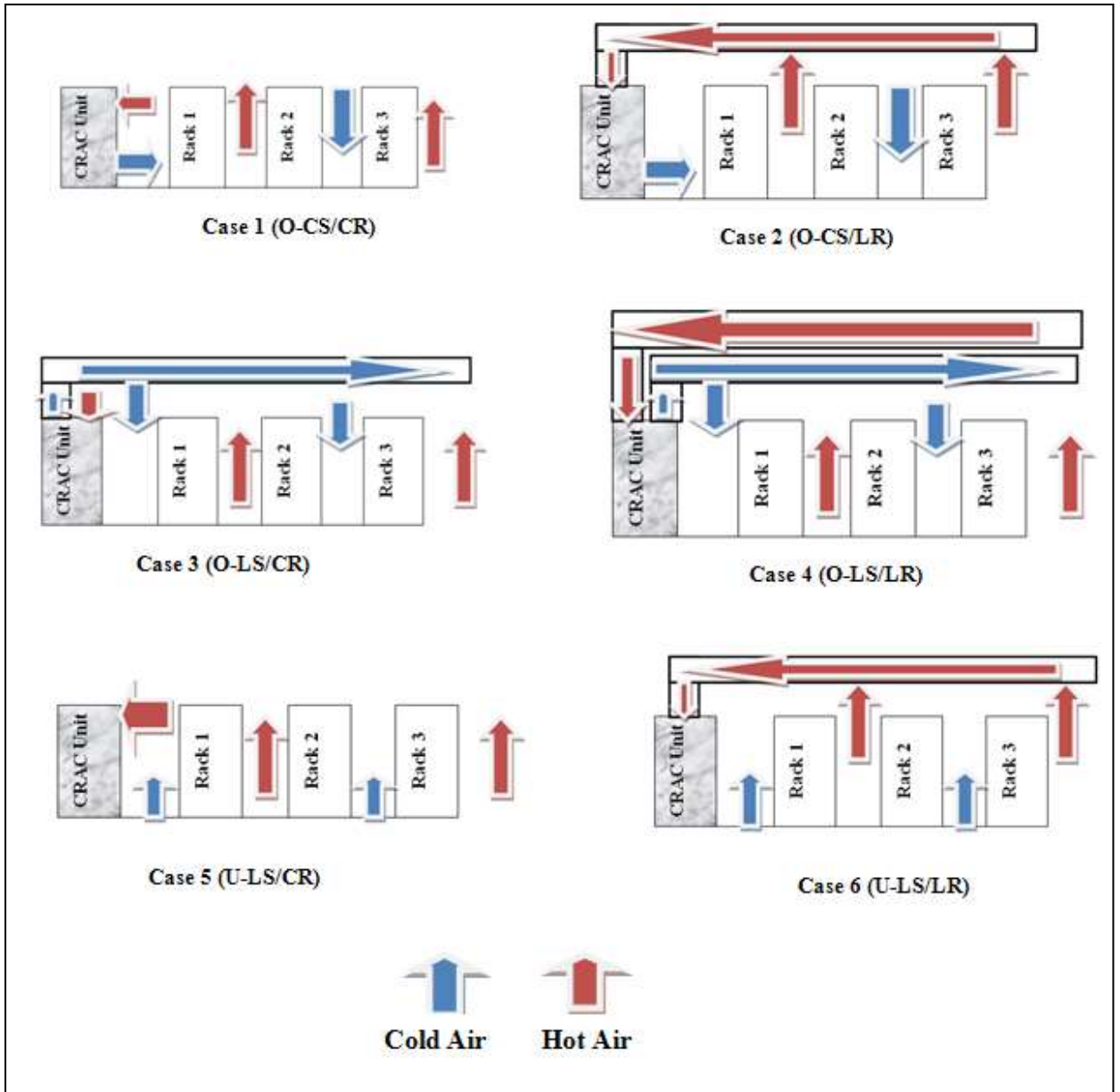


Figure 2.11 Six types of air distribution systems [11].

It is shown from Figure 2.11 that the main difference between the air distribution methods is the way in which they provide the supply air and take out the exhaust air. So, it is shown that the supply air can be provided directly from the CRAC unit, underfloor or overhead by using ducts. Similarly, the exhaust air can be taken out by the CRAC unit, or by using the ducts connected to the CRAC unit. As an example, in case 4, the supply air is introduced to the rack inlet by using overhead supply ducts that are connected with the CRAC unit. Whereas, the exhaust hot air is sucked in also by using the overhead return duct, the return hot air then is cooled down by the CRAC unit, which then supplies it again to the data centre.

It is shown from the results that case 4, which is an O-LS/LR, is a suitable method with respect to air flow and temperature fields inside the data centre; this is because in this case, the recirculation problem is reduced due to using the ducts for both supply and return. Therefore, the hot spots inside the data centre are minimized.

The effect of installation of blanking panels (installed in the unused vertical space in the rack) on the cooling performance was discussed by Rasmussen [35]. Blanking panels are physical barriers used to fill the vertical space between the servers in the rack, as shown in Figure 2.12. The blanking panels are not commonly used because of a lack of knowledge of this technology and also because of the difficulty of installation. Figure 2.12 shows the effect of the blanking panel on the inlet air temperature of the servers. The experiment was carried out to test the effect of blanking panels on the inlet air temperature to the servers in the rack. The inlet air temperature at the servers can be reduced between 2.8°C to 8.3°C by deploying blanking plate technology because the mixing is reduced between cold and hot air.



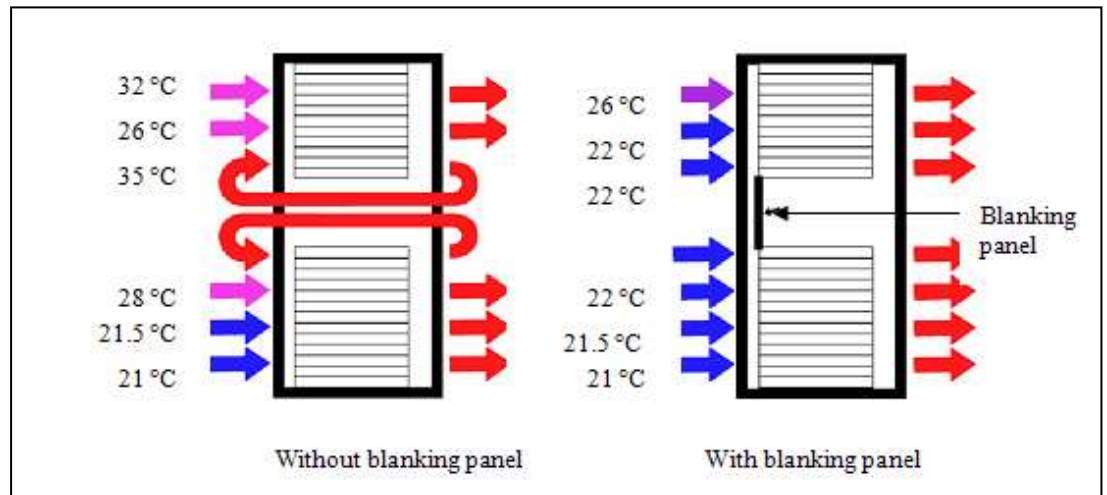


Figure 2.12 Effect of installation of blanking panel on server air inlet temperature [35].

Karki et al. [36] discussed a number of techniques that can be used for controlling airflow distribution. These techniques include changing the plenum height and opening area of the perforated tiles, and installing thin (solid and perforated) partitions in the plenum. A number of case studies, using a mathematical model, are presented to demonstrate the effectiveness of these techniques. Also a computational study of various techniques for controlling the airflow distribution in raised-floor data centres has been presented. The key to controlling the airflow distribution is the ability to influence the pressure distribution (or the flow field) in the plenum. For specified (horizontal) floor dimensions and total flow rate, the pressure distribution is governed by parameters such as the plenum height, the open area of perforated tiles, the distribution of the vents on the floor, the relative positions of CRAC units and perforated tiles, and the presence of underfloor blockages.

The results of this study have been summarized, as following:

- The pressure distribution becomes more uniform as the plenum height is increased. (So the plenum depth must be taken into account in the design

stage, because the changing of plenum depth for the existing data centre is very difficult.)

- The results indicated that the thin partitions offer significant flexibility for controlling the airflow distribution, especially in an existing data centre.

The effect of the air supply flow rate coming from vents in both cold and hot aisles on the inlet air temperature of the racks was analyzed by Schmidt et al.[37]. In addition, CFD models based on Flotherm [37] have been applied to show the temperature distribution along the racks in a data centre. The analysis includes the effect of the CRAC units' location to the inlet air temperature of the racks. The result shows the following:

- As the flow rate of supply air coming through the vents increases, the room temperature of the data centre decreases and vice versa because as the flow rate increases, the heat transfer increases, leading to a decrease in the room temperature.
- The inlet air temperature of the rack increases, as more supply air is utilized in the hot aisle than in the cold aisle.
- The location of the CRAC units has an insignificant effect on the inlet air temperature.

Most strategies to manage the environment of data centres consider the return air temperature to the CRAC units; so the hotter the supply air to the CRAC units, the more efficient their operation. Boucher et al. [38] studied several ways to improve the thermal management and energy performance of the data centre by using three main actuators placed on the CRAC supply to control the supply temperature, the CRAC fan to control the flow rate, and the plenum vent tile opening. Furthermore, the new non-dimensional index that describes the amount of hot and cold air mixing

(recirculation) is called the Supply Heat Index (SHI) [38] and it is defined, as follows:

$$SHI = \frac{(T_i - T_v)}{(T_o - T_v)} \quad (2.5)$$

Where ,

$T_i$  = the inlet temperature.

$T_o$  = the corresponding outlet temperature at the same rack at the same height.

$T_v$  = the air temperature from the adjacent plenum vent.

The results show that in the linear relationship between the CRAC temperature and the inlet temperature, the fan speed has significant effect on the SHI; additionally, the opening area of the vents tile has a direct relation with the rack closer to the CRAC and an inverse relation to the rack farther away.

The cooling and energy efficiencies of the data centre were analysed by Herrlin [39]. Herrlin defined two indices used to indicate both cooling and energy performances. These indices are rack cooling index (RCI) and return temperature index (RTI). Rack cooling index (RCI) measures the cooling efficiency of the equipment in the data centre, whereas the return temperature index (RTI) measures the energy efficiency of the data centre. Also the CFD analysis has been implemented to calculate these indices by obtaining both return and supply temperatures of the CRAC unit. There are two indices,  $RCI_{HI}$  and  $RCI_{LO}$ , can which be extracted from RCI at both ends of high allowable intake temperature and low allowable intake temperature.

ASHRAE describes that the range of intake temperature varied between 20°C and 25°C. However, the allowable range is between 15°C and 32.5°C. Return temperature index (RTI) is written, as follows:

$$RTI = \left[ \frac{T_{Return} - T_{Supply}}{\Delta T_{Equip}} \right] 100\% \quad (2.6)$$

Where:

$T_{Return}$ : return temperature

$T_{Supply}$ : supply air temperature.

$\Delta T_{Equip}$ : temperature rise across the electronic equipment.

The explanation of the RTI index is as follows:

RTI=100% target (the best energy performance)

RTI<100% by-pass (the cold air return to the CRAC without cooling the racks)

RTI>100% recirculation (mixing between hot and cold air)

And the  $RCI_{HI}$  definition is as follows:

$$RCI_{HI} = \left[ 1 - \frac{Total\ over-Temp}{Max\ Allowable\ over-Temp} \right] 100\% \quad (2.7)$$

Where the total over-temperature refers to the summation of the server intake temperature subtracted from the maximum recommended temperature; whereas, the maximum allowable over temperature refers to the subtraction of maximum allowable temperature and the maximum recommended temperature multiplied by the number of servers.

The interpretation of the index is as follows:

$RCI_{HI} = 100\%$  All intake temperatures  $\leq$  max recommended temperature.

$RCI_{HI} < 100\%$  At least one intake temperature  $>$  max recommended temperature.

The  $RCI_{LO}$  definition is as follows:

$$RCI_{LO} = \left[ 1 - \frac{\text{Total Under-Temp}}{\text{Max Allowable Under-Temp}} \right] 100\% \quad (2.8)$$

Where the total under-temperature refers to the summation of the subtraction of the minimum recommended temperature and the server intake temperature, when the server intake temperature is less than the minimum recommended temperature.

$RCI_{LO} = 100\%$  All intake temperatures  $\geq$  min recommended temperature

$RCI_{LO} < 100\%$  At least one intake temperature  $<$  min recommended temperature

And these indices are useful to ensure that all the server racks within the acceptable range of temperature (15°C-25°C)[17].

### **Air, water and refrigeration cooling systems in a data centre**

Hannemann and Chu [6] reported the comparison between five alternative cooling systems for a data centre to achieve the best one based on the cooling performance and the total cost (capital and operation). This study considered a 30 kW heat dissipation rack in a high-density data centre in order to compare these systems. The five alternative cooling approaches are:

(1) Standard air cooling, which is used, chilled air coming from the CRAC unit to cool the rack, as shown in Figure 2.13(a), where the pink and the blue lines are hot return refrigerant and cold supply refrigerant in the condenser respectively.

(2) Water augmentation cooling, in which the heat dissipation from the rack is removed by both chilled air from the CRAC unit and the back door water heat exchanger, as shown in Figure 2.13(b), where the light green and dark green lines are cold supply water and hot return water in the chiller, respectively. In this case, the

heat will be removed directly from the rack. However, this method has a high cost of installation and maintenance, and also the risk of forming the condensation at the rear heat exchanger may lead to a failure in the system.

(3) Refrigerant based augmentation; in this approach, the idea is the same as the water approach, except the refrigerant type R134a in back door heat exchanger is used rather than a water heat exchanger, as illustrated in Figure 2.13(c).

(4) Water touch cooling system; in this approach, the cooling water plates are introduced inside the rack to accomplish the direct cooling of heat source and the CRAC unit is used to remove the part of heat dissipation by the rack, as shown in Figure 2.13(d).

(5) Refrigerant touch cooling, which is the same idea as the water touch approach, but the refrigerant R134a plates are used rather than water plates. Also, this system does not need a chiller unit, as shown in Figure 2.13 (e).

In case (a), the typical air cooling is used to cool the rack inside the data centre. In this system, the refrigeration cycle is used to cool the hot return air from the data centre. Both condenser and compressor are kept outside the data centre, whereas the evaporator and expansion are located inside the CRAC unit where the heat exchange takes place between the hot return air and the refrigerant agent. The results show that the refrigerant touch cooling approach has the best results among all of the approaches for saving floor space, cooling power, capital cost and operational costs [6].

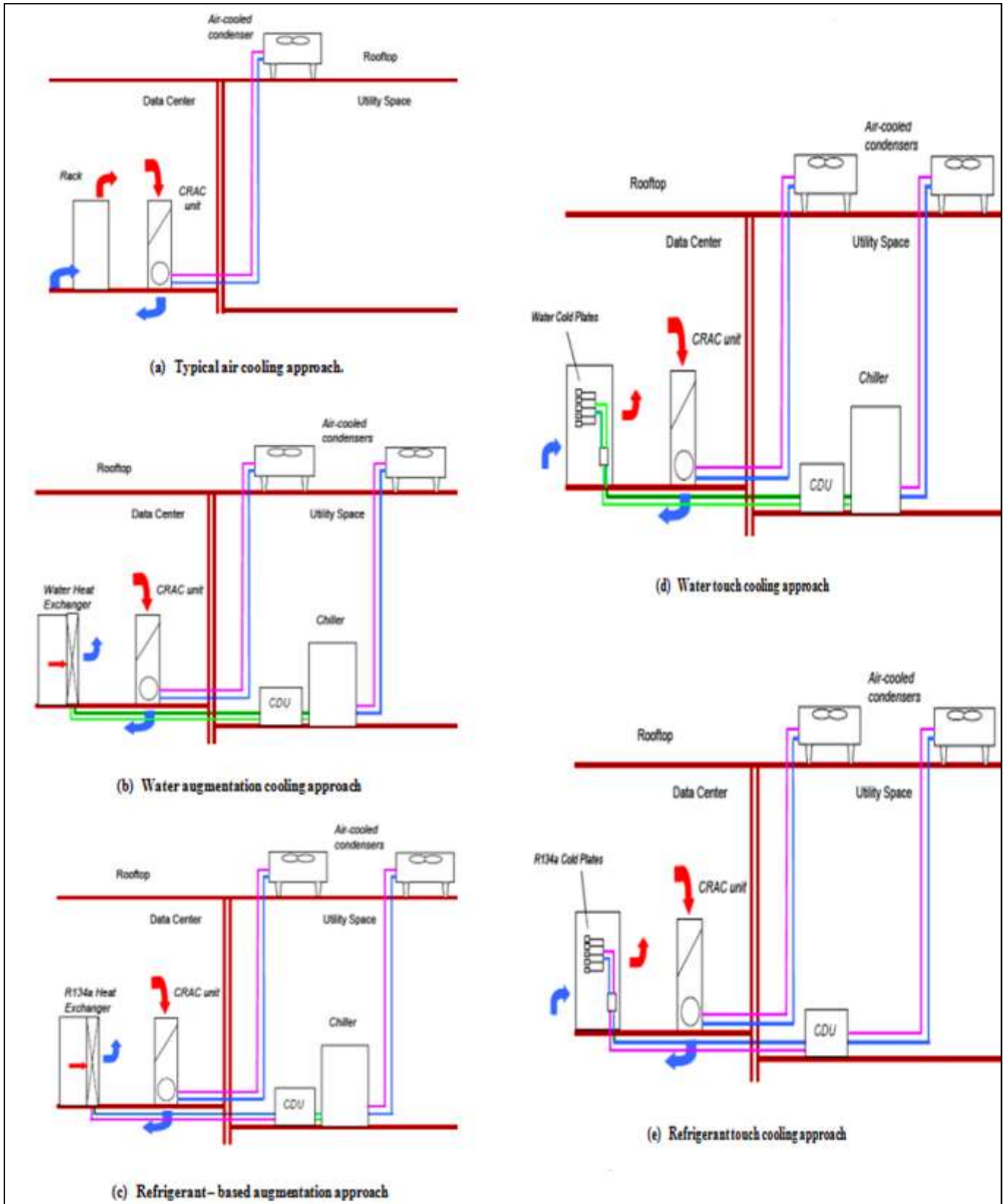


Figure 2.13 Five alternative cooling systems for data centre [6].

### Air side economised system

An air side economizer is discussed here as the alternative solution that could be used under the category of air flow management solutions. An air side economiser is a mechanical device that is used to regulate the outside air brought inside the data centre. A full study of economiser systems for data centres was presented by Anubhav et al. [40], and it was found that the energy of the chiller could be reduced up to 50% with increasing the inlet temperature from 20°C to 25°C. The two main economiser systems are airside economiser systems and fluid-based economiser systems. The air side economiser system uses the fresh outside air to cool the data centre with cooperation from the fan and filter systems, as shown in Figure 2.14.

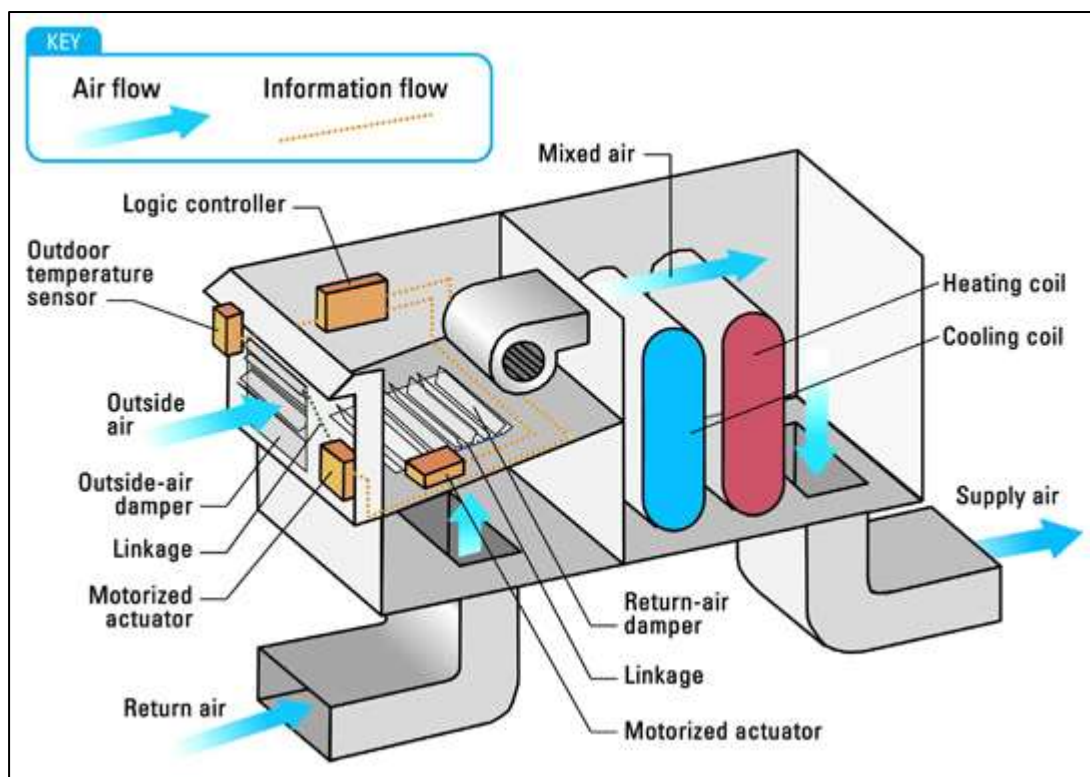


Figure 2.14 Air side economizer system [40].



The principle of an airside economiser can be described as introducing the fresh outside air to the cold aisle, whereas the hot return air is rejected directly to the outside ambient environment. Next, the room air mixed with cold outside air is fed back to the CRAC unit. In this technique, the humidification and dehumidification are critical parameters that have been taken into account to achieve the recommended relative humidity (40%-55%) in the data centre. As a result, the saving of cost and energy using this system can reach up to 40% compared with using the traditional cooling system in a data centre. However, this system cannot be used in hot or humid weather because it is used to supply the data centre air with low temperature and suitable humidity.

### **Overhead cooling method**

A heat exchanger cooling system for the data centre was implemented by Patel et al. [41]. The data centre prototype with a cooling system was analysed by using CFD. The cooling system simply has water-air heat exchangers located in the ceiling of the data centre that are called the Data Cool system. These heat exchangers have been deployed such that a heat exchanger is located above each rack, as shown in Figure 2.15.

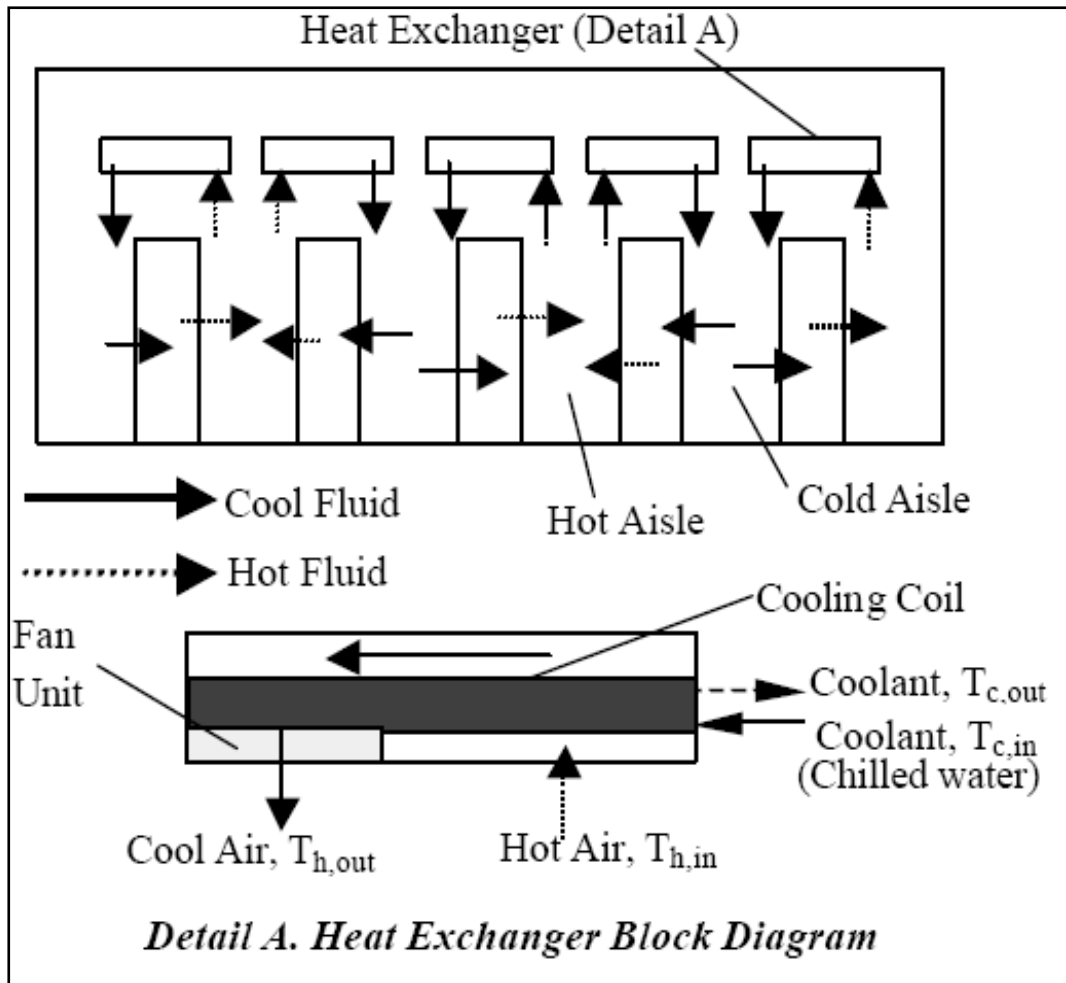


Figure 2.15 Data Cool system in cold-hot aisle arrangement [41].

The idea of this system is to cool the exhaust air coming from the hot aisle in the heat exchanger by using chilled water. The main advantage of this system is a reduction in usage of floor area compared with the traditional system (hot-cold aisle arrangement data centre). It was found that the Data Cool system which is described by Patel et al. [41] is an efficient system to reduce the rack inlet temperature, leading to reduction of the probability of recirculation problems compared to the raised floor system.

A further development to the smart cooling system was invented by Patel et al. [42]. This approach provides a controlled amount of the cooling fluid flow rate to each heat exchanger based on the heating dissipation required for each rack. This system contains variable capacity compressors and variable speed fans in order to control both the volume flow rate of the air and the speed of the cooling fluid. This approach leads to a reduction of the power consumption by the CRAC units. Also in this technique, the data centre layout (CRAC units) may be changed based on the heating dissipation by the racks in order to achieve the optimal operating manner for CRAC units.

An alternative of cooling that uses overhead units to cool the data centre was described by Stahl et al. [43]. As per Patel et al. [41], the cooling heat exchangers are located in the ceiling of the data centre to provide the cooling air to the racks; it is called the overhead cooling system. This system has a heat exchanger associated with the fan to draw the hot air from the rack exhaust and flow it again at a low temperature to the rack intake, as shown in Figure 2.16. The heat exchanging occurs between the hot air and the coolant (either chilled water or refrigerant) used inside the pipe of the heat exchanger.

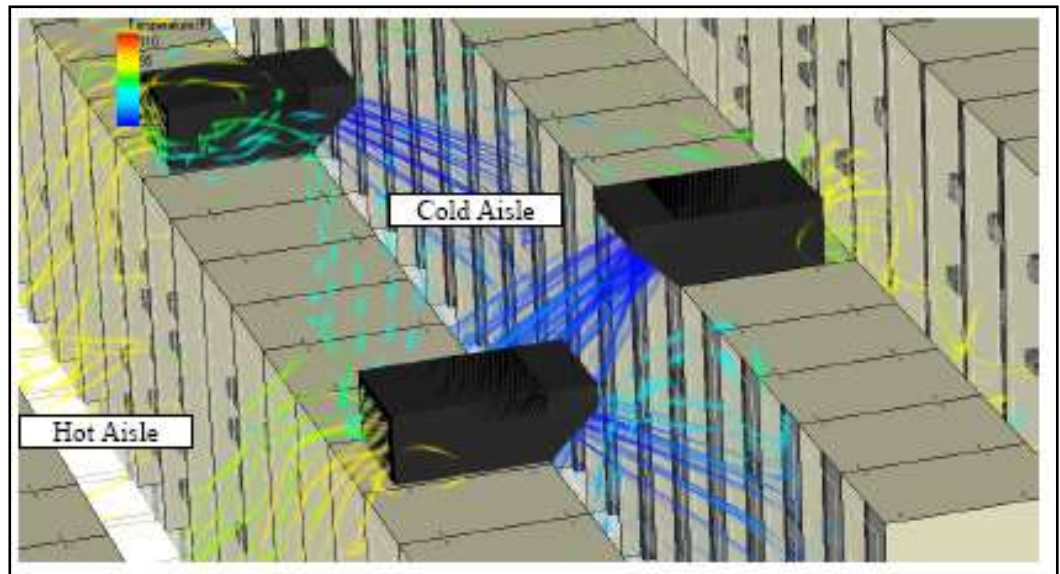


Figure 2.16 Overhead cooling system in a data centre [43].

### **Portable data centre with a cooling system**

Ice cube data centres are produced by SGI [44]. They are portable data centres with easy mobility. The cooling concept of this data centre is represented by using the rows of heat exchangers and each heat exchanger consists of two opposite rack servers, as shown in Figure 2.17. The hot air is drawn from the back of each server in the same heat exchanger and it flows through the plenum, located at the back of the rack. The hot air then is cooled down by the heat exchanger using a closed loop, chilled water system. Finally, the cooled air is introduced again in the cold aisle at a temperature of 24°C. This technique can operate up to 1500 W per square foot of complete data centre space.

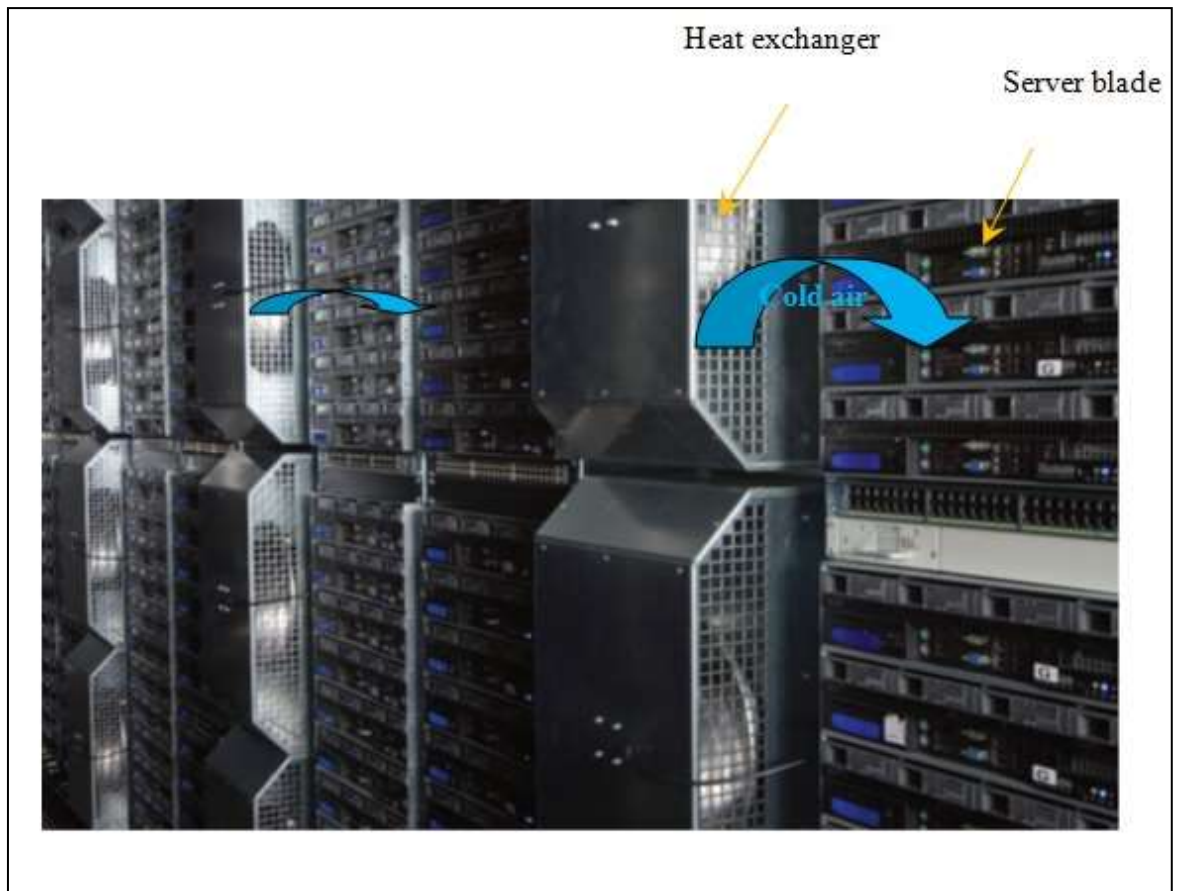


Figure 2.17 Ice cube cooling technique [44].

### Back door cooling system

In high density data centres, where the server rack produces up to 30 kW, the back door cooler is one technique used to maintain the thermal environment. Figure 2.18 shows a typical arrangement of a back door cooler (heat exchanger). According to Almoli et al. [45], up to 90% of the heat could be removed from CRAC unit by deploying both an active and passive back door cooler. Both active and passive back door coolers can be defined as an air-water heat exchanger attached at the rack exhaust to reduce the rack exhaust temperature. In an active back door cooler, the additional fan is used to increase the air flow rate to the heat exchanger. In the passive heat exchanger, the server fans are only used to push the air through the heat

exchanger. It is considered as an efficient way to cool the racks cooperating with CRAC units; also, this technique uses less space than traditional data centre (cold-hot aisle arrangement) and has the ability to control the environment inside the data centre.

However, this technique is expensive because each rack needs a chilled water system. Also it may lead to water leakage on the floor of the data centre due to a large amount of couplings connecting the chilled water pipes [14].

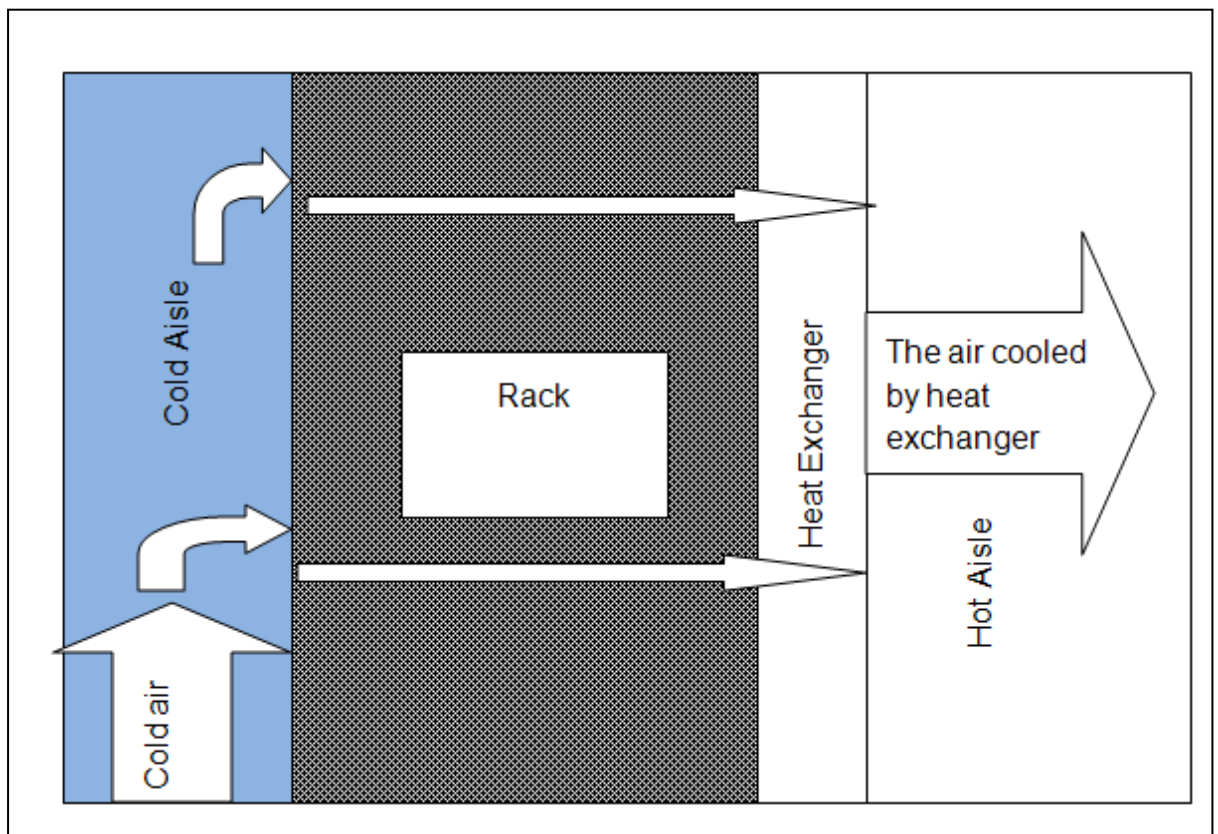


**Figure 2.18 Rack backdoor cooler.**

The hybrid cooling system for the racks in a data centre was tested by Udakeri et al. [46]. The effect of using a water-air heat exchanger (hybrid cooling system) at the back of the rack is observed in this study with two different supply arrangement types, which are over-feed supply and under-feed supply. With the over-feed supply,

the chilled air is provided from the top of the rack; in the under-feed supply, the chilled air is provided from the raised floor vents as in a hot-cold aisle configuration data centre. The idea of the hybrid cooling system is to use a water-air heat exchanger, which is either a plate and fin or tube and fin heat exchanger. The results show that the hybrid cooling system has a significant effect on inlet temperature, return temperature and the thermal energy. The inlet temperature could be reduced by up to 15°C and the return temperature can be reduced by using the hybrid solution for both overhead feed supply and underfloor feed supply arrangements. Moreover, the energy consumed by the CRAC unit can be reduced up to 55% because the hybrid system gets rid with a lot of heat [46].

## **2.7 High Performance Computing (HPC) data centre**

High Performance data centre (HPC), also are sometimes called super computer data centres and can be defined as the data centre that uses multiple processors to run programs in less time and to run advanced applications with a reliably fast turnaround [47]. The term HPC is mainly used for a system that can function above a teraflop, which is a measure of the computer performance in trillions of floating point operations per second [47]. The HPC data centre is usually used to execute complex applications by academic, military and government research facilities. HPC data centres have large volumes of internal components inside the server racks that provide large amounts of primary memory and processors. The level of usage of the CPUs in these centres is greater than that of normal data centres, which can lead to large power consumption per rack. The power consumption per rack typically reaches 20 kW and sometimes reaches more than 30 kW per rack [48]. High-performance computing equipment that uses blade servers consumes much more power per rack than a traditional data centre, leading

to more heat production. In such, efficient cooling systems are required to reduce the risk of server failures [49] and [50].

Some HPC systems have racks with 30 kW or more [51], so the HPC data centre requires special cooling systems to maintain an appropriate range of temperature and humidity, as specified by ASHRAE [16]. According to the TOP500 organization [52], an organization that ranks the supercomputers by their performance to determine the world's 500 fastest super computers, the United State possesses the majority of the world's supercomputers; however, there are 14 other countries that also possess them, as of June 2010, as shown in Figure 2.19.

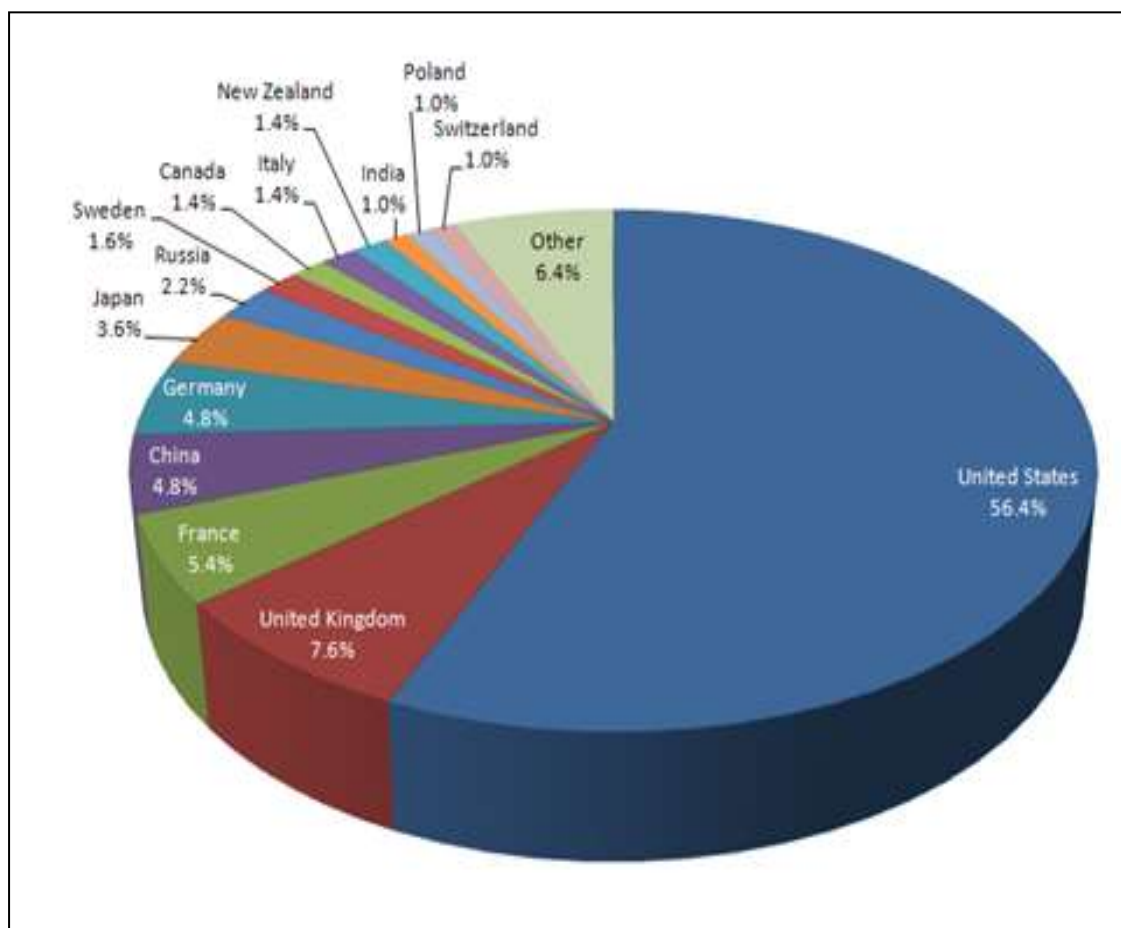


Figure 2.19 Supercomputers countries share [52].



The high density data centre can be defined as a data centre with a rack that produces at least 14 kW [53], which clearly produces more heat than a low data centre density of less than 10 kW per rack. The traditional cooling approach (cold-hot aisle arrangement) cannot provide high density data centres with sufficient cooling [53]. Therefore, other techniques are usually adopted to cool this type of data centre.

The reliability of the servers inside data centres has been discussed by Moore et al. [51]. It is shown from these studies that the reliability (i.e., the mean time between failure (MTBF) or mean time to failure (MTTF)) of the servers could be decreased by 50% when the temperature is increased by 10°C over 21°C. Moreover, the failure rate can increase by factors of two for servers that operate at a temperature that is 15°C over 21°C [51].

### **HPC data centre cooling configurations**

In most data centres, CRAC units are used to provide the cold air, as heat is exchanged between the IT exhaust hot air streams and the chilled water. Heat exchange takes place inside the liquid (or refrigerant) coils, which are placed inside the CRAC units within the data centre and this is the most common approach for commercial data centres. However, this cooling method is limited for a data centre with a rack of up to 8 kW as a maximum limit for heat dissipation [54]; whereas, in the HPC data centres, a large amount of heat is produced and this is considered to be the greatest challenge in cooling the data centre. Racks with heat dissipation of 30 kW are now more common in HPC data centres, and as such, are difficult to cool via normal CRAC units, causing difficulty in keeping the data centre in the ASHREA temperature limits [53]. Therefore, new cooling methods, such as liquid cooling,

could be used in order to cool down the rack inside the HPC data centre. The water has approximately 1000 times more heat carrying capacity than air [55]. Thus, liquid cooling techniques are becoming more widely used in HPC data centres to maintain temperatures inside allowable ranges. Usually, the chilled water, which is used in liquid cooling techniques, is supplied between 8°C and 15°C when the air conditioner is used [54]. The liquid cooling of HPC data centres can be implemented in different configurations [53], such as the following:

- Using a back door liquid loop heat exchanger, which sits in front of the rack exhaust (either active, with fans, or passive back door coolers).
- Using cooling pipes that come close to the CPU, which is the main heat source of the server.
- Overhead heat exchangers, which are placed above the rack to cool the hot exhaust air and supply cold air to the rack inlet. In this technique, an air-water heat exchanger is used.

Air cooling techniques can also be implemented to remove heat inside HPC data centres with either cold or hot aisle containment. Containment is an efficient air management technique, since it prevents the mixing between cold and hot air inside the data centre [53]. Managing heat loads inside HPC data centres with the cooling load for the CRAC units will be analysed in the following section.

## **2.8 Thermodynamics of a data centre**

The heat that is produced inside data centres by the IT equipment is removed by the cold air coming from the CRAC unit. The equation that is used to evaluate the amount of heat removed from the data centre and chiller unit can be expressed as

$$Q = \dot{m} C_p \Delta T \quad (2.9)$$

Where,

$Q$  : is the amount of heat (W)

$\dot{m}$  : is the mass flow rate of air (kg/s)

$C_p$  : is the specific heat of the air or water (J/kg.K)

$\Delta T$  : Temperature difference (K)

From Equation 2.9, the amount of heat removed from the data centre exactly equals the amount of heat removed from the air by the chiller water inside the CRAC unit for a set supply or return air temperatures.

### **2.8.1 CRAC unit types**

#### **Direct Expansion (DX) CRAC Units**

The Direct Expansion (DX) CRAC unit was presented by Evans [56]. In this type of CRAC unit, the simple vapour compression refrigeration cycle is used to cool down the hot return air coming from the rack exhaust, as shown in Figure 2.20. The indoor unit components (evaporator and expansion valves) are located inside the CRAC unit, whereas the outdoor unit components (compressor and condenser ) are located outside the data centre. Refrigerants such as R-134 which is used as the cooling agent. In this thesis, this type of CRAC unit will be implemented because the studied data centre which will be shown in chapter 7 is small relative to the real data centres that would use the chiller system. The chiller system is predominantly used to provide cooling for a large data centre (200 kW or more) because it has greater heat removal capacity than a CRAC unit [57].

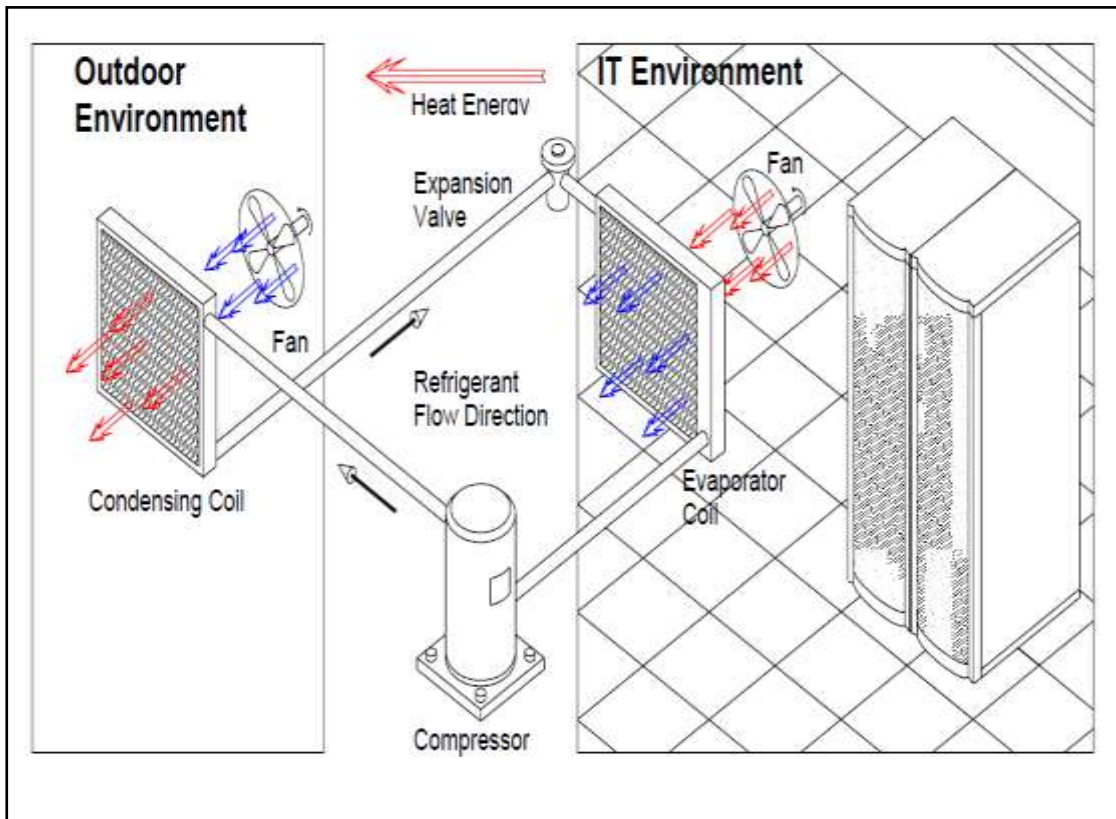


Figure 2.20 Direct expansion CRAC unit type [56].

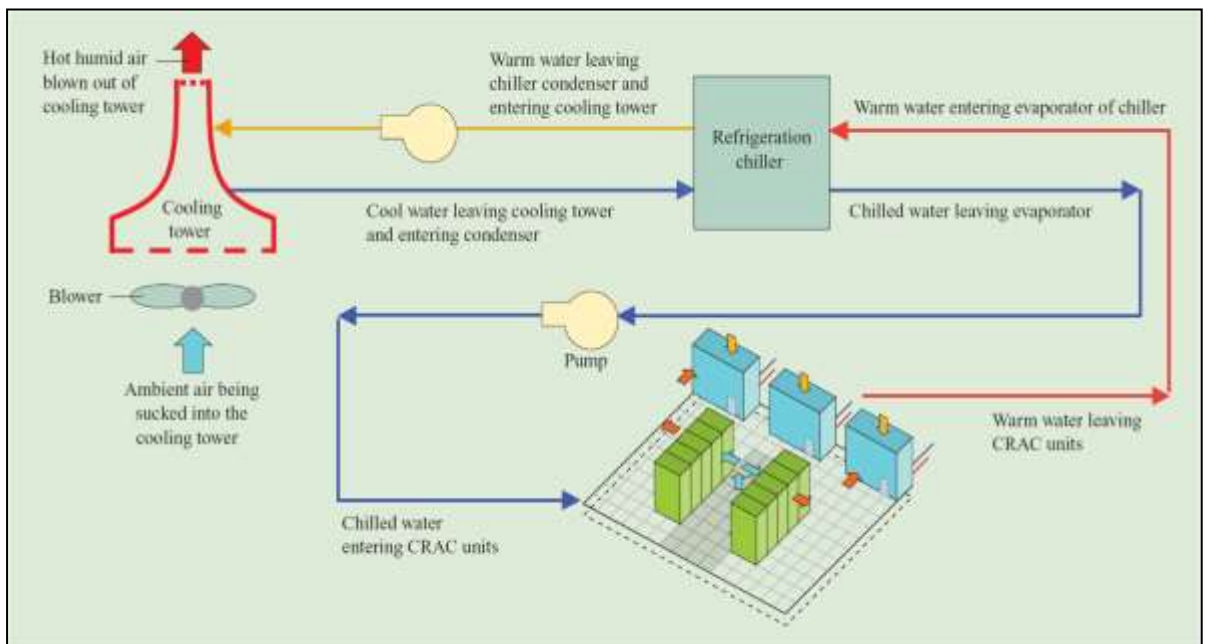


Figure 2.21 Cooling loop for the data centre with chiller system[58]

### **Chiller system CRAC unit**

Figure 2.21 shows the cooling loop of the data centre by using a refrigeration chiller cycle and cooling tower. The refrigeration chiller is a simple vapour compression cycle with a refrigerant cooling agent. Whereas, the cooling tower cools the water by an evaporative cooling concept. The cooling procedure can be described as follows

First of all, the chilled water (8°C-15°C) [58] is pumped from the chiller unit to the CRAC unit in order to remove the heat inside the data centre. The chilled water is used to cool the air that is introduced to the data centre. The hot exhaust air from the data centre then flows to the cooling coil inside the CRAC unit. The heat exchange happens between the hot air and chilled water inside the cooling coil to cool the supply air again by transfer sensible heat (heat transfer by changing the temperature) and latent heat (heat transfer during phase change with constant temperatures), from the air to the chilled water. Finally, the warm water is pumped into the chiller unit to be cooled again by using cooling towers. In the cooling towers, the warm water is sprayed and then the heat is transferred to the outside environment by the evaporative cooling concept. In the evaporative cooling, the temperature of the water can be significantly reduced during the phase change between the liquid water to the water vapour .

### 2.8.2 Coefficient of Performance (COP) of the data centre

The Coefficient of Performance (COP) is a term that is used to represent the efficiency of the refrigerator [59]. The main purpose of a refrigerator is to carry out the heat from the refrigerated space. To achieve this, the supply power should be enough to carry out the heat from refrigeration space.

The aim of calculating the COP of the CRAC unit is to detect the efficiency of the CRAC unit inside the data centre. In this chapter, the COP of the DX-CRAC unit will be used to detect the effectiveness of different data centre configurations.

The COP of the refrigeration cycle in each CRAC unit can be expressed as

$$COP = \frac{\text{Cooling Load (kW)}}{\text{Compressor Work (kW)}} \quad (2.10)$$

Where the cooling load in each CRAC unit can be determined, as shown in Equation (2.9)

$$\text{Cooling Load} = \dot{m} C_p (T_i - T_{ref}) \quad (2.11)$$

Where,

$\dot{m}$  : is the air mass flow rate at the CRAC intake (kg/s)

$C_p$ : is the specific heat of air at constant pressure (kJ /kg. °C)

$T_i$ : is the air inlet temperature of CRAC unit (°C)

$T_{ref}$ : is the CRAC air supply temperature (°C)

Also, the COP can be calculated from the Carnot refrigeration cycle to give an indication of the effect of the supply temperature on the COP values, as follows:

$$COP_{R,Carnot} = \frac{T_L}{T_H - T_L} \quad (2.12)$$

Where  $COP_{R,Carnot}$ ,  $T_L$  and  $T_H$  are the coefficient of performance of the Carnot refrigeration cycle, the supply temperature to the data centre from the CRAC unit (15°C), and the outside environmental temperature (23°C), respectively.

The COP of the DX CRAC unit of a traditional data centre (raised floor, hot-cold aisle arrangement) varies between 3 to 4.5 [60]. Moore et al. [51] found the relationship between the COP of the chiller system and the supply temperature inside the data centre, as shown in Figure 2.22. The relationship can be expressed as

$$COP = 0.0068T^2 + 0.0008T + 0.458 \quad (2.13)$$

Where, T is the CRAC supply temperature in (°C) and it is between 10°C and 30°C.

The Moore et al. [51] study was completed for the HP labs utility data centre. It was found that as the supply temperature increases within the allowable limit, the COP also increases, while the CRAC unit uses less energy. So, raising the inlet temperature by 5°C within the temperature range (15°C-25°C) leads to a saving of up to 40% of the CRAC power [51]. Also, the COP of the chiller system has been tested against the rack inlet temperature by Breen et al. [61]. It was found that the COP of the chiller system for a data centre can be increased by 8% when the rack inlet temperature is increased by 5°C within the temperature range (15°C-25°C).

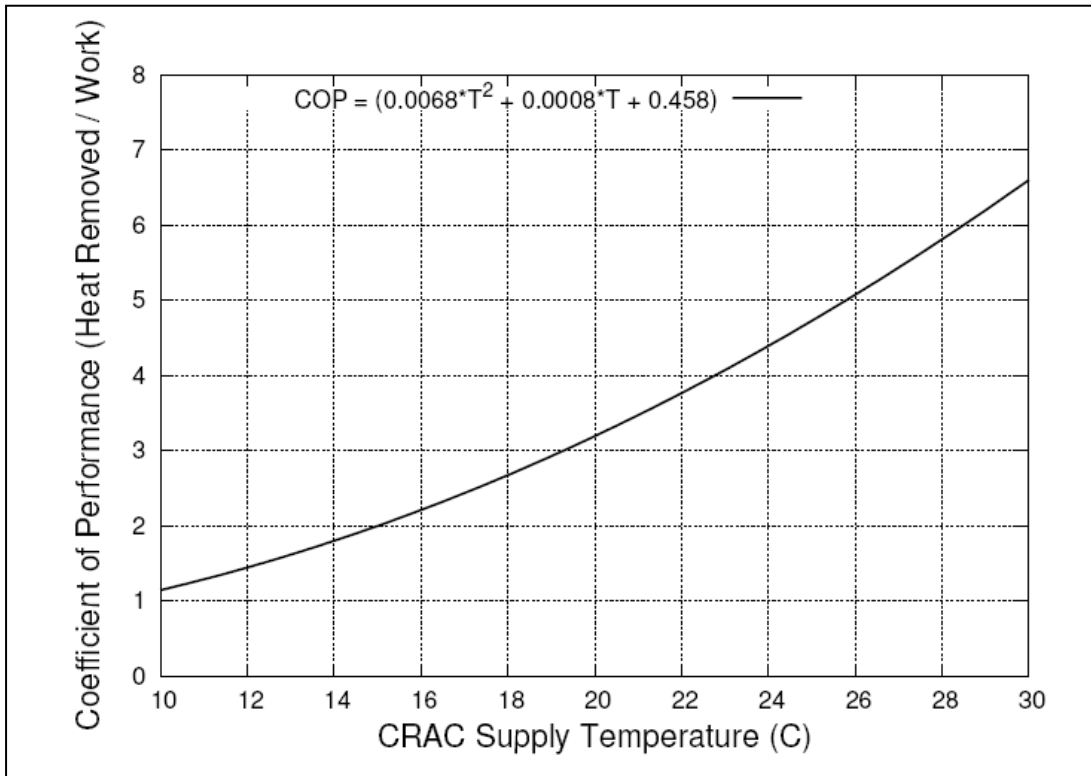


Figure 2.22 COP vs. CRAC supply temperature from the HP experiment [51].

## 2.9 Conclusion

The literature review for the data centre cooling technology has been presented in this chapter. Several ways are used to reduce the temperature inside the data centre as the following:

- Controlling air distribution inside the data centre to reduce the mixing between hot and cold air.
- Using some cooling configuration such as cold aisle containment, hot aisle containment and back door heat exchanger to reduce the data centre temperature.



- Changing the data centre layout in order to reduce the mixing between cold and hot air.

Finally the HPC data centre has been presented in this chapter. Where The power consumption per rack typically reaches 20 kW and sometimes reaches more than 30 kW per rack [48]. Furthermore, the COP of data centre also has been mentioned to detect the efficiency of the CRAC unit inside the data centre. It was found from the previous studies that as the supply temperature increases within the acceptable range (15°C-25°C) as the COP of CRAC unit increases.

## **CHAPTER 3: THE SCOPE OF THE CURRENT WORK**

### **3.1 Introduction**

The cooling techniques and energy consumption inside the data centre are the most concern for the mechanical engineering area as it was mentioned in a lot of previous studies as in chapter 2. The objective and the new knowledge (novelty) that have been used in this thesis will be described in this chapter.

### **3.2 Objective and new knowledge**

The objective of this thesis is to build up the design of the data centre from the server level to the room level as will be described later. Also to test different cooling configurations for the data centre. Finally the power of the CRAC unit that used to supply the chilled air to the data centre will be measured.

In this thesis, the air cooling method is used to cool the rack inside the data centre because it is a popular cooling method due to easy maintenance and low cost [6]. The air flow management cooling methods are represented by using CFD analysis. The CFD models are also developed to study the component of a data centre (i.e., air flow through servers' racks). The new model which is a porous media model will be used to simulate the server by using CFD model and also different turbulence models (standard  $k-\varepsilon$  model, RNG  $k-\varepsilon$  model, and Realizable  $k-\varepsilon$  model) have been tested by CFD and validated with the experimental data. Also the boundary conditions which are used for server and rack simulation will be clearly specify to describe the physics of the problem. The porous approach assumption is made because the air flow has the ability to flow through the rack

servers, but is restricted by the internal components of the servers. Normally the supply of chilled air enters the data centre by the vents via the plenum. After that, the air is sucked to the front of servers due to the internal server fans. Finally, the air carries away the heat dissipated by the server and returns back to the CRAC unit to cool it down again. Furthermore, server blade and rack will be analyzed to simplify the data centre by using both Gambit and Fluent software. Server, rack and room levels are included in this study to determine both velocity field and temperature distribution inside the data centre. Moreover, some techniques have been implemented to increase the data centre efficiency and reduce the hotspots inside the data centre. Finally, the compressor energy of the direct expansion CRAC unit will be calculated and compared with the different types of the cooling configurations inside the data centre. The scope of the current work can be represented as shown in Figure 3.1.

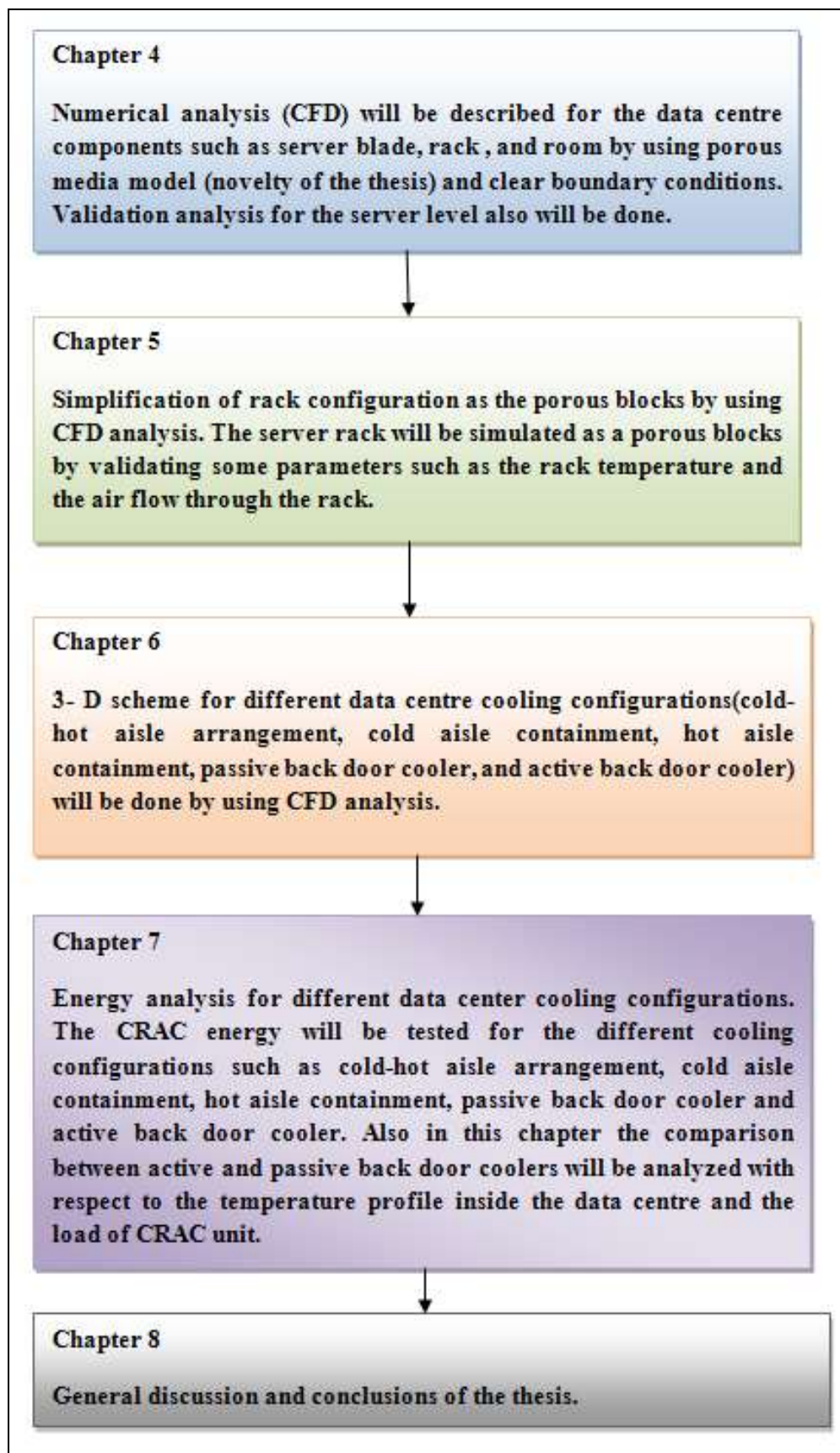


Figure 3.1 Scope of the thesis work.

## CHAPTER 4 : MODELLING

### 4.1 Introduction

The modelling analysis of the data centre will be described in this chapter. This chapter also describes the numerical solution that is used to solve the thermal analysis of the data centre. The data centre can be broken down to three main levels, which are the server level, the rack level, and finally, the room level. The flow characteristics such as temperature, velocity and pressure fields will be obtained for the above three levels (server, rack and room levels). The porous media model will be used to simulate the server blade with its internal components. Finally, three different turbulence models (standard  $k-\epsilon$  model, RNG  $k-\epsilon$  model, and Realizable  $k-\epsilon$  model) will be tested and validated with experimental data. Figure 4.1 shows some CFD figures for the server as in (a), rack as in (b) and room as in (c). Computational Fluid dynamics (CFD) is used to simulate the flow through server, rack and room. The commercial code that is used in this study is the Fluent and the Gambit software. The novel method which is used to present the server and rack is done by considering the porous media concept, where the internal components of the server and rack are assumed to be porous media with experimental validation.

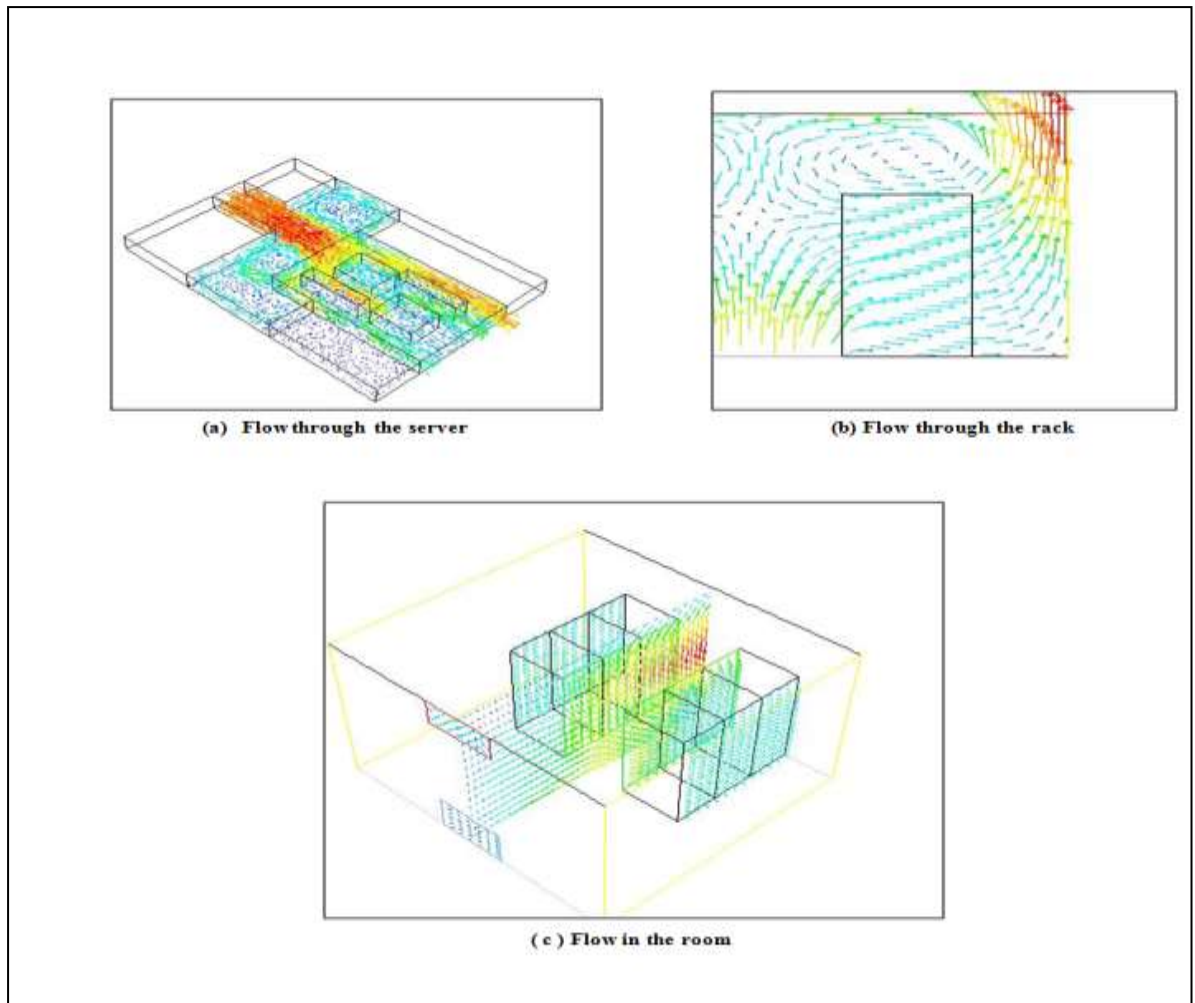


Figure 4.1 Flow analysis in server, rack and room of the data centre.

## 4.2 Computational Fluid Dynamics (CFD) modelling

The CFD analysis is the numerical solution that is used to analyze the governing equations in the data centre, which are continuity, momentum and energy equations [62]. The numerical approximation method is used instead of the analytical solution to simplify the solution and save the calculation time. In this thesis, the finite volume method is used to discretise the governing partial differential equations. In the finite volume method, the governing equation is integrated over the control volume to obtain the discretized equation at the nodal point [62]. CFD analysis for turbulent model cannot give an exact solution because

it just a model and due to turbulence conditions, and due to geometry complication of data centre [63],[64] and [65]. However, it predicts approximate solution for the flow field inside data centre

CFD codes are the codes that use numerical methods to solve and analyse the fluid flow problems [62]. Some popular commercial codes of CFD are CFX/ANSYS, FLUENT, PHOENICS, STAR-CD, Six Sigma, etc. CFD consists of three main elements, which are pre-processor, solver and post-processor. The function of each element is briefly described, as follows:

1. Pre-processor: In this stage, the mesh is generated to divide the domain into a small number of cells. The solution takes place at each node. The accuracy of solution usually depends on the number of the cell; so as the number of the cell increases, the accuracy increases, and vice versa.
2. Solver: in the solver, the numerical method such as the finite volume method is implemented to solve the governing equations (continuity equation, momentum equations and energy equation) which will be explained in the next section.
3. Post-processor: the analysis of the solution takes place in the post-processor. Furthermore, the results can be processed and represented in the figures. Also 2-D or 3-D representation might be obtained.

In this project, the CFD model has been done to break down the components of the data centre (servers, racks and room). Furthermore, each component has been analyzed to simplify the data centre by using both Gambit and Fluent software. Both traditional and blade servers are included in this study to give a comprehensive idea with respect to the data centre and with a combination of both types of servers. Moreover, different cooling configurations have been

implemented to reduce the temperature in data centre and this leads to reduction of hotspots inside the data centre. A new model is applied to treat the data centre components as a porous media, which will be explained in Section 4.4. The 3-D CFD geometry of the data centre has been built by using the Gambit program, version 2.4.6, and run by using Fluent Software, version 6.3.26. CFD could be used to give a good expectation about the thermal model inside the data centre before building the data centre [66].

#### 4.2.1 CFD modelling of data centre air flows

The governing equations in the laminar region for velocity, pressure and temperature fields are described for three-dimensional analysis in this section.

- a) Continuity equation: this equation describe the conservation of mass in the control volume.

$$\frac{\partial \rho}{\partial t} + \text{div}(\rho \underline{U}) = 0 \quad (4.1)$$

The momentum equations in each direction are derived from Newton's second law and state that the force is equal to acceleration times mass.

- b) X-momentum equation:

$$\frac{\partial(\rho u)}{\partial t} + \text{div}(\rho u \underline{U}) = -\frac{\partial p}{\partial x} + \text{div}(\mu \text{grad } u) + S_u \quad (4.2)$$

- c) Y-momentum equation:

$$\frac{\partial(\rho v)}{\partial t} + \text{div}(\rho v \underline{U}) = -\frac{\partial p}{\partial y} + \text{div}(\mu \text{grad } v) + S_v \quad (4.3)$$

- d) Z-momentum equation:

$$\frac{\partial(\rho w)}{\partial t} + \text{div}(\rho w \underline{U}) = -\frac{\partial p}{\partial z} + \text{div}(\mu \text{grad } w) + S_w \quad (4.4)$$



e) Energy equation: which is the equation that is derived from the first law of thermodynamics, which state that the net heat transfer into control volume plus the net work done by the same control volume is equal to the energy difference of the control volume.

$$\rho C_p \frac{\partial T}{\partial t} + \text{div}(\rho C_p T \underline{U}) = -p \text{div} \underline{U} + k \text{div}(\text{grad} T) + Q \quad (4.5)$$

For incompressible flow  $\rho$  is constant so that  $\frac{\partial \rho}{\partial t} = 0$

Where :

$\rho$ : The density (kg/ m<sup>3</sup>)

$u$ : The velocity in x-direction (m/s)

$v$ : The velocity in y-direction (m/s)

$w$ : The velocity in z- direction (m/s)

$p$ : The pressure (Pa)

$S_u$ : The source term in x-direction, where this represent the effect of the permeability in the X direction for the server and racks.

$S_v$ : The source term in y-direction, where this represents the effect of the permeability in the Y direction for the server and racks.

$S_w$ : The source term in z-direction, where this represents the effect of the permeability in the Z direction for the server and racks.

$C_p$ : is the specific heat (kJ/kg.K)

$T$ : temperature (K)

$\underline{U}$  : velocity vector ( $\underline{U} = ui + vj + wk$ )

k : thermal conductivity (W/m.K)

Q: energy source term (kW/m<sup>3</sup>)

μ: dynamic viscosity (kg/m.s)

In this study the steady state situation is assumed. Therefore the variables do not change with the time in equations 4.2, 4.3, 4.4, and 4.5.

#### 4.2.2 Non-dimensional analysis for the governing equations

The non-dimensional analysis is very important to reduce the dimensional parameters to non-dimensional groups, leading to a good understanding of the physics of the problem. As an example, the laminar or turbulent modes can be known by using dimensionless analysis to obtain the Reynolds number (Re) inside the data centre. The non-dimensional coordinates, velocities, pressure and temperature are defined, as follows:

$$x^* = \frac{x}{L}, y^* = \frac{y}{L}, z^* = \frac{z}{L} \quad (4.6)$$

$$u^* = \frac{u}{V_0}, v^* = \frac{v}{V_0}, w^* = \frac{w}{V_0} \quad (4.7)$$

$$p^* = \frac{p}{\rho V_0^2} \quad (4.8)$$

$$T^* = \frac{T - T_s}{T_\infty - T_s} \quad (4.9)$$

Where:

$x^*$  : dimensionless coordinate in x-direction;  $y^*$  : dimensionless coordinate in y-direction;  $z^*$  : dimensionless coordinate in z-direction;  $x$  : Eulerian coordinate in x-direction (m);  $y$  : Eulerian coordinate in y-direction (m);  $z$  : Eulerian coordinate

in z-direction (m); L : characteristic length of the design system (m);  $u^*$  : dimensionless velocity in x-direction;  $v^*$  : dimensionless velocity in y-direction;  $w^*$  : dimensionless velocity in z-direction; u : velocity in x-direction (m/s); v : velocity in y-direction (m/s); w : velocity in z-direction (m/s);  $V_0$ : characteristic velocity of the system (m/s);  $p^*$  : dimensionless pressure; p : pressure field (Pa);

$\rho$  : density of the fluid ( $\text{kg/m}^3$ );  $T^*$  : dimensionless temperature; T : Temperature field ( $^{\circ}\text{C}$ );  $T_{\infty}$ : Surrounding temperature ( $^{\circ}\text{C}$ ); and  $T_s$  : surface temperature ( $^{\circ}\text{C}$ ).

Therefore, the non-dimensional governing equations can be expressed by substituting equations (4.6), (4.7), (4.8) and (4.9) into equations (4.1), (4.2), (4.3), (4.4) and (4.5), as follows:

•Non- dimensional continuity equation:

$$\frac{\partial}{\partial x}(\rho u^*) + \frac{\partial}{\partial y}(\rho v^*) + \frac{\partial}{\partial z}(\rho w^*) = 0 \quad (4.10)$$

For incompressible flow that means  $\rho = \text{constant}$ , then the continuity equation can be written as

$$\frac{\partial}{\partial x}(u^*) + \frac{\partial}{\partial y}(v^*) + \frac{\partial}{\partial z}(w^*) = 0 \quad (4.11)$$

•Non- dimensional x-momentum equation:

$$u^* \frac{\partial u^*}{\partial x^*} + v^* \frac{\partial u^*}{\partial y^*} + w^* \frac{\partial u^*}{\partial z^*} = \frac{1}{\text{Re}} \left( \frac{\partial^2 u^*}{\partial x^{*2}} + \frac{\partial^2 u^*}{\partial y^{*2}} + \frac{\partial^2 u^*}{\partial z^{*2}} \right) - \frac{\partial p^*}{\partial x^*} + S_u^* \quad (4.12)$$

•Non- dimensional y-momentum equation:

$$u^* \frac{\partial v^*}{\partial x^*} + v^* \frac{\partial v^*}{\partial y^*} + w^* \frac{\partial v^*}{\partial z^*} = \frac{1}{\text{Re}} \left( \frac{\partial^2 v^*}{\partial x^{*2}} + \frac{\partial^2 v^*}{\partial y^{*2}} + \frac{\partial^2 v^*}{\partial z^{*2}} \right) - \frac{\partial p^*}{\partial y^*} + S_v^* \quad (4.13)$$

•Non- dimensional z-momentum equation:

$$u^* \frac{\partial w^*}{\partial x^*} + v^* \frac{\partial w^*}{\partial y^*} + w^* \frac{\partial w^*}{\partial z^*} = \frac{1}{\text{Re}} \left( \frac{\partial^2 w^*}{\partial x^{*2}} + \frac{\partial^2 w^*}{\partial y^{*2}} + \frac{\partial^2 w^*}{\partial z^{*2}} \right) - \frac{\partial p^*}{\partial z^*} + S_w^* \quad (4.14)$$

•Non-dimensional energy equation :

$$u^* \frac{\partial T^*}{\partial x^*} + v^* \frac{\partial T^*}{\partial y^*} + w^* \frac{\partial T^*}{\partial z^*} = \frac{1}{\text{Re Pr}} \left( \frac{\partial^2 T^*}{\partial x^{*2}} + \frac{\partial^2 T^*}{\partial y^{*2}} + \frac{\partial^2 T^*}{\partial z^{*2}} \right) + Q \quad (4.15)$$

Three dimensionless parameters have been obtained from non-dimensional analysis, which are Reynolds number (Re), Prandtl number (Pr) and Peclet number (Pe). The Reynolds number describes the inertia force over the viscous force, the Prandtl describes the molecular diffusivity of momentum over the diffusivity of heat, and the Peclet number measures the relative strengths of convection and diffusion [41]. Thus, Reynolds, Prandtl and Peclet numbers can defined, as follows:

$$\text{Re} = \frac{\rho u L}{\mu} \quad (4.16)$$

Where:

Re: Reynolds number.

$\rho$ : The density of the air = 1 m<sup>3</sup>/kg

u: the average velocity (m/s)

L: characteristic length (m)

$\mu$ : the dynamic viscosity of the air = 1.78×10<sup>-5</sup> N.s/m<sup>2</sup> at atmospheric pressure and

T= 300K.

$$\text{Pr} = \frac{\mu C_p}{k} \quad (4.17)$$

$$\text{Pe} = \text{Re} \cdot \text{Pr} \quad (4.18)$$

The Reynolds number gives an indication for the flow being either laminar or turbulent. In our thesis, the turbulent model is used; however, the laminar flow is presented to compare between the laminar and turbulent concepts.

### **4.3 Laminar flow**

Laminar flow is the flow that moves in laminar layers [46]. The character that gives indication either the flow is laminar or turbulent is called the Reynolds number and equals the inertia force over the viscous force. Thus, the Reynolds number can be expressed as equation 4.16.

If  $Re \leq 10^6$ , then the flow over the flat plate (server blade) is called the laminar flow [59] and this can be applied over the vent flow in data centres.

The typical flow rate of supply air coming from the CRAC should be maintained between  $0.1 \text{ m}^3/\text{s}$  to  $0.65 \text{ m}^3/\text{s}$  per tiles, with a 25% opening area [67]. The approximate Reynolds numbers in this research in server and room are  $1 \times 10^7$  and  $1 \times 10^6$ , respectively. The values of Reynolds numbers are calculated by detecting the velocity profile for both server and room. Therefore, the turbulent condition occurs, meaning that the turbulent model is the most suitable model to simulate the flow in the data centre.

### **4.4 Turbulent flow**

The turbulent condition can be defined as small instabilities associated with disturbances in the fluid streamlines of laminar flow that can eventually lead to a chaotic and random state of motion [62], as shown in Figure 4.2.

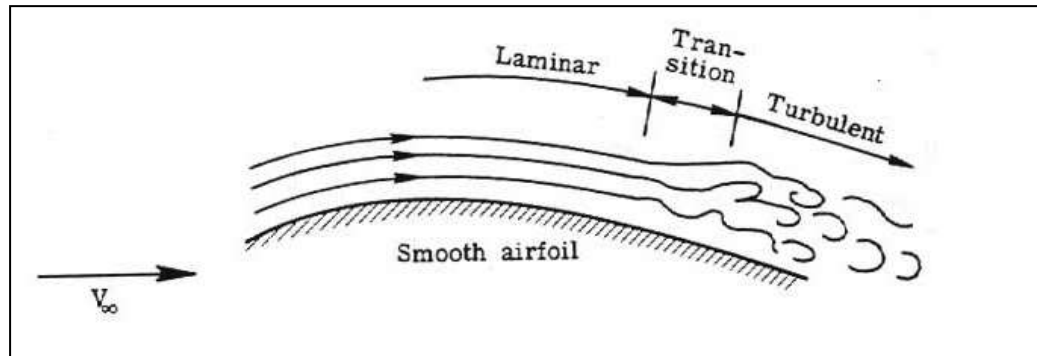


Figure 4.2 The flow modes over the smooth airfoil [68].

The turbulence is caused by high flow rates, low viscous force or surface roughness of the system. The turbulence is associated with fluctuation terms and the flow becomes random. The rotational flow structure, called eddies, appears due to the turbulence flow. These eddies have a characteristic length and velocity. The large eddies are dominated by the inertia force; thus, they are inviscid. Transport of these eddies occurs due to the extraction of energy of mean flow and this phenomena is called vortex stretching. After that, the small eddies are created from the large eddies due to this phenomena. This process continues until the eddies become so small that the viscous effect becomes more significant. The transfer of energy of large eddies to small eddies is called energy cascade [69].

#### 4.4.1 Reynolds Averaged Navier-Stokes model (RANS)

The governing equations can be solved for the turbulent flow by considering the fluctuation terms due to the turbulence. Thus, each property term on the previous governing equations (4.1, 4.2, 4.3 and 4.4) should be substituted by the property term that has two parts: the average property part and the fluctuation part. The new

governing equation is called the Reynolds Average Navier-Stokes equation (RANS) and this model is used widely in practical application [62]

The governing equations in vector form can be expressed for the RANS model as a continuity equation

$$\text{div}(\underline{U})=0 \quad (4.20)$$

Momentum equation (RANS equations)

$$\frac{\partial}{\partial t}(\underline{U}) + \text{div}(\underline{U}\underline{U}) = \frac{1}{\rho} \text{div}(\underline{\underline{\sigma}} - \rho \overline{u'u'}) + \frac{1}{\rho} \underline{S} \quad (4.21)$$

Where

$$\underline{\underline{\sigma}} = -P \underline{I} + \mu (\text{grad}(\underline{U}) + \text{grad}(\underline{U}^T)) \quad (4.22)$$

Where  $\underline{U}$ ,  $\underline{\underline{\sigma}}$ ,  $\underline{u}'$ , and  $\underline{S}$  are the average velocity vector, average stress tensor, velocity fluctuation vector, and additional momentum source term, respectively.

Energy equation

$$\frac{\partial T}{\partial t} + \text{div}(\underline{UT}) = \text{div} \left( \left( \frac{\nu}{\text{Pr}} + \frac{\nu_T}{\text{Pr}_T} \right) \text{grad}T \right) + \frac{1}{\rho C_p} S_Q \quad (4.23)$$

Where T,  $\nu$ , Pr, and  $S_Q$  are temperature, dynamic viscosity, the Prandtl number, and energy source term. The subscript T means the Turbulent flow.

$$\text{Pr} = \frac{\nu}{\alpha} \quad (4.24)$$

$$\alpha = \frac{k}{\rho C_p} \quad (4.25)$$

Also, there is another turbulence model called Large Eddy Simulation (LES) that could be used to solve time-dependent simulation for the large eddies problem. In this model, filtering of the size of eddies is applied rather than averaging over time, as in RANS. In such, this model solves each size of eddies and then gives a more exact solution than RANS. Finally, Direct Numerical Solution (DNS) could be used to solve the continuity equation and Navier-Stokes equation, with a starting point to come up with a transient solution that solves even the small eddies.



The finite volume method which is the numerical model that is integrating the governing equations over the control volume in each node. So that each node will be solved to obtain velocity, pressure and temperature. Whereas the second up-wind scheme is used to give an approximate solution for the discretised equation. This scheme considering the flow direction when determining the value of the cell face [62] and the pressure-based algorithm, and this algorithm is based on initial guess for the pressure to run the momentum equation. And it is used in the Fluent software to solve the governing equations, as shown in Figure 4.3.

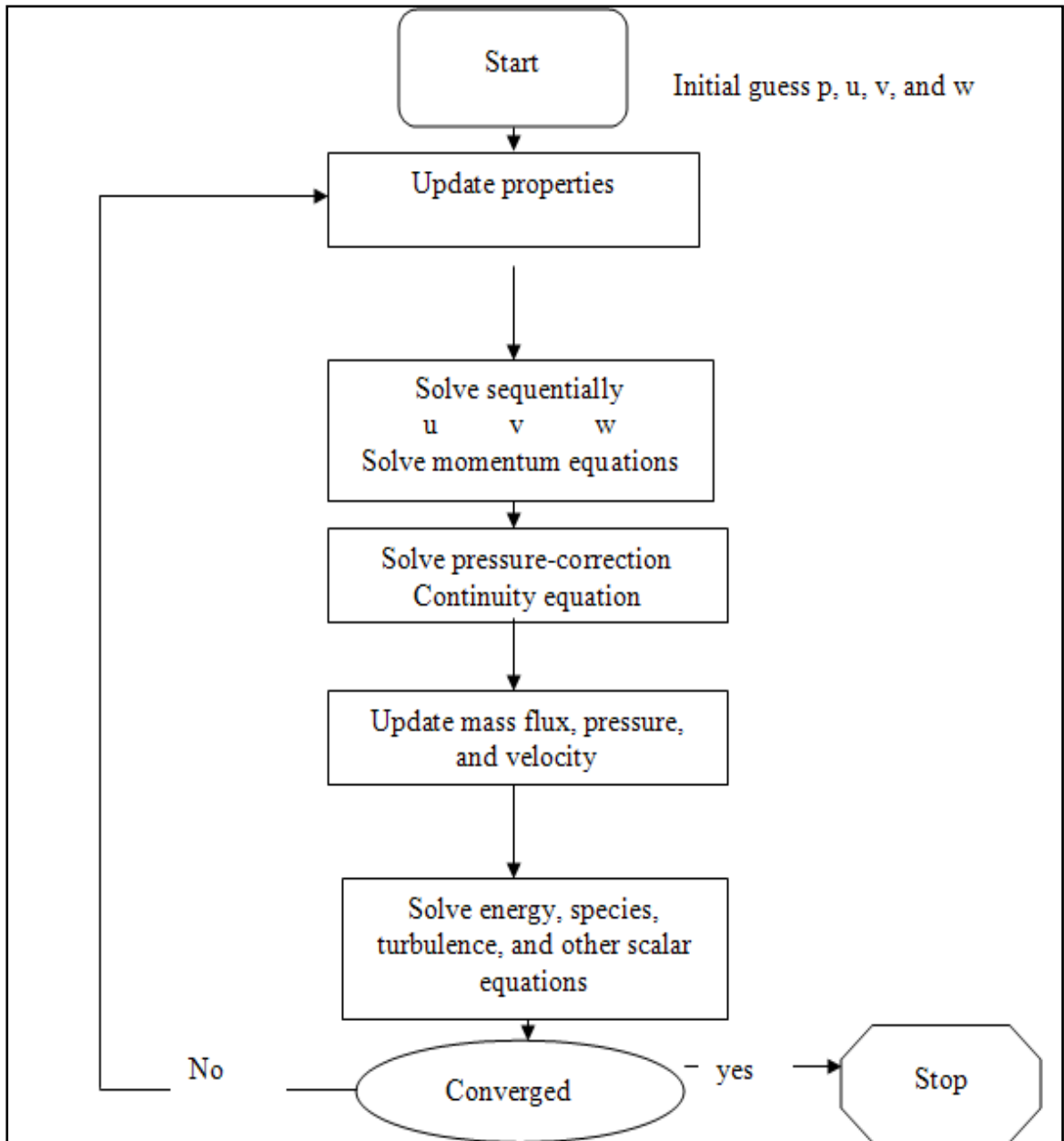


Figure 4.3 Pressure-based method to solve governing equations [69].

#### 4.4.2 Turbulence k-ε models

In this section, the different k-ε models will be presented. The main difference between them can be summarized as follows:

1. The calculation method for the turbulent viscosity.
2. The dissipation equation form and constants.

#### 4.4.3 Standard k-ε model:

The k-ε model, as developed by Launder and Spalding [70] is widely used in industrial application for a fully turbulent model. Two more partial differential equations are used for the k-ε model, with the Reynolds Averaged Navier-Stokes (RANS) equations, as follows:

$$\frac{\partial(\rho k)}{\partial t} + \text{div}(\rho k \underline{U}) = \text{div} \left[ \frac{\mu_t}{\sigma_k} \text{grad } k \right] + 2\mu_t (\text{grad}(\underline{U}) + \text{grad}(\underline{U}^T)) \cdot (\text{grad}(\underline{U}) + \text{grad}(\underline{U}^T)) - \rho \varepsilon \quad (4.26)$$

$$\frac{\partial(\rho \varepsilon)}{\partial t} + \text{div}(\rho \varepsilon \underline{U}) = \text{div} \left[ \frac{\mu_t}{\sigma_\varepsilon} \text{grad } \varepsilon \right] + C_{1\varepsilon} \frac{\varepsilon}{k} 2\mu_t (\text{grad}(\underline{U}) + \text{grad}(\underline{U}^T)) \cdot (\text{grad}(\underline{U}) + \text{grad}(\underline{U}^T)) - C_{2\varepsilon} \rho \frac{\varepsilon^2}{k} \quad (4.27)$$

Where :

$\underline{U}$  : average velocity vector,  $\underline{U}^T$  : average velocity transport vector.

$\rho$  : density (kg/m<sup>3</sup>),  $\mu_t$  : turbulent viscosity(kg/m.s)

$\sigma_k$  : Prandtl number of k ,and  $\sigma_\varepsilon$  : Prandtl number of ε.

And  $\sigma_k$ ,  $\sigma_\varepsilon$ ,  $C_{1\varepsilon}$ ,  $C_{2\varepsilon}$  , and  $C_\mu$  are constant and equal, as in 1, 1.3, 1.44, 1.92 and 0.09, respectively.

The turbulent viscosity (Eddy viscosity) can be specified as

$$\mu_t = \rho C_\mu \frac{k^2}{\varepsilon} \quad (4.28)$$

With respect to the advantage of using the standard k-ε model, it is the simplest model among the models that can be used for a wide range of the industrial application and validated turbulent models [62]. However, the k-ε model gives inaccurate results for some cases, such as some unconfined flow, curved boundary layer, rotating flow and flow in non-circular ducts [62]. Cho et al. [11] implemented the k-ε model to solve the temperature field of a data centre because it is the most effective model to solve the turbulent viscosity and conductivity for large and open-space environments [11].

#### 4.4.4 RNG k-ε model:

The derivation of the new renormalized group (RNG) from the Navier Stokes equations in order to account the effect of the small turbulence was done by Yakhot et al. [71], so that the small-scale turbulence is involved in the large-scale turbulence and in the effective viscosity in the governing equations. The governing equations of both k and ε of this model can be represented as

$$\begin{aligned} \frac{\partial(\rho k)}{\partial t} + \text{div}(\rho k \underline{U}) = \text{div}[\alpha_k \mu_{\text{eff}} \text{grad } k] + 2\mu_t (\text{grad}(\underline{U}) + \text{grad}(\underline{U}^T)) \cdot (\text{grad}(\underline{U}) + \text{grad}(\underline{U}^T)) \\ - \frac{2}{3} \rho k (\text{grad}(\underline{U}) + \text{grad}(\underline{U}^T)) \cdot (\text{grad}(\underline{U}) + \text{grad}(\underline{U}^T)) - \rho \varepsilon \end{aligned} \quad (4.29)$$

$$\begin{aligned} \frac{\partial(\rho \varepsilon)}{\partial t} + \text{div}(\rho \varepsilon \underline{U}) = \text{div}[\alpha_\varepsilon \mu_{\text{eff}} \text{grad } \varepsilon] + C_{1\varepsilon}^* \frac{\varepsilon}{k} [2\mu_t (\text{grad}(\underline{U}) + \text{grad}(\underline{U}^T)) \cdot (\text{grad}(\underline{U}) + \text{grad}(\underline{U}^T))] \\ - \frac{2}{3} \rho k (\text{grad}(\underline{U}) + \text{grad}(\underline{U}^T)) \cdot (\text{grad}(\underline{U}) + \text{grad}(\underline{U}^T)) - C_{2\varepsilon} \rho \frac{\varepsilon^2}{k} \end{aligned} \quad (4.30)$$

Where :

$$\mu_{eff} = \mu + \mu_t, \mu_t = \rho C_\mu \frac{k^2}{\varepsilon} \quad (4.31)$$

$$C_{1\varepsilon}^* = C_{1\varepsilon} - \frac{\eta(1 - \eta/\eta_0)}{1 + \beta\eta^3} \quad (4.32)$$

$$\eta = \frac{k}{\varepsilon} \left( 2 \left( \text{grad}(\underline{U}) + \text{grad}(\underline{U}^T) \right) \left( \text{grad}(\underline{U}) + \text{grad}(\underline{U}^T) \right) \right)^{0.5} \quad (4.33)$$

And  $\alpha_k, \alpha_\varepsilon, C_{1\varepsilon}, C_{2\varepsilon}, C_\mu, \eta_0, \beta$  and are constant and equal in 1.39, 1.39, 1.42, 1.68, 0.0845, 4.377 and 0.012, respectively.

In terms of the RNG k- $\varepsilon$  model, the  $\varepsilon$  equation is now not a main source of the error, as in the standard k- $\varepsilon$  model. The RNG k- $\varepsilon$  model is highly recommended for indoor environment simulation due to its accuracy and ability to save time in computing [72]. Moreover, the RNG k- $\varepsilon$  model is used for forced convection with low turbulence level [72].

#### 4.4.5 Realizable k- $\varepsilon$ model:

A new k- $\varepsilon$  model was derived by Shih et al. [73] to fill the deficiencies of both standard and RNG k- $\varepsilon$  models. This model satisfies some mathematical constraints on the normal stresses from the physics of turbulent flows. In this model, the dynamic equation of the mean vorticity fluctuation at a large Reynolds number has been used to describe the dissipation rate, whereas the positive Reynolds stress constraint is applied to define the new eddy viscosity.

The transport equations for both k and  $\varepsilon$  can be expressed as:

$$\frac{\partial(\rho k)}{\partial t} + \text{div}(\rho k U) = \text{div} \left[ \left( \mu + \frac{\mu_t}{\sigma_k} \right) \text{grad } k \right] + G_k - \rho \varepsilon \quad (4.35)$$

And

$$\frac{\partial(\rho \varepsilon)}{\partial t} + \text{div}(\rho \varepsilon U) = \text{div} \left[ \left( \mu + \frac{\mu_t}{\sigma_\varepsilon} \right) \text{grad } \varepsilon \right] + \rho C_1 S_\varepsilon - \rho C_2 \frac{\varepsilon^2}{k + \sqrt{\nu \varepsilon}} \quad (4.36)$$

Where

$G_k$  is the generation of the turbulent kinetic energy due to the mean velocity ,

$$G_k = 2\mu_t (\text{grad}(\underline{U}) + \text{grad}(\underline{U}^T)) (\text{grad}(\underline{U}) + \text{grad}(\underline{U}^T)), C_1 = \max \left[ 0.43, \frac{\eta}{\eta + 5} \right] \quad (4.37)$$

$$\eta = Sk / \varepsilon \quad (4.38)$$

and the turbulent viscosity is calculated as

$$\mu_t = \rho C_\mu \frac{k^2}{\varepsilon} \quad (4.39)$$

$C_\mu$  is now not constant, as in both standard and RNG k-  $\varepsilon$  models. So this term now

is obtained, as follows:

$$C_\mu = \frac{1}{A_0 + A_s \left( \frac{U^* k}{\varepsilon} \right)} \quad (4.40)$$

Where

$$U^* = \sqrt{S_{ij} S_{ij} + \tilde{\Omega}_{ij} \tilde{\Omega}_{ij}} \quad (4.41)$$

And

$$\tilde{\Omega}_{ij} = \Omega_{ij} - 2\varepsilon_{ijk} \omega \quad (4.42)$$

Where

$$\Omega_{ij} = \overline{\Omega_{ij}} - \varepsilon_{ijk} \omega_k \quad (2.43)$$

Where

$\overline{\Omega_{ij}}$  is the mean rate of the rotation tensor,  $\varepsilon_{ijk}$  is alternating symbol or Levi-Civita symbol;  $\varepsilon_{ijk} = +1$  if i,j and k are different and in cyclic order ( $\varepsilon_{123} = \varepsilon_{231} = \varepsilon_{312} = 1$ ) and  $\varepsilon_{ijk} = -1$  if i,j and k are different and anti-cyclic order ( $\varepsilon_{321} = \varepsilon_{132} = \varepsilon_{213} = -1$ ) ;  $\varepsilon_{ijk} = 0$  if any two indices are the same.  $\omega_k$  is the angular velocity, and both  $A_0$  and  $A_s$  are constant with values of 4.04, and  $\sqrt{6} \cos \phi$ , respectively. Whereas  $S_{ij}$  is the mean strain rate tensor.

Where

$\phi$  can be written as

$$\phi = 1/3 \arccos(\sqrt{6}W), \quad W = \frac{S_{ij} S_{jk} S_{ki}}{\tilde{S}}, \quad \tilde{S} = \sqrt{S_{ij} S_{ij}}$$

And finally, the remaining constants of the transport equations which are  $C_{1\varepsilon}, C_2, \sigma_k$  and  $\sigma_\varepsilon$  are equal to 1.44, 1.9, 1.0 and 1.2, respectively.

The advantages of this model (Realizable k-  $\varepsilon$  model) can be summarized as follows:

- It is widely used and gives good performance for the rotating flow and free flow [73].
- It is used for the flow in the channel.

Three k- $\varepsilon$  models, which are standard k- $\varepsilon$ , RNG k- $\varepsilon$  and realizable k- $\varepsilon$ , have been tested in this research. Cho et al. [11] recommend the use of standard k- $\varepsilon$  models for the environment inside a data centre; whereas, the simulation of the RNG

k- $\epsilon$  could be the best model [72] to represent the server racks, as will be shown in Chapter 3.

#### **4.4.6 Boundary conditions**

The boundary conditions are considered to be an important part in formulating the mathematical model, which is represented by governing equations [62] and [74]. The right boundary conditions should be selected to obtain the right solution. Actually, the boundary conditions represent the reality of the problem. As an example, the wall boundary condition represents the real wall for the problem. The boundary conditions which is used in this thesis will be described in detail in the following chapters.

### **4.5 Porous flow modelling**

A new (novel) model is applied in this thesis to treat the data centre components as porous media. This assumption is made because the air has the ability to flow through the rack servers but is restricted by the internal components of the servers. The obstructions inside the server rack can be replaced by the viscosity resistance and the inertia resistance for the porous media. Similarly, the internal components of the server can be treated as porous media with both viscosity and inertia resistances. Therefore, a step-by step-design has been incorporated to build up the data centre components from the server's internal components level to the data centre room level.

Porous media can be defined as media that contains particles separated by voids, as shown in Figure 4.4. The fluid can flow through this voids. The resistance to the fluid flow is affected by the amount of the particles [75] so that as the amount of particles increases, the resistance increases, and vice versa.

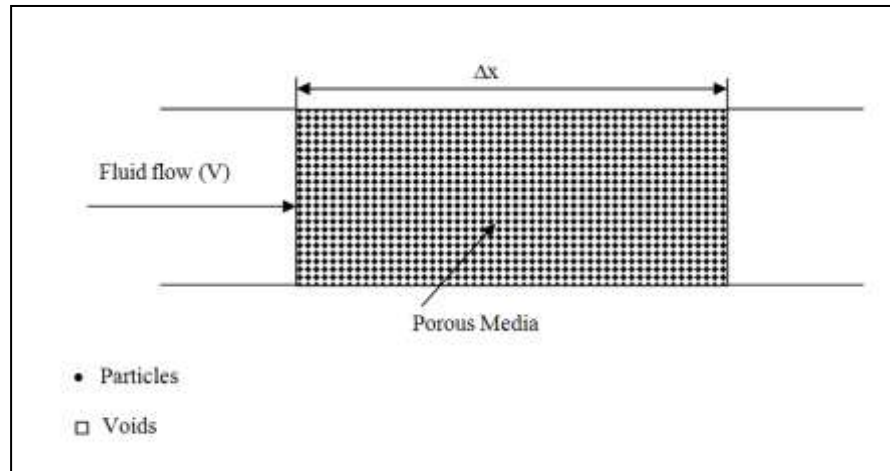


**Figure 4.4 Schematic of the fluid flow across the porous block [55].**

The pressure drop across the porous block is presented due to the friction between the particles and the fluid flow. This pressure drop can be obtained, as shown in Section 4.5.1 and Section 4.5.2.

#### **4.5.1 Darcy's law**

Darcy's law has been established to measure the pressure drop across the porous media, as follows:

$$\Delta P = \frac{-\mu}{\alpha} V \Delta x \quad (4.44)$$

Where ,

$\mu$ : is the viscosity of the fluid (kg/m. s)

$\alpha$ : is the permeability of the porous medium ( $m^2$ )

$V$ : is the axial velocity (m/s)



$\Delta x$ : is the thickness of the porous medium in x-direction.

Darcy's Law is limited just for the laminar flow (low Reynolds number) because the inertia resistance does not have any effect where the viscosity resistance is dominant [76].

In our simulation design, Darcy's Law has been implemented for the internal components to evaluate the permeability, which gives an indication for the viscosity resistance because the flow across these components has a low Reynolds number, around  $1 \times 10^3$ . Whereas, the inertial losses have been taken into account for the server, rack and the room levels, as described in Section 4.5.2.

#### 4.5.2 Inertial losses in porous media

The inertia loss term can be added for Darcy's law for the turbulence mode [76] and can be expressed as:

$$\Delta P = \frac{\mu}{\alpha} lV + \frac{1}{2} C\rho lV^2 \quad (4.45)$$

The first term in this equation represents the pressure difference due to viscous effect. Whereas, the second term represents the pressure difference due to inertia.

Where,

$\Delta P$  : is the pressure drop through the porous media (Pa)

$\mu$  : is the viscosity of the fluid (kg/m.s)

$\alpha$  : is the permeability of the porous media ( $m^2$ )

$l$  : is the thickness of the porous media (m)

$V$  : is the axial velocity (m/s)

$C$  : is the inertial resistance

$\rho$  : is the density ( $\text{kg/m}^3$ )

The server then can be simulated as a porous block. After that the porous blocks will be used instead of server blades inside the rack . It is shown from our analysis that the flow through the server and rack are in turbulent mode. Therefore, Darcy's Law is no longer applicable.

## 4.6 Fan modelling

In this section, the fan modelling of 1U server fan is described. The fan of the 1U server is directly attached at the server exhaust, as shown in Figure 4.5.

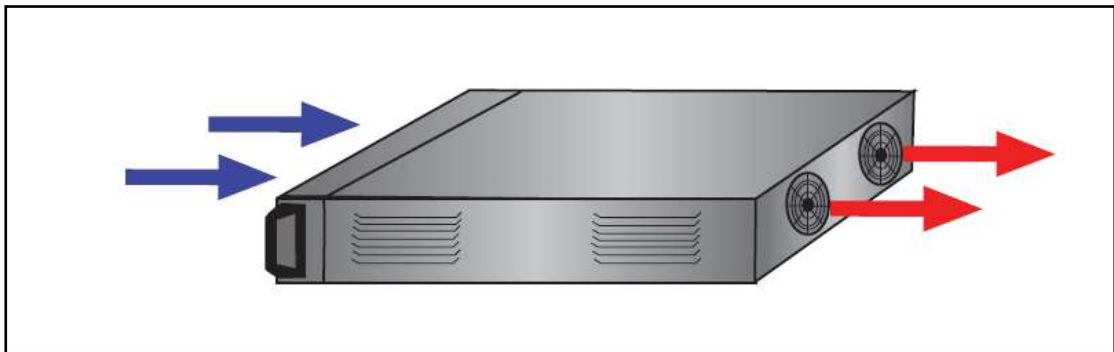


Figure 4.5 Location of the fan on the traditional server [32].

### 4.6.1 Fan modelling for the traditional rack server

The fan is attached at the server exhaust, as shown in Figure 4.5. The fan is considered as a drive force to suck the chilled air from the cold aisle and pass it through the server to carry out the dissipated heat. The fan specification is chosen from the Camair rotron company's website [77] and is considered to be the fan of

the traditional server in our research. The fan used in this research is represented in Tables 4.1 and 4.2, and Figure 4.6.

The fan is selected for the traditional servers with specification [77], as follows:

**Table 4.1 Electrical specification of studied fan [77].**

Electrical Specifications:	
Rated Voltage	115 VAC
AC Frequency	60 Hz
Power Supply	59.0 Watts
Line Current	0.49 Amps
Locked Rotor Current	1.35 Amps
Nominal Speed	3350 RPM

**Table 4.2 Mechanical specification of studied fan [77].**

Mechanical Specifications:	
Dimensions	6.93in x 4.41in
Weight	80.0 oz
Max Airflow @ 0 in H <sub>2</sub> O	330.0 CFM
Max Pressure @ 0 CFM	0.871 in H <sub>2</sub> O
Noise	65.4 dBA

Where CFM is cubic feet per minute.

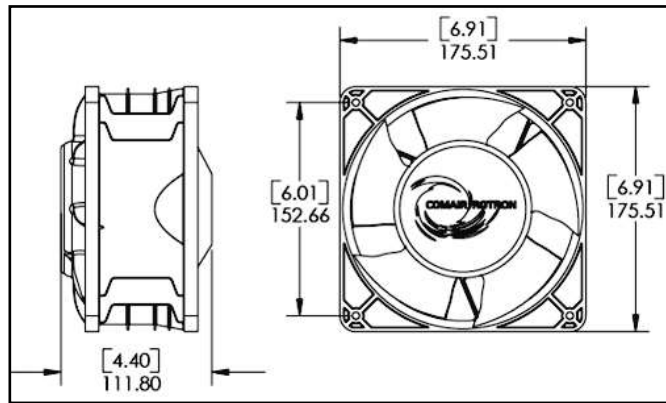


Figure 4.6 Fan drawing [77].

Table 4.3 Pressure distribution against the velocity for fan [77].

Velocity (m/s)	Pressure (Pa)
0.00	216
2.07	137
3.38	92
4.60	42
5.03	0

Table 4.3 can be represented as a polynomial profile between the pressure difference and the velocity, as follows:

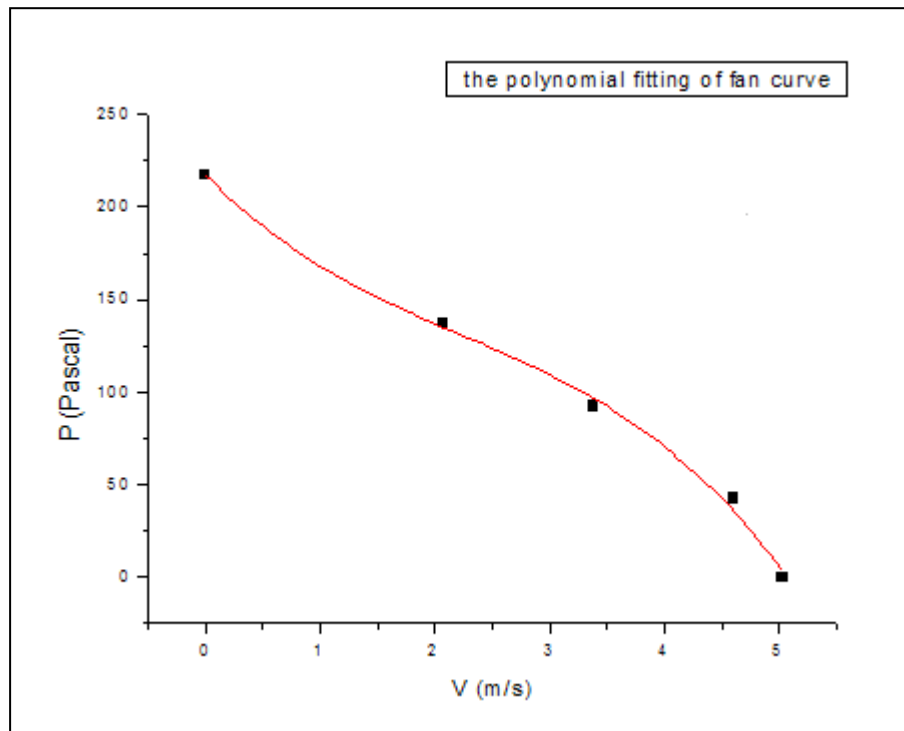


Figure 4.7 Polynomial fitting of fan curve.

Thus, the pressure of the fan can be represented by a polynomial of third order

$$\Delta P = 217.21 - 62.87V + 16.20V^2 - 2.413V^3 \quad (4.46)$$

The third order polynomial pressure drop is implemented in the Fluent software, where the fan curve is required. Only the coefficients are required as an input in Fluent.

### 4.6.2 Fan modelling for active back cooler

The fan modelling for the active back door has taken place in the Airedale Ltd. company. The pressure drop versus the velocity has been obtained, as per Table 4.4.

**Table 4.4 Pressure distribution against the velocity at 15000 RPM for active back door cooler fan.**

Velocity (m/s)	Pressure (Pa)
0.0	4350.0
9.2	2746.9
15.1	1847.9
20.5	849.0
22.5	0.0

The fan curve can be fitted as a third order polynomial, as in Figure 4.8:

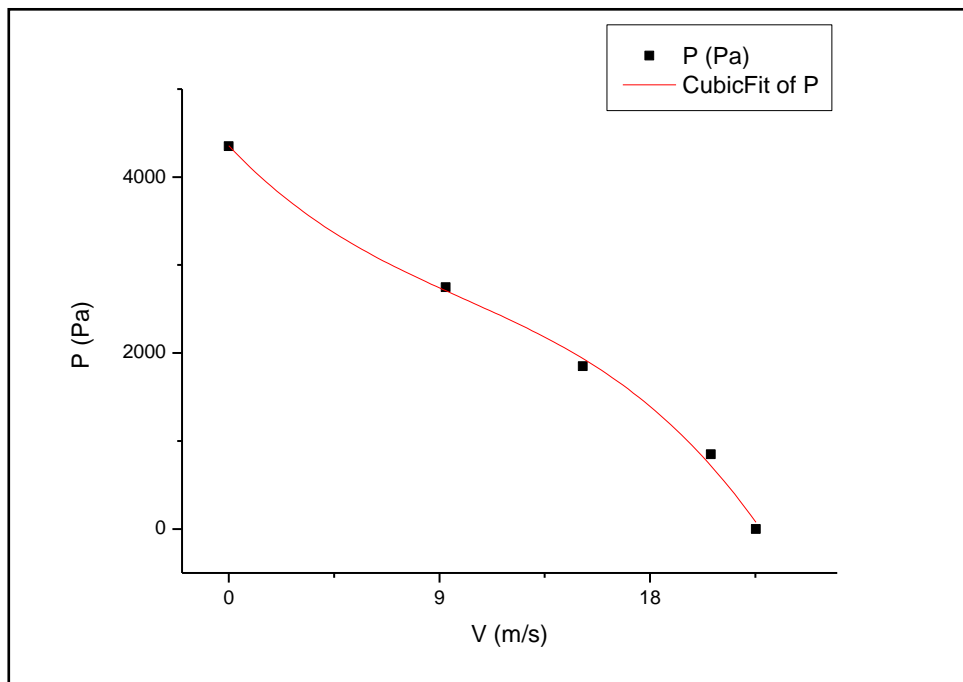


**Figure 4.8 Fitting curve of the pressure difference with respect to the fan velocity at 15000RPM for active back door cooler fan.**

Thus, the pressure of the fan can be represented as the polynomial of third order

$$\Delta P = 4354.91 - 281.55V + 16.2V^2 - 0.54V^3 \quad (4.47)$$

The above equation will be used to specify the fan boundary condition for the active back door cooler in the Fluent program. It is shown that the pressure drop for the active back door cooler fan is bigger than the pressure drop for each fan that is used in the server; this is because the fan that is used for the active back door cooler is just one big fan compared to the fan for each server.

#### **4.7 CFD analysis of server blade**

The numerical method for the data centre is described in detail in sections 4.2 and 4.4. Also, a new approach, which is the porous media model, has been explained in section 4.5 to represent the server blade and the rack inside data centres. Thus, in this section, CFD analysis will be implemented by using both Gambit and Fluent programmes to simulate the server as a porous model, and then will be compared with the experimental data. Thermodynamic properties, such as temperature distribution, pressure across the server and the velocity field, will be obtained for both the 1U server and the blade server. The server is considered to be a main component of the rack inside the data centre; whereas, other components, such as switches and storage, are used to connect between the servers inside the rack and to manage the digital information, respectively [14]

In this study, both switches and storage components will be assumed to be porous blocks where the air flows through them. The storage component is treated as a porous block with lower permeability than the switch component and this assumption takes place because the storage component is more dense than the switch component. In this chapter, the server component is the most considerable component inside the rack. The new technique will be presented, which is a porous approach to simulate the server, such that it verifies both temperature and pressure differences across the server. In such, the experiment has been done to test temperature and pressure drops across the server. Then the agreement between the CFD analysis and the experimental work has been tested. Both 1U server and blade server have been included in this study. The study is carried out with the server of a mother board model Thunder K8SPro (S2882) [78] and the HP blade server [79], as shown in Figure 4.9 and Figure 4.10 respectively. The simulation of blade server for the Hp C7000 is conducted, as this type of blade server is available at Leeds University. The above models for both 1U server and blade server have been selected because these types are widely used for the medium load data centre.

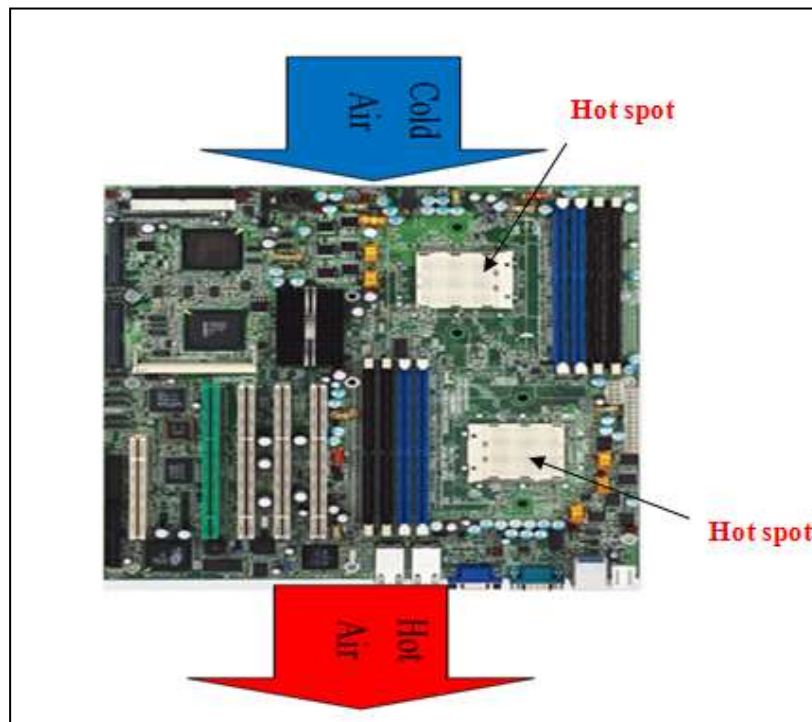


Figure 4.9 Thunder K8S Pro S882 server mother board [78].



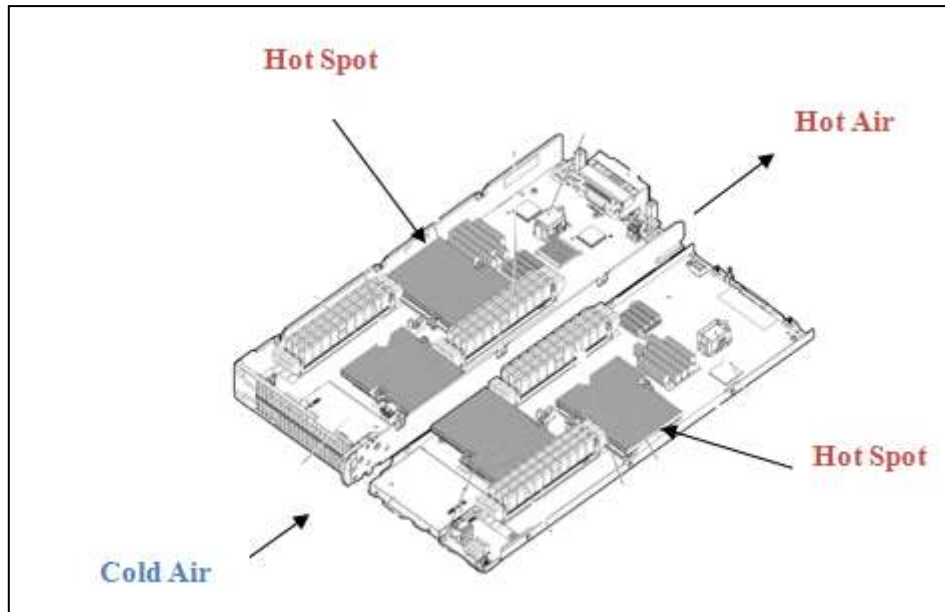


Figure 4.10 Hp G7 server blade [79].

## 4.8 Traditional server (1U server)

The 1U server (4.2cm×60cm×1.1 m) model Thunder K8S Pro S882 is chosen for this study because this type of server is available at Leeds University. Furthermore, the 1U servers are almost identical in their inside components. This type of server dissipates around 300 W of heat. In this section, discussion regarding the traditional server is broken down into two main parts. The first part discusses the simulation of internal components of the server, whereas the second part discusses the whole server's geometry.

### 4.8.1 CPU analysis in the 1U traditional server

Several papers were written to study CPU thermal analysis, such as Mohan and Govindarajan [80], in which they discussed the comparison between the experimental data and the CFD analysis to detect the temperature profile of the CPU

with changing the CPU geometry. Furthermore, cooling analysis of the CPU in consideration of the CPUs geometry has been done by Arularasan and Velraj [81] to carry out the optimization design for the heat sink (CPU). With respect to the server analysis, Choi et al. [82] conducted 3-D CFD by using Phoenics software analysis to study the temperature profile inside the server rack. In such, the ThermoSat which is a thermal modelling tool (software tool), which is used to represent the temperature profile for the internal components of the server [82]. Moreover, experimental works have been done to validate the CFD results. It has been found that the temperature inside the server in different points for both experimental data and CFD analysis are close to each other, where the error is just 9%.

A dual processor server has been selected for this study. The emergence of using Thermo-Stat is due to the difficulty of fitting the thermal sensor at the right place inside the server. Thus, use of the LVEL turbulence model is suggested, which indicates that the model needs the nearest wall distance ( $L$ ), the local velocity ( $VEL$ ), and laminar viscosity to calculate the effective viscosity and to present the flow inside the rack server [82]. The LVEL turbulence model is used to represent the flow at a low Reynolds number. The concept of this model is to use the Algebraic equation by solving the Poisson equation in order to obtain the maximum local length scale and local distance to the nearest wall. After that, the Reynolds number is obtained by using the above length scales and local speed. Finally, the effective viscosity (turbulence viscosity) is solved by solving the Reynolds number and the universal law of the wall.

In this section, the internal components of the 1U server are analyzed and the CPU component is chosen as an example. The main constraint from the cooling point of view are the pressure and the temperature differences across the

components. Therefore, the internal components such as CPU, memories (Dimms) and power supply are simulated to meet these constraints. Due to this, the porous media model is tested to ascertain if it satisfies the temperature and the pressure differences constraints or not. The real CPU has been compared with the porous CPU. The temperature, the pressure and the velocity fields have been obtained in this study.

CPU simulation is carried out in this study. The actual CPU is compared with the approximation method by assuming the CPU to be a porous model. Both actual and approximation CPUs are built by the Gambit Software with geometry of 7cm in width, 2.5 cm in height and 10 cm in length, as shown in Figure 4.11.

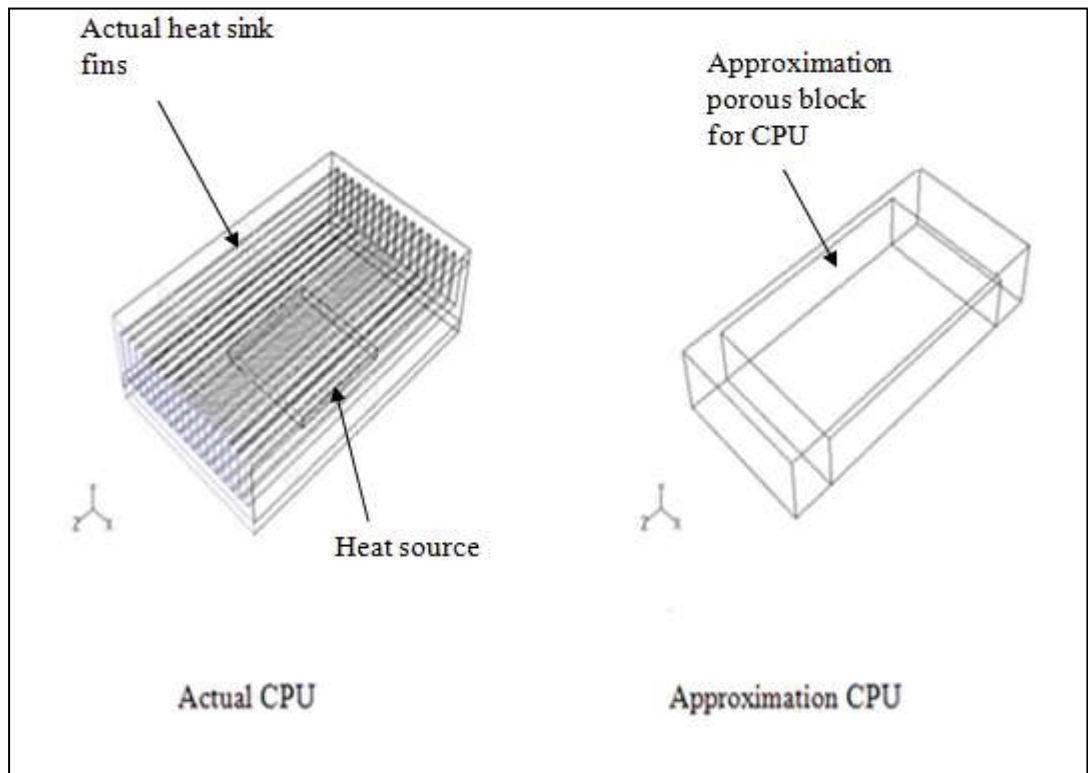


**Figure 4.11 Actual and approximated CPU geometries.**

The permeability of the CPU could be calculating in order to apply the porous media model. The value of the permeability can be obtained by equalizing

the pressure drop across the rectangular channel and Darcy's Law. The rectangular channel represent the geometry of the actual CPU inside the server.

The pressure drop across the channel, which represents the actual case, can be expressed as per Michael et al. [83], as shown in Figure 4.12. This study has been done to compare between the pressure drops in both the empty channel and the channel with a bubble.

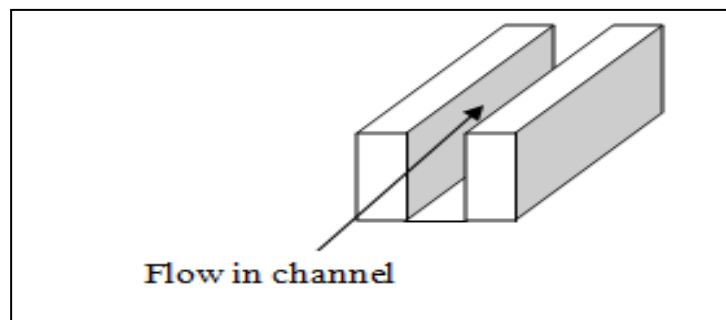


Figure 4.12 Diagram for the flow-through channel

$$\Delta P = \frac{a\mu QL}{WH^3} \quad (4.48)$$

Where

a : is the dimensionless parameter

$$a = \left[ 1 - \frac{192H}{\pi^5 W} \tanh\left(\frac{\pi W}{2H}\right) \right] \quad (4.49)$$

$\mu$  is the air viscosity (kg/m.s), Q is the volumetric flow rate (m<sup>3</sup>/s), Q=VA, L is the length of channel (m), W is the Width of the channel (m), and H is the height of the channel (m).

On other hand, the Darcy pressure drop, which represents the approximation method, can be written as:

$$\Delta P = \frac{\mu}{\alpha} VL \quad (4.50)$$

Where  $\alpha$  is the permeability ( $m^2$ ) and  $V$  is the linear velocity (m/s).

The permeability value in Z direction can be obtained from equations (4.48) and (4.50) with the CPU geometry values, as mentioned above, and it is equal to  $2.9 \times 10^{-7} m^2$ .

the Nusselt number [84] can be expressed as:

$$Nu = \frac{hS}{k} \quad (4.51)$$

Where  $h$  is the heat transfer coefficient ( $W/m^2 \cdot K$ ),  $S$  is the spacing between the plates (m) = 3mm and  $k$  is the thermal conductivity ( $W/m.K$ ).

The Nusselt number of the vertical plate with constant heat flux by the processor [52] can be expressed as:

$$Nu = \left[ \frac{48}{Ra_s(S/L)} + \frac{2.51}{(Ra_L(S/L))^{0.4}} \right]^{-0.5} \quad (4.52)$$

Where  $L$  is the length of the plate (m),  $S$  is the spacing between the fin (m),  $T_f$  is average temperature (K),  $T_\infty$  is the surrounding temperature (K),  $q$  is the heat flux ( $W/m^3$ ),  $\nu$  is Kinematic viscosity ( $m^2/s$ ),  $\beta$  is Volume expansion coefficient ( $1/K$ )

$\beta = \frac{1}{T_f}$ ,  $T_f = \frac{(T_s + T_\infty)}{2}$ , and  $Ra$  is the Rayleigh number and can be written as

$$Ra_s = \frac{g\beta q S^4}{k\nu^2} Pr, \quad Ra_L = \frac{g\beta q L^4}{k\nu^2} Pr.$$

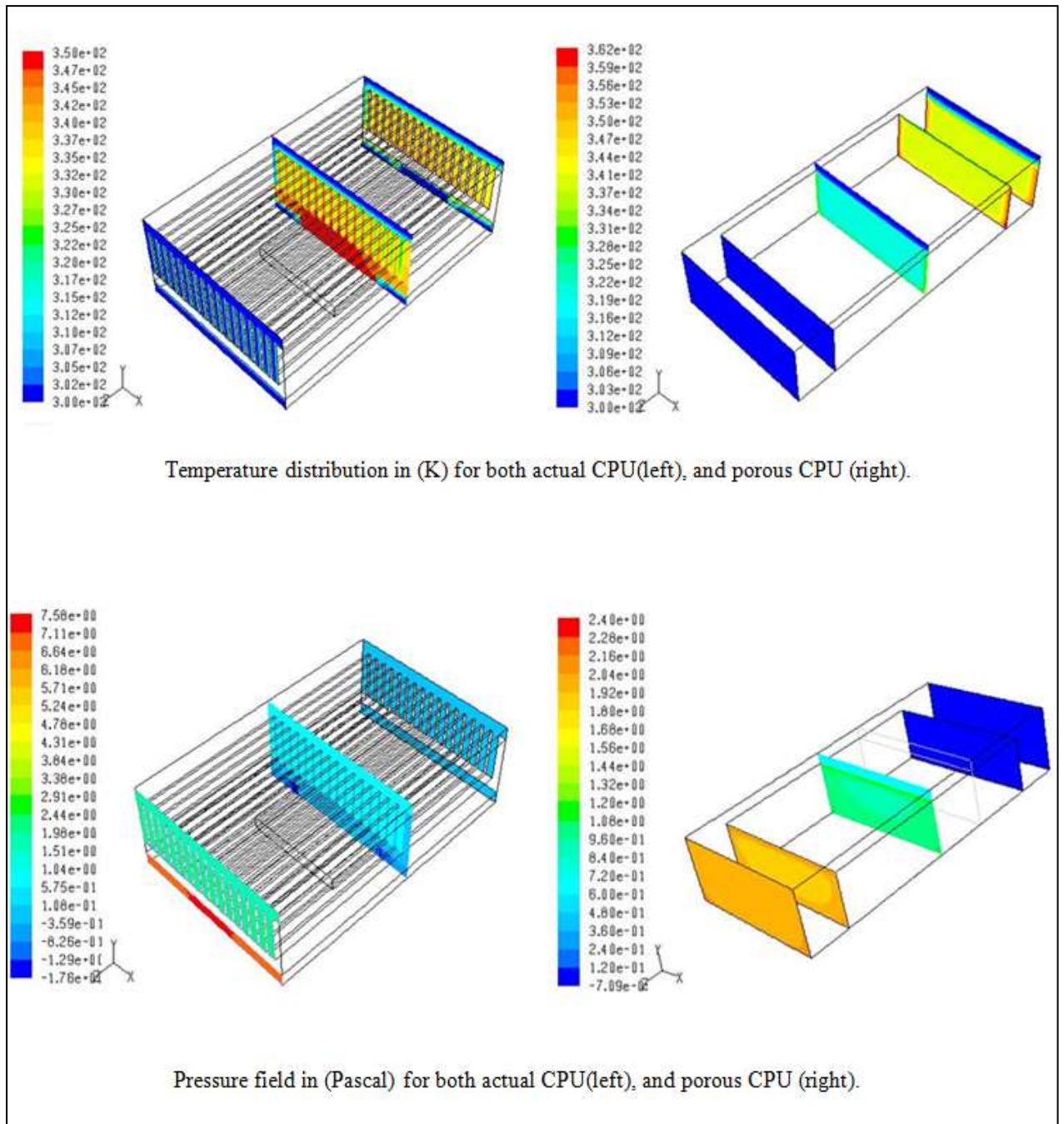
The heat transfer mode between the processor and the CPU is conduction with constant processor temperature at  $50^\circ C$ . The value of thermal conductivity ( $k$ ) has been chosen for the Aluminium and it equals to  $237 W/m.K$ .

## **Results and Discussion**

### **CPU thermal analysis**

The numerical solution to solve temperature, pressure and velocity fields inside the CPU of the server has been developed by applying the porous approach. The porous flow analysis, with the permeability of  $2.9 \times 10^{-7} \text{ m}^2$  in the Z direction, has been implemented to simulate flow through the CPU; whereas, permeability in both the X and Y direction is assumed to be  $1 \times 10^{-20} \text{ m}^2$ . This assumption for the previous permeability values has been done because in real situations, the air has the ability to flow in the Z direction with a neglected flow in both X and Y directions, as shown in Figure 4.14. Figure 4.13 shows the comparison of CFD study between the actual and porous flow model to simulate the CPU. Figure 4.13 shows the comparison between the real CPU and the porous CPU, with respect to the temperature distribution and the pressure field. It is shown that there is good agreement between both cases in temperature distribution. In this study, the surface at the CPU middle is chosen. It is shown that the temperature at the middle surface for both CPU cases equals approximately 330 K. Similarly, the pressure has been obtained for both cases and also shows good agreement. The CFD analysis has been implemented to compare between the methods by using Gambit software to build the geometry and Fluent software to obtain the results. The processor dissipates 89 W inside the server, so that the heat from the processor is transferred to the heat sink by conduction mode for the real case. Whereas, in the porous flow model, the heat generation divided by the porous volume is added as a source term in the energy equation. Figure 4.14(a), Figure 4.14(b) and Figure 4.14(c) show a good agreement between the actual case (red line) and the assumption case (black line) with respect

to temperature, pressure and the velocity fields, respectively. In such, the assumption of the CPU as a porous media is a good approximation to simplify the



actual geometry of the CPU.

Figure 4.13 Comparison between the actual analysis and approximation analysis of the CPU.

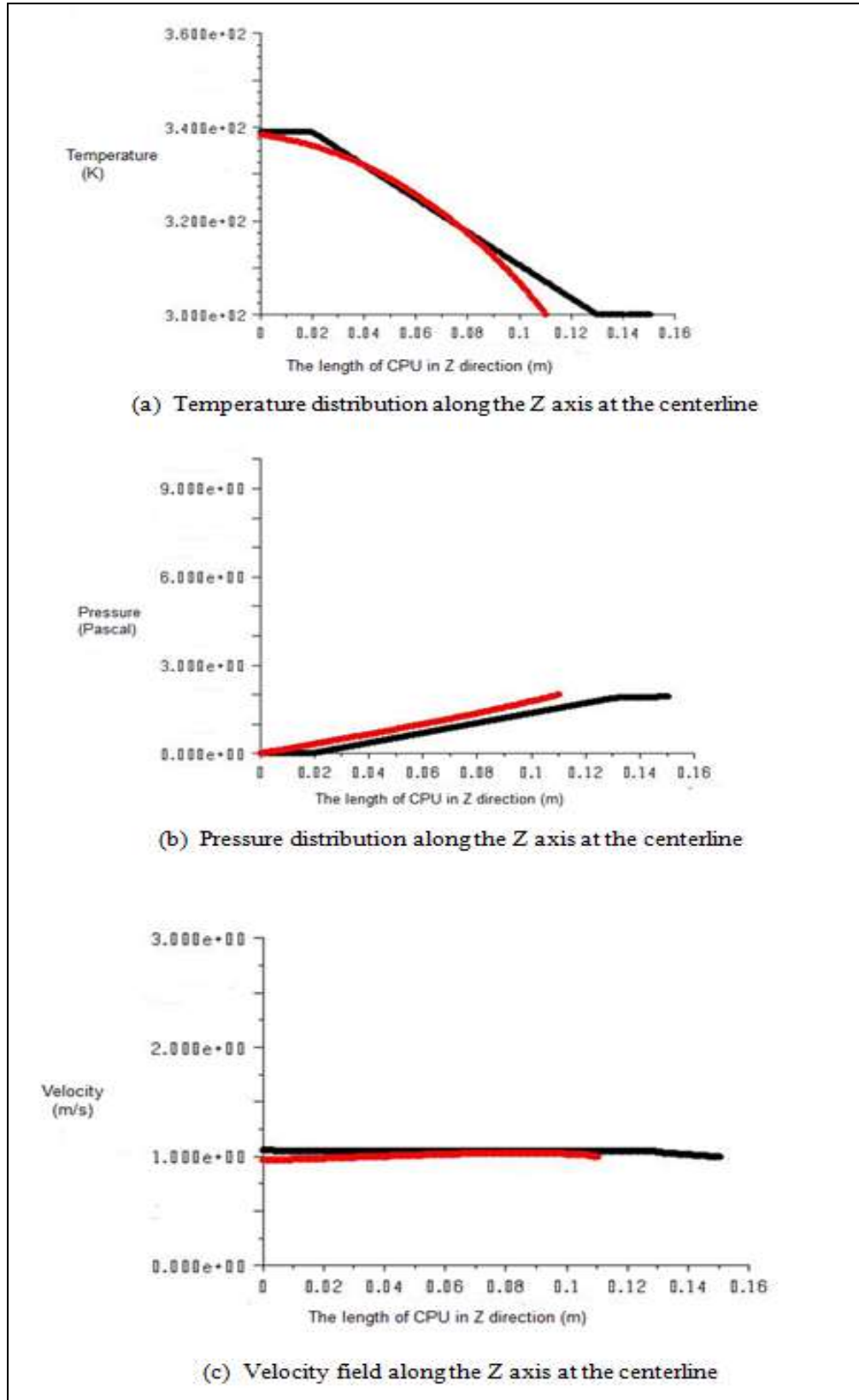


Figure 4.14 Temperature, pressure and velocity gradient for both actual and approximation CPUs in the longitudinal direction (Z) of the CPU.



Figure 4.14 (a) shows the temperature distribution across the CPU centre line. The red line indicates the real CPU case and the black line indicates the porous CPU. It is shown that the maximum temperature equals 340 K and it occurs at the CPU inlet; this is because at the CPU inlet, the cooled air does not take a reasonable time to reduce the fin temperature and the temperature reduces as the air goes through the fins. Whereas, the static pressure in both cases builds up until it reaches 2.5 Pa, as shown in Figure 4.14 (b). Thus, the porous media approach shows good agreement with the real situation. Therefore, the porous approach could be used to simulate the internal parts of the server.

## **4.8.2 Server Modelling**

### **Actual server**

The actual server schematic based in the real structure is shown in Figure 4.15. The actual server has CPUs, DIMMs, fans and a power supply. It is shown from in Section 4.8.1 that the CPUs can be simulated as a porous media with a permeability of  $2.9 \times 10^{-7} \text{ m}^2$  in the Z direction and  $1 \times 10^{-20} \text{ m}^2$  in both X and Y directions. Similarly, the DIMMs and power supply have been assumed to be porous media models. In this study, the fan effect is ignored to simplify the model and this assumption does not affect the purpose of the validation study. Furthermore, the tunnel has been attached to the actual server to represent the experimental situation, as shown in Figure 4.16.

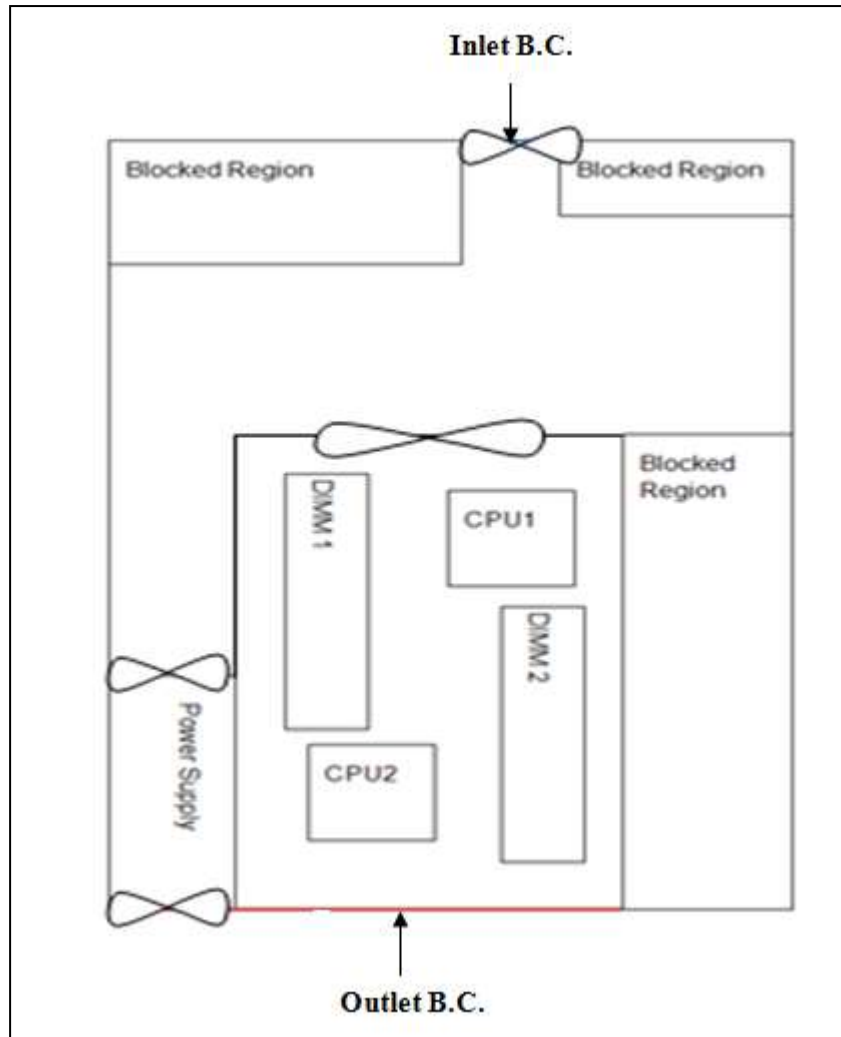


Figure 4.15 The block diagram of the server's internal parts.

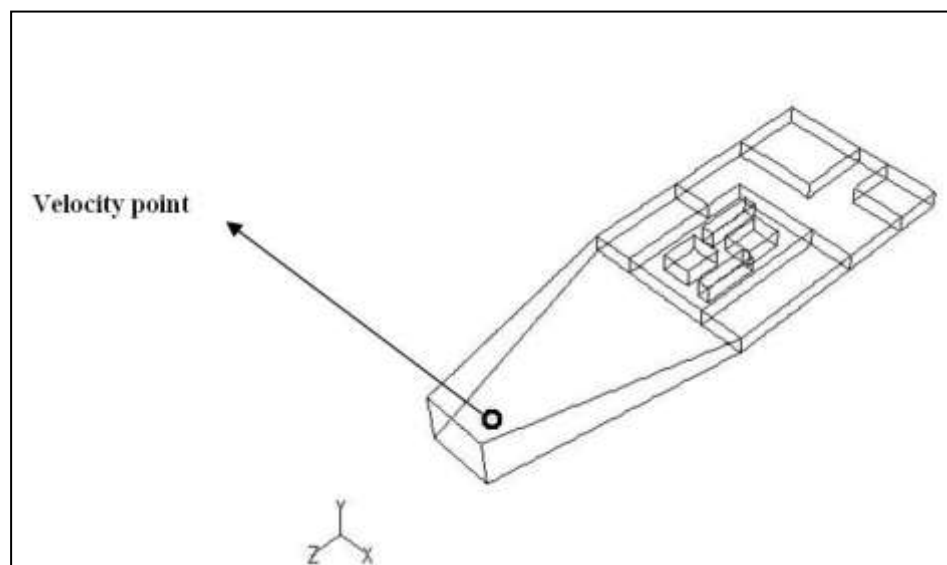


Figure 4.16 Experimental set-up geometry for the 1U server.

Different pressure drop values across the server have been used to detect the point velocity as the experimental setup was done by a fellow PhD student (private communication) [85], as shown in Figure 4.16. The velocity is measured 0.48m away from the server outlet at the centre line. The aim of this study is to simulate the actual server rack as a porous block by comparing between the CFD analysis and the experimental velocity values at different pressure drop across the server. Three turbulence models with respect to k-ε model have been tested for the 1U server, as shown in Figure 4.15. The aim of this study is to identify the most suitable k-ε model that provides good agreement with the experimental data, and to identify whether the porous media approach can be used. CFD analysis has been created to implement these models. The turbulence intensity for both inlet and outlet are assumed to be equal to 5% and 1%, respectively. Furthermore, the different turbulence intensity values are assigned to check if either of the results change or not. Whereas, the hydraulic diameter for the inlet and the outlet are 0.05508m and 0.12m, respectively. The velocity field for different pressure drops is obtained to compare with experimental data.

It is necessary to define the hydraulic diameter for the inlet and the outlet to process both in the Fluent program. The hydraulic diameter can be defined as

$$D_h = \frac{4A}{P} \quad (4.53)$$

So the hydraulic diameter at the inlet and the outlet are 0.05508m and 0.12m, respectively.

### **Approximation server**

The relationship between the velocity profile and the pressure gradient across the server has been fitted as a second order polynomial by using the RNG k- $\epsilon$  model as

$$\Delta P = -5.9202V + 6.3966V^2$$

Whereas, the fitted curve for the experimental data has been expressed as

$$\Delta P = -5.2743V + 6.8206V^2$$

The second order polynomial pressure equation is equivalent to the equation of the pressure drop for the porous media, which describes Darcy's Law plus the inertial loss term, as in the following equation:

$$\Delta P = \frac{\mu}{\alpha} lV + \frac{1}{2} C\rho lV^2 \quad (4.54)$$

Where  $\Delta P$  is pressure drop through the porous media (Pa),  $\mu$  is the viscosity of the fluid (kg/m.s),  $\alpha$  is the permeability of the porous media ( $m^2$ ),  $l$  is the thickness of the porous media (m),  $V$  is the axial velocity (m/s),  $C$  is the Inertial resistance and  $\rho$  is the density ( $kg/m^3$ ). In such, the values of both permeability  $\alpha$  and inertial resistance  $C$  are equal to  $1.889 \times 10^{-6} m^2$  and 20.46 m, respectively.

### **4.8.3 Boundary Conditions**

The inlet boundary condition for actual and approximation servers are assumed to have an intake pressure inlet of 0 Pa gauge pressure. With respect to the outlet boundary condition, it is assumed that the static pressure is constant over the outlet. Different pressure values have been assigned for the outlet condition to obtain the velocity field in order to sketch the relationship between the pressure and

the velocity field. All other surfaces are assumed to be no-slip walls, as shown in Figure 4.17.

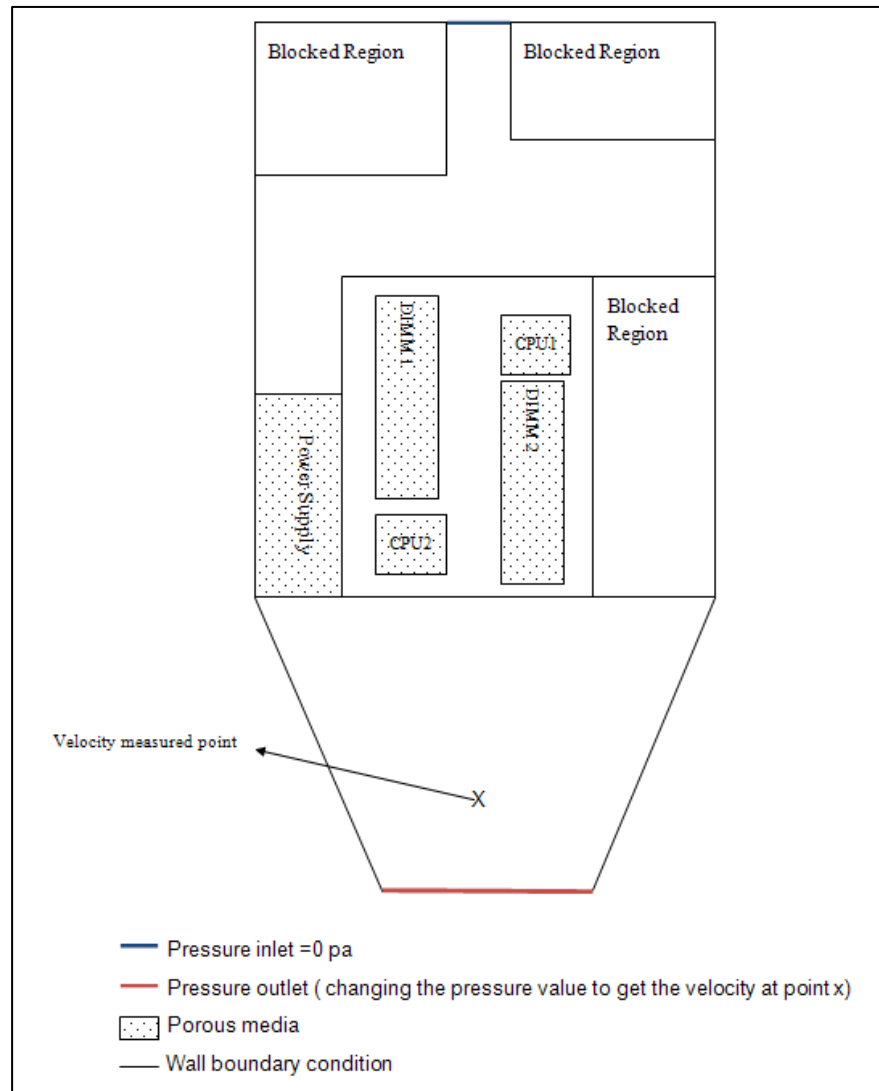


**Figure 4.17** The boundary condition used in the CFD analysis of a 1U server rack.

### Server air flow analysis

In this section, three turbulent models with respect to the k- $\epsilon$  model have been tested for the server rack, as shown in Figure 4.16. The aim of this study is to simulate the server blade as a porous block by identifying the most suitable k- $\epsilon$  model that provides good agreement with the experimental data. CFD analysis has

been created to implement these models. The turbulence intensity for both inlet and outlet are assumed to be equal to 5% and 1%, respectively, as per the experiment procedure. Also, the additional range of the turbulent intensities are included in this study, which are 1% at the inlet and 1% at the outlet, 10% at the inlet and 1% at the outlet, 5% at the inlet and 5% at the outlet, 10% at the inlet and 5% at the outlet, and 10% at the inlet and 10% at the outlet. Whereas, the hydraulic diameter for the inlet and the outlet are 0.05508m and 0.12m, respectively. The turbulence intensities are tested for a range between 1% and 10% to detect how the solution is sensitive for this parameter. The velocity point for different pressure drops is obtained to compare with the experimental data.

#### **CFD modelling of the server**

A tunnel has been attached at the exhaust of the actual server in order to represent the experimental situation. The length of the tunnel is assumed to be equal to 0.575m, whereas the velocity is measured at 0.48m from the sever exhaust, as in the experimental setup. The point velocities for different pressure drops across the server have been obtained by using the standard  $k-\varepsilon$  , RNG  $k-\varepsilon$  and Realizable  $k-\varepsilon$  models. The velocity field for different  $k-\varepsilon$  models has been obtained, as shown in Table 4.5. The velocity field is compared with the velocity field that was obtained from the experimental procedure. It is shown that the RNG  $k-\varepsilon$  model is the best behaviour and gives a good agreement with the experimental data compared with other  $k-\varepsilon$  models.

**Table 4.5 Velocity for different k- $\epsilon$  models against the pressure drop.**

<b>Turbulence model</b> <b><math>\Delta P</math> (Pa)</b>	<b>Standard k-<math>\epsilon</math></b> <b>model</b> <b>(m/s)</b>	<b>RNG k-<math>\epsilon</math></b> <b>model</b> <b>(m/s)</b>	<b>Realizable</b> <b>k-<math>\epsilon</math> model</b> <b>(m/s)</b>	<b>Experimental</b> <b>Data</b> <b>(m/s)</b>
25	1.3	1.5	1.8	2.31
50	2.6	3.5	3.3	3.10
100	4.5	4.7	5.1	4.41
160	9.2	5.5	7.7	5.04
200	10.9	6.0	8.95	5.71

The point velocities for different pressure drops across the server have been obtained by using the RNG k- $\epsilon$  model. The velocities have been tested for the following range of the turbulent intensities at the inlet and the outlet as shown in Table 4.6 to detect the effect of changing the turbulent intensities on the point velocity.

**Table 4.6 Turbulent intensity specification for both inlet and outlet.**

<b>Case</b>	<b>Turbulent intensity at the inlet</b>	<b>Turbulent intensity at the outlet</b>
1	1%	1%
2	5%	1%
3	5%	5%
4	10%	1%
5	10%	5%
6	10%	10%

It is shown in Figure 4.18 that as the turbulent intensity at the inlet increases, the velocity slightly increases and vice versa; whereas, the turbulent intensity at the outlet does not have any significant effect on the velocity. Therefore, turbulence intensity does not have any significant effect on the results in this specific case.



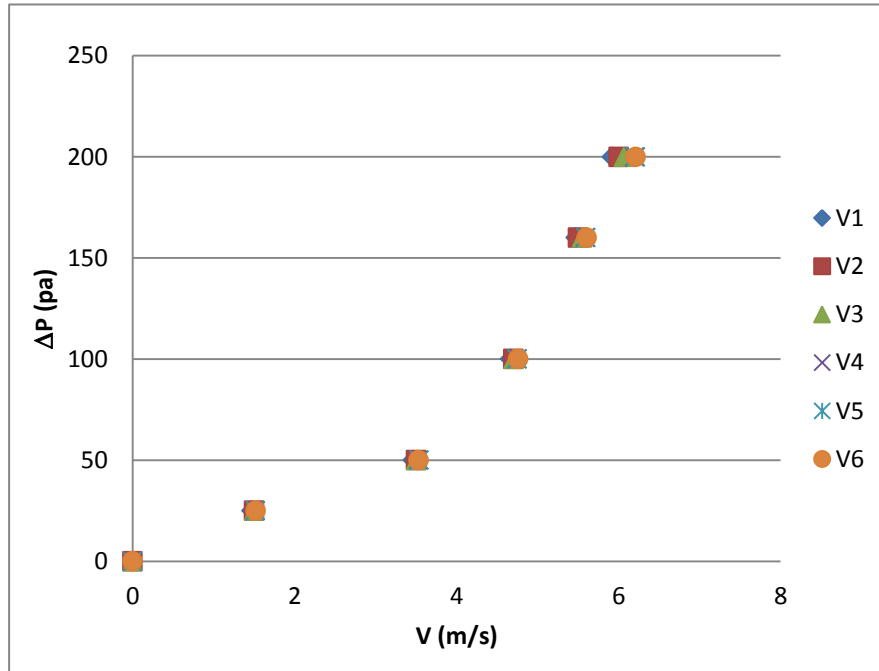


**Figure 4.18 Velocity versus the pressure drop for different turbulence intensities.**

Figure 4.19(a), Figure 4.19(b) and Figure 4.19(c) show the comparison between the k-ε models and the experimental data, and all points are fitted as second order polynomials. Figure 4.19(a) shows the comparison between the standard k-ε model and the experimental data for the pressure difference against the point velocity. It is shown that the trend between the two curves are totally different. The intersection point between the two curves at the velocity point equals to 4 m/s, where the pressure difference equals 75 Pa. Figure 4.19 (b) shows the relationship between the pressure difference across the server and the velocity point in the tunnel for both the Realizable k-ε model and the experimental data. It is shown from the Figure that the trend behaviour for this k-ε model shows greater improvement than the behaviour in Figure 4.19(a) for the standard k-ε model.

The intersection point between the Realizable  $k-\varepsilon$  model and the experimental data occurs at a velocity of 3 m/s and the pressure difference equals 50 Pa. Finally, in Figure 4.19 (c), it is shown that the RNG model is the best model to represent the experimental data in trend. The reason for this is that the RNG  $k-\varepsilon$  is the most suitable model for the forced convection with low turbulence level [78]. It is shown from previous studies [82] and [86] that the Reynolds number for the flow through the electrical components is low, such that the turbulence level inside the server is low. As shown by Zhang [72], the RNG is the best model for this specific situation. The RNG  $k-\varepsilon$  model is suitable turbulence model to represent the forced convection, because the fan is used at tunnel exhaust, with low Reynolds number as in this thesis. This is due to usage of modified equation of dissipation and the constants that is used in the two partial differential equations to calculate the kinetic energy ( $k$ ) and the dissipation rate ( $\varepsilon$ ).

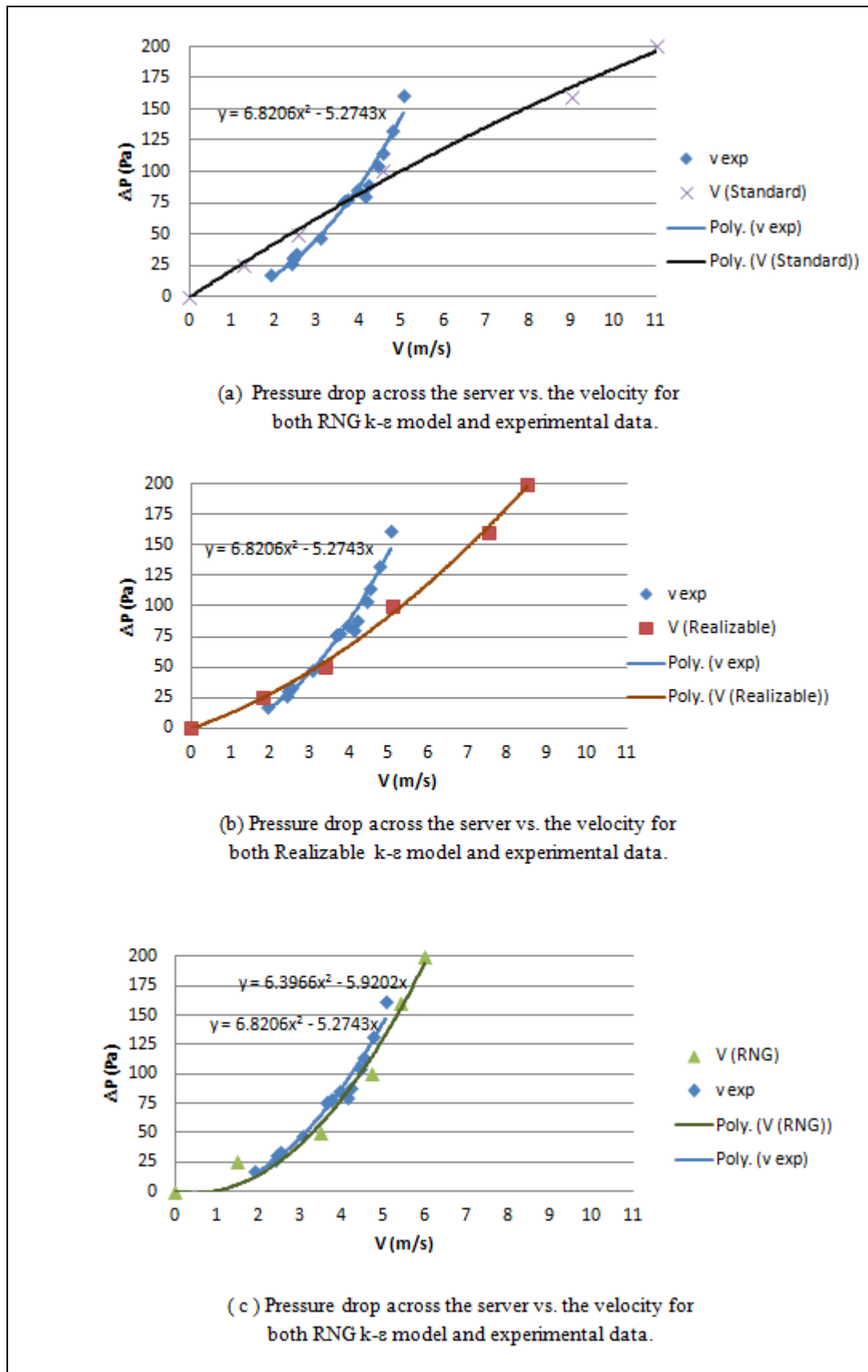


Figure 4.19 The comparison between k-ε models and the experimental data for the server.

So the porous media technique can be implemented for the server blade due to the good agreement between the CFD analysis of the actual server and the experimental data.

The solution domain for this study is specified by using 470590 cells and 926450 nodes. The mesh study has been done for this case to ensure that the mesh independence is achieved and does not affect the results. The mesh study of the 1U server blade has been done as follows in table 4.7. The testing of this problem is the velocity point at  $\Delta P=200$  Pa for RNG k- $\epsilon$  model as shown in Figure 4.20 .

**Table 4.7 Number of cells vs. the velocity point for 1U server blade.**

<b>No. Of Cell</b>	<b>Velocity point (m/s)</b>
335010	4.92
371020	5.59
431030	5.93
470590	6
512010	6
550300	6

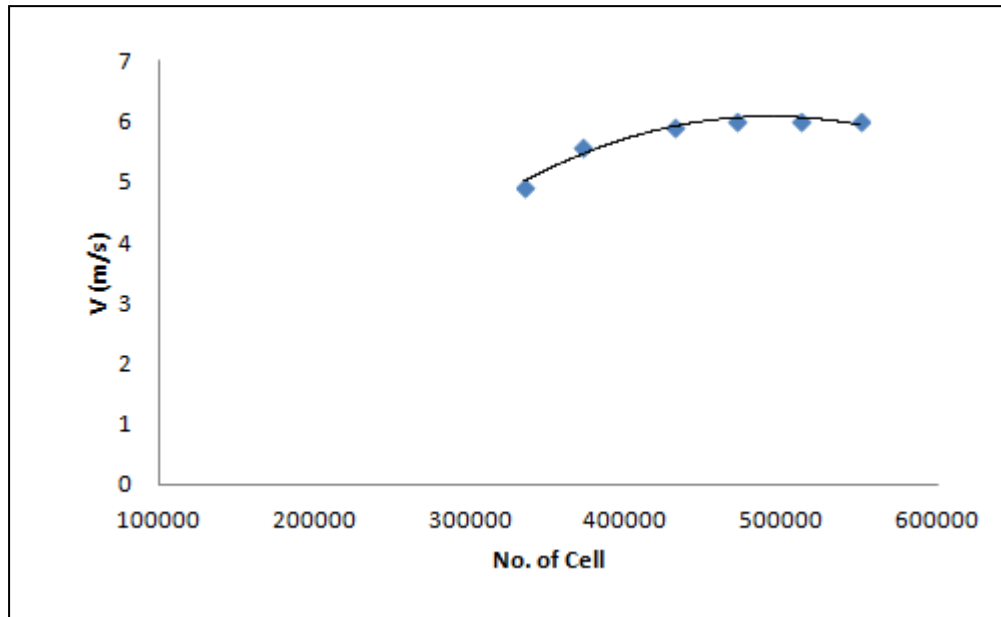


**Figure 4.20 Mesh independence study for 1U server blade.**

It is shown from Figure 4.20 that the number of cells that were used to solve the problem was 470590. Therefore, the number of cells that were used is the right choice because after increasing the number of cells, the velocity point remains constant.

#### **Temperature difference across the server.**

In this study, the temperature difference across the server has been measured by experimental work and compared with CFD analysis. It is shown from both Figure 4.21 and Table 4.8 that the temperature measurement from the experimental work is in good agreement to the temperature, which is measured by CFD analysis. Now both pressure drop and temperature difference across the server are validated with experimental data, so that the porous media approach can be used for this type of server.

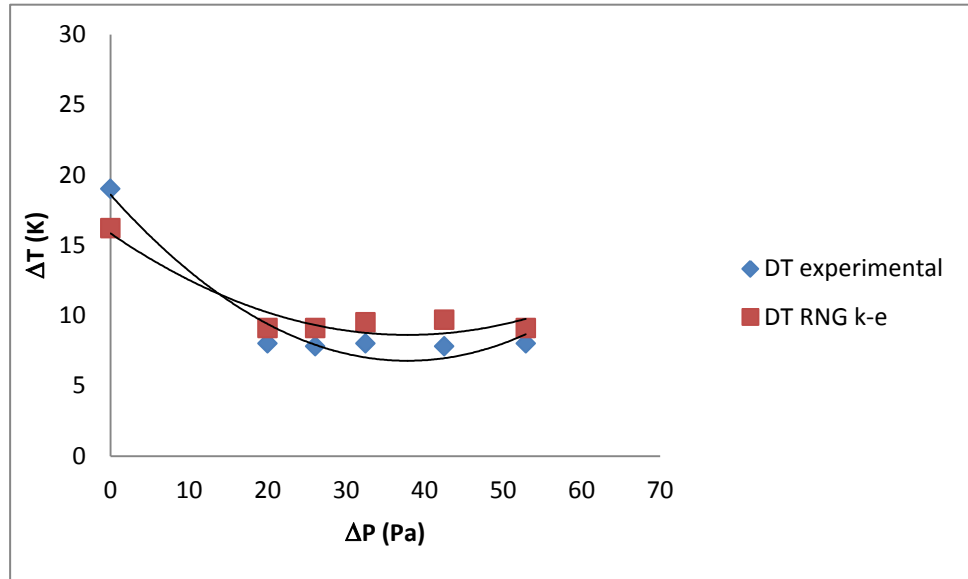


**Figure 4.21 Comparison between experimental measurements and CFD analysis with respect to the temperature difference across the server.**

**Table 4.8 Comparison between experimental and CFD (RNG k-ε model) with respect to the temperature difference across the server.**

$\Delta T$ (K) $\Delta P$ (Pa)	Experimental temperature difference (K)	CFD (RNG k-ε model) temperature difference (K)
52.9	8	9.1
42.5	7.8	9.7
32.5	8	9.5
26.1	7.8	9.1
20	8	9.1
0	19	15

## 4.9 Blade server

The difference between the blade server and 1U server in the dimension and the dense of the internal components. The thickness of the 1U server is equal 4mm. Whereas, the thickness of blade server is higher and it is equal approximately 5 mm or more depend on the dense of the internal components. Moreover, the blade server is more in dense of the internal components than 1U server. The fan is existing in each 1U server. Whereas, the blade server doesn't have any fan, so the fans are located at the chassis which hold the blade servers, Blade server chassis [87] can be defined as a chassis that contains the complete computer panel with all necessary parts, such as the processer and memory boards. The blade server has been used instead of the rack server for the following reasons:

1. Space limitation, where some elements such as cables and the bulk volume of rack in the traditional server rack can be eliminated by using the blade server. Therefore, a high number of blade servers can be used in the data centre.
2. Cooling, as the chassis provides the cooling facility to the blades via the fans and these fans are connected to the control system to detect the temperature values. In such, the fan will operate when the temperature increases above a certain value (25°C), and this is mean that the fans will operate in the intermittent mode. As a result, the chassis will consume less power than the traditional rack server, with more cooling efficiency.
3. Hot swapping. This is the ability to add or remove and replace the units without powering off the device and this concept is applicable in the blade server. In such, the usage of the blade inside the chassis is dependent on the

demand of each blade and this concept provides advantages from the maintenance point-of-view, so maintenance can be done for each blade without affecting the other blades.

The advantages of introducing the blade servers to the data centre were discussed by Intel [88]. It is claimed that there are a lot of significant benefits that can be achieved by using the blade servers, such as:

- Lower price than the traditional rack server.
- Lower maintenance and operation cost than the traditional server.
- Lower cooling and power requirements, as shown in Figure 4.22.
- Saving space inside the data centre.

Therefore, the usage of a blade server is highly recommended due to the above benefits.

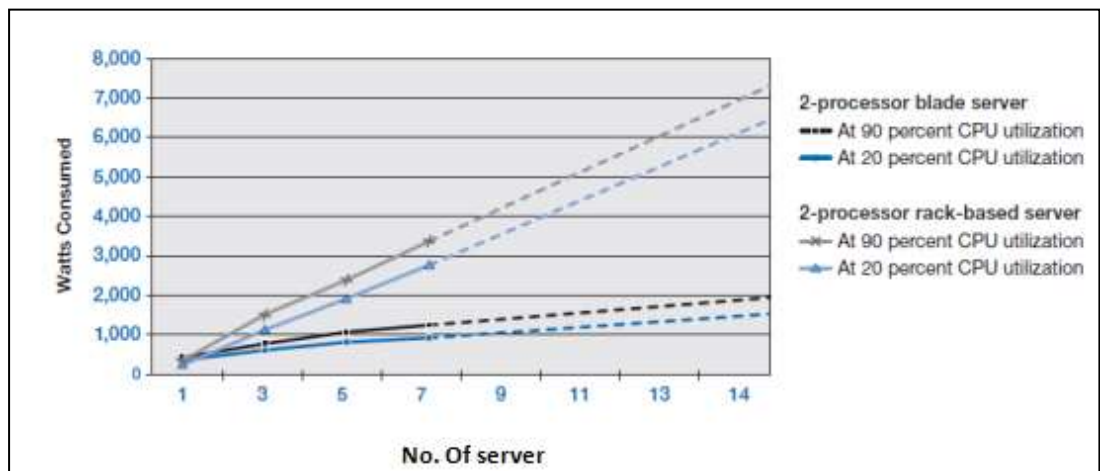


Figure 4.22 Power consumption for both blade and rack servers with two processors [88].

However, the disadvantages of blade servers can be summarized by stating that the blade server system has an expensive configuration and the blade server needs a large amount of cooling to reduce the high temperatures produced by the blade server chassis compared with the traditional rack server. Furthermore, due to



the high density of blade servers inside the chassis, high-speed fans are required, leading to noise problems [88].

#### 4.9.1 HP server modelling

The aim of this section is to simulate the HP blade server using the porous flow modelling approach. CFD analysis will be done for the HP blade server. The HP blade server, as shown in Figure 4.23, is built by using Gambit software, as shown in Figure 4.23.

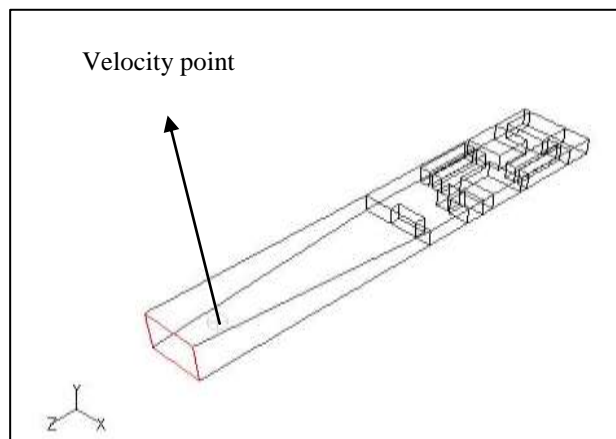


**Figure 4.23 HP blade server geometry with attached tunnel [77].**

The RNG k- $\epsilon$  model has been implemented to obtain the velocity field for the HP server. This is used because it provides excellent agreement with experimental data for the traditional server, as shown in Section 4.8.2.

#### 4.9.2 Boundary Conditions

Similar to what is done in Section 4.8.3 for 1U server, the boundary condition for HP blade server is shown in Figure 4.24. The inlet boundary conditions for actual and approximation servers are assumed to be intake pressure inlets of 0 Pa gauge pressure. With respect to the outlet boundary condition, it is assumed to be the same as the pressure outlet boundary condition. Different pressure values have been

assigned for the outlet condition to obtain the velocity field in order to sketch the relationship between the pressure and the velocity field. All other surfaces are assumed to be wall surfaces.

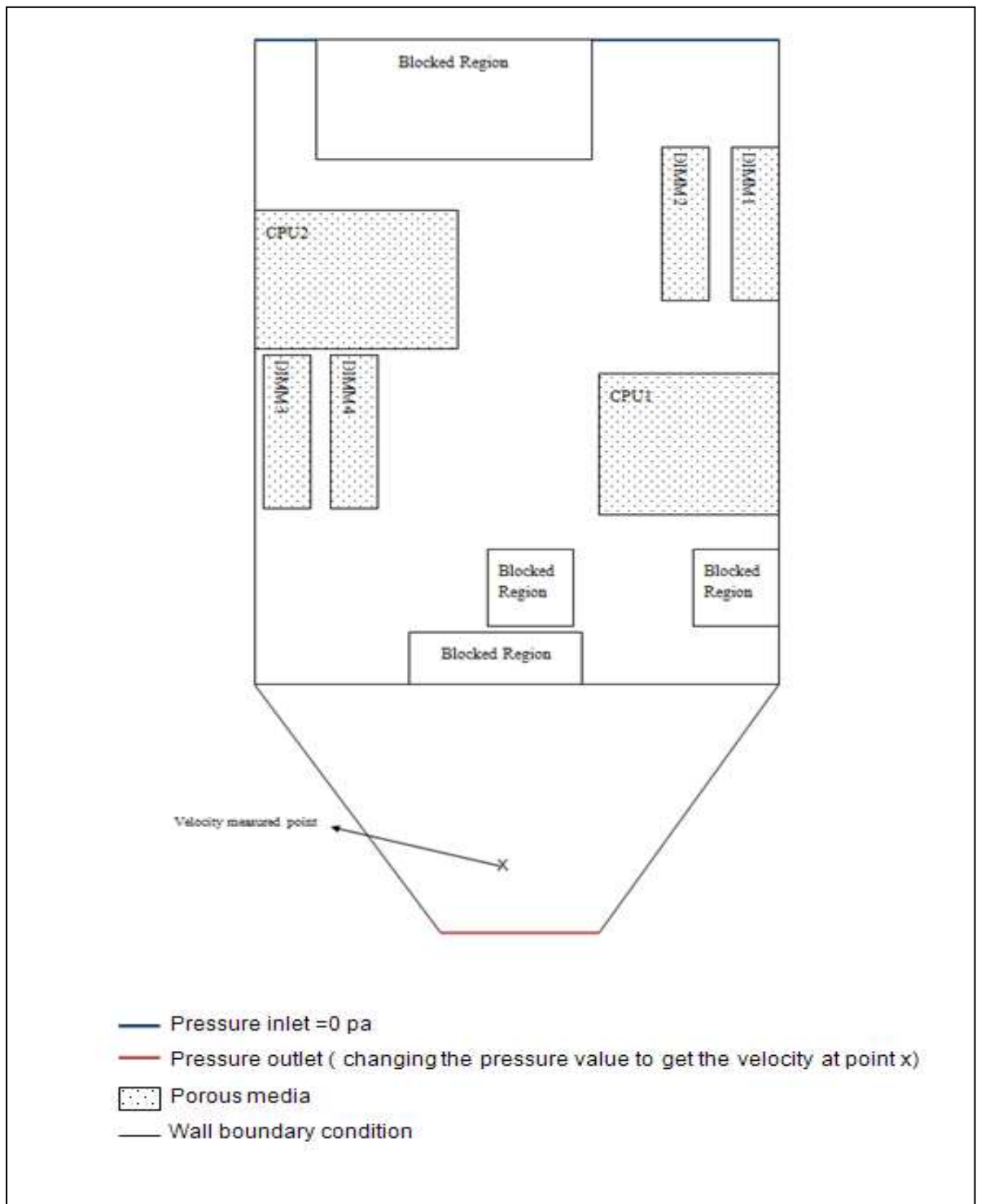


Figure 4.24 Boundary condition used in the CFD analysis of an HP blade server.

### 4.9.3 Results and Discussion

**Table 4.9 Velocity profile for HP blade server with respect to the pressure drop across the server.**

$\Delta P$ (Pa)	Velocity (m/s)
25	0.9
50	1.7
100	2.4
160	3.0
200	4.1

Table 4.9 shows the obtained values of the velocity point which is obtained from CFD for different pressure drops across the server. Also, this table can be represented as a second order polynomial, as shown in Figure 4.25. The pressure equation from the fit curve is equivalent to the equation of the pressure drop for the porous media, which describes Darcy's Law plus the inertial loss term as follows

$$\Delta P = \frac{\mu}{\alpha} lV + \frac{1}{2} C\rho lV^2$$

Where,  $\Delta P$  is pressure drop through the porous media (Pa),  $\mu$  is the viscosity of the fluid (kg/m.s),  $\alpha$  is the permeability of the porous media ( $m^2$ ),  $l$  is the thickness of the porous media (m),  $V$  is the axial velocity (m/s),  $C$  is the Inertial resistance and  $\rho$  is the density ( $kg/m^3$ ).

The fitted curve for the pressure drop against velocity can be expressed as

$$\Delta P = 28.494V + 5.5377V^2 \quad (4.55)$$

So that the values of both permeability  $\alpha$  and inertial resistance C for the porous block which represents the HP blade server are equal to  $3.08 \times 10^{-7} \text{ m}^2$  and 22.6 m, respectively

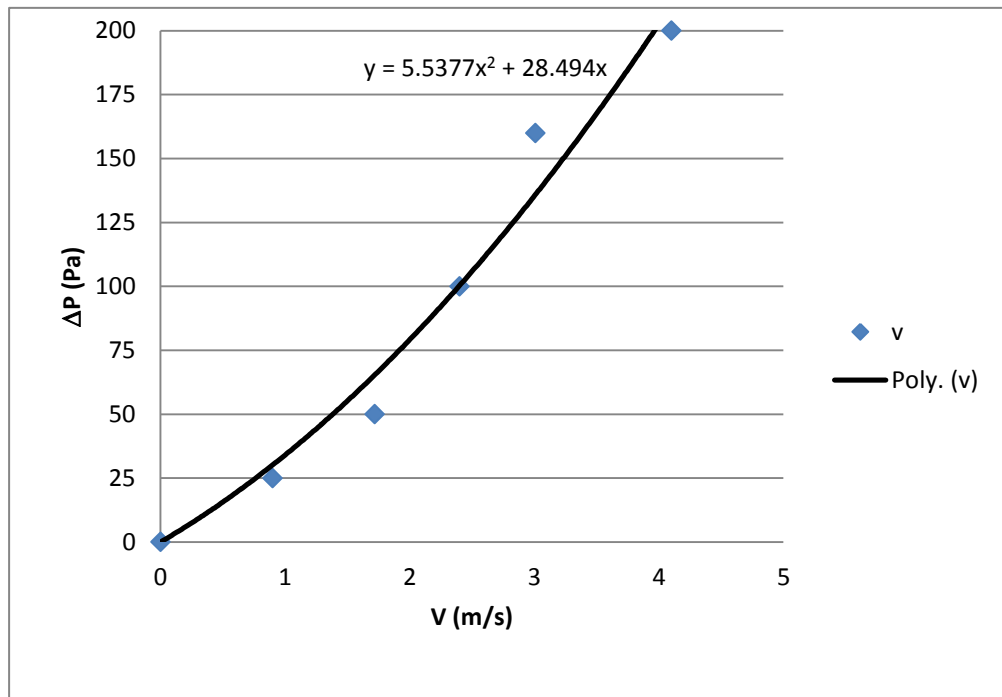


**Figure 4.25 Velocity profile vs. pressure drop in a HP blade server.**

Figure 4.25 shows the relationship between the point velocity and the pressure drop across the blade server. It is shown that the trend of this relation is almost second order polynomial. This relationship has been obtained by using the RNG k- $\epsilon$  model. This model has been used because it gives good agreement in cases involving 1U servers, as shown in Section 4.8.2. The results show that the permeability value ( $\alpha$ ) of the HP blade server is lower than the permeability value of the traditional server; this make sense, considering that the HP blade server is

more dense with internal components than the traditional server (1U server). Moreover, the value of the inertial resistance ( $C$ ) of the blade server is higher than the traditional server due to the same reason mentioned above.

In this situation the comparison between the CFD analysis and experimental data is not performed because the method used to obtain the pressure drop across the server has already been conducted for the traditional server and validated with experimental data by using the RNG  $k$ - $\epsilon$  turbulent model. So, the study which is done for the traditional server by using the RNG  $k$ - $\epsilon$  model is considered as a sufficient condition and can be applied to the Hp blade server. However, the theoretical results for HP blade server could be validated using pressure drop sensors in the high performance computing data centre. It is shown from Section 4.8.2 that the porous media model provides excellent agreement with the experimental data. Thus, the porous media principle can be implemented for the blade server, as well. Furthermore it is shown in the same section that the turbulence intensities do not have any significant effect. Therefore, the turbulence intensities have not been changed and values for the inlet and outlet have been assumed to be 5% and 1%, respectively.

#### 4.10 Conclusion

The numerical solution method (finite volume method) is represented in this chapter to solve the governing equations in data centre. Also the porous model is tested to simulate the server blade and its internal components with clear boundary conditions. It is found that from this chapter that the CPU can be simulated as a porous media by using Darcy's law and the pressure drop across the heat sink channel. After that, three turbulence models which are k-ε model, RNG k-ε model, and Realizable k-ε model have tested for the server blade (1U). It is found that the RNG model is the best model among others by comparing the results with the experimental data. The same analysis has been done for the HP blade server So that the server blade and internal components are simulated as a porous block with permeability as the following table 4.10.

**Table 4.10 Permeability values for CPU, 1U server, and HP server blade.**

<b>Components</b> <b>Permeability</b> <b>Direction</b>	<b>Permeability of</b> <b>CPU</b> <b>(m<sup>2</sup>)</b>	<b>Permeability of</b> <b>1U server</b> <b>(m<sup>2</sup>)</b>	<b>Permeability of</b> <b>HP blade server</b> <b>(m<sup>2</sup>)</b>
<b>X</b>	$1 \times 10^{-20}$	$1 \times 10^{-20}$	$1 \times 10^{-20}$
<b>Y</b>	$1 \times 10^{-20}$	$1 \times 10^{-20}$	$1 \times 10^{-20}$
<b>Z</b>	$2.9 \times 10^{-7}$	$1.88 \times 10^{-6}$	$3.08 \times 10^{-7}$

## **CHAPTER 5 : CFD ANALYSIS OF FLOW-THROUGH LEVEL RACKS**

### **5.1 Introduction**

In the previous chapter, the server blade has been simulated as a porous media model and shows good agreement with the experimental data. In this chapter, the simulation of the rack, consisting of a number of blades, will be explored in detail. As was carried out for a single server, the simplification of treating the rack as a porous block will be discussed. Thus, this will be used to verify servers to be simulated as porous blocks inside the data centre. Following this, cooling techniques will be applied to the porous models to ascertain how these techniques can reduce the hot spots inside the data centre. The cooling of the rack is the most important thing to reduce the temperature inside the data centre, to reduce occurrence of hot spots and address the recirculation problem. The components of the rack are the servers, switches and storage; the servers have been discussed earlier in Chapter 4.

The rack that encloses the servers is shown in Figure 5.1. In a data centre where the cold-hot aisle arrangement is used, the racks are arranged to face each other with the intake and additional row sections forming the cold aisle. The rear of the racks exhausts the air to form the hot aisle. This arrangement is important to eliminate the mixing of both hot and cold air streams. Typical rack dimensions that are used inside the data centre are 1.1m×0.8m×2.1m [11]. Typically, the average heat dissipation per rack is 4 kW [6], although it can reach 20 kW or above per rack in a high density data centre [89].

CFD analysis will be described in this chapter to study the geometry simplification for the rack of 32 server blades (porous blocks). In this chapter the temperature profile for a rack of 32 servers (porous blocks) will be compared with different rack configurations such as 16 porous blocks, 8 porous blocks, 4 porous blocks, 2 porous blocks and 1 porous block. This study is done to find the minimum number that can be used to simplify 32 porous blocks rack.

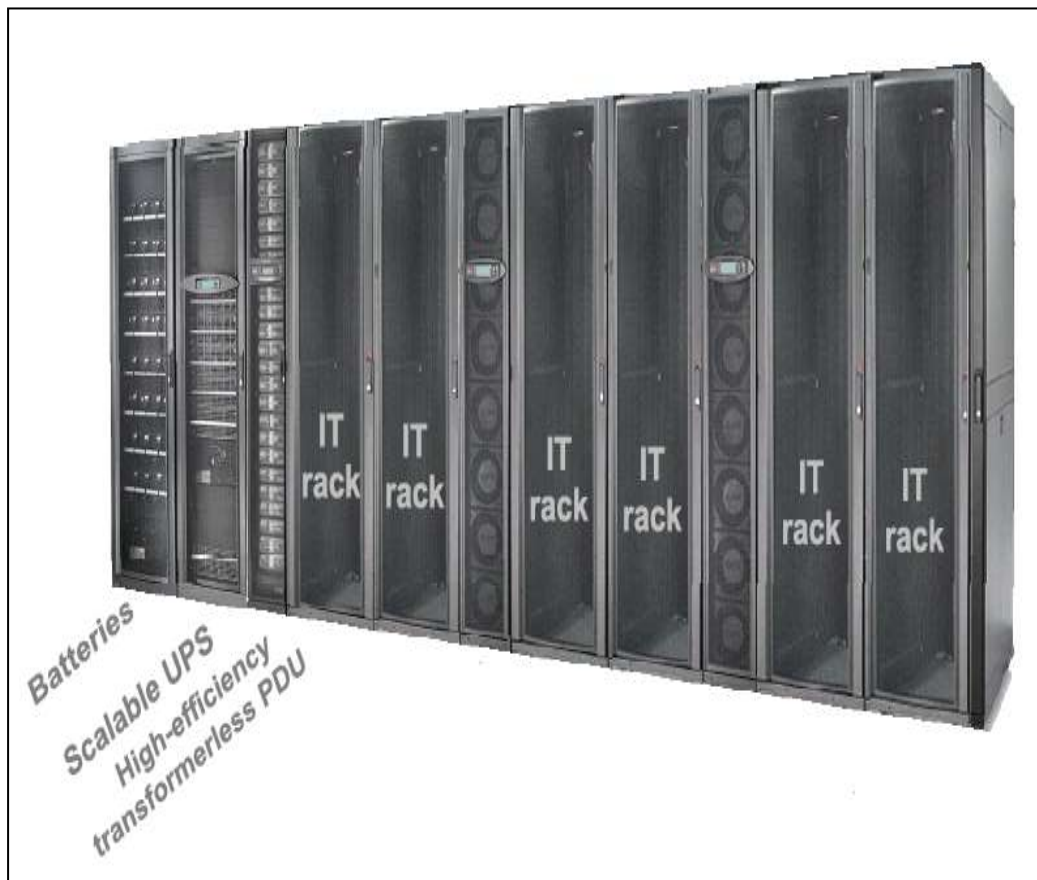


**Figure 5.1 IT rack inside the data centre [89].**



## 5.2 Rack Cooling Scenarios

In this section, the simplification of racks by using a porous media approach will be presented by deploying the CFD model for 2-D schemes. This simplification will be done to build the geometry easier.

### 5.2.1 Traditional cooling for the rack

Usually, the data centre is cooled by the chilled air, which is supplied by the CRAC unit and then is introduced by the vents in the cold aisle for the cold-hot aisle arrangement. After that, the chilled air is sucked by the server fans inside the rack, as shown in Figure 5.2.

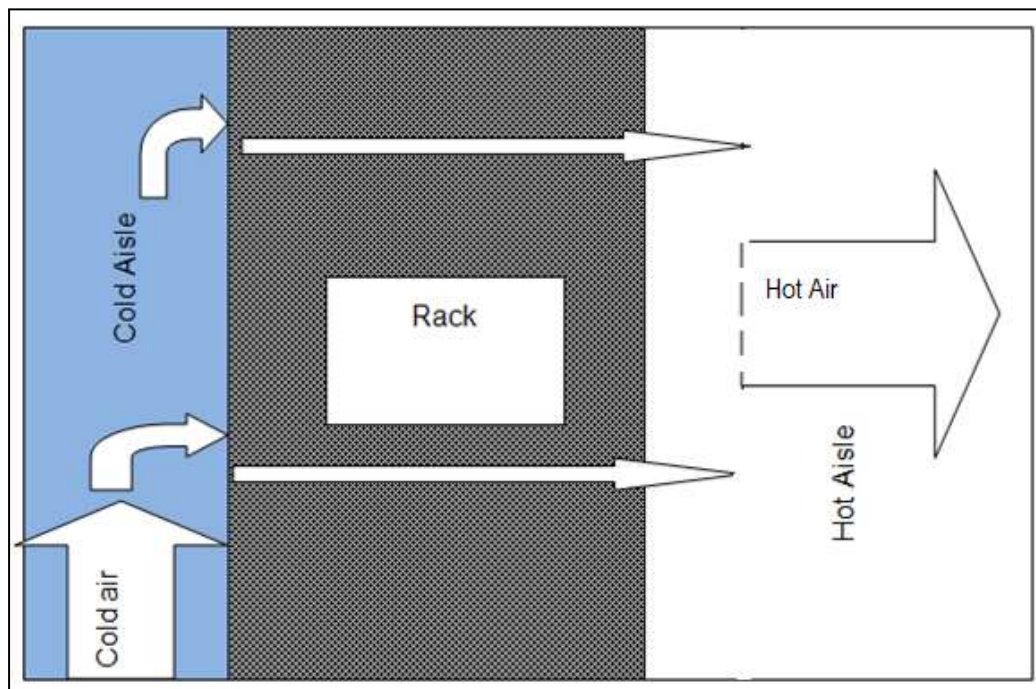


Figure 5.2 Plan view of air flow through racks in a data centre.

### 5.2.2 CFD analysis for the rack

The aim of this section is to develop a simple model of a rack, which then can be used to understand influence of multiple racks on the air flow within a data centre. The rack containing 32-servers will be analysed using Fluent to calculate both inlet and outlet temperatures of the rack. After this step, the assumption of using porous blocks configurations will be tested with respect to the inlet and outlet rack temperatures in order to simplify a 32-server rack.

The 2-D CFD analysis is used to create the rack geometry by using both Gambit software and Fluent software. 32-servers (1U in height) are located inside the rack, as shown in Figure 5.3. The basis of this analysis can be assumed as per Cho et al. [11]. Where the temperature profile has been tested for six air distribution configurations as described in section 2.6.2 by Cho et al.[11] by using CFD analysis (STAR-CD software) for different high level inside the data centre.

- The cold aisle width equals 1.2m.
- The hot aisle width equals 1m.
- The rack volume equals 1.1m×0.8m×1.9m.
- The vent cross- sectional area equals 0.6m×0.6m.

The flow and thermal specifications have been designed as follows:

- Each rack dissipates 8 kW.
- The supply air velocity through each vent equals 1 m/s.
- The inlet temperature of supply air via the vents equals 15°C.

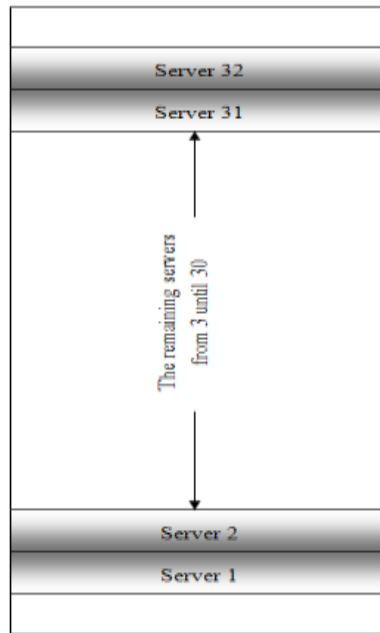


**Figure 5.3 Rack configuration.**

Each server dissipates 250 W of heat in this case. The servers have been assumed to be porous blocks with both permeability and inertial resistance of  $1.88 \times 10^{-6} \text{ m}^2$  and 20.46 m, as mentioned in table 4.10 and section 4.8.2 respectively. Each server has been inserted inside the rack with the above specifications.

Five porous block configurations will be tested to evaluate the accuracy of the models. The five configurations are 16 porous blocks, 4 porous blocks, 2 porous blocks and 1 porous block. Figure 5.4 shows the five porous block configurations.

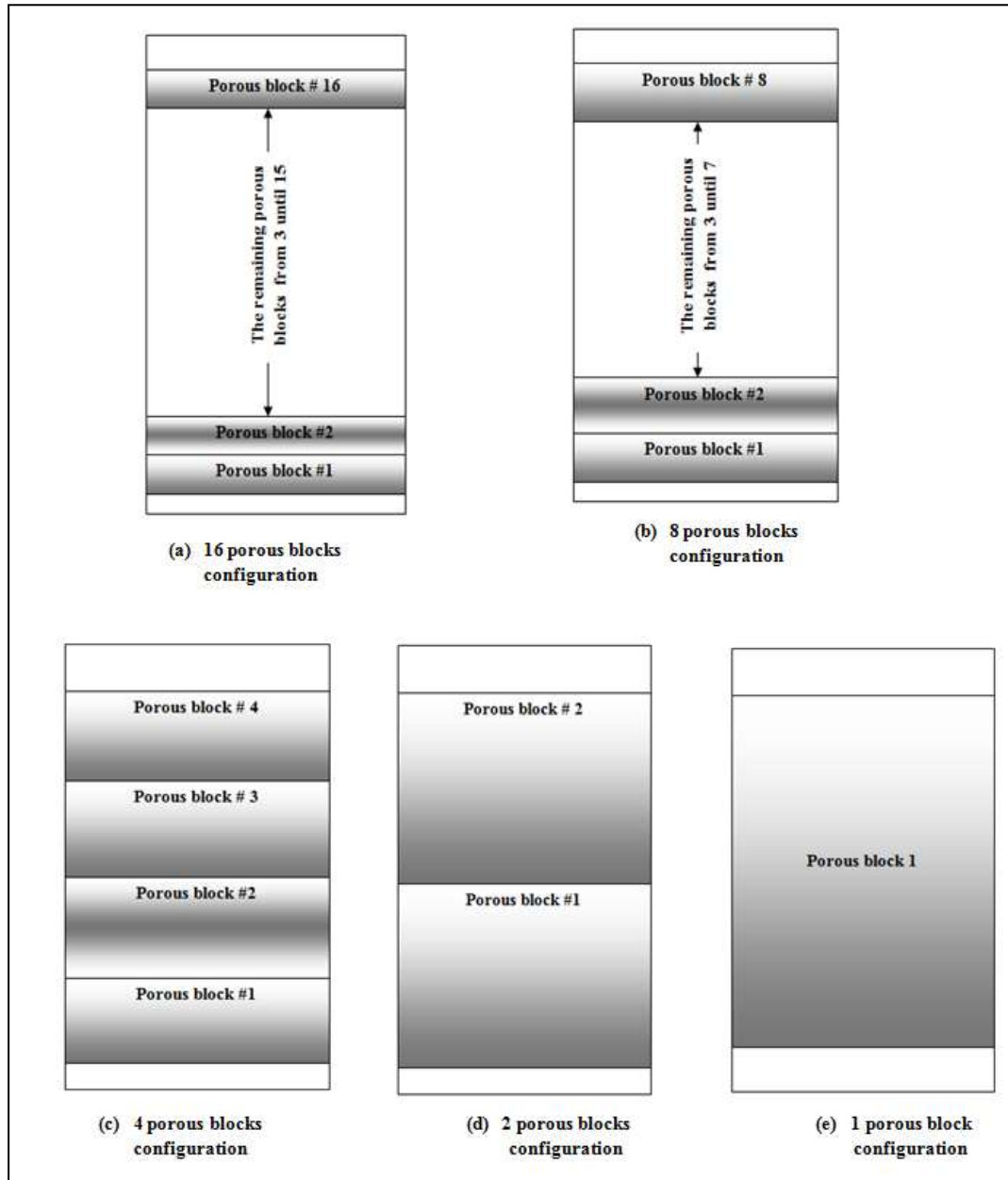


**Figure 5.4 Five porous blocks approximation.**

The porous block permeability is affected by using the combination approximation due to the resistance of the wall between the servers, so that the permeability decreases as the number of porous blocks decreases. So that the permeability values for 16 porous blocks, 8 porous blocks, 4 porous blocks, 2 porous blocks and 1 porous block are  $1.75 \times 10^{-6} \text{ m}^2$ ,  $1.62 \times 10^{-6} \text{ m}^2$ ,  $1.48 \times 10^{-6} \text{ m}^2$ ,  $1.35 \times 10^{-6} \text{ m}^2$  and  $1.2 \times 10^{-6} \text{ m}^2$ , respectively. These values have been obtained by using the role

of equivalent resistance in parallel, where the inverse of equivalent resistance equals to the accumulation of inverses of each resistance, as shown in Equation 5.1

$$\frac{1}{R_{eq}} = \sum_{i=1}^n \frac{1}{R_i} \quad (5.1)$$

Where  $R_{eq}$  is the equivalent resistance and  $n$  is the number of the servers. In this case, the resistance is considered as the permeability. The above permeability values for the combinations are simply obtained by using role of the resistance in the parallel.

With respect to the fan model, the specification of the server fan is previously shown in Chapter 4. An equivalent fan is used to represent the fan for two or more servers by considering the fans as parallel units.

The boundary conditions of this study are specified as the normal physical situation of a data centre, which include a velocity inlet at the vent, a pressure outlet at the top right of the room, a fan at the server exhaust, an interior space at the server inlet, and symmetrical at the end of cold aisle. Finally, all other surfaces were selected as a wall boundary condition, as shown in Figure 5.5.

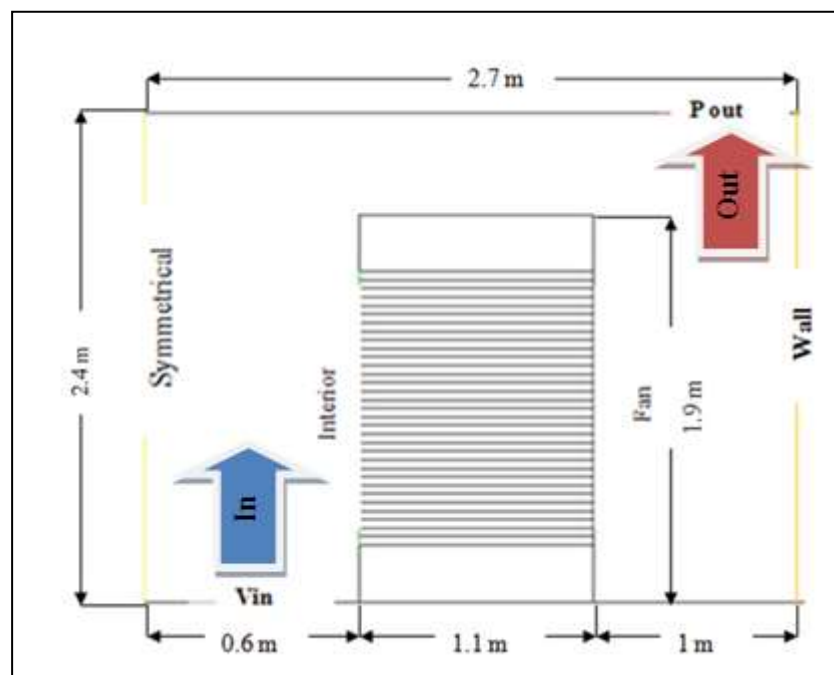


Figure 5.5 Boundary conditions for tested rack inside a data centre.

The boundary conditions also can be represented, as per Table 5.1.

**Table 5.1 Boundary conditions used in Fluent**

<b>Boundary</b>	<b>Boundary condition in Fluent</b>
Air inlet	Inlet velocity ( 1m/s)
Air exhaust	Pressure outlet ( $P_{out}=0$ Pa)
Rack intake	Interior
Rack exhaust	Fan, as described in Chapter 4
Cold Aisle	Symmetrical
Hot Aisle	Wall
Other boundaries	Wall

### **5.3 Results and Discussion**

The temperature distribution on the rack is used to characterize the data centre. The study is carried out with inlet velocity of 1 m/s. The inlet temperature of the air is 287K. The Reynolds number for the flow through the vent that is calculated to detect either the laminar or turbulent model by using equation 4.16. Where the length scale for the vent equals to 0.6 m. The Reynolds number is equal to 33708 . Thus, the turbulence model should be implemented in this case. It is shown that the Reynolds number is relatively low in the turbulent region. However, the most suitable turbulence model for this case is the standard k- $\epsilon$  model, as

mentioned by Cho et al. [11]. Cho et al [11] have used this model and obtained good accuracy.

Figure 5.6 shows the temperature distribution of the rack inside the data centre. It is shown that the hot spot occurs at the top of the rack; that is due to flow recirculation of the hot air in the hot aisle. These hot spots affect the IT equipment reliability and lifespan. This figure shows the temperature at the inlet increasing along with the height of the rack. This happens because of the mixing between the hot exhaust air and cold supply air, causing an increase in the inlet air temperature. In such cases, the supply temperature comes from the vent lower than the rack inlet temperature and does not reflect the real rack intake temperature, because the mixing between the hot and cold air in the cold aisle raises the air temperature coming from the vents.

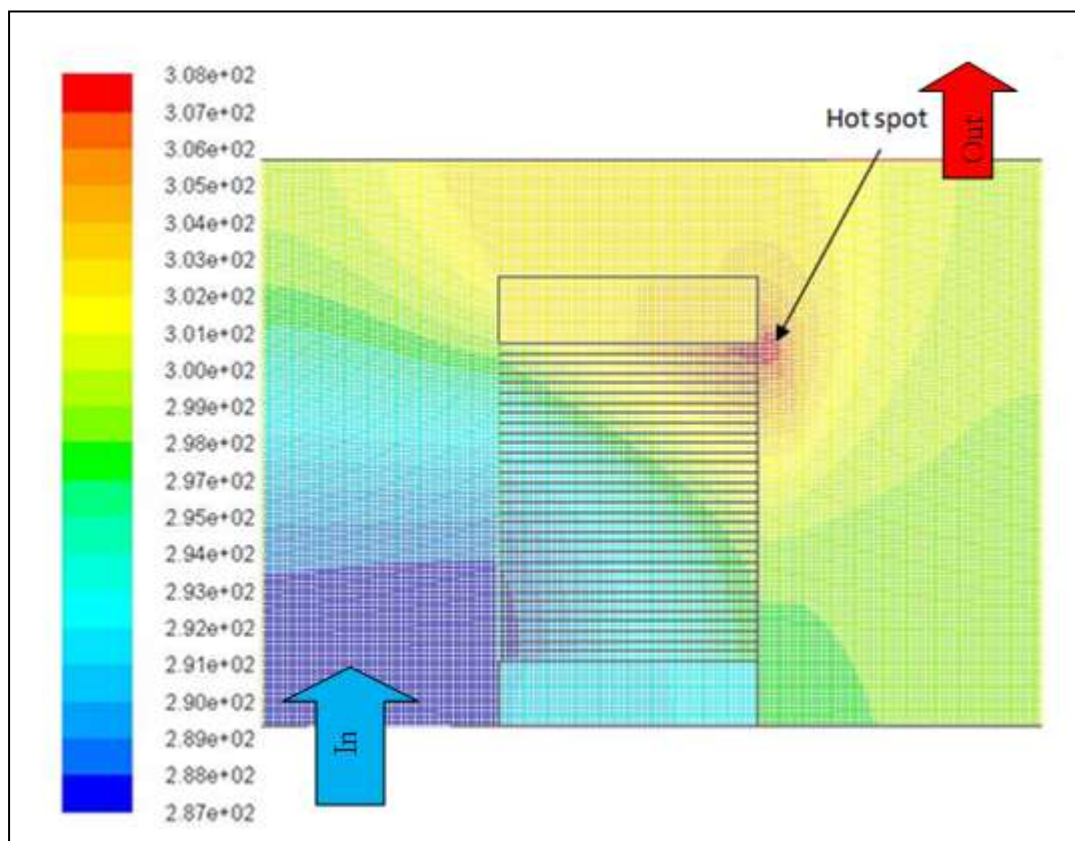
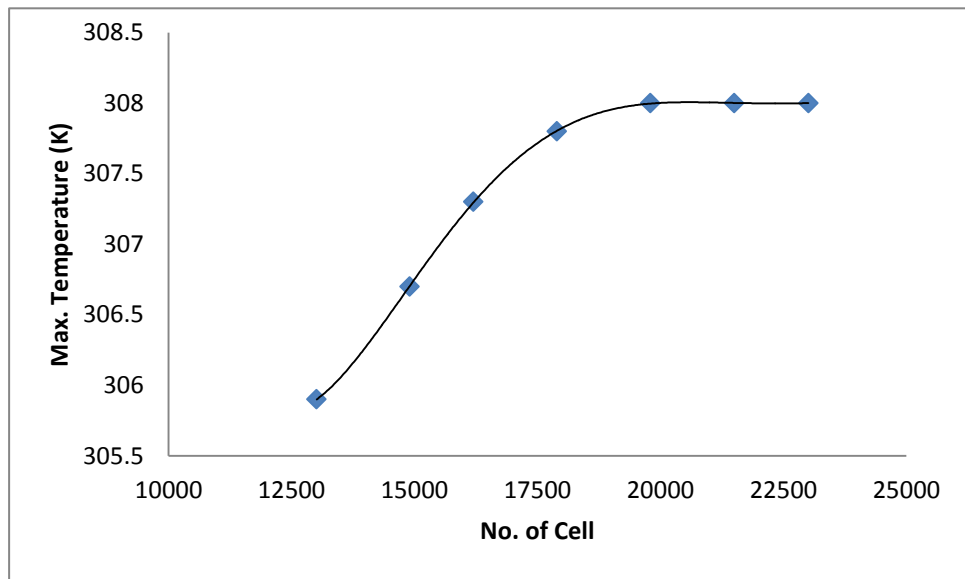


Figure 5.6 Temperature distribution in a rack inside the data centre.

The solution domain for this study is specified by using 19800 cells and 22000 nodes. The mesh study has been done for this case to ensure that the mesh independence is achieved and does not affect the results. The mesh study of the rack of 32 server blades has been done as follows in table 5.2. The testing of this problem is the maximum temperature that forming hot spot as shown in Figure 5.6.

**Table 5.2 Number of cells vs. the maximum temperature for the rack of 32 server blades.**

No. Of Cell	Max. Temperature (K)
13010	305.9
14960	306.7
16200	307.3
17900	307.8
19800	308
21500	308
23010	308



**Figure 5.7 Mesh independence study for the 32 server rack.**



The temperature distribution along with both the rack inlet (red curve) and rack outlet (black curve) are shown in Figure 5.8. This illustrates that the rack inlet temperature increases along the rack's height, while the temperature difference between the inlet and the outlet decreases for the upper server; this is a gain due to the recirculation problem.

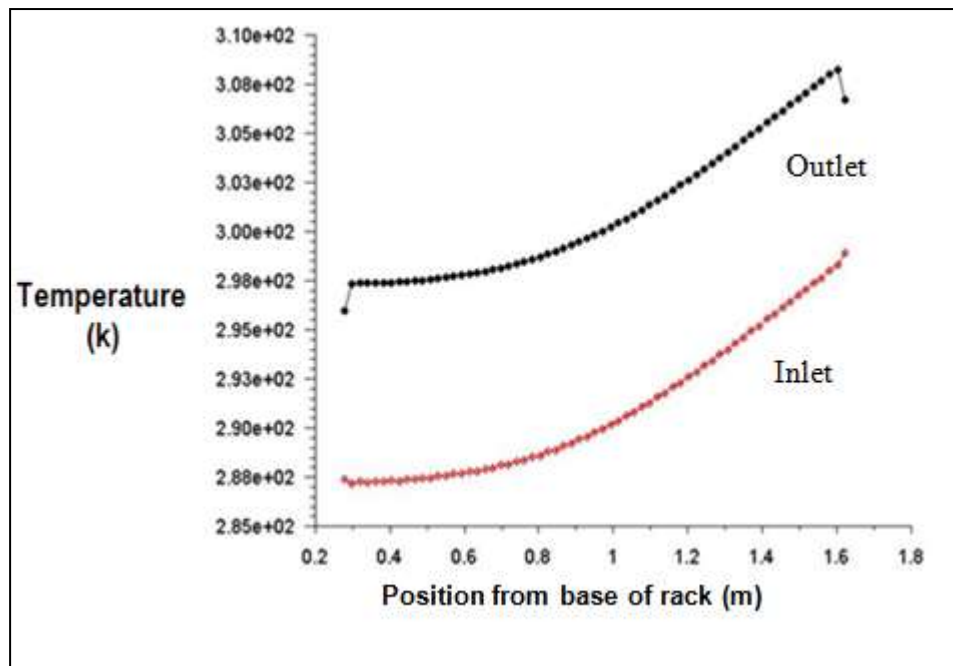


**Figure 5.8 Temperature distribution along both rack inlet and rack exhaust.**

The recirculation problem when the hot air mixes from the hot aisle to the cold aisle is shown in Figure 5.9. The hot air stream is recirculated in the upper servers due to the density difference between the cold and hot air in both cold and hot aisles. It is also shown from Figure 5.9 that the flow of the hot air streams, which is in blue arrows, mixes with supply cold air and this leads to increase in the temperature for the upper servers.

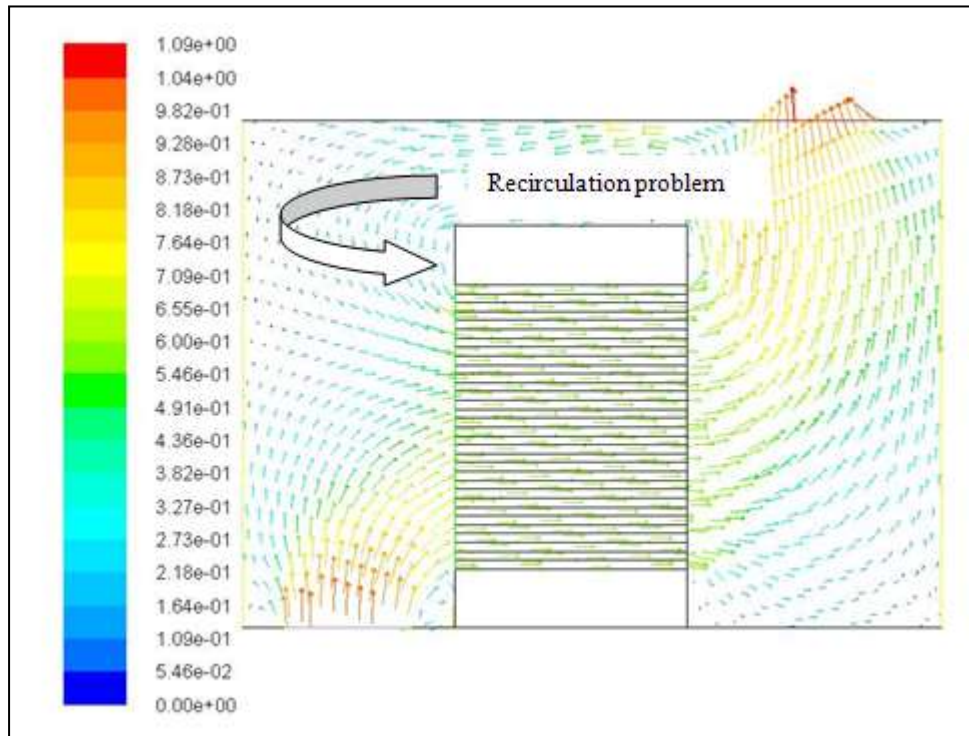
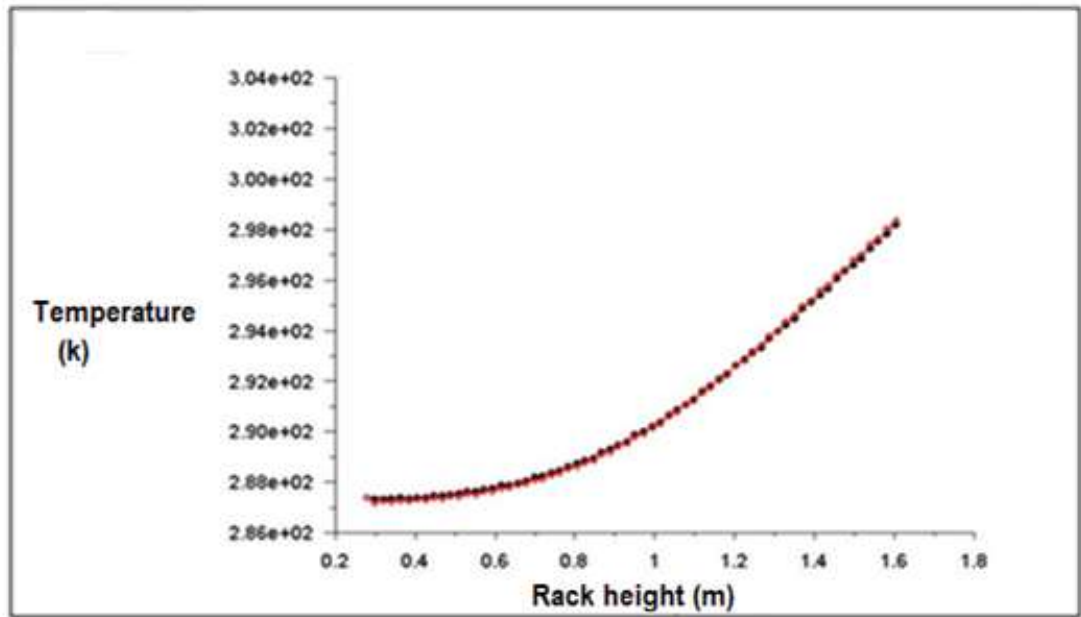


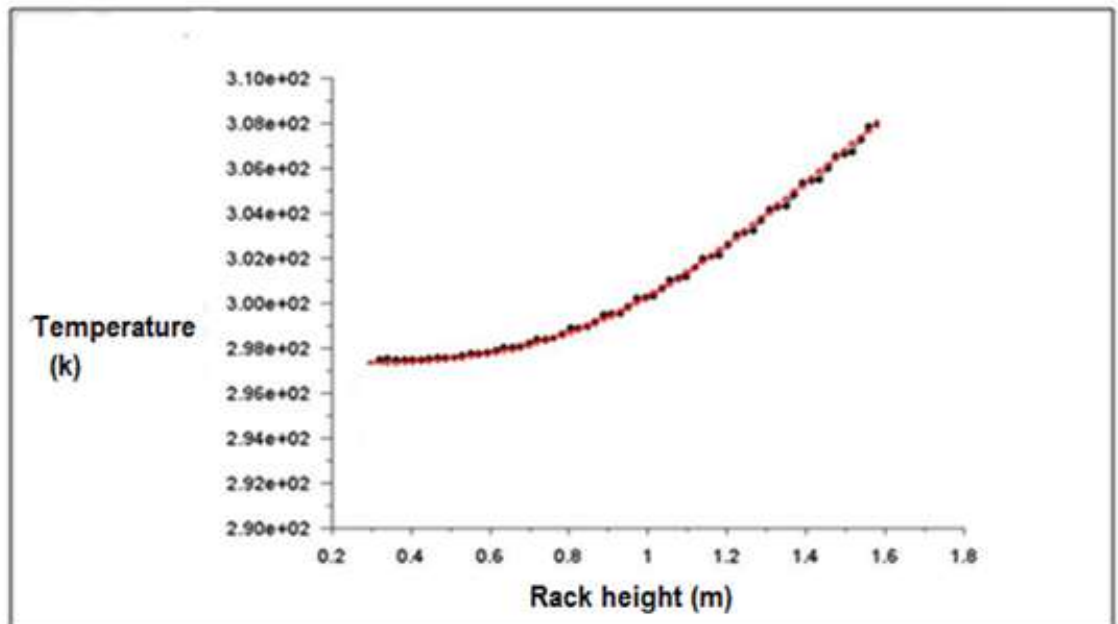
**Figure 5.9 Velocity field (m/s) for a 32-server rack inside a data centre.**

The configurations, which are shown in Figure 5.4, are tested. Figures 5.10 to 5.14 show the comparison between the temperature distributions for the 32-server rack and the simplified models. Both inlet rack and outlet rack temperature distributions are compared between the actual rack (32-server rack) (red curve) and the assumptions (black curves). The temperature distributions between the 32-server rack and the assumption should be the same to apply the assumption of rack configurations; otherwise, this assumption is no longer valid. It is shown from Figures 5.10 and 5.11 that the temperature distributions are almost the same for both the 32-server rack and the assumption analysis for the first two configurations (16 porous blocks and 8 porous blocks); whereas, the assumptions for 4 porous blocks, 2 porous blocks and 1 porous block, as shown in Figures 5.12, 5.13 and 5.14, respectively, are not judged as realistic because the temperature distributions for both rack inlet and rack outlet are different than the temperature distribution for the 32-server rack. As a result, it is shown from Figure 5.10 that both the rack inlet and

outlet temperature for the 32-server (red dots) and the rack intake temperature for the 16 porous blocks configuration (black dots) are almost the same. Thus, the temperature distribution for both rack and rack exhaust are identical, so this combination assumption of 16 porous blocks could be used instead of the 32-server rack. Analysis shows that the 8 porous blocks also behaves like the 32-server rack. Thus, the 8-server combination can be used to represent the 32-server rack. On the other hand, the configurations of 4 porous blocks, 2 porous blocks and 1 porous blocks, as shown in Figure 5.12, Figure 5.13 and Figure 5.14, respectively, do not match that of the 32-servers with respect to the rack inlet and rack exhaust temperatures.

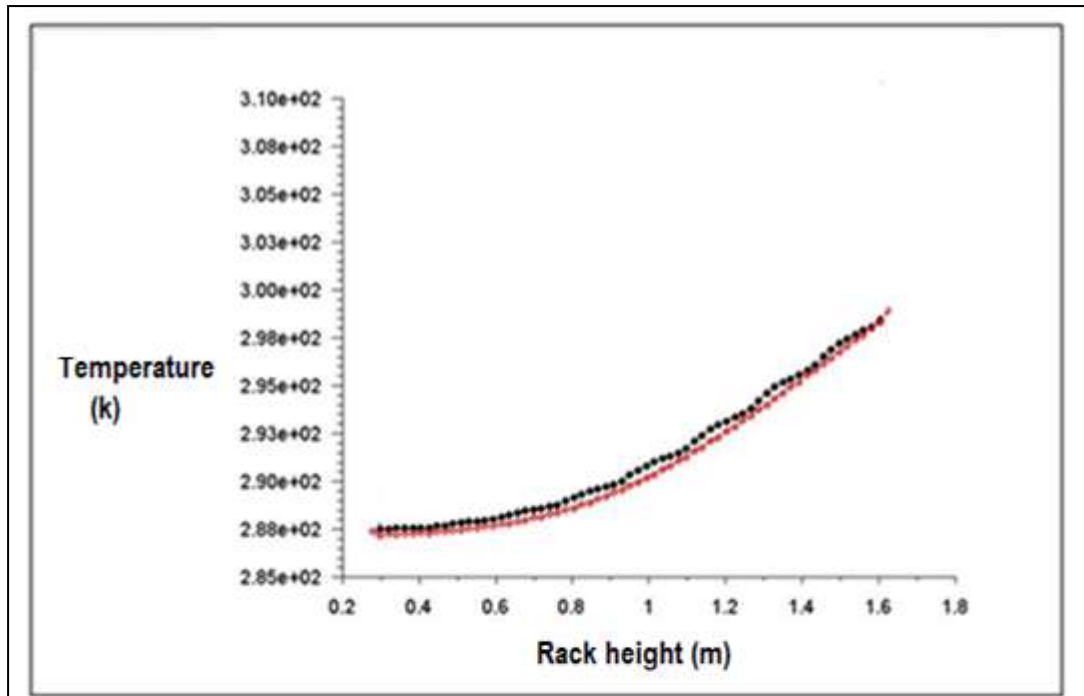


(a) Comparison between the inlet temperature for 16 porous blocks and 32 server rack configuration

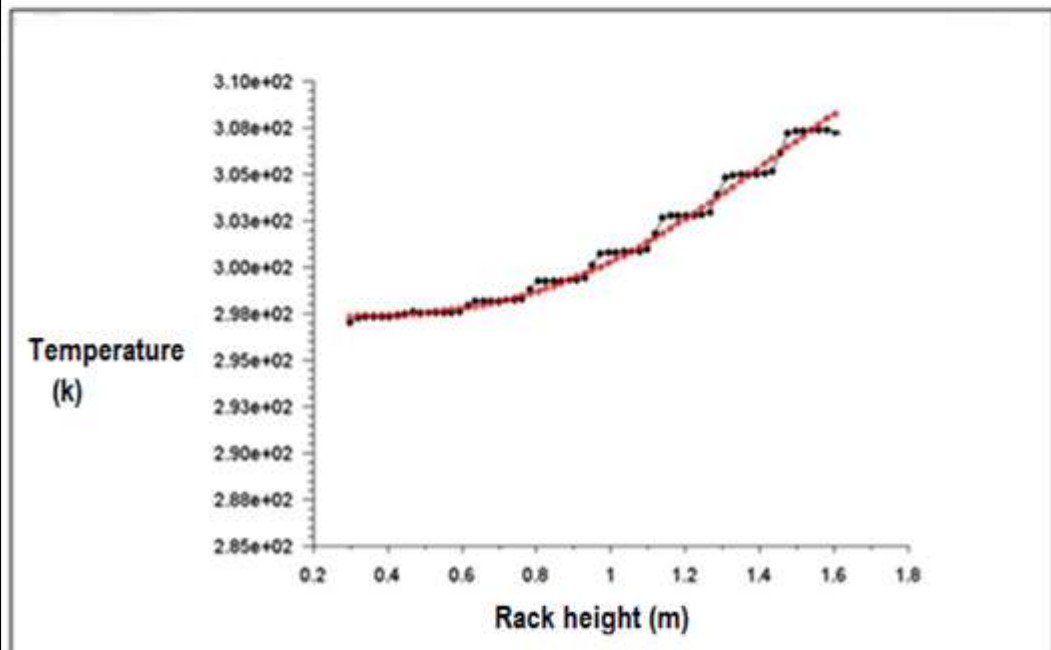


(b) Comparison between the outlet temperature for 16 porous blocks and 32 server rack configuration

Figure 5.10 Comparison between inlet and outlet temperature distributions for the 32-server rack and 16 porous blocks.

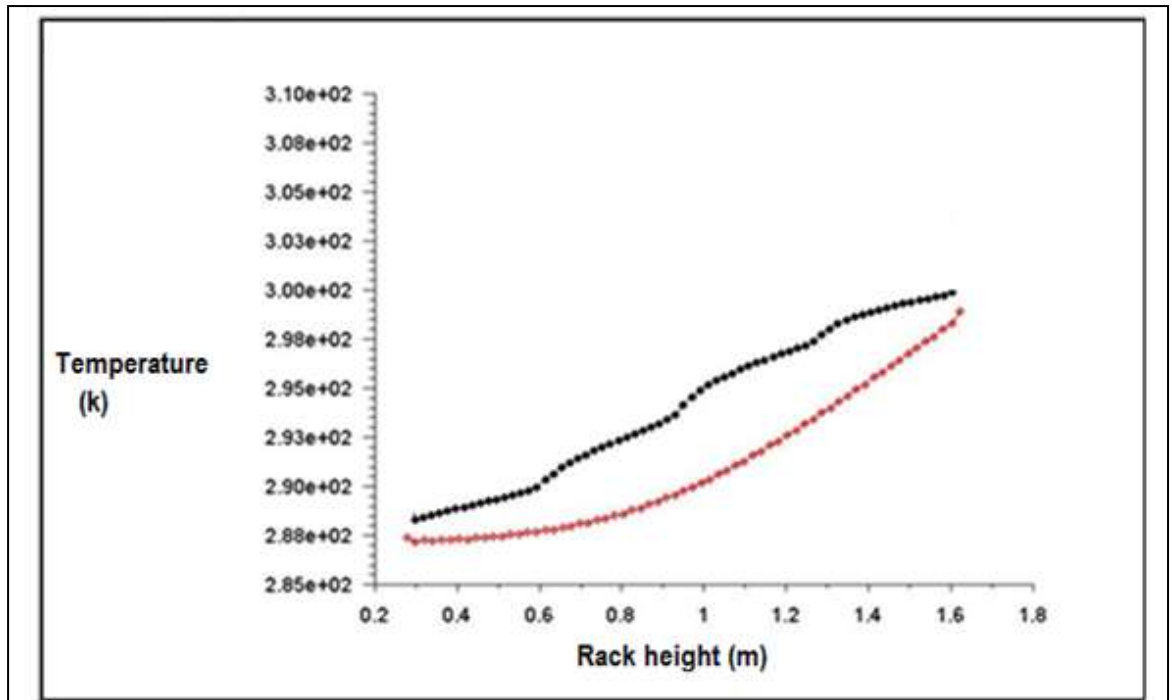


(a) Comparison between the inlet temperature distributions for 8 porous blocks and 32 server rack

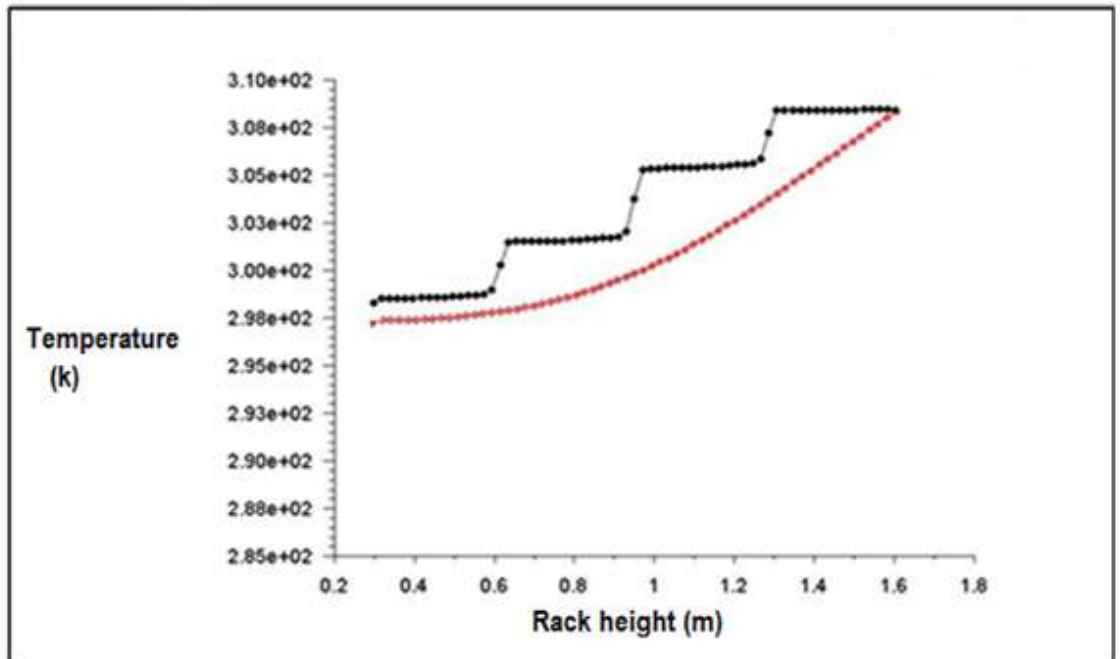


(b) Comparison between the outlet temperature distributions for 8 porous blocks and 32 server rack

Figure 5.11 Comparison between inlet and outlet temperature distributions for the 32-server rack and 8 porous blocks

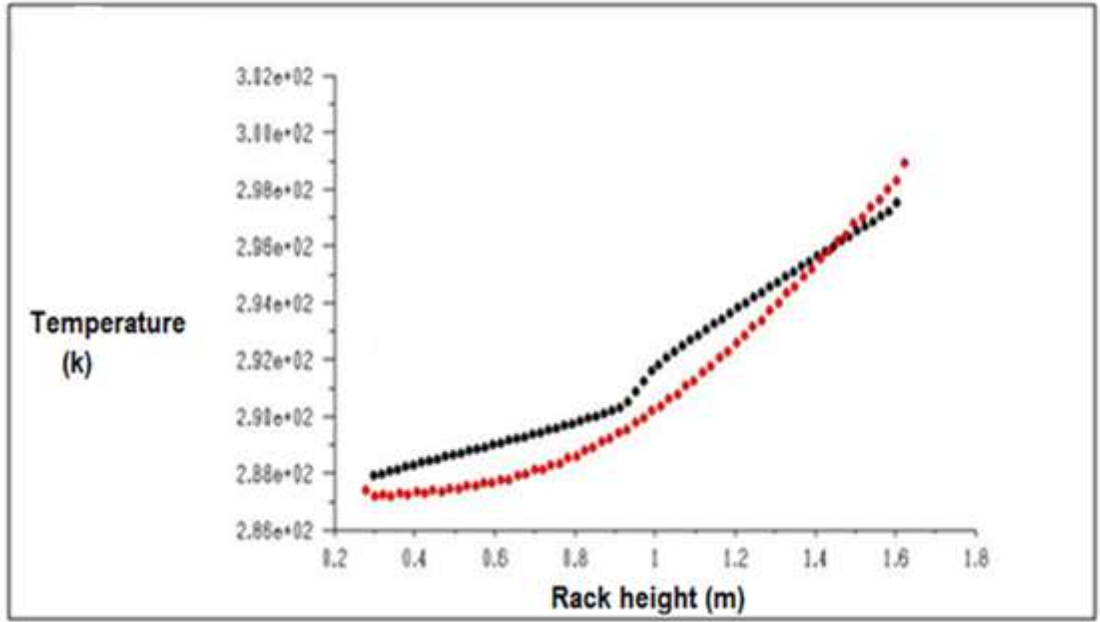


(a) Comparison between the inlet temperature distributions for 4 porous blocks and 32 server rack.

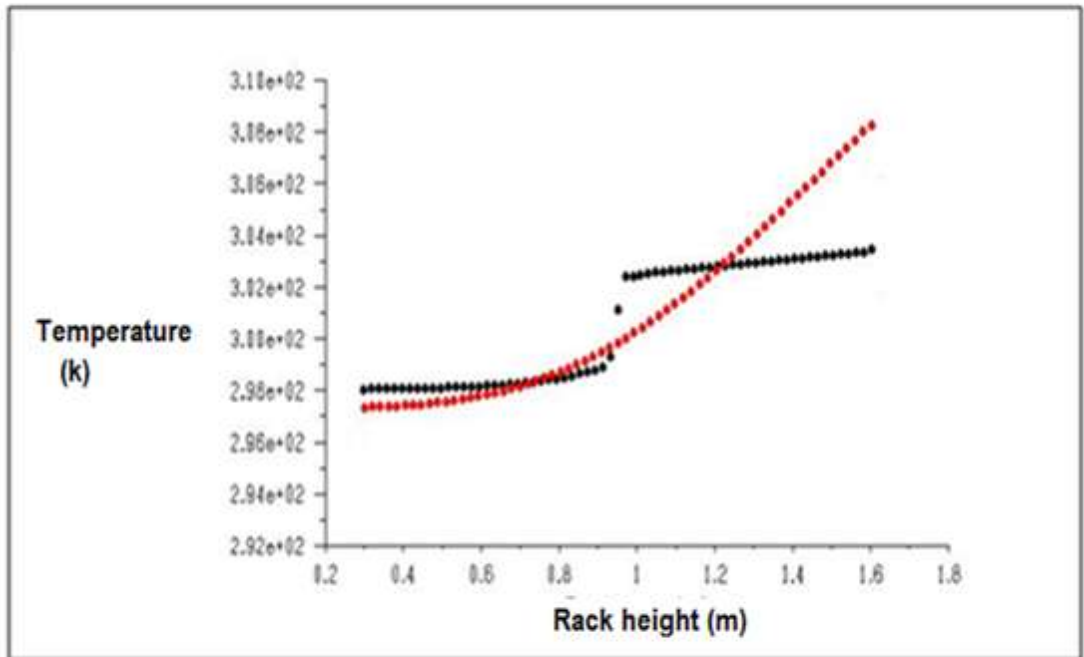


(b) Comparison between the outlet temperature distributions for 4 porous blocks and 32 server rack.

Figure 5.12 Comparison between inlet and outlet temperature distributions for the 32-server rack and 4 porous blocks.



(a) Comparison between the inlet temperature distributions for 2 porous blocks and 32 server rack.



(b) Comparison between the outlet temperature distributions for 2 porous blocks and 32 server rack.

Figure 5.13 Comparison between inlet and outlet temperature distributions for the 32-server rack and 2 porous blocks.

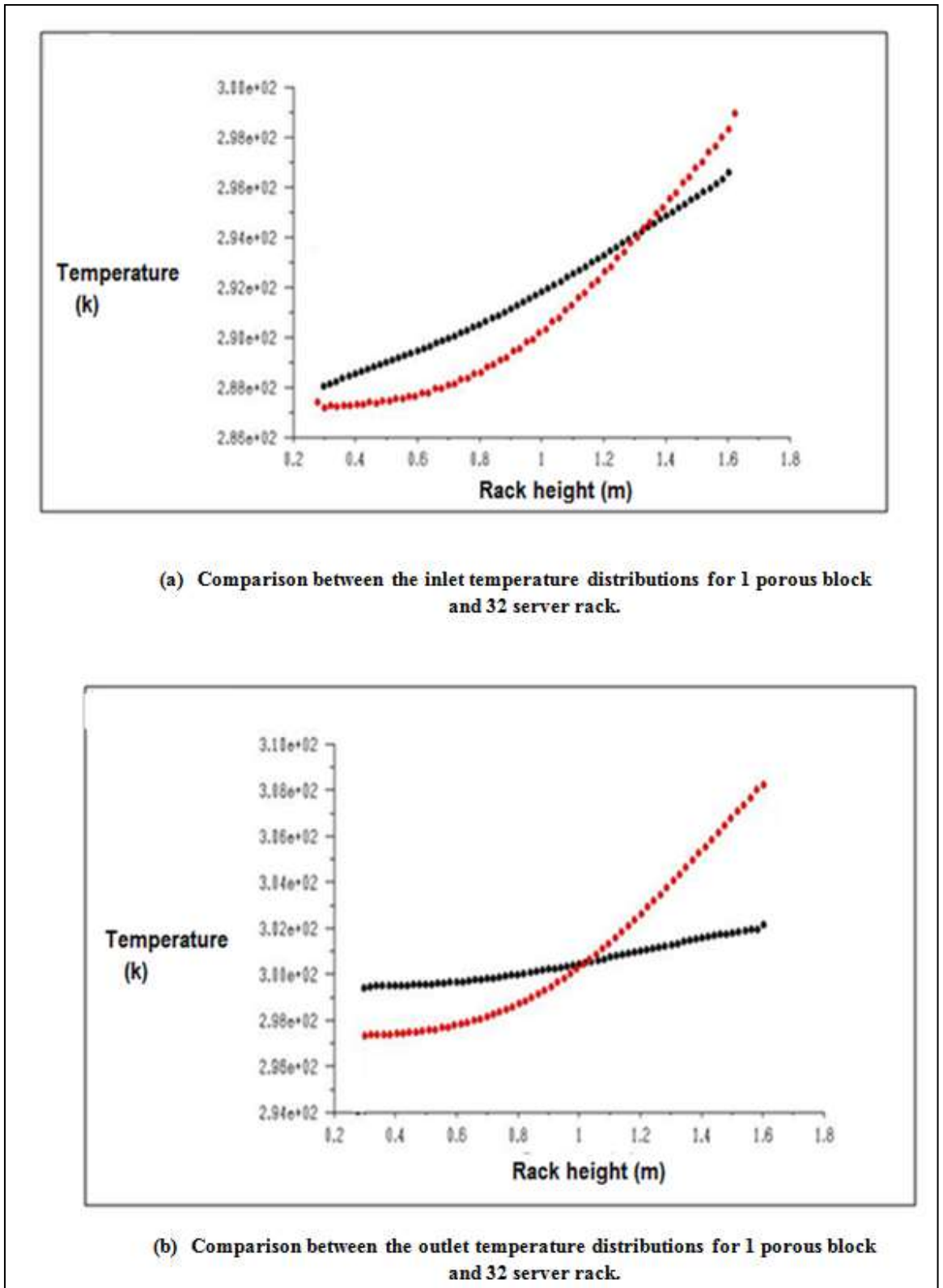
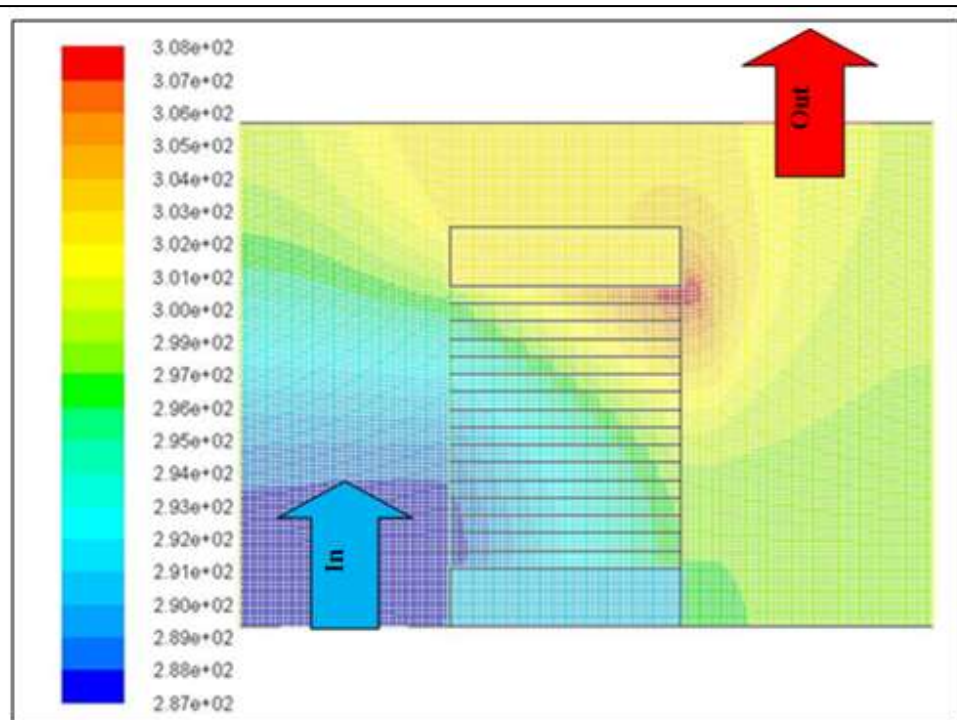


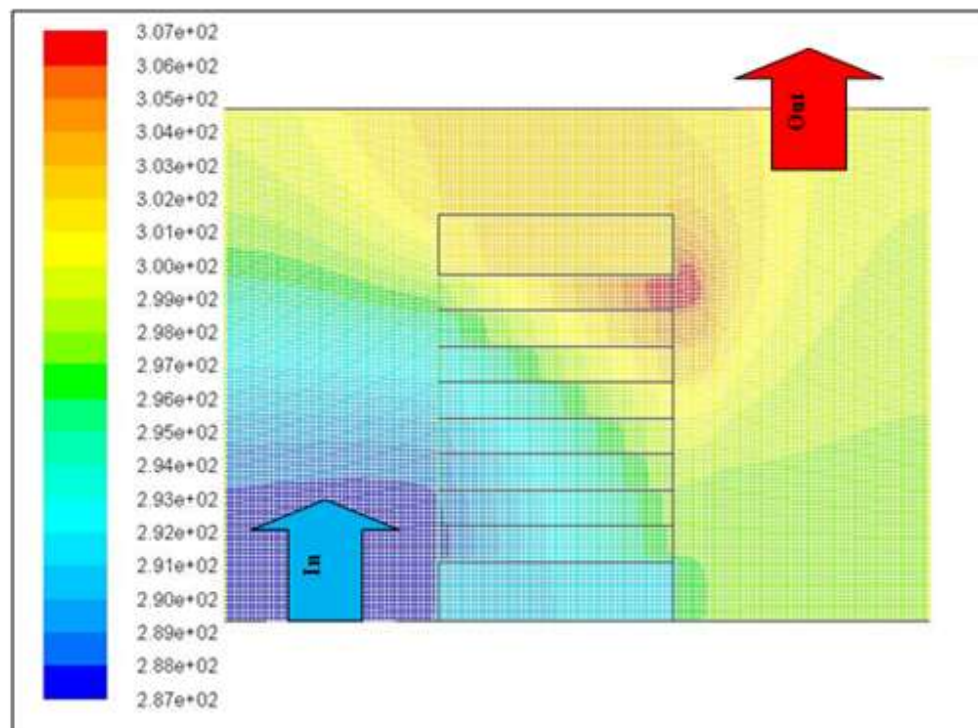
Figure 5.14 Comparison between inlet and outlet temperature distributions for the 32-server rack and 1 porous block.



The temperature distribution for the porous block configurations inside the data centre are shown in Figure 5.15, Figure 5.16 and Figure 5.17. Figure 5.15 illustrates that the temperature distribution for both 16 porous blocks and 8 porous blocks are very close to the temperature distribution for the 32-server rack, as shown in Figure 5.6. The temperature distribution for other configurations is markedly different than the 32-server rack case. Thus, the minimum number of porous blocks representing a 32-server rack in this study is 8 blocks. Relying on this conclusion, the 3-D geometry could be built of 8 porous blocks instead of a 32-server rack. The accuracy of this approach is compared to the 32-server rack with respect to both the inlet and exhaust temperatures for the rack. It is shown from the results that the average inlet temperature difference between the 32-server rack and the 8 porous blocks is 0.8 K, whereas the average exhaust temperature difference is 1.5 K. Therefore, the temperature in the case of the 8 porous blocks configuration is almost the same as that of the 32-server rack.

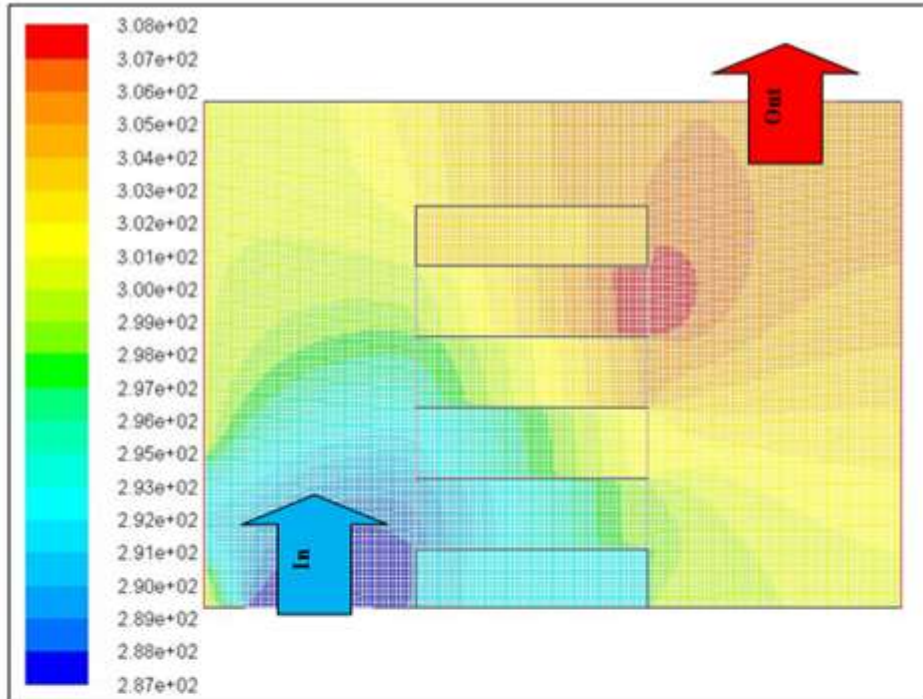


(a) Temperature distribution for 16 porous blocks configuration

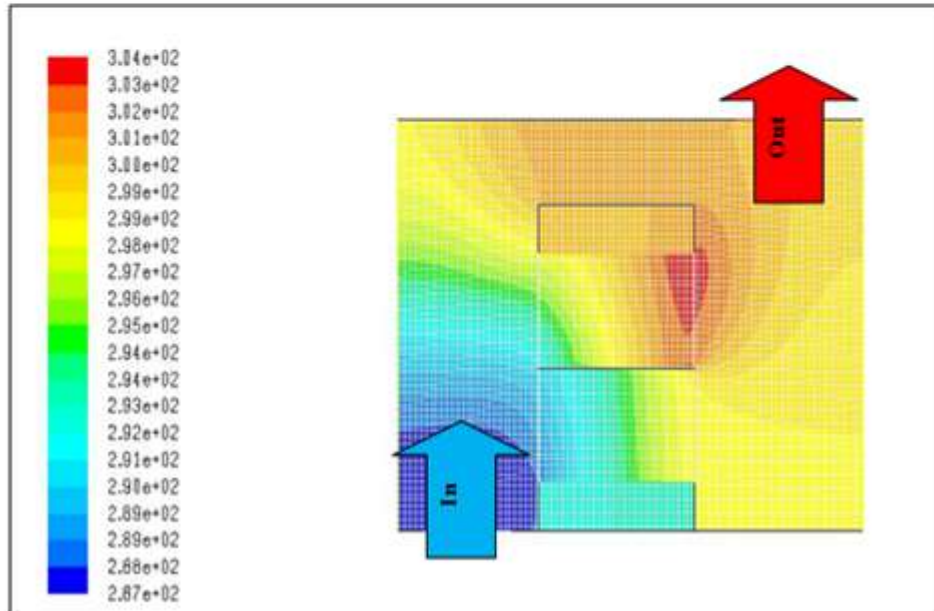


(b) Temperature distribution for 8 porous blocks configuration

Figure 5.15 Temperature fields for the 16 and 8 porous blocks configurations.

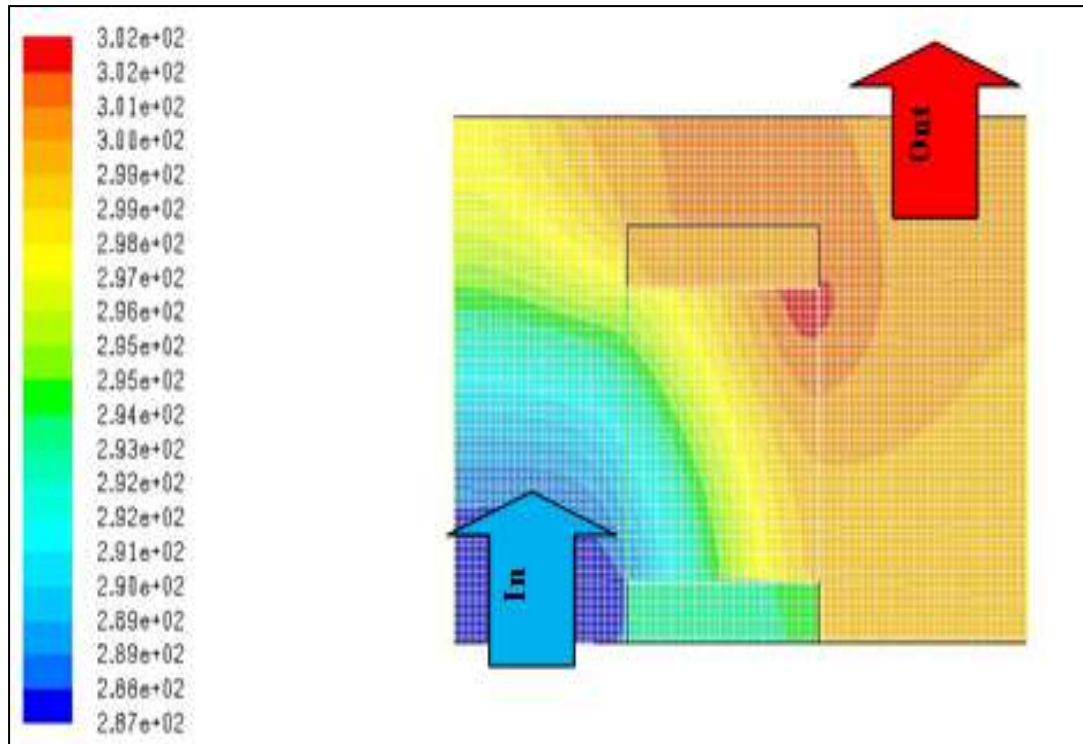


(a) Temperature distribution for 4 porous blocks configuration



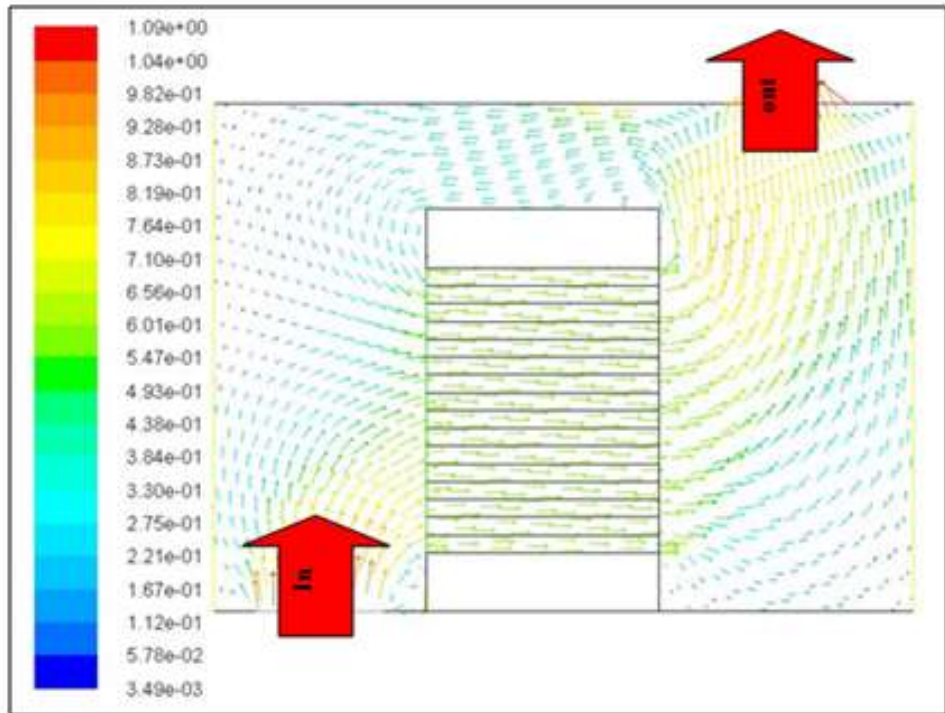
(b) Temperature distribution for 2 porous blocks configuration

Figure 5.16 Temperature fields for the 4 and 2 porous blocks configurations.

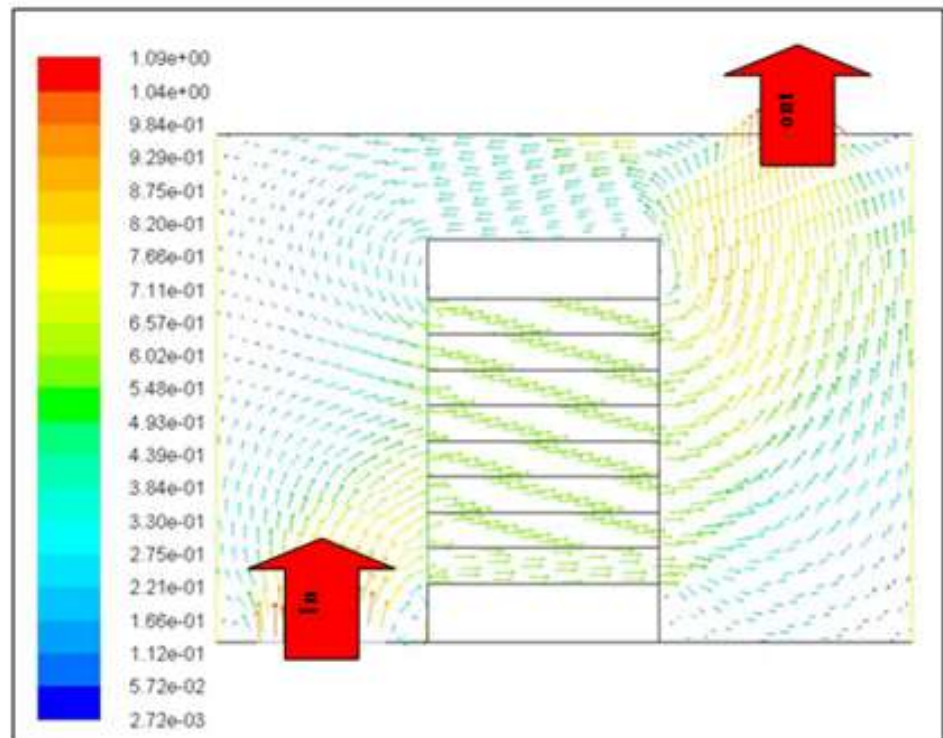


**Figure 5.17 Temperature fields for 1 porous block configuration.**

Figure 5.18 shows that the velocity distribution for 16 servers and 8 servers and the maximum velocity is equal 1.09 m/s for both cases. The assumption of 16 and 8 porous blocks configurations have been taken into account because they provide good agreement with the 32-server rack as shown in Figure 5.9.



(a) Velocity field for 16 porous blocks configuration



(b) Velocity field for 8 porous blocks configuration

Figure 5.18 Velocity fields (m/s) through 16 and 8 porous blocks configurations.

## **5.4 Conclusion**

In this chapter five rack configurations as shown in Figure 5.4 have been compared with 32 porous blocks rack. It is found from the results that the temperature profiles at rack inlet and exhaust for 16 porous blocks and 8 porous blocks configuration are matching the temperature profile for the 32 porous block rack. Furthermore the velocity field for 32, 16, and 8 porous blocks are same. So that, Based on the results the minimum number of porous blocks that could be used to represent 32 porous blocks rack is 8 porous blocks configuration. This simplification will be implemented in next chapter to simplify the geometry building in 3-D scheme.

## **CHAPTER 6: DATA CENTRE COOLING CONFIGURATIONS**

### **6.1 Introduction**

In this chapter, a 3-D analysis will be considered for the small section of a data centre that used by Cho et al. [11]. In chapter 5, the 2-D analysis for the rack has been carried out to simplify the rack. The results show that the 8 porous blocks configuration can be used instead of the 32-server rack. So the 8 porous blocks inside the small data centre will be presented as a traditional data centre (cold-hot aisle arrangement). The cooling techniques, such as cold aisle containment, hot aisle containment and passive back door cooler will be tested to define the effect of these techniques on the temperature distribution inside the data centre.

### **6.2 3-D Analysis for cold-hot aisle arrangement.**

It is shown from chapter 5 that the 32-server rack can be simplified by using just 8 porous blocks to represent each rack. This assumption has been verified by comparing the temperature fields at both rack inlet and exhaust between both the 32-server rack and 8 porous blocks. The agreement for the temperature field for both the 32-server rack and 8 porous blocks was good. Figure 6.1 shows the top view of the data centre that will be tested with a cold- hot aisle arrangement, as is commonly found in data centres. Four racks with 8 porous blocks have been built using Gambit software. The Navier Stokes equations (Equations 4.20 and 4.21) and the energy equation (Equation 4.23) will be solved by using Fluent software. The dimensions of the tested data centre are shown in Figure 6.1, with room height of 2.4 m. The dimensions of the rack have been selected, as per Section 5.2.2.

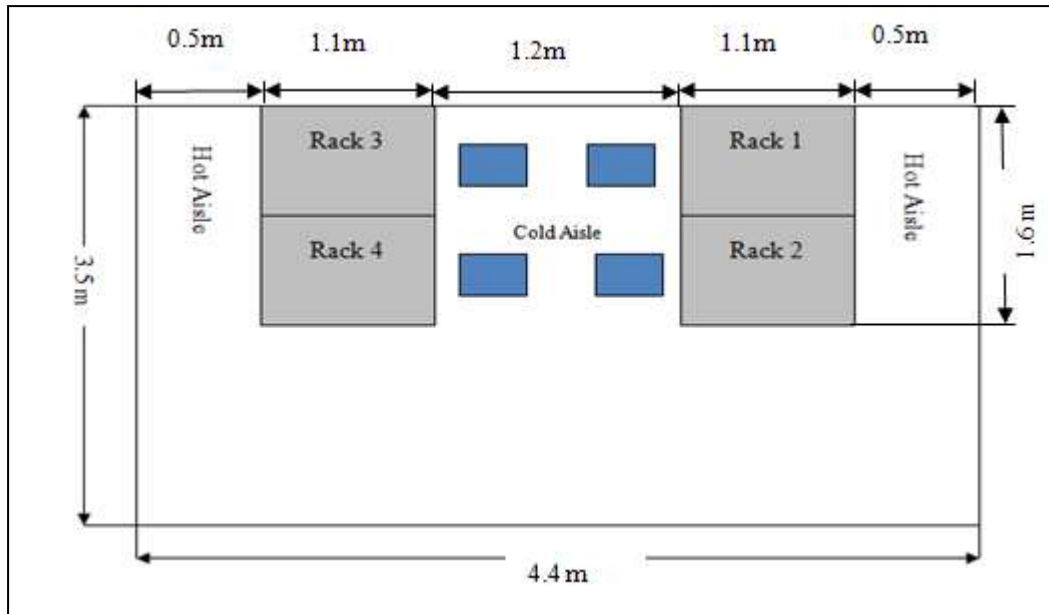


Figure 6.1 Top view for the tested data centre with a cold-hot aisle arrangement.

Each vent with blue colour (as shown in blue in Figure 6.1) provides the cold air that comes from the CRAC unit through the under-floor plenum. The data centre exhaust is located at the top of each hot aisle. The dimensions of the tested data centre have been selected, as per Cho et al. [11]. Cho et al.'s [11] dimensions for the tested data centre were 1.2 m and 1m for the cold and hot aisle, respectively; however, the selected study is just a section of Cho et al.'s [11] data centre.

The standard  $k-\epsilon$  model is used in this study due to justification provided by Cho et al. [11], who showed that is  $k-\epsilon$  model may be used for a large and open-spaced environment. The velocity of the air from each vent is set to 1 m/s, with the temperature of 15°C. The heat dissipation from each rack is 8 kW.



The solution domain for this study is specified by using 403703 cells around the rack where the hot spots will appear. The mesh study has been done for this case to ensure that the mesh independence is achieved and does not affect the results. The mesh study of the traditional data centre has been done as follows in table 6.1.

**Table 6.1 Number of cells vs. the maximum temperature for the traditional data centre.**

Number of cells	Maximum temperature (K)
203560	306.51
305021	308.72
350100	309.55
403703	310.24
454501	310.24
473112	310.24
502310	310.24

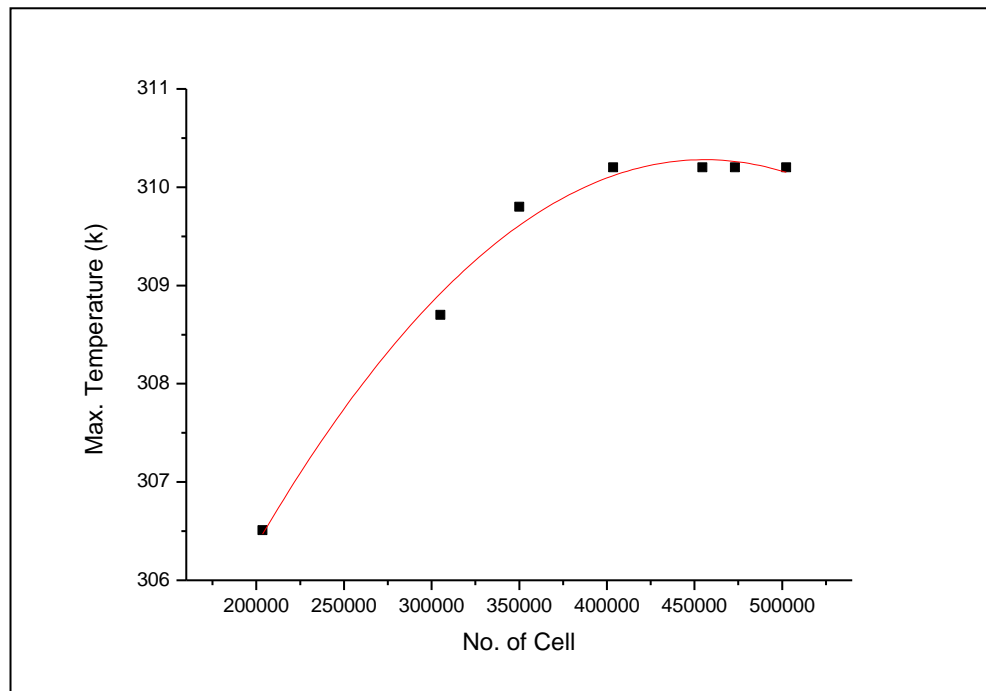


**Figure 6.2 Mesh independence study for the traditional data centre.**

The number of cells that were used to solve the problem was 403703. In such, the number of cells that were used is the right choice because after increasing the number of cells the maximum temperature remains constant as shown in Figure 6.2.

### **6.3 An Assessment of the cold aisle containment technique**

Cold aisle containment is a technique that is used to prevent the recirculation phenomena in order to provide the cold air stream to the rack inlet without any mixing with the hot air from the hot aisle. A physical barrier is used to cover the cold aisle in order to overcome any mixing between the cold and hot air. This prevents hot spots. The energy will be saved and the cooling efficiency will be improved, while the humidification and dehumidification can be reduced when the

cold aisle containment is used because the hot and cold air streams are separated [30].

The cold aisle containment technique will be tested to compare the traditional data centre (cold-hot aisle arrangement) and this technique to detect whether the cold aisle containment technique is good technique to reduce the data centre temperature. Figure 6.3 shows the top view of the data centre with the cold containment technique where the inlet is the blue colour vents, and the outlet on the top of hot aisle

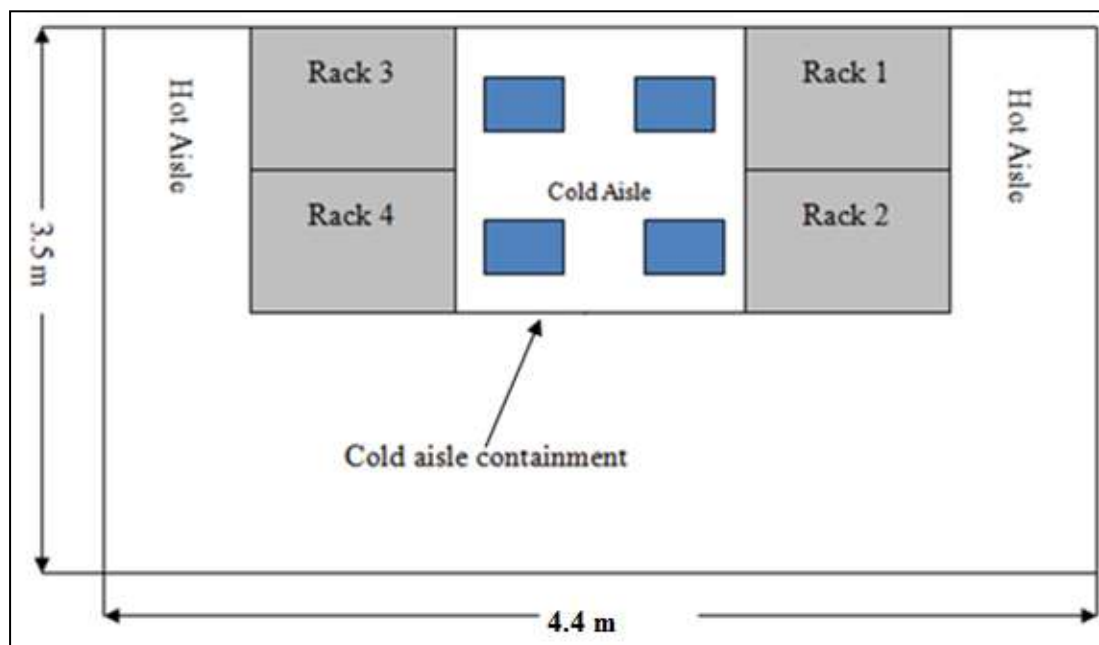


Figure 6.3 Cold aisle containment in the data centre.

#### 6.4 An Assessment of the hot aisle containment technique

The principle of the hot aisle containment technique is similar to the cold aisle technique but the physical barrier is used to cover the hot aisle rather than cold aisle. The hot aisle technique is a technique that is used to prevent mixing between the cold and hot air inside the data centre [30]. This technique also will be tested in

this stage to detect the effect of this strategy on the cooling point inside the data centre. The geometry has been built using Gambit software, as shown in Figure 6.4 and the governing equations have been solved in Fluent software to obtain the velocity, the pressure and the temperature fields. The inlet and outlet for this configuration is same as cold aisle containment configuration.

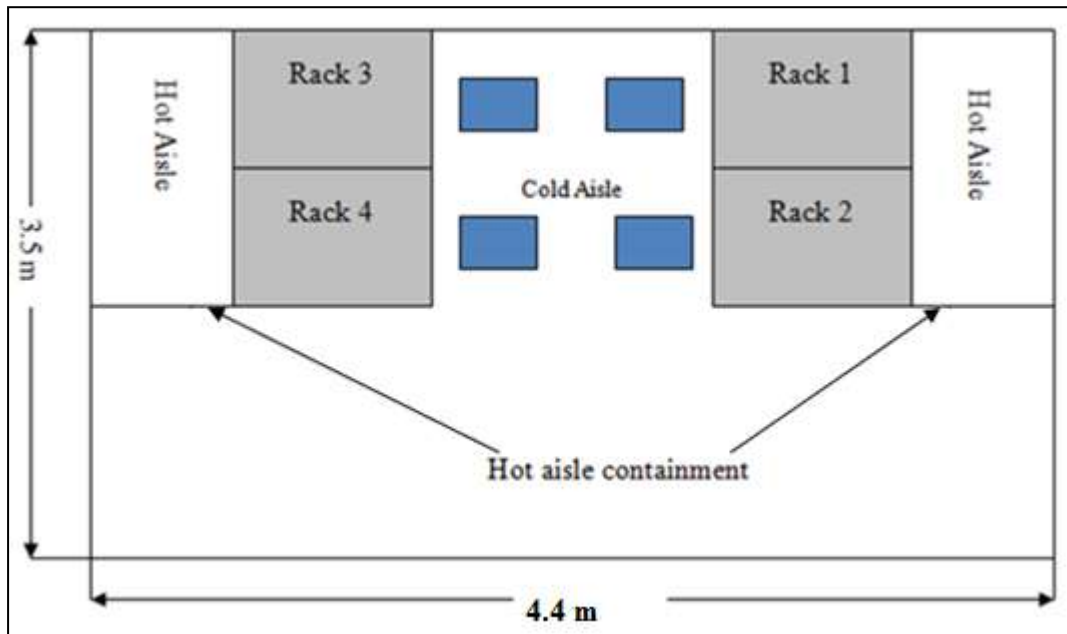


Figure 6.4 Hot aisle containment in the data centre.

In this technique, the room temperature will be expected to be at supply temperature because the hot air will be contained and exhausted outside the data centre. Thus, a uniform intake temperature along the rack height will be expected. These assumptions will be tested by using the CFD analysis.

## 6.5 An assessment of a back door cooler

There are two different types of back door coolers: the active back door cooler and the passive back door cooler. With respect to the active back door cooler, the fan is utilized to draw the air in order to increase the air flow rate, leading to an

increase of heat transfer between the hot air stream and the chilled water inside the back door cooler. In terms of the passive back door cooler, the heat exchanger is installed at the rack exhaust without using fans. A full comparison will be done between these two types to examine the most suitable technique to maintain the temperature inside the data centre.

### 6.5.1 Active back door cooler

In the active back door cooler, the water air heat exchanger is installed at the rack exhaust. The system is provided by using the fan at the heat exchanger, as shown in Figure 6.5. The chilled water is provided to the heat exchanger to cool down the hot air stream coming from the rack exhaust.

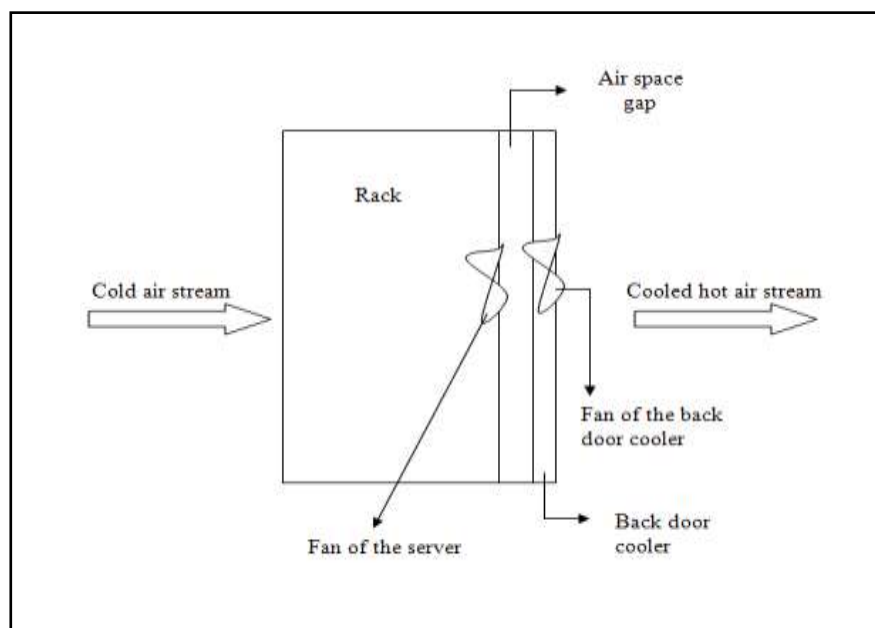


Figure 6.5 Schematic of the active back door cooler.

### 6.5.2 Passive back door cooler

In the passive back door cooler, the water air heat exchanger is installed at the rack exhaust without using any auxiliaries such as a fan, as shown in Figure 6.6. The chilled water is provided to the heat exchanger to cool down the hot air stream coming from the rack exhaust. The forced convection heat transfer occurs due to the

fan of the servers. As before, after the chilled water carries the heat from the hot air, the temperature of the water increases and the temperature of the air decreases. Finally, the hot water is sent to the cooling tower to cool the water and then send it back to the heat exchanger.

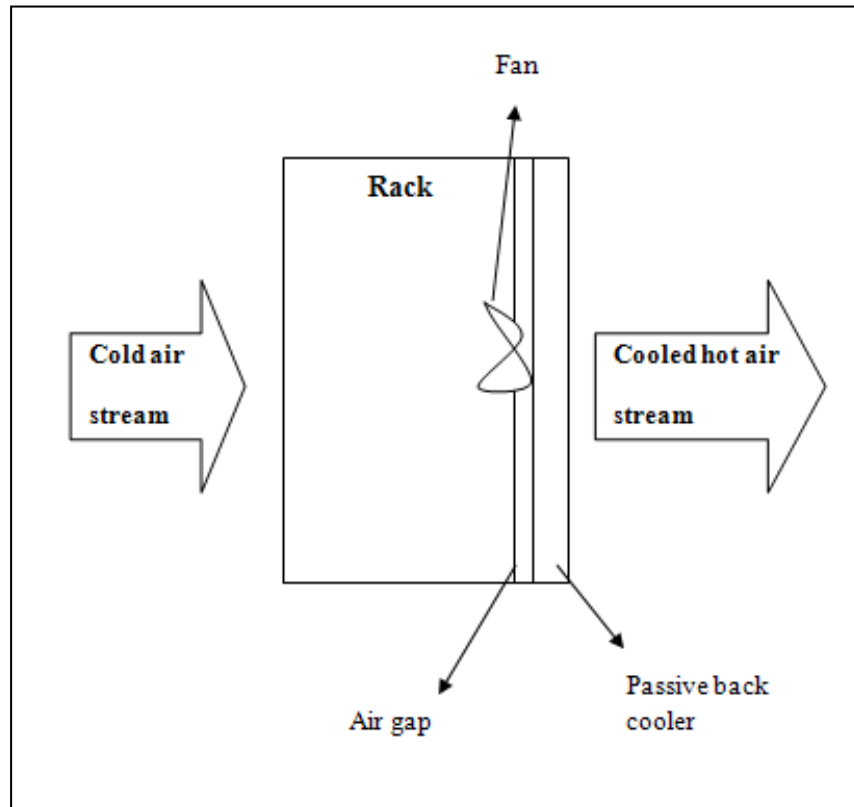
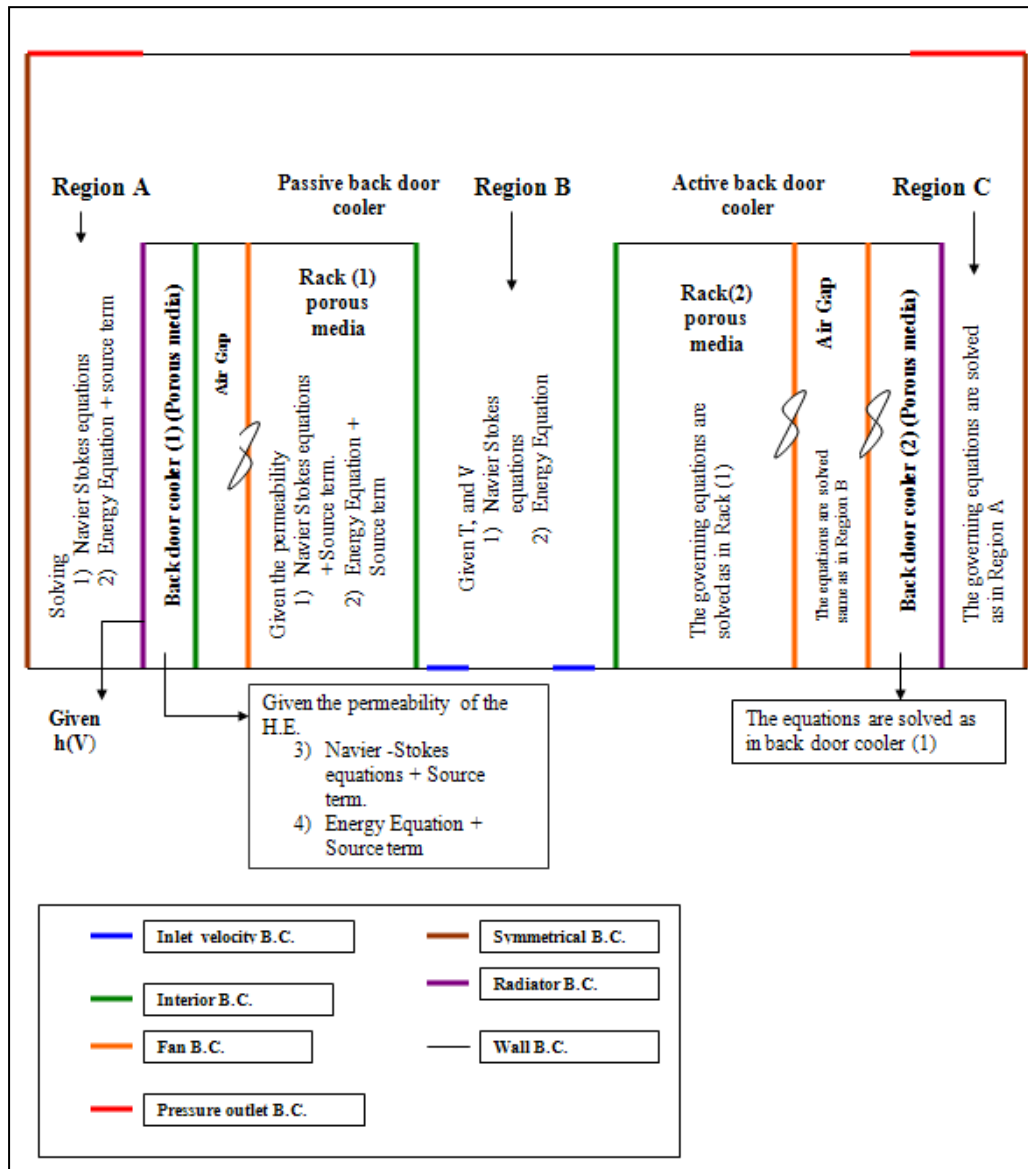


Figure 6.6 Schematic of passive back door cooler.

### 6.5.3 CFD analysis of the back door cooler

The server rack is simulated as a porous media with permeability in the x, y and z directions, which are  $1.889 \times 10^{-6} \text{ m}^2$ ,  $1 \times 10^{-20} \text{ m}^2$  and  $1 \times 10^{-20} \text{ m}^2$ , respectively, as mentioned in table 4.10. The back door cooler is also simulated as a porous media with the same permeability value, except in the X direction, the permeability equals  $1 \times 10^{-8} \text{ m}^2$  because the heat exchanger has a greater resistance to flow than the rack and this permeability value has been obtained based on the pressure drop across the

heat exchanger by the experimental work [85]. In both active and passive back door coolers, the following boundary conditions and governing equations have been specified, as per Figure 6.7.



**Figure 6.7** The boundary conditions and governing equations that are used to solve back door coolers.

Three regions have been specified: region A, region B and region C. Region A and region C represent the hot aisles, where region B represents the cold aisle. At the boundaries of region B, both temperature and velocity have been specified as

inlet boundary conditions. With respect to the passive door cooler at the left of Figure 6.7, both rack and back door heat exchanger have been assumed as porous media. The rack exhaust has been assumed as the fan boundary condition; whereas, the back door cooler exhaust has been assumed as a radiator, where the forced convection heat transfer occurs between the hot air and the cold water in the radiator. Similarly, for the active back door cooler at the right of figure, the boundary conditions have been assumed exactly the same as the passive back door cooler; however, an additional fan has been installed at the air gap exhaust.

The heat transfer coefficient  $h$  can be obtained for the fin and tube heat exchanger (back door cooler), as per Tang et al. [90].

$$h = C|U|^{0.71} \quad (6.1)$$

Equation 6.1 is calibrated to obtain the constant value  $C$  by using experimental curve between heat transfer coefficient and velocity which is obtained by Thompson[85].

The second order polynomial curve is obtained as follows

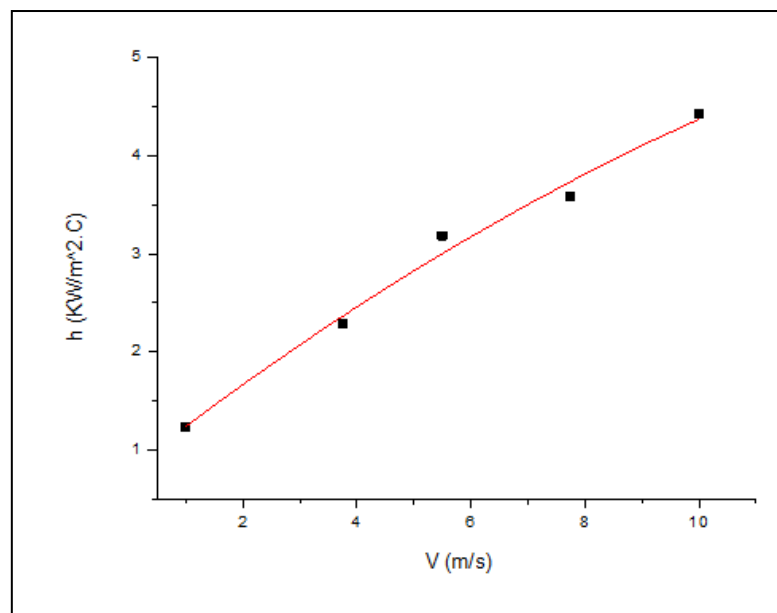


**Figure 6.8 The experimental data for air side convective heat transfer coefficient for different speed values.**



$$h = 794 + 450V - 9.7V^2 \text{ (W/m}^2\text{.K)}$$

The constant C is calibrated by using experimental data and it equals 900  
The fitting curve between the heat transfer coefficient (h) and the velocity (V) for  
the Tang's equation 6.1 can be represented as

$$h = 900|U|^{0.71}$$

Whereas the loss coefficient for the radiator can be represented as

$$K = \frac{2\Delta P}{\rho V^2} \quad (6.2)$$

## 6.6 Result and Discussion

Five cooling techniques have been simulated in order to examine the choice of techniques on both temperature and velocity fields inside the data centre. In the first stage, the CFD analysis has been done for the traditional data centre, which is a cold-hot aisle arrangement, to test both the temperature and velocity fields inside the data centre. In this case, the 8 porous blocks rack is used to represent the 32-server racks. This representation has been implemented due to the results in chapter 5. It is shown from Figure 6.9 that the intake temperature for the rack increases at the top of the rack and this happens due to the recirculation problem when the hot air mixes with the cold air in the cold aisle. The temperature is not uniform at the rack inlet due to this flow recirculation.

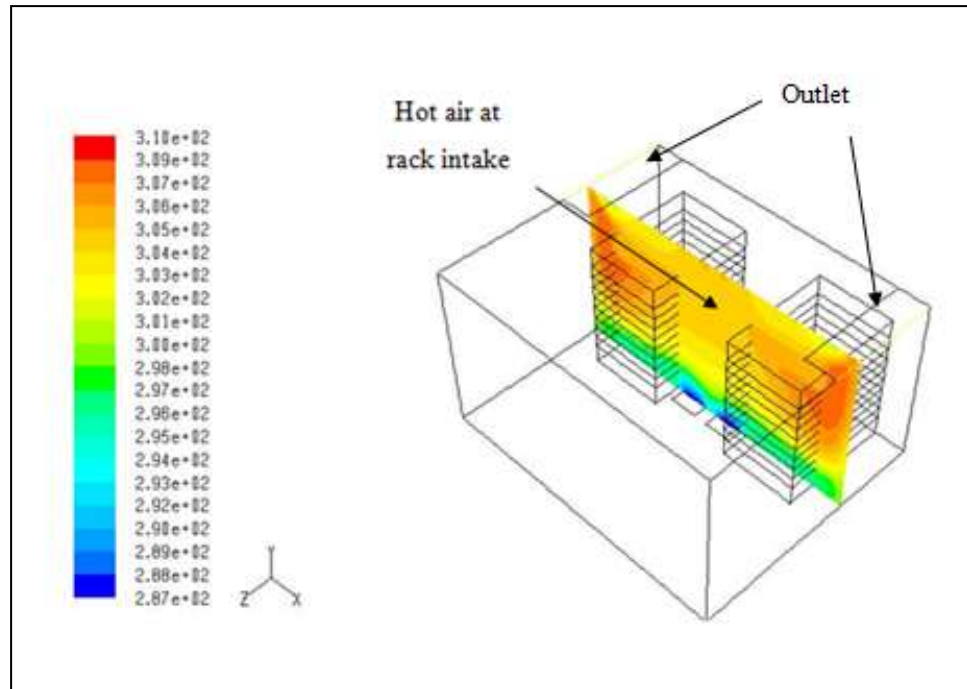


**Figure 6.9 Temperature fields for the cold-hot aisle arrangement.**

The model shown in Figure 6.9 has been validated with Cho et al. [11] section and the temperature profiles are matched.

Cooling techniques have been implemented in order to overcome the flow recirculation problem. The first technique that is applied in this study is the hot aisle containment, as shown in Figure 6.10 (a). Whereas, Figure 6.10 (b) shows the cold aisle containment.

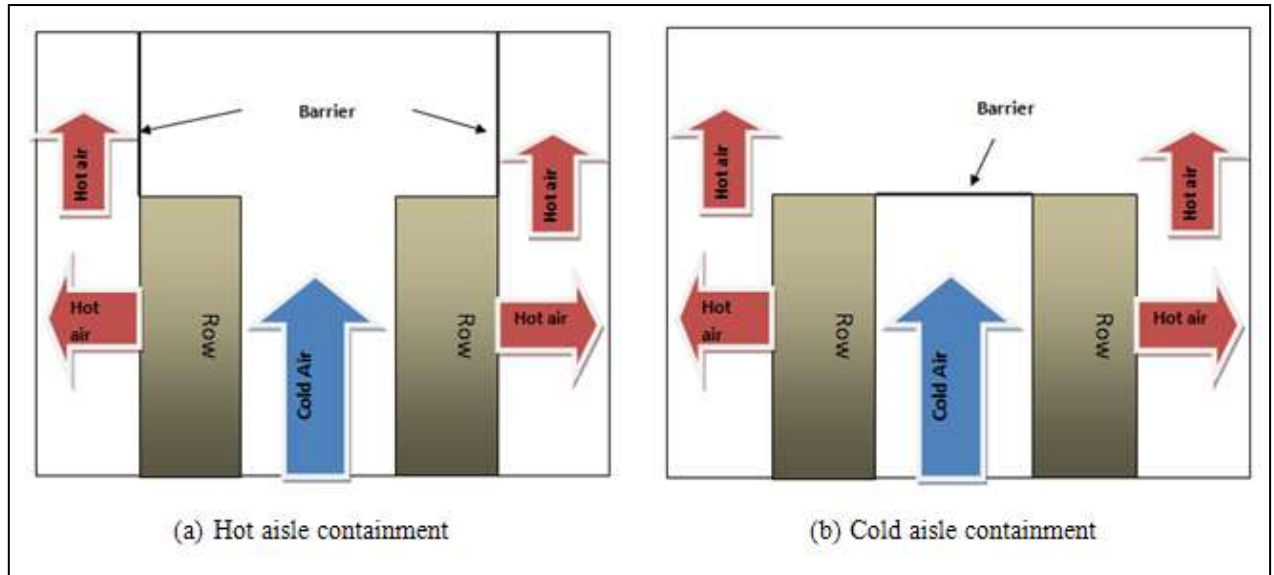


**Figure 6.10 Cold and Hot aisle containment techniques [29].**

Figure 6.11 shows the comparison between the cold aisle containment and the hot aisle containment with respect to the temperature distribution. It shows that the intake temperature for both techniques is almost same and it verifies that the temperature is between 15°C and 19°C.

Also, it is shown in Figure 6.11 that the hot spots are overcome due to covering the cold aisle in the cold aisle containment case and the hot aisle in the hot aisle containment case, so there is no longer mixing between the hot and cold air in the data centre.

Concerning the rack intake temperature, it is shown that the rack intake temperature has been improved by using either cold aisle or hot aisle containment techniques. As an example, the average rack intake temperature in the traditional data centre (cold-hot aisle arrangement with no containment), as shown in Figure 6.9, equals 304 K and it was measured in the Fluent program. Whereas, the average rack intake temperature for both cold aisle containment and hot aisle containment is 288 K and 290 K, respectively. This means that the rack intake temperature is improved by 16 K with the cold aisle containment technique and 14 K with the hot

aisle containment technique. It is shown that the rack intake temperatures in both cold and hot aisle containment techniques are close to the inlet temperature (i.e., 288 K). The reduction of rack inlet temperature leads to an increase in the lifespan of the server racks inside the data centres.

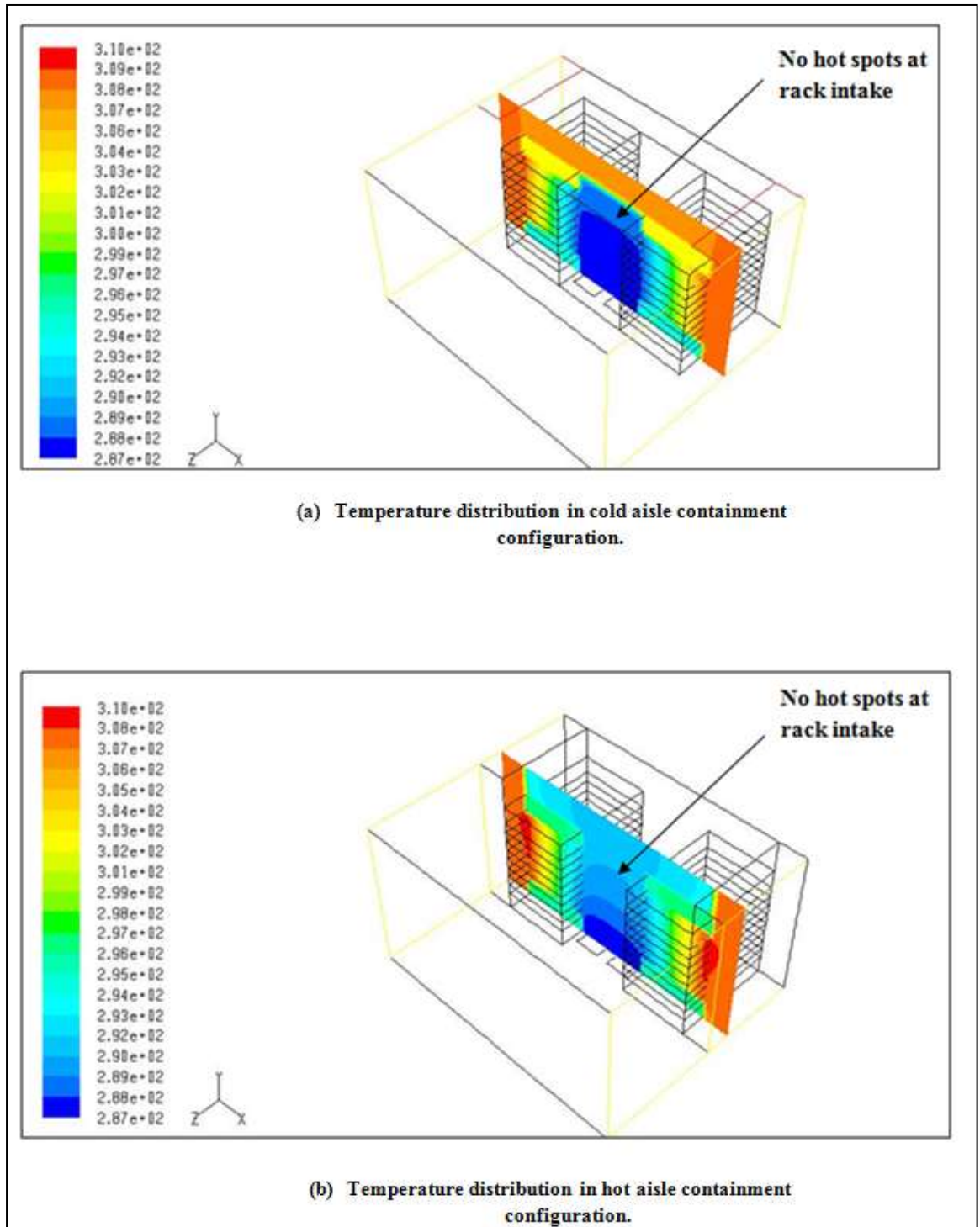
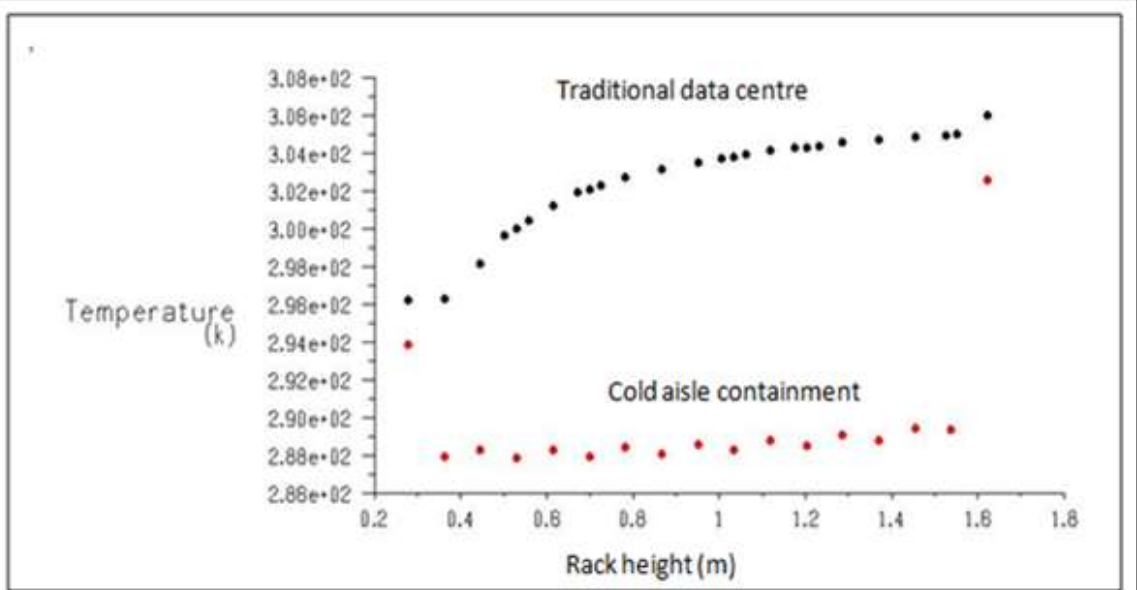
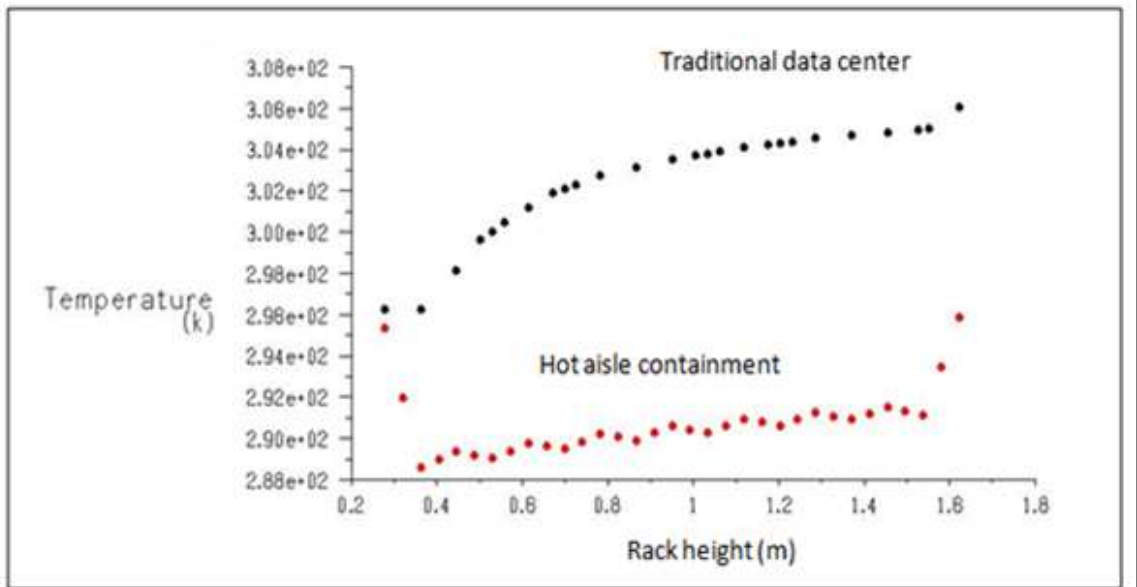


Figure 6.11 CFD analysis for both hot and cold aisle containments with respect to temperature distribution.

The comparison between the temperatures at rack intake and rack exhaust for cold aisle containment, hot aisle containment, and traditional data centre is shown graphically in Figure 6.12 and 6.13. Figure 6.12 clearly shows that the rack inlet temperatures for the both cold aisle containment technique, as in Figure 6.12 (a) (red dots), and hot aisle containment technique, as in Figure 6.12 (b) (red dots), are lower than that of the traditional data centre (black dots), even for the upper servers. This happens because of recirculation in the traditional data centre as opposed to the recirculation in both hot and cold aisle containment techniques, which is absolutely overcome by separating the cold and hot air streams. Therefore, using either cold aisle containment or hot aisle containment techniques decreases the rack intake temperature and reduces the hot spots inside the data centre. Also, it is shown from Figure 6.13 (a) and (b) that the rack exhaust temperature for both cold aisle containment and hot aisle containment techniques are almost constant along the rack height and equal to 35°C. Whereas, the rack exhaust temperature for the traditional data centre is not constant and this is due to the bypass for the cold air to the hot aisle.

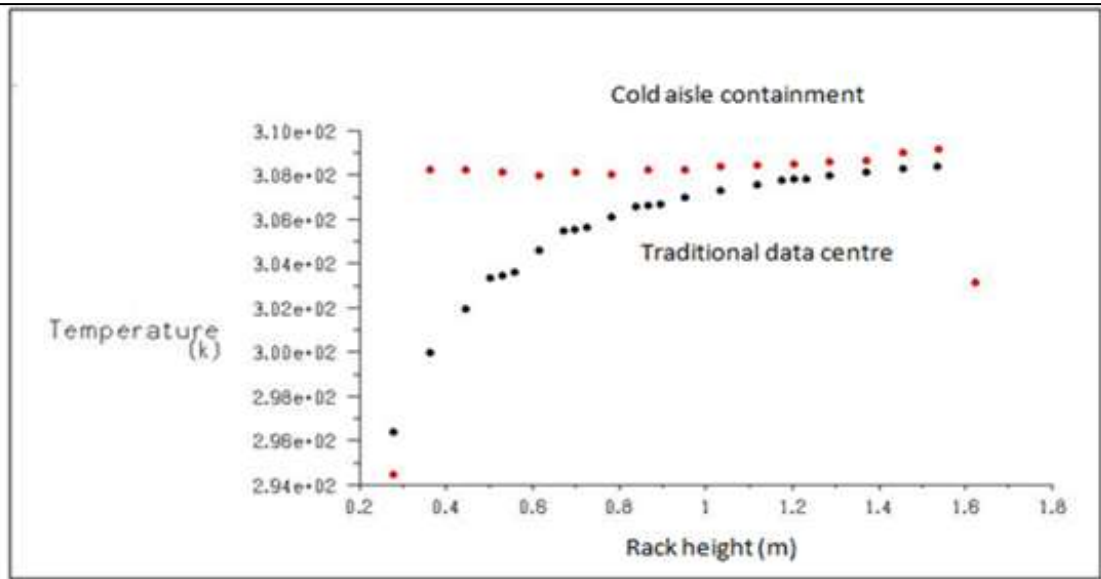


(a) Rack inlet temperature for both cold aisle containment and traditional data centre.

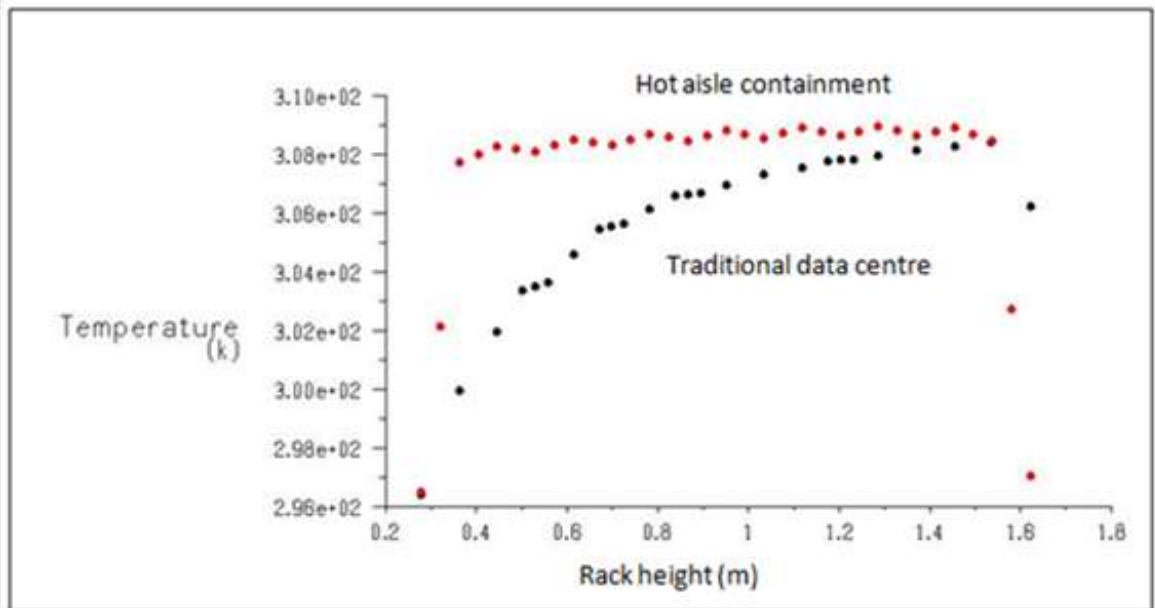


(b) Rack inlet temperature for both hot aisle containment and traditional data centre.

Figure 6.12 Comparison between the cold aisle containment technique, the hot aisle containment technique and the traditional data centre with respect to rack inlet temperature.



(a) Rack exhaust temperature for both cold aisle containment and traditional data centre.



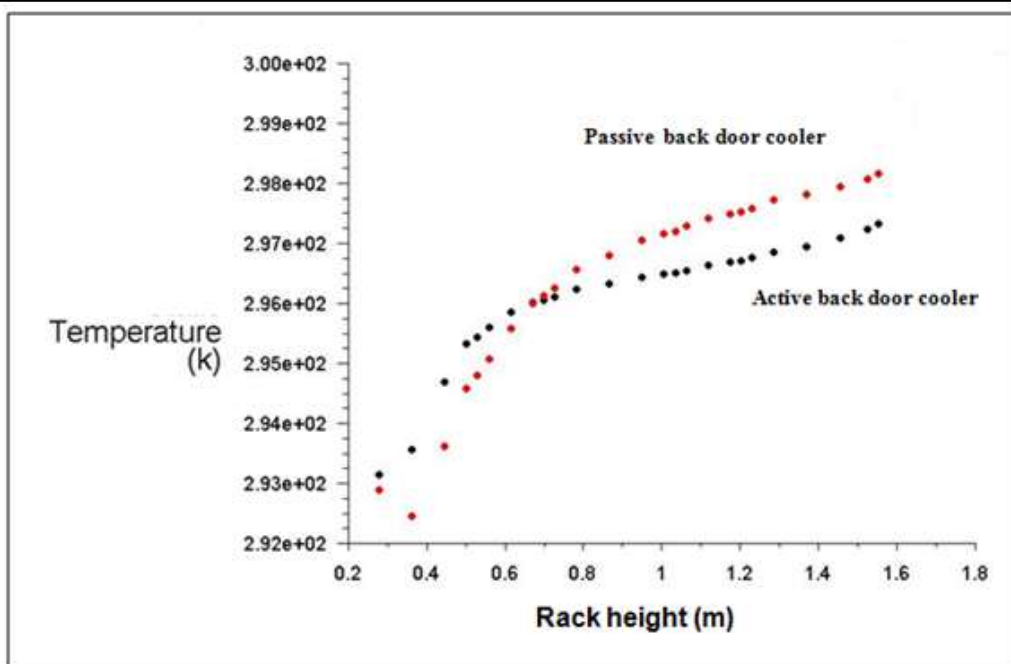
(b) Rack exhaust temperature for both hot aisle containment and traditional data centre.

Figure 6.13 Comparison between the cold aisle containment technique, the hot aisle containment technique and the traditional data centre with respect to rack exhaust temperature.

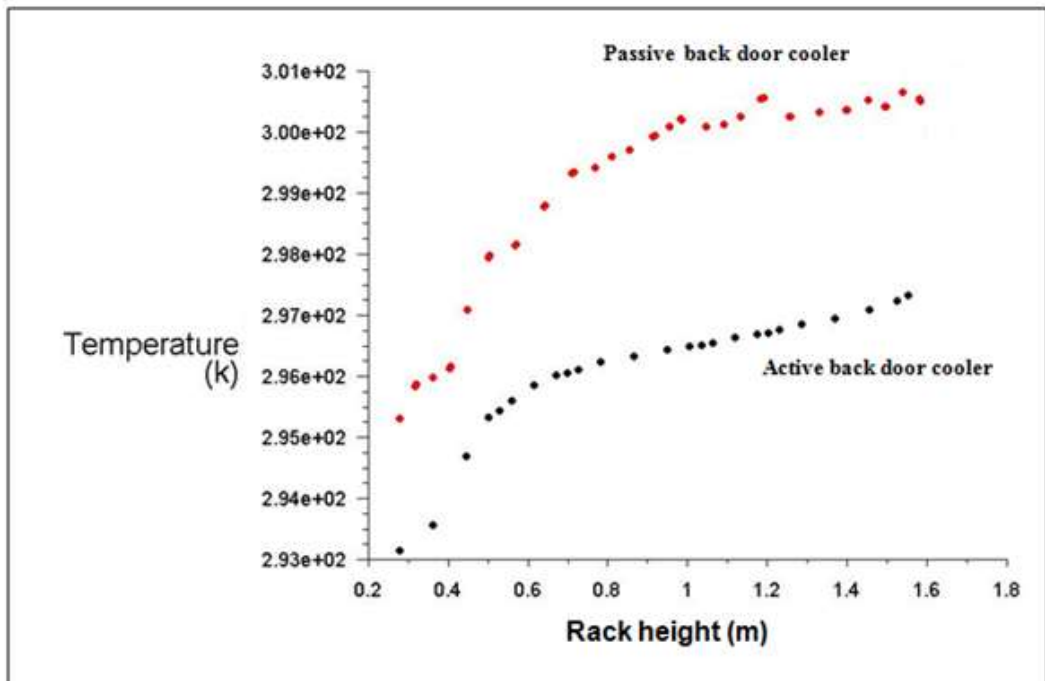
The comparison between the active back door cooler and passive back door cooler with respect to the temperature at the rack inlet and rack exhaust is shown in Figure 6.14. It is shown that the exhaust rack temperature of the active back door cooler is lower than that of the passive back door cooler. Likewise, the inlet rack temperature in the active back door cooler is lower than that of the passive back door cooler. It is shown from Figure 6.14 that the active back door cooler reduces the temperature field inside the data centre because in the active back door cooler, the additional fan has been insulated before the back heat exchanger. The maximum temperatures inside the data centre reach 29°C and 31°C for the active back door cooler and the passive back door cooler, respectively

In terms of the comparison between the back door cooler technique and traditional data centre, it is shown that the intake temperature at the rack can be decreased by using either a passive back door cooler or an active back door cooler. That is means that the hot spots inside the data centre can be reduced by using the back door cooler technique. The specific heat of liquid (water), which is used in the back door cooler, is much greater than the air ( $mC_p$ ). And this depends on the flow rate of water. In such, the temperature inside the data centre will be reduced by using the back door cooler technique.



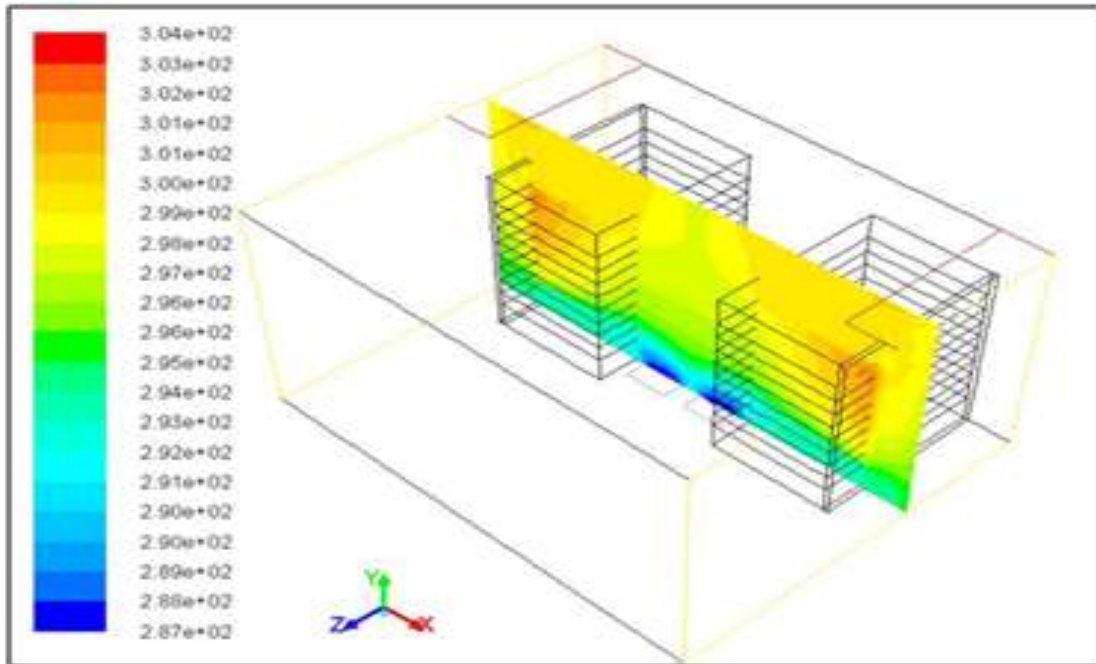


(a) Rack intake temperature for both active and passive back door coolers.

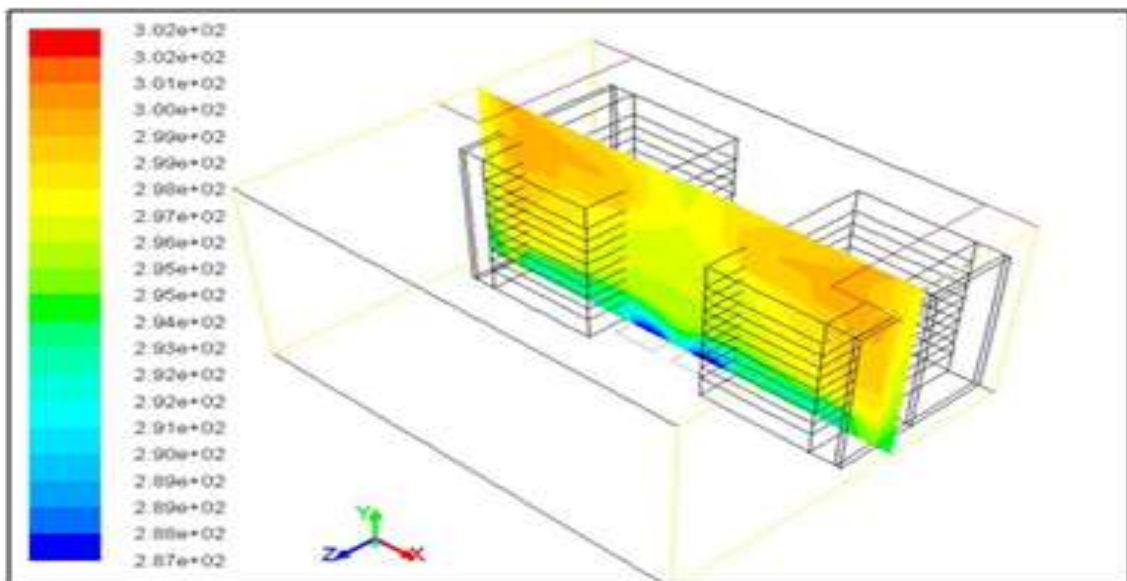


(b) Rack exhaust temperature for both active and passive back door coolers.

Figure 6.14 Rack inlet and exhaust temperatures for both active and passive back door coolers.



**(a) Temperature profile for case of passive back door**



**(b) Temperature profile for case of active back door cooler**

**Figure 6.15 Temperature field inside the data centre for the back door cooler technique.**

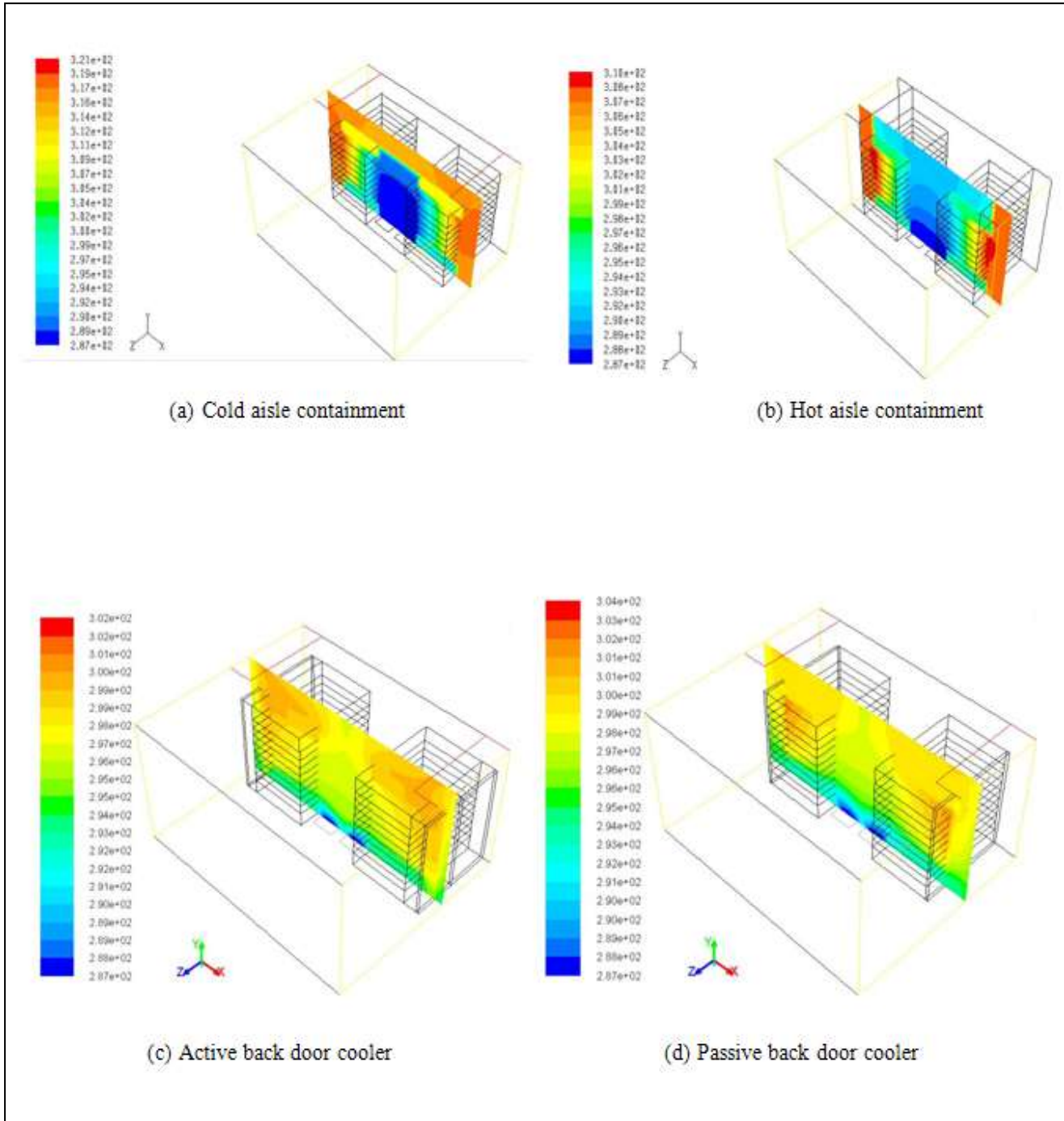


Figure 6.16 Temperature profile for cold aisle containment, hot aisle containment, active back door cooler, and passive back door cooler.

## **6.7 Conclusion**

In this chapter 3-D analysis has been tested to detect the temperature profile for five cooling configurations inside the data centre which are cold-hot aisle arrangement, cold aisle containment, hot aisle containment, passive back door cooler and active back door cooler as shown in Figure 6.16. It is shown that the recirculation problem can be reduced by using either cold aisle containment or hot aisle containment instead of using traditional data centre (cold-hot aisle arrangement) and this leads to reduction of the hot spots inside the data centre. Furthermore, the temperature distribution inside the data centre could be reduced by using either a passive back door cooler or an active back door cooler. The reduction in temperature is due to the back door heat exchanger which is used in both the active and passive back door cooler. However, using the back door cooler consumes extra power to run the heat exchanger and this means that further studies are needed in energy analysis for the back door cooler to check if it is economic or not . Finally, the comparison between active and passive back door coolers is made. It is shown from the results that the maximum temperature in the active back door cooler case is lower than the maximum temperature of the passive back cooler case due to using an additional fan in the active back door cooler. The additional fan that is used in the active back door cooler increases the air flow which leads an increase in the heat transfer between the cold air and exhaust hot air dissipated from servers inside the rack. This point should be taken into account when the comparison between the active and passive back door coolers is made.

## **CHAPTER 7 :CFD ANALYSIS OF DIFFERENT COOLING CONFIGURATIONS OF HPC DATA CENTRES**

### **7.1 Introduction**

HPC data centres will be discussed in this chapter, particularly within the context of different cooling configurations. Different cooling approaches, as discussed in Chapter 6, could be used to reduce the power consumption inside HPC data centres; at the same time, the Coefficient of Performance (COP) of cooling components can be improved by slightly increasing the supply temperature of data centres within the acceptable range (15°C-25°C) [16], leading to an increase of the COP of the cooling unit. Thus, the power input for the CRAC unit will be tested for different cooling configurations inside the data centre when a COP is assumed. The cooling configurations that will be investigated theoretically in this chapter are: cold-hot aisle arrangement, hot aisle containment, cold aisle containment, and active and passive back door coolers. Furthermore, the comparison between the active and passive back door coolers will be drawn to detect which approach is better with respect to reducing the CRAC power consumption.

### **7.2 CRAC power input for different cooling configurations**

The power input to the CRAC unit will be obtained for both direct expansion (DX) and chiller systems. Three cooling configurations—cold-hot aisle arrangement (traditional data centre), hot aisle containment, and cold aisle containment—will be analysed. In this section, the data centre with 8 kW per rack will be tested. The cooling configurations that will be tested are the same as those in

Chapter 6. The CRAC power input values for each cooling configuration will be compared to detect the best cooling configuration that provides the lowest value of power input to the CRAC for the same COP value.

### 7.2.1 CRAC power input for cold-hot aisle arrangement

The CRAC power input (electrical power input) value for a traditional data centre will be presented in this section. The dimensions for the tested data centre are assumed to be the same as in Section 6.2 and shown in Figure 6.1. Each rack will dissipate 8 kW; that is, each server block dissipates 1000 W, and each rack contains 8 server blocks. The calculation for the CRAC power input of a DX CRAC unit requires the air supply temperature to be set at 15°C, the return temperature that will be obtained by using CFD analysis, and the COP for the DX CRAC unit. In a traditional data centre, the supply temperature could not be increased because the room temperature will increase. The maximum allowable data centre temperature is 38 °C, as per ASHRAE [17]. This is maximum temperature in which the equipment can operate without its reliability being affected.

For this case, the COP for the DX CRAC unit can be assumed to be between 3 to 4.5 [60]. In this analysis, the COP will be assumed to be 3.5. Then, the CRAC power input can be obtained as

$$W_{in} = \frac{Q_L}{COP} \quad (7.1)$$

Where ,

$W_{in}$  is the CRAC power inlet (kW)

$Q_L$  is the cooling load (kW), and can be calculated as per Equation 2.11.

From the CFD analysis, the return temperature is found to be 36 °C at a 15°C supply temperature when the cold-hot aisle configuration is used. The return temperature is a bit high because in this situation, each rack dissipates 8 kW so the total amount of heat is around 32 kW in a small data centre volume ( 36.96 m<sup>3</sup>). In such, more mixing between hot and cold air can be expected. Also, the mass flow rate for the air through the vent is found via the CFD calculations to be 1.45 kg/s. The specific heat capacity C<sub>P</sub> for the air equals 1.05 kJ/kg.K at air temperature equals 20°C and atmospheric pressure.

Then the DX CRAC power input can be calculated, as follows:

$$Q_L = \dot{m} C_p (T_R - T_S) = 1.45 \times 1.05 (36 - 15) = 31.9 \text{ kW}$$

Then

$$W_{in} = \frac{Q_L}{COP} = \frac{31.9}{3.5} = 9.1 \text{ kW}$$

So, as the supply temperature increases, the return temperature increases, too. For example, when the supply temperature is increased to 18°C, the return temperature is calculated via the CFD analysis to be 38°C and this is the maximum allowable temperature at the inlet condition inside the data centre. In such, the supply temperature cannot be increased above 18°C.

Whereas, the indication for the COP of a CRAC chiller unit can be obtained using Equation 2.13; for example, the COPs are 2 and 2.67 with 15°C and 18 °C supply temperatures, respectively. This COP value is not the exact value; rather, it is just an indication for the COP value because Equation 2.13 is only valid for the special HPC data centre. However, this equation gives a good indication for the

variation in COP value with respect to the supply temperature of the chiller CRAC unit.

### **7.2.2 CRAC power input of cold aisle and hot aisle containment configurations.**

The aim of this section is to assess the effect of changing the inlet supply temperature on the power of the CRAC unit in data centres, which adopt either cold or hot aisle containment strategies, and to determine which technique provides better performance for both CRAC power input and maintaining room temperature. The configurations of both cold aisle and hot aisle containment systems are assumed as per sections 6.3 and 6.4, respectively. The cold aisle containment solution was presented by Fakhim et al. [91] and demonstrated results that show that the temperature of the hot spots reduces and the temperatures for both cold and hot aisles are decreased. The different supply temperatures have been applied and analysed in the CFD analysis to calculate the required CRAC power input of the DX unit.

The maximum recommended supply temperature is 25°C as per ASHRAE [17]. Thus, the range of supply temperatures from 15°C to 25 °C could be applied. Tables 7.1 and 7.2 show the relationship between the supply temperature, the return temperature, the room temperature and the CRAC power input. All temperatures are obtained from the CFD analysis, apart from the supply temperature, which is assigned as an inlet boundary condition.



**Table 7.1 CRAC power input values for different supply temperatures in cold aisle containment technique at COP =3.5.**

<b>Supply temperature (°C)</b>	<b>Return temperature (°C)</b>	<b>Room temperature (°C)</b>	<b>CRAC input power (kW)</b>
15	35	34.5	8.64
18	37.1	37	8.25
21	39.1	39	7.81

**Table 7.2 CRAC power input values for different supply temperatures in hot aisle containment technique at COP=3.5.**

<b>Supply temperature (°C)</b>	<b>Return temperature (°C)</b>	<b>Room temperature (°C)</b>	<b>CRAC input power (kW)</b>
15	35.3	21	8.76
18	37.6	22.5	8.46
21	39.3	25	7.90

It can be seen from Tables 7.1 and 7.2 that as the supply temperature increases, the CRAC power input values decrease because the temperature difference decreases; however, improvement could be greater with the elevated temperatures. Also it is shown that the hot aisle containment is better than the cold

aisle containment with respect to the room temperature, which is obtained via the CFD analysis. It is shown that for cold aisle containment, the temperature of the room reaches 39°C when the supply temperature is set to 21°C. Whereas, the temperature of the room reaches 25°C at the same supply temperature in the hot aisle containment. Therefore, in terms of the comfort criterion inside the data centre, the hot aisle containment is highly recommended [29]. It is also shown that the CRAC power input values at a COP of 3.5 for both cold and hot aisle containment techniques are almost the same because the return CRAC temperatures are almost equal according to the CFD results. The relationship between the supply temperature and the CRAC power input for the DX CRAC unit in both cold aisle and hot aisle containments can be represented by the following Figure 7.1.

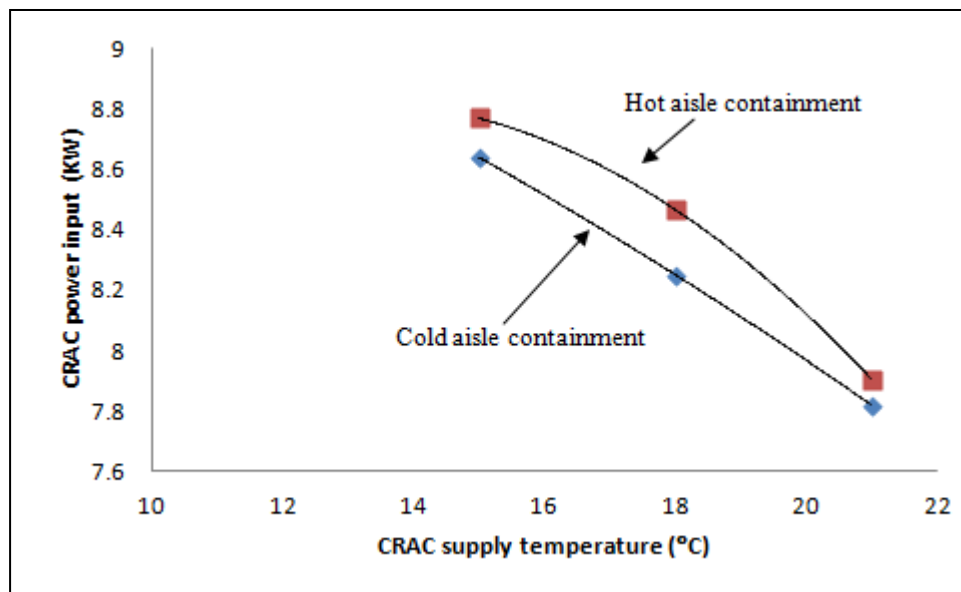


**Figure 7.1 Relationship between CRAC power input and supply temperature for both cold and hot aisle containments at COP=3.5.**

It is shown from Figure 7.1 that as the CRAC supply temperature increases, the compressor power decreases, and vice versa. This will lead to an increase of the COP for DX CRAC units inside data centres.

Figure 7.2 shows the relationship between the CRAC power input (kW) and the room temperature for both cold aisle containment and hot aisle containment. It is shown that as the room temperature increases, the CRAC power input decreases. However, the room temperature in the hot aisle containment configuration is still in the recommended region (21°C-28°C), as per ASHRAE's standard for indoor environments [92]. Whereas, the room temperature reaches 39°C in the cold aisle containment because in this case, the rack exhaust temperature is exactly the same as the room temperature, so that there is no mixing between cold and hot air to reduce the room temperature. This temperature is out of the recommended region.

With respect to comparison between the traditional data centre and both cold and hot aisle containments configurations, it is shown that the compressor power (CRAC power input) can be reduced by around 1.1 kW when either cold or hot aisle containment configurations are used versus the normal arrangement of cold and hot aisles.

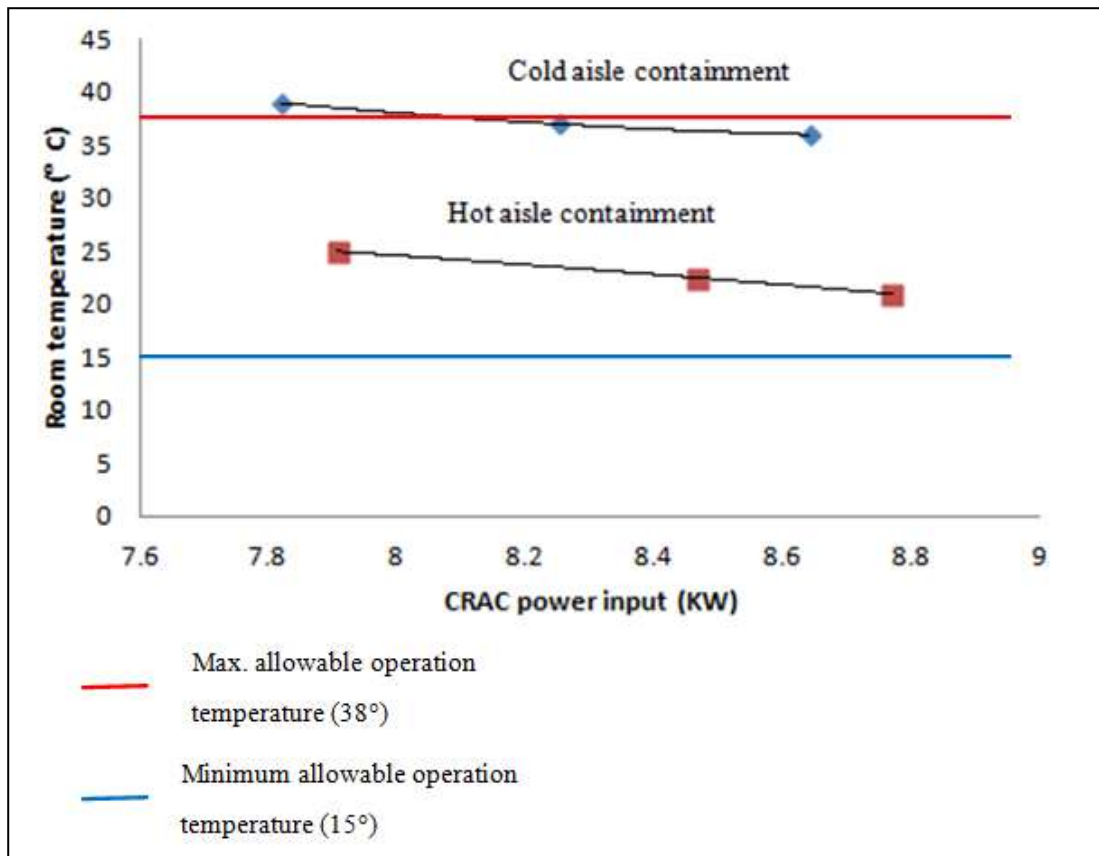


Figure 7.2 CRAC power input vs. room temperature for both hot and cold aisle containments at COP=3.5.

In terms of the chiller CRAC, the indication of COP can be obtained for both cooling configurations by using only the supply temperature, as is mentioned in Section 2.8.2. The values of COP of the chiller system can be calculated by using Equation 2.10. The values of COP for supply temperature of 15°C, 18°C and 21°C are 2, 2.67 and 3.47, respectively.

### **7.2.3 CRAC power input for active and passive backdoor coolers**

The aim of this section is to analyse the effect of using both active and passive back door liquid loop heat exchangers on the CRAC power input and to detect which configuration has better performance. The configurations used in this study are cold aisle containment, hot aisle containment, passive back door cooler and active back door cooler. The configuration of both active and passive back door heat exchangers have been addressed in Section 6.5. The different supply temperatures have been applied and analysed by CFD to calculate DX CRAC unit power requirements. A COP of 3.5 will be assumed. In this study, different CRAC supply temperatures will be applied within the allowable range to find the effect of changing the supply temperature on the DX CRAC compressor unit.

The CFD is used to calculate the CRAC power input by measuring the return CRAC temperature for different supply temperatures. Tables 7.3 and 7.4 show the relationship between the supply temperature, the return temperature, and the total power input for passive and active back door liquid loop heat exchanger, respectively.

**Table 7.3 Power input values for different supply temperatures in passive back door cooler at COP =3.5.**

<b>Supply temperature (°C)</b>	<b>Return temperature (°C)</b>	<b>CRAC input power (kW)</b>	<b>Chiller power input for the passive back door cooler (kW)</b>	<b>Total power input (kW)</b>
15	27.1	5.22	3.14	8.36
18	27.6	4.14	2.81	6.95
21	28.1	3.06	2.53	5.59

**Table 7.4 Power input values for different supply temperatures in active back door cooler at COP =3.5.**

<b>Supply temperature (°C)</b>	<b>Return temperature (°C)</b>	<b>CRAC input power (kW)</b>	<b>Chiller power input for the active back door cooler (kW)</b>	<b>Total power input (kW)</b>
15	25.5	4.53	3.71	8.24
18	25.9	3.41	3.25	6.66
21	26.3	2.28	2.91	5.19

It is shown from both Tables 7.3 and 7.4 that the CRAC power input decreases when the supply temperature increases within the acceptable range (15°C-25°C), and this is due to decreasing in the temperature difference between the supply and return temperatures. Also the total power decreases when the supply temperature decreases too. This leads to reduction in the amount of cooling load, which results in a corresponding decrease in the CRAC power input and the total power for both active and passive back door coolers. Also, it is shown from these tables that the CRAC power input (compressor work of the refrigeration cycle) could be reduced to around 0.7 kW when an active back door cooler is installed. However, the pumping of the water, which is used to remove the heat from the back door cooler and the fans consume power.

The relationship between the supply temperature and the CRAC power input for the DX CRAC unit for both active and passive back door heat exchanger configurations is represented in Figure 7.3.

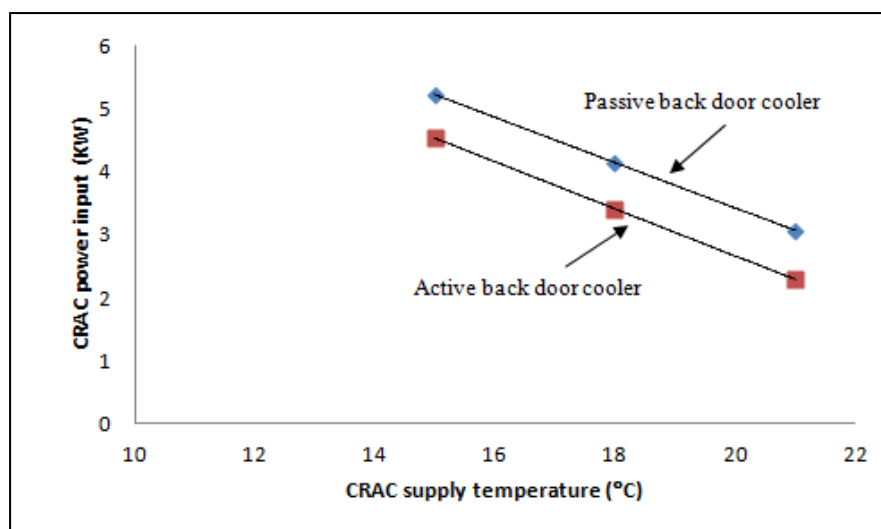
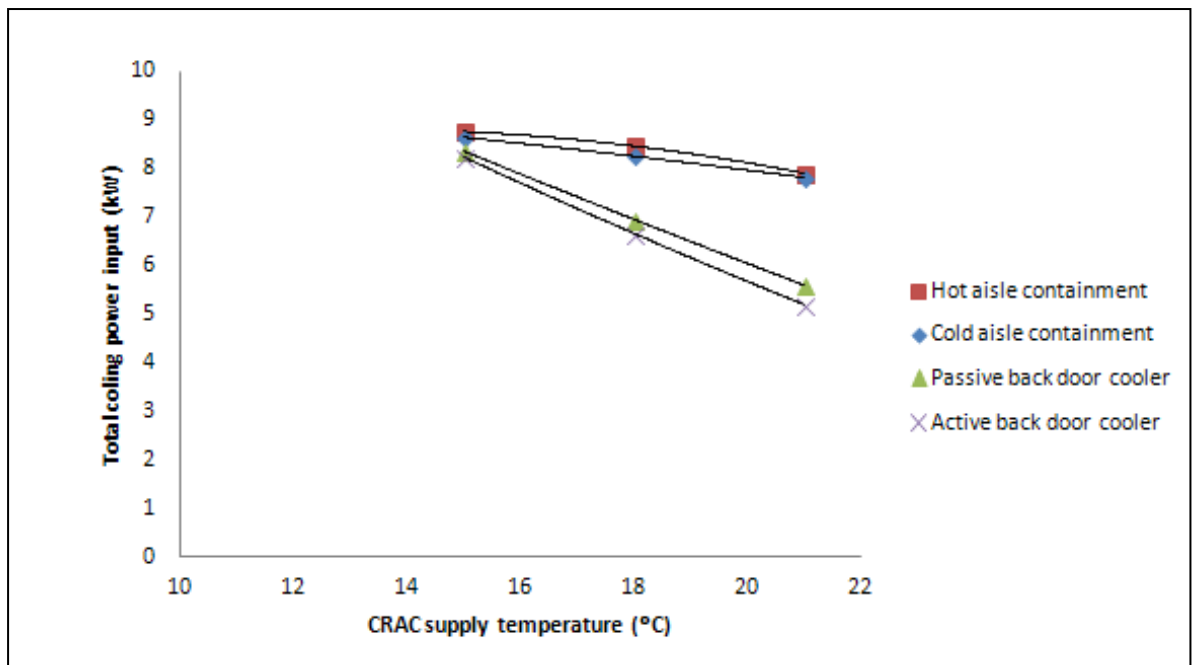


Figure 7.3 Relationship between CRAC power input and supply temperature for both passive and active back door coolers at COP=3.5.

At the end of this study, the full comparison has been done between four cooling configurations—cold aisle containment, hot aisle containment, passive back door cooler and active back door cooler—as per Figure 7.4. This comparison has been done at specific conditions, when the DX CRAC unit is used with a COP of 3.5, and chiller unit with COP of 3.5 to operate back door coolers. It is shown from Figure 7.4 that the lowest total cooling power input can be achieved when the active back door cooler is used among the four cooling configurations. Therefore, the cost of the electrical work used in the CRAC unit and chiller unit can be reduced when the active back door cooler is used. However, the cost of installation of back door coolers is not considered in this study.



**Figure 7.4 Total cooling power input of DX CRAC and chiller units vs. CRAC supply temperature four cooling configurations at COP=3.5.**



Further study of active and passive back door coolers in high density data centres will be presented in Section 7.3 to detect the effect of using active and passive back door coolers in HPC data centres and how they affect on the temperature inside the data centres and the CRAC power consumption.

### **7.3 Back door cooler in HPC data centre.**

In this section, the comparison between active and passive back door coolers that are used in an HPC data centre will be presented. The rack will be analysed to use with both an active and passive back door cooler. The comparison is based on changing the heat dissipation load of the rack for both active and passive back door coolers. The comparison between the active and passive back door heat exchangers with respect to the rack intake and exhaust temperatures will be assessed using a CFD analysis. The heat load from the IT systems takes values of 15 kW, 25 kW and 30 kW per rack.

The same specifications for both active and passive back door coolers is assumed, as per Section 6.5, and has been published by Almoli et al. [45], where they considered two rows of three racks and each rack had 4 server blocks. The Hagen-Poiseuille equation is used to determine the pressure drop across the 1U server where a hydraulic diameter,  $D_h=2R$ , of 1U servers is used to give

$$\Delta P = \frac{8\mu v}{R^2} L \quad (7.2)$$

Where ;

$\mu$ : is the viscosity of the fluid (kg/m. s)

$R$  : is the hydraulic radius of the channel (m)

$v$ : is the axial velocity (m/s)

$L$ : is the length of channel in the X direction

Whereas, the hydraulic diameter of the server is calculated, as follows:

$$D_h = \frac{4A}{P}$$
$$R = \frac{D_h}{2} = 0.012m$$

Then, the pressure drop across the channel is calculated as

$$\Delta P = \frac{8\mu v}{R^2} L \Rightarrow \frac{\Delta P}{L} = \frac{8\mu v}{R^2}$$
$$\frac{\Delta P}{L} = 0.9941v \tag{7.3}$$

This approach enables the permeability,  $\alpha$ , of the servers to be calculated, where Darcy's Law is assumed to calculate the pressure drop across the porous model, as follows:

$$\Delta P = \frac{-\mu}{\alpha} v \Delta x \tag{7.4}$$

Then,

$$\frac{\Delta P}{\Delta x} = -\frac{1.7894 \times 10^{-5}}{\alpha} v \tag{7.5}$$

The value of permeability then can be obtained by comparing Equations (7.3) and (7.5), giving  $\alpha=1.8\times 10^{-5} \text{ m}^2$ .

The permeability above has been obtained by using Equations (7.2) and (7.4), pressure drop across the pipe, and Darcy's Law, respectively, as described by Almoli et al. [45]. However, the permeability of the server blocks in this chapter has been obtained by measuring the pressure drop across the server for different flow rates, as described in Chapter 4.

### 7.3.1 CFD analysis of back door cooler inside a HPC data centre

Chapter 4 has demonstrated that the porous approach to represent the server rack is valid. Therefore, here, a rack with 8 servers is assumed as in Chapter 5 and it was shown that 8 server blocks in a rack can be used to represent 32-rack servers. The momentum equations and the energy equations will be solved with the additional source terms, as follows:

$$\underline{S}_i = -\frac{\mu}{\alpha_{rack}} \underline{U} \quad \text{and} \quad S_Q = \frac{Q_{rack}}{V_{rack}} \quad (7.6)$$

In equation (7.6),  $\alpha_{rack}$  is the permeability of the rack,  $Q_{rack}$  is the rate of heat generation inside the rack and  $V_{rack}$  is the volume of the rack equalling  $1.182\text{m}^3$ . The value of  $\alpha_{rack}$  is  $1.889\times 10^{-6} \text{ m}^2$  as in table 4.10, and  $S_Q= 12682\text{W}/\text{m}^3$ ,  $21137.8\text{W}/\text{m}^3$ , and  $25365.2\text{W}/\text{m}^3$ , which represents 15 kW, 25 kW and 30 kW per rack, respectively.

The back door cooler is assumed to be a porous media with permeability values of  $1\times 10^{-8} \text{ m}^2$ ,  $1\times 10^{-12} \text{ m}^2$  and  $1\times 10^{-20} \text{ m}^2$  in X, Y and Z directions, respectively as highlighted in Chapter 6. Therefore, the momentum equations are also solved with an additional Darcian source term that is expressed as

$$\underline{S}_i = - \frac{\mu}{\alpha_{backdoorcooler}} \underline{U} \quad (7.7)$$

The amount of heat that passes the back door cooler is removed by the following equation:

$$\dot{Q} = \dot{m} h A (T_{air} - T_{ref}) \quad (7.8)$$

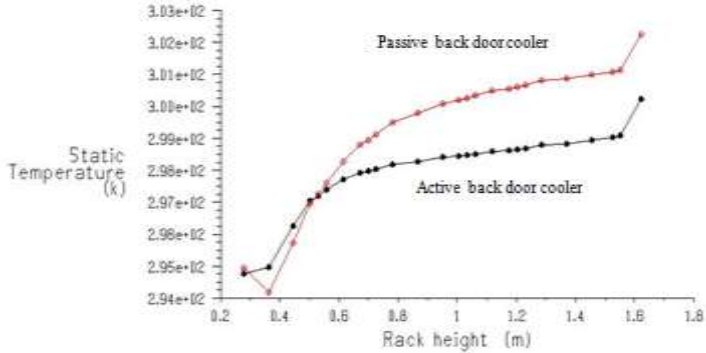
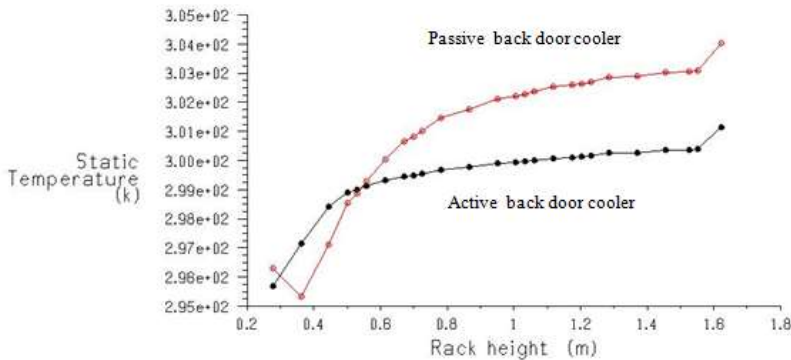
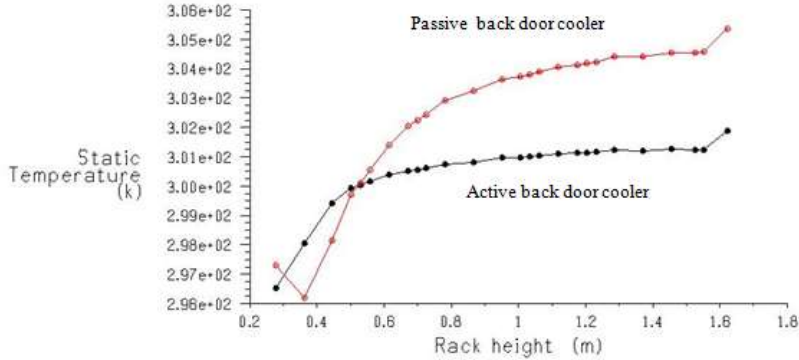
Where,  $\dot{m}$  is the mass flow rate of air across the back door cooler;  $h$  and  $A$  are its average convective heat transfer coefficient and surface area of back door cooler, respectively;  $T_{air}$  is the temperature of the air stream coming from the rack exhaust; and  $T_{ref}$  is the set point temperature of the back door cooler that varies between 13°C and 18°C in an HPC system liquid loop back door cooler at the University of Leeds. Therefore, it is assumed to be the average value, which is 15.5°C in this study. The convective heat transfer coefficient ( $h$ ) is actually a function of  $\underline{U}$  and its variation is based on equation 6.1, as suggested by Tang et al. [90], for a fin and tube heat exchanger.

### 7.3.2 Results and discussion

In this section the comparison between active and passive back door coolers will be discussed. Also, the power consumption of the CRAC will be obtained for a cold-hot aisle arrangement (traditional data centre), active back door cooler and passive back door cooler. Both inlet and exhaust rack temperatures are obtained by using CFD analysis. It is shown from Table 7.5 and Table 7.6 that both rack inlet and rack exhaust temperatures for the active back door cooler are lower than those of the passive back door cooler. The difference of temperature is due to the additional fan that is installed in the active back door cooler. The additional fan in the active back door cooler increases the heat transfer rate between the back door

heat exchanger and the hot air stream by increasing the air stream velocity, thus leading to an increased heat transfer coefficient. The exhaust temperature for the active back door cooler is consistently lower than the temperature of the passive back door cooler for heat loads of 15, 25 and 30kW per rack. The exhaust temperature for the active back door cooler is around 4-5°C less than that of the passive back door cooler for all rack heat dissipations. This implies that the power consumption by the CRAC will be reduced due to the decrease of the exhaust temperature. However, the cost of installing either a passive back door cooler or an active back door cooler, and the cost of cooling the water passing in the door heat exchanger, should be taken into account.

**Table 7.5 CFD analysis for rack intake temperatures for both active and passive back door cooler for different rack heat consumption (kW).**

Heat dissipation load	Rack intake temperature
15 kW	 <p>The graph for 15 kW shows static temperature (k) on the y-axis (ranging from 2.94e+02 to 3.03e+02) and rack height (m) on the x-axis (ranging from 0.2 to 1.8). Two data series are plotted: 'Passive back door cooler' (red line with circles) and 'Active back door cooler' (black line with circles). Both series show an initial increase in temperature with rack height, followed by a slight decrease and then a final increase. The passive cooler consistently shows higher static temperatures than the active cooler.</p>
25 kW	 <p>The graph for 25 kW shows static temperature (k) on the y-axis (ranging from 2.95e+02 to 3.05e+02) and rack height (m) on the x-axis (ranging from 0.2 to 1.8). Two data series are plotted: 'Passive back door cooler' (red line with circles) and 'Active back door cooler' (black line with circles). The trends are similar to the 15 kW case, with the passive cooler showing higher static temperatures throughout the rack height range.</p>
30 kW	 <p>The graph for 30 kW shows static temperature (k) on the y-axis (ranging from 2.96e+02 to 3.06e+02) and rack height (m) on the x-axis (ranging from 0.2 to 1.8). Two data series are plotted: 'Passive back door cooler' (red line with circles) and 'Active back door cooler' (black line with circles). The trends are consistent with the previous two cases, showing that the passive cooler results in higher static temperatures compared to the active cooler.</p>

**Table 7.6 CFD analysis for rack exhaust temperatures for both active and passive back door cooler for different rack heat consumption (kW).**

Heat dissipation load	Rack exhaust temperature
15 kW	<p>Static Temperature (k)</p> <p>Rack height (m)</p> <p>Passive back door cooler</p> <p>Active back door cooler</p>
25 kW	<p>Static Temperature (k)</p> <p>Rack height (m)</p> <p>Passive back door cooler</p> <p>Active back door cooler</p>
30 kW	<p>Static Temperature (k)</p> <p>Rack height (m)</p> <p>Passive back door cooler</p> <p>Active back door cooler</p>

The mass flow rates across the CRAC unit and the back door coolers are obtained from the CFD analysis. The mass flow rate across the CRAC unit is 3.5 kg/s, and the mass flow rate across the active and passive back door coolers are 4.57 kg/s and 3.25 kg/s, respectively. In Table 7.7, the temperature differences across both active and passive back door coolers are 4 K and 5 K, respectively.

The CRAC loads are presented in Table 7.7, where the calculations are based on a data centre with 4 racks, with each rack producing 25 kW of heat load. It is shown that the CRAC unit load decreases when the back door coolers are used. For the CRAC alone inside the data centre, it must remove 100kW of heat. Whereas, the CRAC load is reduced by up to 69% when the passive back door cooler is applied, and when the active back door cooler is used, the CRAC load can be reduced by up to 77% over configurations with no back door heat exchangers. Therefore, the active back door cooler is more efficient than the passive back door cooler in reducing the load on the CRAC unit.

**Table 7.7 Heat load calculations for the CRAC unit and a back door cooler for a data centre with four racks at 25 kW each.**

Data centre configuration	Heat load on CRAC	Heat load on back door cooler
CRAC	$m_{CRAC} C_p (T_{inlet} - T_{outlet}) = 100 \text{ kW}$	$m_{backdoor} C_p \Delta T_{acrossbackdoor} = 0$
CRAC + passive	32.12 kW	68.16 kW
CRAC + Active	23.45 kW	76.8 kW



## 7.4 Conclusion

This chapter includes the comparison between different cooling configurations, such as cold aisle containment, hot aisle containment, active back door cooler and passive back door cooler. It is shown that the cooling power input for the CRAC unit could be reduced when both active and passive back door coolers are used. However, these results do not reflect the actual situation for the back door cooler because in this study it is shown that the total cooling power input for all cooling configurations are close to each other as shown in Figure 7.4 . however, the minimum total cooling power input could be achieved when the active back door cooler is used. After that, a comparison between an active back door cooler and a passive back door cooler in a HPC data centre was conducted. The additional fan in the active back door cooler increases the heat transfer rate between the back door heat exchanger and the hot air stream by increasing the air stream velocity, thus leading to an increased heat transfer coefficient. It is shown from this study that the CRAC load could be decreased up to 77% when the active back door cooler is used, and 69% when the passive back door cooler is used. However, the back door cooler techniques need greater study to define the true economical energy efficiency benefits for a range of data centres. In such, more detailed cost/benefit analysis should be considered. Also, the energy, maintenance, and installation costs should be taken into account when the back door coolers cooling configurations are used.

## CHAPTER 8: CONCLUSIONS

### 8.1 General discussion

Air cooling methods are commonly used to cool server racks inside data centres because of their low capital cost and maintenance [6]. This thesis focuses on the use of CFD methods to optimise air cooling in data centres. Previous CFD studies, such as those undertaken by Cho et al. [11], for instance, are difficult to reproduce for comparison owing to insufficient details about the boundary conditions being used. Also, CFD analysis has been used by Beitemal et al. [15] to test the effect of the failure of the CRAC unit on the cooling of the data centre without any clarification of the boundary conditions that have been used in CFD analysis. It was shown that the smart redundant cooling system could be used to prevent the rack failure by removing the load in high density areas and redistributing the load to other low density areas inside the data centre. Additionally, a lot of CFD studies have been done to detect the rack inlet temperature, such as [28] and [37], with different room layouts. Also, the boundary conditions that have been used are not clear in previous CFD studies. Therefore, in this thesis, the boundary conditions are clearly described to give a full picture of how the server and rack are treated inside a data centre.

CFD analysis is used in this thesis to analyse data centre design and to detect the effect of managing the air flow in server racks. Consequently, the cooling air flows for the components of data centres, such as servers and racks, have been analysed by using CFD analysis to determine the environmental condition inside the data centre (temperature, pressure and velocity fields). First, a porous approach to modelling flow in server racks has been tested to simulate the server inside the data

centre in order to simplify the components' geometry. The results obtained, which are pressure drop and temperature distribution across servers and server outlet velocity, have been validated with experimental data for a single blade. Secondly, the rack level has been simplified by using an 8 porous block rack instead of 32-server rack. Finally, the compressor work of the direct expansion CRAC unit has been evaluated for different cooling configurations. The various cooling configurations studied in this thesis are cold-hot aisle arrangement, cold aisle containment, hot aisle containments and back door coolers (active back door cooler and passive back door cooler). Furthermore, the comparison between the active and passive back door coolers has been done to study the effect of using these techniques on the CRAC heat load. The following conclusions can be drawn from the results of this study:

1. It is found that the RNG  $k-\varepsilon$  model is more accurate than other  $k-\varepsilon$  models when the 1U server is simulated. This is consistent with studies showing that the RNG  $k-\varepsilon$  is the most suitable model for the forced convection with a low turbulence level [58]. So that, the RNG  $k-\varepsilon$  model is the best Reynolds Averaged Navier- Stokes (RANS) model for this specific situation.
2. The CPU inside a 1U server has been simulated as a porous media and validated with experimental measurements with respect to the temperature distribution and pressure drop. Also, it is shown that the porous media model provides good agreement with experimental data for a 1 U server with respect to both temperature and pressure drop across the server. Therefore, the porous media assumption is made because the air has the ability to flow through the rack servers but is restricted by the internal components of the servers. The

obstructions inside the server rack can be replaced by viscous and internal resistances for the porous media.

3. In order to simplify the geometry of a 32-server rack, a comparison has been carried out on the temperature distribution of a 32-server rack inside the data centre with 16 porous blocks, 8 porous blocks, 4 porous blocks, 2 porous blocks and 1 porous block. The results show that both 16 porous blocks and 8 porous blocks gives an excellent agreement with a 32-server rack with respect to temperature distribution. It is found that 8 porous blocks is the lowest level that can be used to represent a 32-server rack, as discussed in Chapter 5.
4. The Reynolds number is relatively low (i.e., around 5000) in the turbulent region inside the server. However, the Reynolds number would be high in the vent section (i.e.,  $10^6$ ). Therefore, the standard k- $\epsilon$  turbulence model is appropriate inside the room, as mentioned by Cho et al. [11] and Beitemal et al. [15].
5. Based on the CFD model, which is presented in this thesis, hot spots inside the data centre can be reduced by using either cold aisle containment or hot aisle containment configurations because of the usage of the physical barriers to increase the degree of separation between the hot and cold aisles. This reduces the mixing of cold air and hot air in the cold aisle.
6. Using the hot aisle containment technique is better than using the cold aisle containment technique with respect to maintaining comfortable environmental criteria inside the data centre. In the cold aisle containment case, the room temperature is close to the exhaust temperature and it may reach to 35°C; this temperature is out of the comfortable temperature range, which is 21°C -28°C, as described by ASHRAE [92]. Whereas, the room temperature inside the data centre with hot aisle containment is close to the supply temperature and this

temperature is in the acceptable comfortable temperature range. Because of the specific heat of liquid (water), which is much greater than that of the air, the back door cooler could be used to reduce the rack exhaust temperature by using an air-water heat exchanger at the rear of the racks. In such, the liquid cooling loop is close the IT equipment and, in some cases, is used inside the server to remove the heat directly from the CPUs. This solution has an advantage of removing a higher amount of heat than that which can be removed by the air cooling systems. On the other hand, the main disadvantages of the liquid (water) system are its high cost and potential leakage problems. The leakage problem could damage the IT equipment.

7. The CFD analysis shows that the compressor power of a direct expansion (DX) CRAC unit can be reduced when either cold aisle containment or hot aisle containment configurations are used instead of a traditional arrangement. This is because the supply temperature can be increased, and thus, the temperature difference between the return and supply decreases.
8. The back door cooler is a promising technique to reduce the rack exhaust temperature based on the results in Chapter 7. Therefore, the room temperature is reduced, and this leads to reduction of the CRAC unit load.
9. In this study, it is found that the active back door cooler is a better cooling configuration than the passive back door cooler, cold aisle containment, and hot aisle containment configurations, with respect to reducing the total cooling load. The exhaust rack temperature is a main parameter that is considered because it is the main parameter that causes the hot spots inside the data centre and affects the rack lifespan [15]. Therefore, using a back door cooler is an effective way to reduce the exhaust rack temperature because it is close to the heat source; this is accomplished by placing the heat exchanger directly at the rack exhaust. The

additional fan in the active back door cooler increases the heat transfer rate between the back door heat exchanger and the hot air stream by increasing the air stream velocity, thus leading to an increased heat transfer coefficient. However, the back door cooler techniques need further study to define the true economical energy efficiency benefits for a range of data centres. In such, a more detailed cost/benefit analysis should be considered. Also the energy, maintenance and installation costs should be taken into account when the back door cooler cooling configurations are used.

## 8.2 Future Work

In this thesis, the traditional server (1U server) is simulated by using CFD analysis and experimentally validated; then, different cooling configurations have been tested. It is suggested that future studies could be conducted, as follows:

1. In future research, much more experimental work is needed to validate the CFD models of the rack and room levels inside the data centre, and a wide range of data centres can be used to generalize the results because the results presented here are for a limited case.
2. Also, in the case of using back door coolers, further study is needed to calculate the installation, maintenance and energy costs. Therefore, a more detailed cost/benefit analysis of back door coolers could be done.
3. The blade server could be applied in the same way as this thesis is presented. Also, the comparison between the 1U server and blade server could be tested. After that, in the rack level, the rack with 1U servers and the rack with blade server chassis could be compared with respect to the fan power required to operate the blade server chassis rack.
4. Different cooling configurations could be implemented for the rack with blade servers. Also real-time simulations that account for variable server loads could be handled.
5. Free cooling technique could be applied for the back door cooler configuration in a data centre, in which free cooling could be used to the water loop that cools the back door heat exchanger. However, the free cooling depends on the geographic location of the data centre and seasonal conditions.

## **BIBLIOGRAPHY**

- [1] J. Fredrik Karlsson and Bahram Moshfegh. Investigation of indoor climate and power usage in a data centre. *Energy and Buildings* 37 (2005) PP.1075–1083.
- [2] H.S. Sun and S.E. Lee. Case study of data centres' energy performance. *Energy and Buildings* 38 (2006). PP. 522–533.
- [3] Tao Lu, Xiaoshu Lu, Matias Remes and Martti Viljanen. Investigation of air management and energy performance in a data center in Finland: Case study. *Energy and Buildings* 43 (2011). PP. 3360–3372
- [4] Mauricio Arregoces and Maurizio Partolani. *Data center fundamentals*. (2004) Cisco system, Inc. USA. ISBN.1-58705-023-4.
- [5] Rahmat Romadhon, Maisarah Ali, Ayub Mohd Mahdzir and Yousif Abdalla Abakr. Optimization of cooling system in data system in data centre by computational fluid dynamics model and simulation. (2009) CITISIA. PP. 322-327.
- [6] Dr. Robert Hannemann and Herman Chu. Analysis of alternative data centre cooling approaches. *InterPACK-1176* copyright at ASME (2007). PP. 743-750.
- [7] C.E. Bash, C.D. Pate, and R.K. Sharma, Efficient thermal management of data centers—immediate and long-term research needs, *Int. J. HVAC R Res.* 9 (2) (2003). PP. 137–152.
- [8] C. Patel, R. Sharma, C. Bash and A. Beitelmal, Thermal considerations in cooling large scale high computer density data centers, in: *Proceedings of IThERM (2002) the Eighth Intersociety Conference on Thermal and Thermomechanical Phenomena in Electronic Systems*, San Diego, CA, PP. 767–776.



- [9] J. Mitchell-Jackson, J.G. Koomey, B. Nordman and M. Blazek. Datacenter power requirements: measurements from Silicon Valley, *Energy* 28 (8) (2003). PP. 837–850.
- [10] Patterson MK. The effect of datacenter temperature on energy efficiency. In: *Thermal and thermo mechanical phenomena in electronic systems*, (2008) IThERM 11th intersociety conference on Orlando, FL; 2008. PP. 1167–74.
- [11] Jinkyun Cho, Taesub Lim and Byungseon Sean Kim. Measurements and predictions of the air distribution systems in high compute density (Internet) data centres. *Energy and Buildings* 41 (2009) PP. 1107–1115.
- [12] J. Rambo and Y. Joshi, Convective transport processes in data centers, *Numerical Heat Transfer, Part A* 49 (2006). PP. 923-945.
- [13] Donald J. Schumacher, William C. Beckman. Data centre cooling system. United State patent (2004). Patent number: US 6,374,627 B1,2002.
- [14] Luiz Andre Barrosos and Urs Holzle. *The datacentre as a computer: An introduction to the design of warehouse-scale machines*. (2009) by Morgan & Claypool.
- [15] Abdlmonem H. Beitelmal and Chandrakant D. Patel. Thermo-fluids provisioning of a high-performance high density data centre. *Distributed and Parallel Databases*, (2006) Springer science. PP. 227-238.
- [16] Data centre Wikipedia website: [http://en.wikipedia.org/wiki/Data\\_center](http://en.wikipedia.org/wiki/Data_center).
- [17] *Thermal guidelines for data centre processing environments*, ASHRAE, (2004).
- [18] Power usage effectiveness(PUE). Mark Fontecchio. May (2008). Website <http://searchdatacenter.techtarget.com/definition/power-usage-effectiveness-PUE>

- [19] Anna Haywood, Jon Sherbeck, Patrick Phelan, Georgios Varsamopoulos and Sandeep K.S. Gupta. Thermodynamic feasibility of harvesting data center waste heat to drive an absorption chiller. *Energy Conversion and Management* 58 (2012). PP. 26–34.
- [20] The Green Grid. The green grid data centre power efficiency metrics: PUE and DCiE. (2007) The Green Grid. White paper # 6.
- [21] Victor Avelar. Guidance for calculation of efficiency (PUE) in real data centres. White paper # 158. (2009) APC.
- [22] Intel Co.. Reducing data centre energy consumption. White paper (2008).  
Website:  
[http://www.cs.berkeley.edu/~istoica/classes/cs294/09/CERN\\_Whitepaper\\_r04.pdf](http://www.cs.berkeley.edu/~istoica/classes/cs294/09/CERN_Whitepaper_r04.pdf)
- [23] Neil Rasmussen. Avoidable mistakes that compromise cooling performance in data centres and network rooms. White paper # 49.(2003) APC.
- [24] Neil Rasmussen and Wendy Torell. Data centre project: establishing a floor plan. White Paper #144.(2007) APC.
- [25] Amir Radmehr and Kailash Karki. Airflow modelling: An effective tool for improving cooling performance of data centres. Innovative Research. Plymouth, MN55447. Website  
<http://inres.com/assets/files/tileflow/TF10-airflow-modeling.pdf>
- [26] Intel information technology. Air-cooled high-performance data centres: case studies and best methods. White paper (2006).
- [27] Rikke Jensen. Benefits of the air flow calculator. Application note. (2007) APC.

- [28] Siddharth Bhopte, Dereje Agonafer, Roger Schmidt and Bahgat Sammakia. Optimization of data centre room layout to minimize rack inlet air temperature. December (2006). ASME Vol. 128, PP. 380-387.
- [29] John Niemann. Hot aisle vs. cold aisle containment. (2008) APC. White paper #135.
- [30] Mitch Martine, Mukesh Khattar and Mark Germagian. High-density heat containment. (2008-2009) ASHRAE journal, ASHRAE Thailand Chapter. PP. 35-42.
- [31] Kwok Wu. A comparative study of various high density data centre cooling technologies. December (2008). Master of Science thesis at Stony Brook University.
- [32] Chatsworth Products, Inc. Ducted exhaust cabinet~ managing exhaust airflow beyond hot/cold aisle. (2006) CPI. White paper.
- [33] Richard Sawyer. Calculating total power requirements for data centres. (2004) APC. White paper #3.
- [34] Christopher G. Malone, Wade Vinson and Cullen E. Bash. Data Centre TCO benefits of reduced system air flow. Google Inc. and Hewlett Packard company(2008). PP. 1199–1202.
- [35] Neil Rasmussen. Improving rack cooling performance using blanking panels. (2005) American power conservation white paper #44.
- [36] Kailash C. Karki, Suhas V. Patankar and Amir Radmehr. Techniques for controlling airflow distribution in raised-floor data centres. Proceedings of IPACK03 .The Pacific Rim/ASME (2003) International Electronic Packaging. Technical Conference and Exhibition. Volume 2.

- [37] Roger Schmidt and Ethan Cruz. Raised floor computer data centre: Effect on the rack inlet temperatures of chilled air exiting both the hot and cold aisles. (2002) inter society conference on thermal phenomena.
- [38] Timothy D. Boucher, David M. Auslander, Cullen E. Bash, Clifford C. Federspiel and Chandrakant D. Patel. Viability of dynamic cooling control in data centre environment. Journal of Electronic Packaging. June (2006), Vol. 128. PP. 137-144.
- [39] Magnus K. Herrlin. Airflow and cooling performance of data centres: two performance metrics. (2008) ASHRAE, Vol.114, part2.
- [40] Anubhav, Kumar, Yogendra, and Joshi. Use of airside economizer for data centre thermal management. (2008) IEEE.
- [41] Chandrakant D. Patel, Cullen E. Bash and Christian Belady. Computational fluid dynamics modelling of high compute density data centres to assure system inlet air specifications. ASME international electronic packaging technical conference and exhibition (2001).
- [42] Chandrakant D. Patel, Cullen E. Bash and Abdlmonem H. Beitelmal. Smart cooling of data centres. United State, Patent Application publication. Pub. No.:2003/0067745 A1 (2003).
- [43] Lennart Stahl, Christian Belady and Liebert Corporation. Overhead cooling system with selectively positioned path of airflow. United States Patent. May 20 (2003).
- [44] Sgi. Next generation data centre infrastructure. ICE cube modular data centre overview and features. White paper. Website : <http://www.sgi.com/pdfs/4172.pdf>.

[45] Ali Almoli, Adam Thompson, Nikil Kapur, Jonathan Summers, Harvey Thompson and George Hannah. Computational fluid dynamic investigation of liquid rack cooling in data centres. Applied energy, volume 89, issue 1, January (2012), PP. 150-155.

[46] Ravi Udakeri, Veerendra Mulary and Dereje Agonafer. Comparison of overhead supply and underfloor supply with rear heat exchanger in high density data centre clusters. (2008) IEEE. PP. 165-172.

[47] High-performance computing (HPC). Website

<http://searchenterpriselinux.techtarget.com/definition/high-performance-computing>

[48] HPC power and cooling: Introduction-part 1. HPC at Dell home. Website

<http://en.community.dell.com/techcenter/high-performance-computing/w/wiki/2294.aspx>

[49] Jayantha Siriwardana, Saman K. Halgamuge, Thomas Scherer and Wolfgang Schott. Minimizing the thermal impact of computing equipment upgrades in data centers. Energy and Buildings 50 (2012). PP. 81–92.

[50] J. Siriwardana, W. Schott and S. Halgamuge, The power grabbers, IEEE Power and Energy Magazine 8 (2010). PP. 46–53.

[51] Justin Moore, Jeff Chase, Parthasarathy Ranganathan and Ratnesh Sharma. Making Scheduling “Cool”: Temperature-aware workload placement in data centres. (2005) USENIX annual technical conference. PP. 61-74.

[52] TOP 500 Supercomputer sites. Website

[www.top500.org](http://www.top500.org)

[53] M.K. Patterson, D.G. Costello, P.F. Grimm and M. Loeffler. Data centre TCO; a comparison of high-density and low-density spaces. Intel corporation. Jan. (2007) White paper. Paper submitted to THERMES 2007 for publication in Santa Fe, NM 2007.

[54] HP modular cooling system: water cooling technology for high-density server installations. Website

<http://h20000.www2.hp.com/bc/docs/support/SupportManual/c00600082/c00600082.pdf>

[55] National Renewable Energy Laboratory (NREL). U.S. department of energy. High-performance computing data center. Website

<http://www.nrel.gov/docs/fy12osti/55423.pdf>.

[56] Tony Evans. Fundamental principles of air conditioners for information technology. (2004- 2007) APC. white paper#57.

[57] R. Schmidt and M. Iyengar. Thermodynamics of information technology data centers. IBM J.RES & DEV. Vol.53, No.3, paper 9 (2009). PP. 1-9.

[58] Tony Evans. The Different Technologies for Cooling Data Centers. APC white paper 59. Website :

[http://www.apcmedia.com/salestools/VAVR-5UDTU5\\_R2\\_EN.pdf](http://www.apcmedia.com/salestools/VAVR-5UDTU5_R2_EN.pdf).

[59] Yunus A. Cengel, and Robert H. Turner. Fundamental of thermal-fluid sciences. 2<sup>nd</sup> edition . Published by McGraw-Hill (2005). ISBN 0-07-245426-1.

[60] Ken Darrow and Bruce Hedman. Opportunities for combined heat and power in data centre. (2009) ICF international. Website

[http://www1.eere.energy.gov/manufacturing/datacenters/pdfs/chp\\_data\\_centers.pdf](http://www1.eere.energy.gov/manufacturing/datacenters/pdfs/chp_data_centers.pdf).

[61] Thomas J. Breen, Ed J. Walsh and Jeff Punch. From chip to cooling tower data center modelling: Part I influence of server inlet temperature and temperature rise across cabinet. (2010) IEEE.

[62] H K Versteeg, and W Malalasekera. An Introduction to computational fluid dynamics: the finite volume method. 2<sup>nd</sup> edition. Pearson education limited (2007). ISBN 978-0-13-127498-3.

[63] A. Radmehr, R. Schmidt, K.C. Karki, and S.V. Patankar. Distributed leakage flow in raised-floor data centers, The Pacific Rim/ASME International Electronics Packaging Technical Conference and Exhibition (2005), IPACK2005-73273.

[64] R. Schmidt, and E. Cruz. Cluster of high powered racks within a raised floor computer data center: Effects of perforated tiles flow distribution on rack inlet air temperature, IMECE-03 ASME International Mechanical Engineering Congress and R&D Exposition (2003).

[65] R. Schmidt, K.C. Karki, S.V. Patankar. Raised data center: Perforated tile flow rates for various tile layouts, 9th Intersociety Conference on Thermal and Thermo mechanical Phenomena in Electronic Systems (2004).

[66] Jinkyun Cho, and Byungseon Sean Kim. Evaluation of air management system's thermal performance for superior cooling efficiency in high-density data centers. Energy and buildings(43) (2011). PP.2145-2155.

[67] James W. VanGilder, and Roger R. Schmidt. Airflow uniformity through perforated tiles in a raised- floor data centre. (2005) white paper # 121.

[68] Fluid flow website

[http://www.centennialofflight.gov/essay/Theories\\_of\\_Flight/Real\\_Fluid\\_Flow/TH9\\_G3,htm](http://www.centennialofflight.gov/essay/Theories_of_Flight/Real_Fluid_Flow/TH9_G3.htm).

[69] Using the solver in Fluent. Fluent manual. Chapter 25. (2006) Fluent Inc.

[70] Launder, B. E. and Spalding, D. B. The numerical computation of turbulent flows. Comput. Methods Appl. Mech. Eng. (1974). Vol. 3. PP.269-289.

[71] Yakhot, V., Orszag, S.A., Thhangam, S., Gatski, T. B. and Speziale, C. G. Development of turbulence models for shear flows by a Double expansion technique. Phys. Fluids A (1992), Vol. 4, No. 7. PP.1510-1520.

[72] Zhao Zhang, Wei Zhang, Zhiqiang Zhai, and Qingyan Chen. Evaluation of various turbulence models in predicting airflow and turbulence in enclosed environments by CFD: part-2: comparison with experimental data from literature. HVAC & R research (2007), 13(6).

[73] Tsan-Hsing Shin, William W. Liou, Aamir Shbbir, Zhigang Yang and Jiang Zhu. A new k- $\epsilon$  eddy viscosity model for high Reynolds number turbulent flows. Computer fluids (1995), Vol. 24, No. 3, PP. 227-238.

[74] Premnath R. Qualitative air flow modelling and analysis of data centre air conditioning as multiple jet array. (2011) PhD thesis.

[75] Fluid flow in porous media. Website

[http://www.particles.org.uk/particle\\_technology\\_book/chapter\\_3.pdf](http://www.particles.org.uk/particle_technology_book/chapter_3.pdf).

[76] Fluent 6.3 user's guide. Chapter 7. (2006) Fluent Inc.

[77] Camair rotron company. Air moving solutions made simple. Website:

<http://www.comairrotron.com/cgi->

[bin/acfandatasht.pl?Pnum=020174&VoltList=115v&FreqList=60hz&airflow\\_val=&airflow\\_unit=CFM&pressure\\_val=&pressure\\_unit=inh2o&diameter\\_val=&diameter\\_unit=in](http://www.comairrotron.com/cgi-bin/acfandatasht.pl?Pnum=020174&VoltList=115v&FreqList=60hz&airflow_val=&airflow_unit=CFM&pressure_val=&pressure_unit=inh2o&diameter_val=&diameter_unit=in)

[78] Tyan Server Soltion, Thunder K8S pro. Server specification based on Thunder K8S pro (S2882). ([www.tyan.com](http://www.tyan.com)).



- [79] Hewlett-Packard Development Company, Quick Specs of HP Proliant BL 2x220C Generation 7 (G7) server blade. Version 6- April8 (2011).
- [80] R. Mohan and Dr. P. Govindarajan. Thermal Analysis of CPU with variable heat sink base plate thickness using CFD. International Journal of the Computer, the Internet and mangment, Vol. 18 No.1(Januaray-April, 2010), PP. 27-36.
- [81] Arularasan R. and Velraj R. CFD analysis in a heat sink for cooling of electronic devices. International Journal of the Computer, the Internet and Mangment, Vol. 16 No.1(September-December, 2008), PP. 1-11.
- [82] Jeonghwan Choi, Youngjae Kim, Anand Sivasubramaniam, Jelena Srebric, Qian Wang and Joonwon Lee. Modeling and managing thermal profile of rack mounted servers with ThermoStat. (2007) IEEE. PP. 205-215.
- [83] Michael J. Fuerstman, Ann Lai, Meghan E. Thurlow, Sergey S. Shevkoplyas, Howard A. Stone and George M. Whitesides. The pressure drop along rectangular microchannels containing bubbles. The Royal Society of Chemistry (2007). PP. 1479-1489.
- [84] Yunus A. Cengel,. Heat Transfer A practical Approach. International edition . Published by McGraw-Hill (1998).
- [85] Adam Thompson. PhD. Student. School of mechanical engineering.University of Leeds.
- [86] Kulvir K Dhinsa, Chris J Bailey and Koulis A Pericleous. Turbulence modelling and its impact on CFD predictions for cooling of electronic components. (2004) IEEE. Inter society conference on thermal phenomena.

[87] Blade server assembly. James L. Carlisi, Keith D. Richeson, Steven R. Testa and John K. Whetzel. United States, Patent application publication. US2008/0266813 A1 (October 30,2008).

[88] Blade server benefits. Intel information technology. White paper. May (2004).

[89] Magnus K. Herrlin. Rack cooling effectiveness in data centres and telecom Central offices: The Rack Cooling Index (RCI). (2005) American Society of Heating, Refrigerating and Air-Conditioning Engineers, Inc. Reprinted by permission from ASHRAE Transactions, Vol. 111, Part 2.

[90] L.H. Tang, M. Zeng and Q.W. Wang. Experimental and numerical investigation on air-side performance of fin-and-tube heat exchangers with various fin patterns. *Experimental Thermal and Fluid Science* 33 (2009). PP. 818–827.

[91] B Fakhim, M. Bchni, S.W. Armfield and N. Srinarayana. Cooling solutions in an operational data centre: A case study. *Applied thermal engineering*, Vol. 31, Issues 14-15, October (2011), PP. 2279-2291.

[92] BSR/ASHRAE standard 55P. Thermal environment conditions for human occupancy. Third public review. February (2003).

## **APPENDIX**

On the following pages, publication resulting from this study [ Almoli et al.,2012] is presented.